Prevention of Aminoglycoside Antibiotic-Induced Ototoxicity of Auditory Hair Cells via Block of Mechano-Electrical Transducer Channels or Intracellular Mechanisms

Submitted for the degree of Doctor of Philosophy

Molly O'Reilly

University of Sussex

September 2018

UNIVERSITY OF SUSSEX

Molly O'Reilly

Submitted for the degree of Doctor of Philosophy

Prevention of Aminoglycoside Antibiotic-Induced Ototoxicity of Auditory Hair Cells via Block of Mechano-Electrical Transducer Channels or Intracellular Mechanisms

SUMMARY

This thesis addresses the pressing concern of clinical drug-induced hearing loss (ototoxicity). Described herein is the mechanism by which ototoxicity emerges following drug administration both in a clinical setting and in an *in vitro* model assay system used for its investigation, through use of mouse cochlear cultures. The predominant nature of this research concerns the identification of novel otoprotectants - compounds that when co-administered alongside clinical drug treatments can prevent the unfortunate ototoxic side-effect from occurring.

Here I present my research, focussing on the identification of a number of novel compounds that have the potential to be taken forward to *in vivo* screening and, ultimately, clinical trials. Moreover, for each identified compound I present my investigation of their mechanism of protection – which could arise either by preventing the entry of the ototoxicity-inducing drugs into the sensory hair cells of the inner ear, or prevent their induction of apoptosis once inside the cell. To investigate their protective mechanism I employed a variety of methods, including: electrophysiology, fluorescent imaging and mitochondrial respirometry.

Conclusively, I have identified at least five novel otoprotectants with the potential for clinical use. I show that three of these compounds likely block the entry of the damaging drugs into sensory hair cells, whereas the remaining two are thought to work intracellularly. Moreover, the two most effective compounds that I have identified seemingly work intracellularly, suggesting this to be the most viable mechanism of otoprotection for further investigation. I also show the potential for compound modification based on their mechanism of protection as a way of improving a compound's otoprotective profile. Lastly, I devised an assay for the screening of clinical drug effects on mitochondria and employ this as a new avenue of screening for otoprotection.

Declaration Statement

Whilst I have collected the vast majority of the data presented in this thesis, due to the collaborative nature of the project a small proportion was obtained from Dr Nerissa Kirkwood and Dr Emma Kenyon, and is presented here with their permission. Any instance of this will be indicated in text, and is detailed below for clarity:

Data obtained from Emma Kenyon: Figures 6.1A-N and 7.4.
Data obtained from Nerissa Kirkwood: Figures: 4.10, 5.2E, 5.3, 5.6G, 6.5, 6.8, 6.10, 7.6 and 8.6.

I hereby declare that this thesis has not been and will not be, submitted in whole or in part to another university for the award or any other degree.

_____

Molly O'Reilly

In loving memory of Sarah Jane O’Reilly.

Acknowledgements

I would first like to thank my supervisors, Corné Kros and Guy Richardson, for the fantastic support they provided throughout my PhD project. A wonderfully-unparalleled combination of intellect, humility, compassion and kindness, I am so thankful for them guiding me through my beginnings as an independent scientist. They were incredibly encouraging and supportive, and without whom my fascination and interest in science would not have blossomed to half the extent that it has.

Richard Goodyear, for teaching me so much of what I now know, for not laughing at all of my silly mistakes, and for being a fantastic friend throughout the entirety of my PhD; Nerissa Kirkwood, for being my electrophysiology guru; Emma Kenyon, for imparting all of her zebrafish knowledge and being such a genuine, lovely human being; Marco Derudas, for designing and supplying all of the compounds that I tested throughout this project; and lastly Luke Young, for all of his help in the mitochondria part of my project and for being a wonderful housemate during my final year.

A special thank you to Kate Fennell, who became one of my best friends on the very first day of our PhD induction; a moment I will never forget. Always there for each other in our many 'hours of need', I am so thankful for all that we have shared these past four years: the endless laughs, the smiles, the tears and all of our wonderfully drunken science chats... I honestly could not imagine the last four years without you. A friendship that I know will last a lifetime.

I would also like to thank my wonderful family. Although small, their love is enormous. Firstly my mother, Jackie O'Reilly, responsible for creating the strong, independent woman that I feel I have become. Also my brothers, Danny and Kai O'Reilly: Danny for being the most wonderful, kind-hearted human being to have ever walked this planet. Your kindness and compassion knows no bounds, and I will forever be grateful for all of the love and support you showered me with throughout this stage of my life. Kai, for making me feel like I can achieve anything. For being a wonderful combination of sweet and sassy, your strength and individuality is inspiring. Not just my brothers, but also my best friends. I would also like to thank my late grandmother, Sarah Jane O'Reilly, for being the most inspirational woman I have ever met. You always believed in me and told me that I could do anything I put my mind to. If I can grow to have even half of the caring kind-heartedness that you did, I will be so happy. Lastly Jane Friedman, my crazy American aunty that has always been supporting me from a far; my number one fan and my kindred spirit.

Last but certainly not least, I would like to thank all of my friends that have helped me along the way. Joanna Packwood; Gabriella Broadley; Alev Treece; Kirsty Walker; Chris Todd; Amy Bunce; Laura Eade; Kirsty Clinton; David Ingleson; Sean Clark; Scott Ensor; James Morgan; Miles Bryant; Kit Harding; Adam Carter; Sam Parsons and Paul Murphy.

I could not have done it without all of your continued support and utter unwavering faith in my abilities, even when I had none of my own! So to everyone that has been a part of this wonderful journey, thank you for everything!

Abstract

Aminoglycoside antibiotics (AGs) are extremely effective clinical agents used to treat serious bacterial infections such as septicaemia. They do however cause permanent hearing loss as an unfortunate side-effect. This is because they are known to specifically enter the sensory hair cells of the inner ear through an ion channel known as the mechano-electrical transducer (MET) channel. Once inside a cell they are thought to interact with mitochondria, causing the production of cytotoxic levels of reactive oxygen species (ROS). It is this process that results in the activation of apoptotic cell death cascades, underlying the hair cell loss and consequent elevation of hearing threshold associated with AG treatments.

It is therefore of pressing concern to identify preventative measures against this side-effect. Presented herein is my investigation, and identification, of potential novel otoprotectants – compounds that when co-administered alongside AG treatment can prevent the associated hearing loss. At least five novel compounds have been identified from a library of ion channel interactors that display otoprotective properties *in vitro* and have the potential for clinical investigation.

Following otoprotectant identification, the mechanism by which they protect was subsequently investigated. Broadly speaking, there are two possibilities: extracellular block of AG entry into hair cells via the MET channel or intracellular prevention of mitochondrial dysfunction and ROS accumulation. Whole-cell electrophysiological approaches were employed to study compound interaction with the MET channel and imaging of a fluorescent AG analogue to assess any prevention of its entry into sensory hair cells. The most effective compound identified, protecting in the low nanomolar range, was found to not prevent AG entry and thus assumed to have an intracellular mechanism of protection. For this reason, an assay was developed to investigate the effect of the AGs on mitochondrial function and subsequently to test whether the compound of interest was able to prevent this effect.

AGs were found to behave as uncouplers of the mitochondrial electron transport chain, affecting respiratory rates by dissipating the mitochondrial membrane potential and thereby inhibiting ATP production. The most efficacious otoprotectant identified herein did not prevent this effect, meaning its mechanism of protection remains to be identified.

Table of Contents

Abbreviations

AG – Aminoglycoside antibiotic

ANOVA - Analysis of variance

BAPTA - 1,2-bis(o-aminophenoxy)ethane-N,N,N’,N’-tetraacetic acid

CI, CII, CIII, CIV and CV – Electron transport chain complexes I, II, III, IV and V

CCCP – Carbonyl cyanide m-chlorophenyl hydrazine

DHS - Dihydrostreptomycin

DIC - Differential interference contrast

DMSO - Dimethyl sulfoxide

dTC – d-Tubocurarine

ECS – Extracellular solution

EP – Endocochlear potential

ER – Endoplasmic reticulum

ETC – Electron transport chain

GTTR – Gentamicin-Texas Red

HBHBSS - Hanks Buffered Salt Solution with 1% Hepes

HC – Hair cell

IC_{50} – Half-effect concentration

ICS – Intracellular solution

IMM – Inner mitochondrial membrane

K_D – Half-blocking concentration

IHC – Inner hair cell

MEM - Eagle’s minimum essential medium

MET – Mechano-electrical transducer

MtMP – Mitochondrial membrane potential

MtROS – Mitochondrial reactive oxygen species

OHC – Outer hair cell

OMM – Outer mitochondrial membrane

P2 – Postnatal day 2

PBS - Phosphate buffered saline

RCM – Rat culture media

RCR – Respiratory control ratio

RNA - Ribonucleic acid

ROS – Reactive oxygen species

RP – Resting potential

SV – Stria vascularis

TMC - Transmembrane channel-like

TRITC - Tetramethylrhodamine

1 Introduction

Our sense of hearing is unequivocally fundamental to our existence as we know it. Not only underpinning our survival, our ability to hear is crucial to the rich plethora of communicatory abilities that we utilise on a daily basis, without which life would certainly lose a little richness at the very least. Those who are unfortunate enough to lose this sensory modality suffer a greatly-reduced quality of life, with an almost-unavoidable impact on every aspect of their livelihood. Progressive and irreversible hearing loss occurs naturally as a result of aging; however other causes of deafness include: prolonged exposure to loud noise, infections such as meningitis and treatment with ototoxic compounds. The aminoglycoside antibiotics are an extremely effective class of clinical agent used to cure serious bacterial infections. They do, however, cause permanent hearing loss as an unfortunate side-effect. The aim of this thesis was to identify compounds that could prevent this effect and uncover their modes of action, thereby improving the quality of life of individuals unfortunate enough to be treated with these clinical agents.

1.1 The Anatomy and Functionality of the Ear

1.1.1 The Outer and Middle ear

The outer ear, consisting of the pinna, concha and external auditory meatus (ear canal), serves to collect and funnel airborne sound information from the external environment and direct it through the ear canal to the tympanic membrane, colloquially known as the ear drum (Figure 1.1). The sound pressure of frequencies of sound around 3 kHz are passively amplified by the auditory meatus due to its anatomical configuration - the frequency of sound at which human speech distinction cues are concentrated (Purves et al., 2012).

The middle ear serves to amplify the sound signal by acting as an impedance matching device. Sound stimuli in the external environment are in a low-impedance medium, air. The inner ear, however, is filled with the higher-impedance medium, aqueous fluid. When sounds travel between these two mediums in the external environment almost all of the acoustic energy is lost due to the process of reflection. The middle ear works to prevent the loss of the acoustic signal by impedance-matching and boosting the pressure measured at the tympanic membrane almost 200-fold by the time it reaches the inner ear (Purves et al., 2012). The structure achieves this amplification pressure gain by two complimentary processes. Firstly, the middle ear contains three bones that connect the tympanic membrane to the oval window (Figure 1.1). These are known as the ossicles, or the malleus, incus and the stapes; colloquially known as the hammer, anvil and stirrup. They are three small, specifically shaped and interconnected bones that serve to amplify and concentrate the sound signal on the oval window; maximising sound intensity with remarkable efficiency. Secondly, the focussing of the force from the relatively large-diameter tympanic membrane onto the much smaller-diameter oval window (where the middle ear bones contact the inner ear) gives a large boost in the pressure signal, enhancing the amplification process (Purves et al., 2012; Kandel et al., 2013).

1.1.2 The Inner Ear

The inner ear is a bony labyrinth comprised of the auditory and vestibular systems; highly-specialised structures that are responsible for the phenomenon of hearing and balance respectively. The vestibular apparatus comprises the saccule, utricle and the semicircular canals; structures that are responsible for the detection of head motion, head orientation and

balance. The cochlea (the organ of hearing) is directly responsible for sound transduction and our ability to perceive sounds emerging from the external environment. It is the location at which sound stimuli are converted into neural impulses that can then be delivered to, and processed by, the auditory cortex. Alongside this, the cochlea also represents the first instance of frequency analysis, with complex sound stimuli waveforms being decomposed into their component parts by the fascinatingly intricate anatomical organisation of the structure.

The stapes joins the cochlea at the oval window, at the base of the structure (Figure 1.1). From the base to the apex, the cochlea is partitioned into three fluid-filled chambers. Either side of this partition are two chambers known as the scala vestibuli and scala tympani, both of which contain perilymph; a sodium-rich fluid. Central to the cochlear partition is a distinct chamber known as the cochlear duct, or scala media, which contains a potassium-rich fluid known as endolymph. Within the scala media sits the organ of Corti – the anatomical structure that is situated between the basilar and tectorial membranes and is directly responsible for sound transduction (Figure 1.2). The cochlear partition is what allows for the flexibility in movement of the basilar and tectorial membrane – important structures that underlie the frequency-selectivity of the transduction apparatus (Purves et al., 2012; Kandel et al., 2013).

When sound stimuli are delivered to the base of the cochlea via the stapes, the basilar membrane resonates depending on the frequency composition of the sound. Due to the geometry of the basilar membrane, being wider and more flexible at the apical end and more narrow and stiff at the base, it vibrates maximally at different locations dependent on the stimulus. High-frequency stimuli induce maximal basilar membrane displacement at the base of the cochlea whereas low-frequency stimuli cause maximal displacement in the apex. This tonotopic gradient is an important characteristic enabling the decomposition of complex sound waveforms into their frequency components, with the basilar membrane acting as a mechanical frequency analyser (Purves et al., 2012; Kandel et al., 2013).

The sensory hair cells (HCs) of the inner ear are situated atop of the basilar membrane (Figure 1.2). On top of the HCs sits the tectorial membrane, a gelatinous structure in which the stereocilia of outer HCs (OHCs) are embedded. When the basilar membrane vibrates in response to sound stimuli, this causes movement of both the organ of Corti and the overlying tectorial membrane. Due to their differing pivoting points this displacement leads to a shearing of the two membranes. This shearing causes a displacement of the stereocilia that adjoin the HC's apical surface, leading to potassium ion entry into the cell, consequent cellular depolarisation and the signalling of sound stimuli to the auditory nerve. Inner HCs (IHCs) are

not directly embedded in the tectorial membrane, but rather their stereocilia are deflected by movement of the fluid beneath the membrane (Kandel et al., 2013) (Figure 1.2).

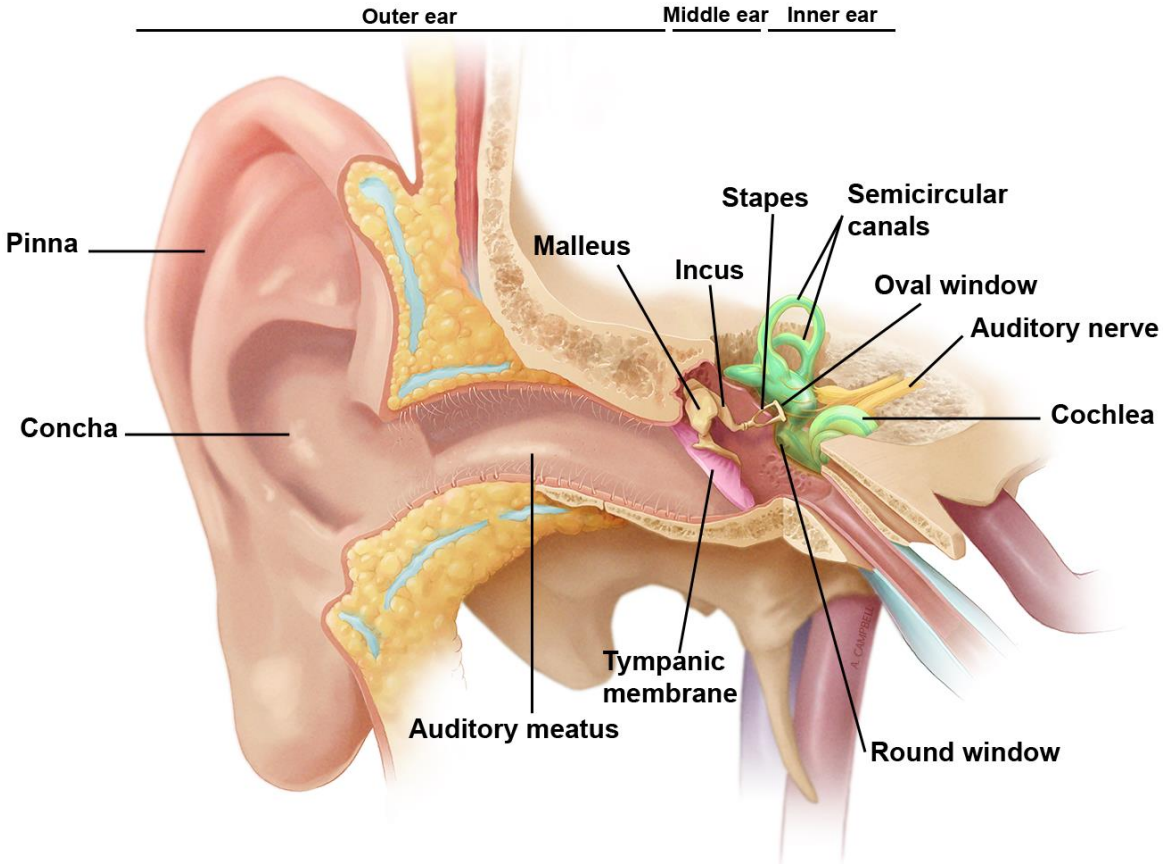

Figure 1.1: *The anatomical organisation of the ear. Figure modified with permission from © University of Dundee School of Medicine, illustrated by Annie Campbell.*

The outer ear, responsible for capturing and funnelling airborne sound information, consists of the pinna, concha and auditory canal. The middle ear, which impedance matches and serves to amplify sound signals, consists of the tympanic membrane and the ossicles (the malleus, incus and stapes). The inner ear, which is responsible for sound transduction, consists of the vestibular apparatus and the cochlea.

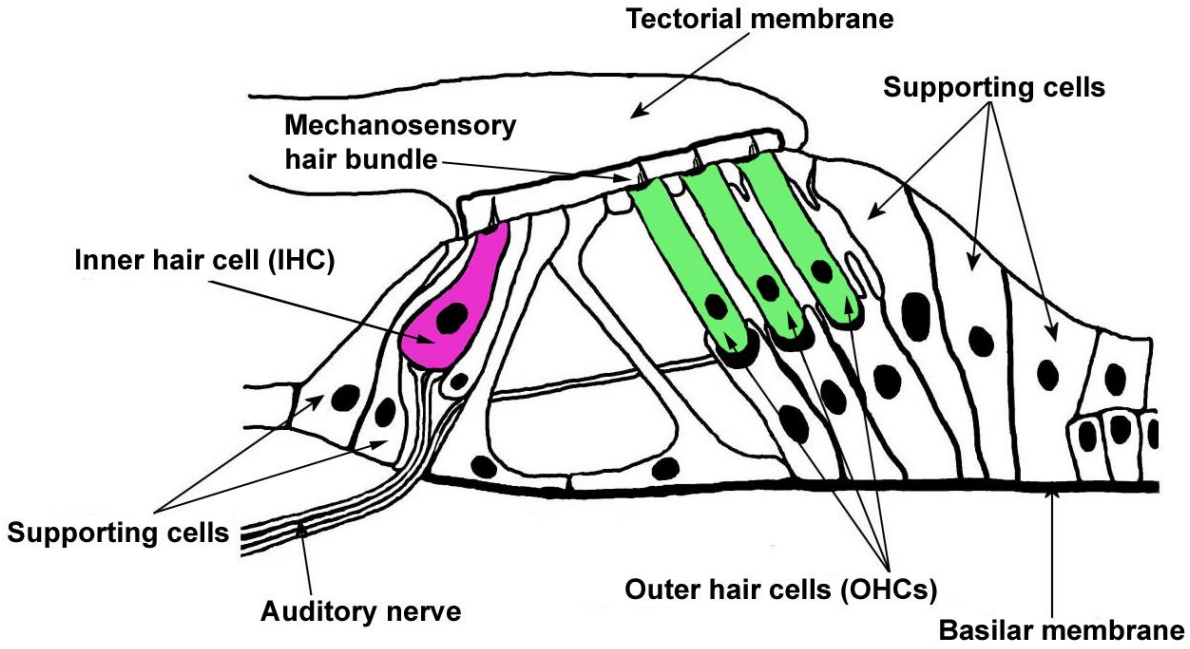

Figure 1.2: *The anatomical organisation of the organ of Corti. Figure modified from Pickles (2008).*

The organ of Corti, which is situated in the cochlear duct, is responsible for the transduction of sound stimuli into electrical impulses that can be interpreted by the brain. Inner HCs (IHCs) directly transduce sound stimuli to afferent nerve fibres, whereas outer HCs (OHCs) are innervated mainly by efferent nerve fibres and serve to fine-tune our hearing sensitivity and frequency selectivity.

1.2 Sensory Hair Cell Anatomy and Function

Along the length of the cochlear sensory epithelium there are typically four rows of sensory HCs - one row of IHCs and three rows of OHCs (Figure 1.2). On average, the human organ of Corti contains approximately 3,500 IHCs and 11,000 OHCs (Kandel et al., 2013). The IHCs are the sensory receptors that are directly responsible for sound stimuli transduction and information transfer to the auditory nerve. They are contacted by many afferent nerve fibre innervations, with approximately 95% of fibres in the auditory nerve originating from the IHCs (Purves et al., 2012). OHCs are primarily contacted by efferent nerve fibres and serve to actively amplify sound signals due to their expression of the motor protein prestin. This gives rise to their unique characteristic of electromotility; frequency-dependent contraction and extension of the cell body in response to electrical stimulation (Brownell et al., 1984; Zheng et al., 2000; 2002; Dallos, 2008).

Located on the apical surface of all sensory HCs is a mechanosensory hair bundle, comprised of multiple rows of stereocilia that are joined together with an assortment of molecular linkers, allowing the hair bundle to move in a cohesive manner upon deflection (Hackney and Furness, 2013). These stereocilia are anchored in the apical membrane in an actin-rich structure known as the cuticular plate, and are able to pivot in response to mechanical deflection. In mammals, the bundle also has a larger kinocilium that disappears shortly after birth – it is absent by postnatal day 12 (Kikuchi and Hilding, 1965; Kimura, 1966). The stereocilia are arranged in a graded pattern with rows of increasing height and are connected at their apical tips by filamentous structures known as tip-links (Pickles et al., 1989). These are molecular structures comprised of cadherin-23 and protocadherin-15 (Kazmierczak et al., 2007), which are anchored in structures known as the upper and lower tip-link densities, alongside an assortment of other proteins such as myosin VIIa, harmonin-b and sans (Figure 1.3). In IHCs, the hair bundle shape is roughly linear, whereas OHCs have a characteristic V-shaped mechanosensory hair bundle located on their apical surfaces (Kandel et al., 2013).

When a mechanical stimulus causes displacement of the stereociliary bundle in the excitatory direction, towards the tallest stereocilia, the tip-links are stretched and put under tension. Located at the lower end of the tip-link is a non-selective cation channel known as the mechano-electrical transducer (MET) channel. The tip-links and MET channels represent the transduction apparatus, in that their functionality is what allows the transformation of hair bundle displacement into a receptor potential. When the tip-links are put under tension in

response to an excitatory stimulus this causes the mechanically-gated MET channels to open and potassium and calcium ions from the endolymphatic fluid to flow into the HC. This process depolarises the cell, causing calcium ions to enter near the basolateral membrane and subsequent neurotransmitter release to the connecting nerve fibre, which then transmits the signal along the auditory pathway, eventually terminating in the auditory cortex of the brain. Deflection in the inhibitory direction, towards the shortest row of stereocilia, closes the MET channels and hyperpolarises the cell.

Evidence of the involvement of tip-links in transduction comes from calcium chelation studies. When calcium chelators such as BAPTA are used to destroy tip-links, transduction disappears (Assad et al., 1991; Goodyear and Richardson, 2003; Marcotti et al., 2014). Upon regeneration, transduction is restored, indicative of tip-link control of HC mechano-transduction (Zhao et al., 1996; Indzhykulian et al., 2013; Kendal et al., 2013).

1.3 The Endocochlear Potential

A crucial driving force of mechano-electrical transduction within the cochlea is the endocochlear potential (EP). The EP is primarily generated by the stria vascularis (SV) – a metabolically-active epithelium located in the lateral wall of the cochlear duct (Quraishi and Raphael, 2008). The SV is responsible for the two endolymphatic properties which enable such efficient signal transduction by mechanosensory HCs - the unusually high extracellular K^+ concentration (> 150 mM) and the large electrical potential (+80 to +90 mV) relative to the perilymphatic fluid (Takeuchi et al., 2000; Wangemann, 2002; Hibino and Kurachi, 2006; Quraishi and Raphael, 2008). The cells of the SV transport and secrete K^+ ions into the scala media compartment (Tasaki and Spyropoulos, 1959), thereby generating the properties that are fundamental to audition (Wangemann, 2006; Nin et al., 2008).

The EP is essential for cochlear function, with the influx of K^+ ions through the MET channel determined by the electrical gradient established by the sum of the EP and the resting potential (RP) of the HC, which is between -70 and -45 mV (Dallos et al., 1982; Dallos, 1996; Takeuchi et al., 2000; Purves et al., 2012). The RP of OHCs is more negative than that of IHCs (Dallos et al., 1982). The EP is non-uniform and increases from the apex to the base, meaning there is a greater electrical driving force across HC MET channels in the basal coil of the cochlea.

Following entry, K^+ must be cleared from HCs to enable continuous sensory receptiveness. This is achieved by basolateral potassium channels that release the K^+ into the perilymph that bathes the basolateral surface of the HCs. A number of ion channels perform this function, including: KCNQ4 (which mediates the current $I_{K,n}$), KCNN2 (ISK2) and KCNMA1 ($I_{K,f}$) (Kros, 1996; Wangemann, 2006).

1.4 The Mechano-Electrical Transducer (MET) Channel

For the sensation of hearing to occur, mechanical sound stimuli must be converted into electrical signals that can be interpreted by the brain. This function is achieved by the sensory HC MET channels. The molecular characterisation of the MET channel has been described as the 'holy grail' of the field of hearing research, due to its obscurity and elusiveness of identification. Pursuit of its molecular identity has spanned over 20 years (Fettiplace, 2016), and the topic is still of controversial debate. Several candidates have been proposed, including members of the transient receptor potential (TRP) channel family (Corey, 2003; Fettiplace, 2009; Lee et al., 2013); however these have since failed under scientific scrutiny (Corey, 2006). Many researchers now consider transmembrane channel-like (TMC) 1 and TMC2 proteins to be the most likely candidates as crucial molecular components of the MET channel (Kurima et al., 2015; Fettiplace, 2016; Pan et al., 2018).

Investigation into the molecular identification of the MET channel has led to a large body of information regarding its functional properties. Firstly, the MET channel is a non-specific, cation-selective ion channel. It primarily permits the flow of potassium, which predominantly underlies the MET current, and also calcium, which partly underlies the adaptation process (Corns et al., 2014). However, other molecules have also been shown to permeate through the channel (Farris et al., 2004). The entry rate of positively-charged molecules is determined by the electrical potential generated across the channel, primarily as a result of the combined sum of the EP and RP of the cell. Cellular depolarisation has been shown to reduce calcium entry (Eatock et al. 1987; Crawford et al. 1989), as direct evidence of this.

Experimental evidence has suggested that there are two MET channels per stereocilium (Fettiplace, 2009), and although researchers remain divided, their location is largely assumed to be at the base of the tip-links on the second and third stereociliary rows atop cochlear HCs, as established by high-speed calcium imaging studies (Beurg et al., 2009) (Figure 1.3). HCs

exhibit adaptation properties in that upon maintained stimulation, the tension in the tip-links is lessened over time to enable a broader dynamic range of the sensory detection response. This is partly due to the non-selective nature of the MET channel. When it opens upon stereocilial deflection calcium ions also flow into the cell and this is what underlies at least one aspect of the adaption process (Vilfan and Duke, 2003; Corns et al., 2014).

The functioning of the MET channel can be investigated with the use of a number of fluorescent dyes. Classically, the styryl dye FM 1-43 has been used for the study of endo- and exo- cytosis (Betz et al., 1996; Smith and Betz, 1996; Amaral et al., 2011). However, researchers have also found that it can rapidly enter HCs through the MET channel (Gale et al., 2001), meaning it provides a reliable marker of HC MET channel function.

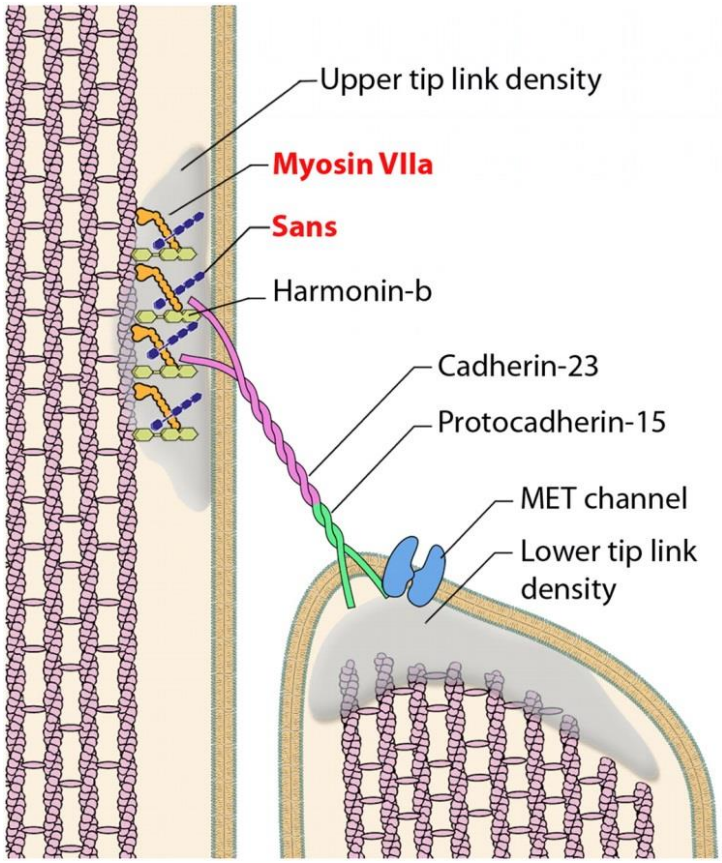

Figure 1.3: *The proposed anatomical localisation of the MET channel. Figure taken from Grati and Kachar, 2011.*

Current theories suggest that the mechano-electrical transducer (MET) channel, which is critical for our ability to hear, is located in the lower tip-link density, on the shorter neighbouring stereocilium.

1.5 Ototoxic Drugs

1.5.1. The Use of Ototoxic Drugs

Ototoxicity is defined as the property of being toxic to the ear. This can manifest as either cochleotoxicity (damage to the cochlea or auditory nerve) or vestibulotoxicity (damage to the vestibular system or nerve). Many ototoxic substances have been identified, including: the aminoglycoside antibiotics (AGs), loop diuretics such as furosemide and chemotherapy agents such as cisplatin. Despite their ototoxic properties they are still widely prescribed due to their effectiveness at treating serious medical conditions and the lack of suitable alternatives.

The AGs are one of the most commonly prescribed antibiotics worldwide due to their remarkable antimicrobial efficacy, their widespread availability due to their ease of storage and also their low cost relative to alternatives (Rizzi and Hirose, 2007; Kushner et al., 2016). They are widely prescribed to treat serious life-threatening bacterial infections such as septicaemia, tuberculosis, meningitis, respiratory infections in cystic fibrosis and complex urinary tract infections (Xie et al., 2011). A recent study on the prescription demographic revealed that the vast majority of AG prescriptions are for neonatal children and the younger population, between 18 and 34 years of age (Kushner et al., 2016).

Although extremely effective clinical agents, the AGs carry the unfortunate risk of common adverse side-effects such as oto- and nephro- toxicity – damage to hearing ability and kidney function respectively (Mingeot-Leclercq and Tulkens, 1999; Forge and Schacht, 2000; Selimoglu, 2007; Wargo and Edwards, 2014). The damage to these tissue types specifically is due to the retention of the AGs within these cells. Most cells take up AGs but are able to efficiently clear them from their cytoplasm (De Groot et al., 1990; Imamura and Adams, 2003; Jiang et al., 2017). Kidney cells and cochlear sensory HCs, however, retain the AGs within their cytoplasm for a prolonged period of time (Imamura and Adams, 2003; Dai et al., 2006). This, together with the greater cellular uptake, leads to the accumulation of an intracellular concentration at which apoptosis is induced. Nephrotoxicity is of a lesser concern due to the regenerative ability of kidney cells, with dying cells replaced through cellular proliferation meaning kidney damage is short-lived and reversible (Heller, 1984; Xie t al., 2001; Jiang et al., 2017). In mammals, unlike in avian species, the sensory cells of the inner ear are unable to regenerate (Stone and Cotanche, 2007), meaning that damage to the inner ear is permanent and irreversible, making AG-induced ototoxicity a much more pressing concern.

In terms of ototoxicity, the AGs can be both cochleo- and vestibulo- toxic, depending on which one is prescribed. Gentamicin (Figure 1.4) and streptomycin are primarily vestibulotoxic, whereas amikacin, neomycin, dihydrostreptomycin (DHS) and kanamycin are primarily cochleotoxic (Selimoglu, 2007; Xie et al., 2011). The likelihood of developing the symptoms of ototoxicity is influenced by several factors, including: the concentration of the dose, the frequency of administration, the duration of treatment and any genetic predisposition, primarily as a result of mitochondrial make-up, with the latter largely due to the A1555G mutation in the mitochondrial 12S rRNA gene (Wu et al., 2002; Xie et al., 2001; Qu et al., 2015). The incidence of ototoxicity varies between studies depending on the method of assessment, but in patients who receive intravenous doses across multiple days, the incidence of ototoxicity has been reported in approximately 20% of all treated patients (Ariano et al., 2008; Al-Malky et al., 2015; Garinis et al., 2017; Jiang et al., 2017). Cochleotoxicity is more commonly observed, with incidence rates as high as 33% reported, compared with 15% for vestibulotoxicity (Fee, 1980; Lerner et al., 1986; Fausti et al., 1999; Kushner et al., 2016).

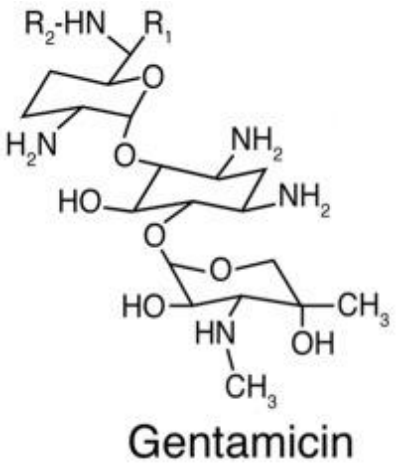

Figure 1.4: *Gentamicin is a large (465 g/mol molecular weight), polycationic molecule that is water soluble at physiological pH. The chemical structures for the gentamicin varieties are as follows: gentamicin C_1: $R_1 = R_2 = CH_3$; gentamicin C_2: $R_1 = CH_3$, $R_2 = H$; and gentamicin C_1A: $R_1 = R_2 = H$. Figure modified from Jiang et al., 2017.*

The prescription demographic is what makes the issue of AG-induced ototoxicity a pressing concern. Neonatal children are the most often treated with the antibiotics due the broad-spectrum nature of AG activity and therefore their effectiveness at curing a wide range of bacterial infections, especially when the underlying cause is unknown. However, neonates are also the most susceptible population to the debilitating consequences of the often-endured

ototoxic side-effect. Hearing ability is vital for the development of language and communication skills, education, psychosocial development and social interaction; those that lose their ability to hear at an early age often struggle to develop in these areas, creating a large socio-economic burden and a greatly-reduced quality of life.

1.5.2 Mechanism of Action of the Aminoglycoside Antibiotics

The way in which the AGs cause the death of bacteria is well understood, with their antibacterial effect attributable to their binding of the bacterial 30S ribosomal subunit. Binding of this subunit causes RNA to be misread, consequent disruption to protein synthesis and thus an accumulation of non-functional proteins leading to bacterial cell death (Cox et al., 1964; Davies and Davis, 1968; Xie et al., 2011). The way in which the AGs cause the death of kidney cells and cochlear sensory HCs is less well understood, however. The damage to these organs is due to the entry and subsequent inefficient clearance from these tissue types specifically, with endocytic and non-selective cation channel-mediated entry routes in kidneys (Nagai and Takano, 2014) and the MET channels in cochlear sensory HCs being proposed entry pathways (Marcotti et al., 2005; Alharazneh et al., 2011).

In order to cause sensory hair cell death the AGs must first be trafficked to the endolymph (in which the sensory hair cell bundles are situated), where they can then proceed to enter cells and induce apoptosis. The AGs are usually administered systemically, and although the endolymph is well shielded from the circulatory system due to the blood-labyrinth barrier, they are still able to enter into this discrete compartment. Endothelial cells line the capillaries within the stria vascularis, forming an impermeable barrier. However, evidence suggests that the tight junctions existing in these cell membranes can allow the passage of AGs into the endolymph, with AGs trafficked from the capillaries, through the marginal cells and into the endolymphatic compartment (Figure 1.5). For a thorough review, see Kros and Desmonds (2015).

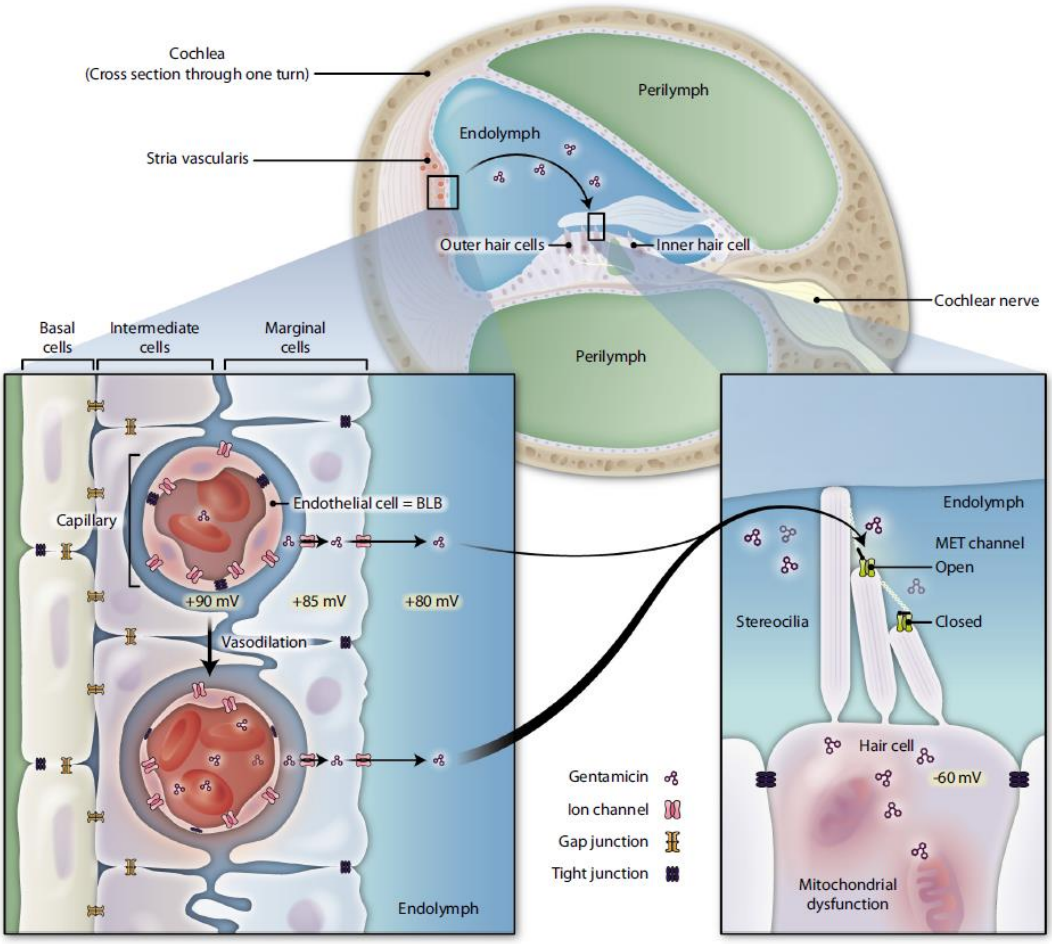

Figure 1.5: *A schematic of a cross-section through a turn of the cochlea, showing the three discrete compartments. AGs are able to cross the blood-labyrinth barrier and enter the endolymph via the marginal cells. Figure taken from Kros and Desmonds, 2015.*

Once inside a cell, however, the AGs are thought to have a conserved mechanism of cell death induction. They are believed to interact with intracellular organelles such as mitochondria, causing their dysfunction and the consequent initiation of apoptotic cell death pathways. The assumption of mitochondrial involvement in AG-induced damage has manifested as a result of several pieces of evidence. Firstly, the remarkable similarity of the structure of mitochondria to that of bacteria (the primary target of AGs) gave the first indication that they may represent a secondary target of the antibiotics, alongside their proposed bacterial origin (Margulis et al., 1970; Gray et al., 2001; Gray et al., 2012). Secondly, fluorescence imaging studies showing the co-localisation of a fluorescent AG conjugate (gentamicin-Texas Red; GTTR) with mitochondrial stains such as Mitotracker (Ding et al., 1995; Steyger et al., 2003), suggested that they are trafficked to these organelles once inside the cell. Moreover, point mutations in mitochondrial

DNA leads to enhanced susceptibility to AG-induced toxicity (Prezant et al., 1993), again signifying mitochondrial involvement. Lastly, prior to cell death, cells treated with AGs show an increase in the intracellular concentration of reactive oxygen species (ROS) (Clerici et al., 1996; Hirose et al., 1997; Sha and Schacht, 1999a); cell signalling molecules produced primarily by mitochondria. Taken together these data suggest that mitochondria are a secondary target of the AGs, and that perhaps their dysfunction is what underlies kidney and sensory HC death following AG entry into these cell types.

As well as these somewhat indirect lines of evidence, researchers have also shown a direct effect of the AGs on the respiratory activities of mitochondria, both in isolated mitochondrial assays and also intact whole-cell systems. Reports suggest that AGs can irreversibly bind to mitochondria *in vitro* (Kornguth et al., 1980), their binding induces the opening of the permeability transition pore (Dehne et al., 2002), this dissipates the mitochondrial membrane potential (Dehne et al., 2002; Miyazono et al., 2018) and leads to a reduction in the amount of ATP that cells can produce (Simmons et al., 1980), thereby causing the death of the cell.

Alternative theories have suggested the involvement of ribosomes and the endoplasmic reticulum (ER) (Steyger et al., 2003), and potentially an extremely complex interaction between combinations of intracellular organelles and their interconnecting systems, including calcium signalling between the ER and mitochondria (Esterberg et al., 2013, 2014; Hailey et al., 2017; O'Sullivan et al., 2017).

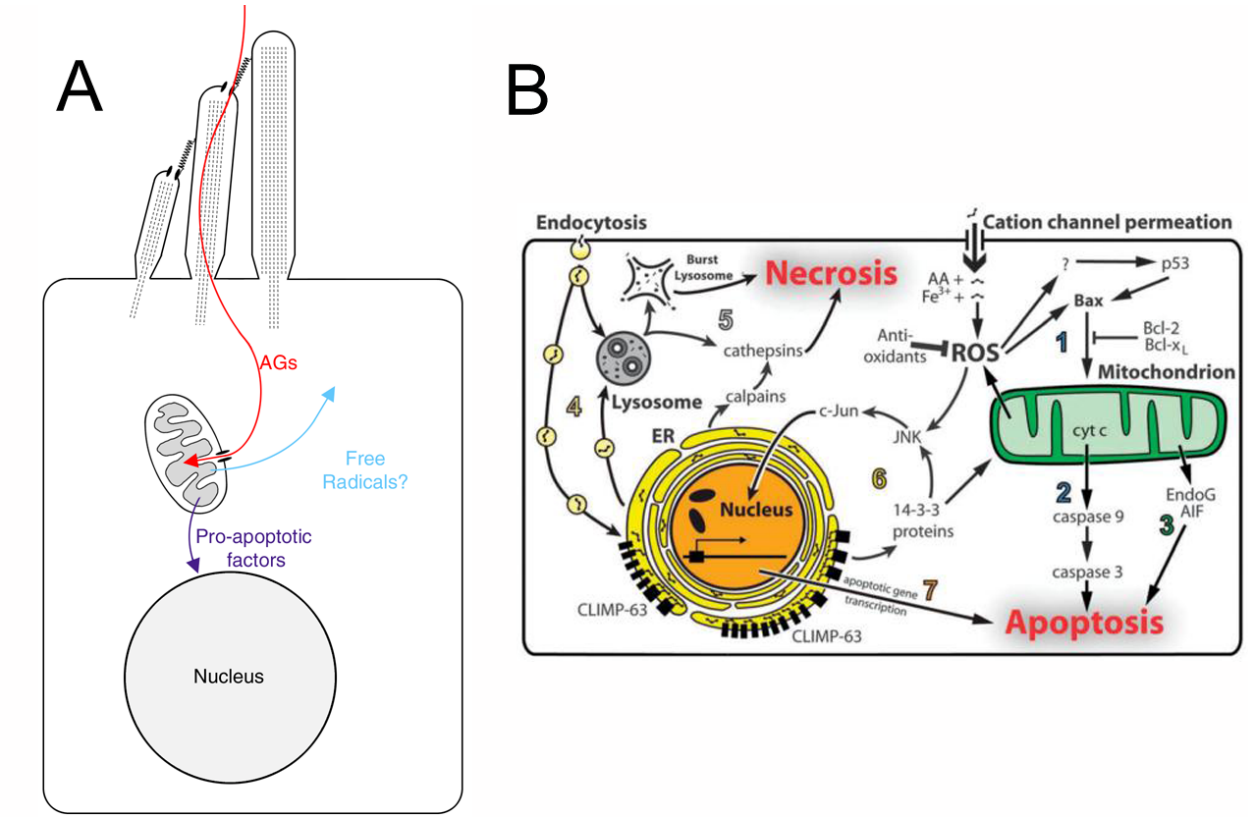

Figure 1.6: *Crude schematics of the mechanisms by which AGs are thought to cause HC death.* ***(A)*** *Figure produced by Richard Goodyear, University of Sussex, and modified by myself.* ***(B)*** *Figure taken from Karasawa and Steyger, 2011.*

The aminoglycoside antibiotics (AGs) are known to enter the sensory HCs of the inner ear through the MET channel. Once inside, they are thought to interact with mitochondria, causing the production of cytotoxic levels of free radicals and the release of pro-apoptotic factors.

1.6 Mechanisms of Otoprotection

Due to the devastating consequences of AG-induced ototoxicity, especially when occurring in the younger demographic, a large number of researchers working in the field of hearing and deafness have focussed on attempting to identify otoprotectants; compounds that when co-administered alongside AG treatment can prevent the unfortunate side-effect form occurring. Broadly speaking, there are two main ways in which a compound could offer protection against AG-induced ototoxicity, as detailed below.

1.6.1 MET Channel Block

One potential method of otoprotection that has been extensively studied is focussed on the entry route of the AGs into HCs. As they are known to primarily enter sensory HCs through their MET channels (Marcotti et al., 2005; Alharazneh et al., 2011), numerous studies have investigated the potential of blocking these channels and thereby preventing AG entry, accumulation and consequent apoptosis-induction. However, when searching for a MET channel-blocking otoprotectant, the compound must show reversibility of the channel block so as to provide only a temporary effect. Furthermore, compounds must not permeate into HCs, as they themselves could cause toxic effects once they have accumulated inside a cell.

1.6.2 Intracellular Protection

An alternative mechanism of otoprotection that has been extensively studied is the prevention of intracellular apoptotic cascades. Once inside a cell, AGs are thought to cause mitochondrial dysfunction and the consequent production of cytotoxic levels of ROS. Intracellular approaches therefore aim to prevent this effect. One approach is to preserve mitochondrial function, for example by way of preventing AG binding to the mitochondrial membranes, preventing the opening of the permeability transition pore, or by preserving the mitochondrial membrane potential (Fu et al., 2006; Ou et al., 2009). Alternatively, these approaches could work post-mitochondrial dysfunction, by way of reducing ROS concentrations within the cell, often by application of antioxidants and other ROS-scavenging molecules (Sha and Schacht, 2000; Sergi et al., 2004; Rybak and Whitworth, 2005; Xie et al., 2011; Negrette-Guzmán et al., 2015).

1.6.3 Otoprotection Method Comparison

The advantage of an intracellular approach is that there would be no interference with MET channel function, so patients treated with the otoprotectant would not experience short-lived hearing loss, as they would with MET channel-blocking approaches. However, once inside a cell the closely-related AGs neomycin and gentamicin have been shown to activate different intracellular cell-death cascades in zebrafish (Owens et al., 2009; Coffin et al., 2013a,b), so

perhaps a MET channel-blocking otoprotectant may be the most effective, all-encompassing approach.

However, mitochondrial dysfunction is known to play a role in a variety of diseases and disorders, including a large number of neurodegenerative conditions such as Alzheimer's disease (Reddy, 2009; Lezi and Swerdlow, 2012). Consequently, if we were to identify a compound that could preserve mitochondrial function, for example by way of mitochondrial membrane potential stabilisation, this could have huge transferable potential in terms of remodelling for a large number of other debilitating conditions.

1.7 Zebrafish as a Model for Otoprotectant Screening

Zebrafish were used for preliminary screening in this thesis as they provide a powerful pre-screening tool when searching for otoprotectants that can prevent the ototoxic side-effect of the AGs in mammals. This is because the sensory HCs that are situated in the neuromasts located along the lateral line system are remarkably similar to those in the mammalian cochlea, both morphologically and functionally. Each neuromast has an aggregation of multiple sensory HCs. On top of each of these HCs sits a mechanosensory hair bundle, consisting of a single kinocilium and multiple stereocilial rows. These are the same morphological features present on the sensory HCs of the postnatal day 2 (P2) mice cochleae used in the subsequent screening experiments detailed in this thesis. Moreover, zebrafish sensory HCs are permeated by FM 1-43 (Seiler and Nicolson, 1999), susceptible to AG damage (Kaus, 1987; Song et al., 1995; Harris et al., 2003) and protected by the same compounds that protect mammalian HCs (Kirkwood et al., 2017), further highlighting their functional similarities.

The use of zebrafish allows for extremely high-throughput screening relative to the use of mammalian models, and numerous otoprotectants have previously been identified using this approach (Ton and Parng, 2005; Ou et al., 2009; Esterberg et al., 2013; Kruger et al., 2016).

1.8 Thesis Aims

Ototoxicity is an extremely unfortunate and debilitating effect associated with AG treatment. Patients already suffering from serious bacterial infections must then also endure the extremely unpleasant experience of losing their hearing ability. For this reason, the main aim of this thesis was to identify novel otoprotectants – compounds that when co-administered alongside AG treatment could prevent the associated hearing loss.

Additionally, I also aimed to establish the mechanism of protection of all of the newly-identified protectants. This would further our knowledge of which approach to otoprotection may be the most viable option; whether that be blockade of the MET channel and prevention of AG entry or, alternatively, the prevention of mitochondrial dysfunction and the consequent initiation of intracellular apoptotic cascades.

Alongside this, I have provided full characterisation of the effects of gentamicin in the mouse cochlear culture assay system developed by Richardson and Russell (1991), which was used for the screening and assessment of otoprotection throughout this thesis and elsewhere throughout the literature.

Lastly, I also aimed to elucidate the effect of the AGs on mitochondrial function and develop an experimental assay for screening for this effect. This then enabled me to investigate the mechanism of protection of identified compounds in regards to preservation of mitochondrial function.

2 Methods

2.1 Animal Husbandry

2.1.1 Mouse Husbandry

CD-1 wildtype, postnatal day 2 (P2) mice of either sex were used for the majority of the experiments detailed herein; for cochlear culture protection screening, GTTR and FM 1-43 live imaging and also for electrophysiological recordings. Animals were bred in house following UK Home Office guidelines. Stock was originally obtained from Charles River.

2.1.2 Rat Husbandry

For the mitochondria experiments detailed in this thesis, Sprague Dawley rats of either sex were used. Their age ranged from 4 weeks to 3 months, with no difference detected in the experimental result across different ages. Rats were bought in from Charles River. Pups were born and raised in house following UK Home Office guidelines.

2.2 Cochlear Culture Preparation

Cochlear cultures were prepared from CD-1 wildtype mice as previously described by Russell and Richardson (1987). In brief, P2 pups were euthanized by cervical dislocation following Home Office guidelines. Decapitated heads were surface sterilised by three one minute washes in 80% ethanol. Sagittal incisions were made down the midline of the head and cochleae were removed. Subsequent dissections were performed in Hank's Buffered Salt Solution (HBSS; Thermo Shandon 14025050) with 1% Hepes (Sigma H0887) (HBHBSS). The cartilaginous capsule surrounding the cochlea was removed, the sensory tissue was then detached from the central modiolus and the stria vascularis was stripped off. The exposed sensory epithelium was explanted onto a collagen-coated (Corning 354236) coverslip. Immersed in rat culture media (RCM; 93% DMEM-F12, 7% fetal bovine serum and 10 µg ml-1 ampicillin), cochlear preparations were sealed in Maximow slide assemblies and left to adhere for 24 hours in a 37°C, 5% CO_2 incubator. All cochlear culture screening was performed after one day (P2 + 1) incubation. Electrophysiology experiments were conducted after one or two (P2 + 2) days incubation time. All procedures described in this thesis complied with the UK Animals (Scientific Procedures) Act 1986.

2.3 Mouse Protection Assay

Following 24 hours incubation, cochlear cultures were quality-checked using differential interference contrast (DIC) optics on an inverted Zeiss IM35 microscope, to assess culture viability. They were then removed from the Maximow slide assemblies, placed in 35 mm petri dishes (Greiner Bio-One 627161) and incubated for 48 hours in the presence of 1 ml RCM:DMEM-F12 (1:4) alongside 5 µM gentamicin (Sigma G3632) and either 0.5% dimethyl sulfoxide (DMSO) or selected concentrations of the compounds of interest, often starting with a dose-response experiment for the parent compound from which subsequent concentrations were chosen. Following 48 hours incubation, cultures were washed once with 2 ml phosphate buffered saline (PBS) and fixed for 1 hour with 3.7% formaldehyde (Sigma F1635) in 0.1 M sodium phosphate buffer (pH ~ 7.3). After fixation, cultures were washed three times with PBS, trimmed off of the coverslips with their adherent collagen and permeabilised with 0.1% Triton X-100 in PBS, in the presence of 10 % horse serum and 1 mM sodium azide. Cultures were then stained with TRITC-phalloidin (Sigma P1951) at a concentration of 1:1000 for at least 24 hours. Additionally, myosin VIIa (1:400) rabbit primary antibody (2B Scientific) followed by Alexa 488 goat α rabbit secondary antibody (1:500) (Invitrogen) were used to specifically stain the HC bodies in some experiments. Cultures were mounted on glass slides with Vectashield (Vector Laboratories) and imaged using a Zeiss Axioplan II microscope and Spot RT digital camera.

2.4 Live Cell Imaging of Gentamicin-Texas Red (GTTR) and FM 1-43 Loading into Sensory Hair Cells

2.4.1 Block of GTTR Loading by 5 minutes Compound Incubation

Coverslips with their adherent cochlear cultures were removed from the Maximow slide assemblies and placed in a Perspex viewing chamber with a glass bottom. They were immersed in 500 µl of HBHBSS and the cultures were then treated with either 100 µM of the potential otoprotectant or 1% DMSO as a control, with all parent compounds and their derivatives being dissolved in this solvent. After 5 minutes incubation time at room temperature (20-25°C), GTTR (obtained from P.S. Steyger, Oregon Hearing Research Center, Oregon Health & Science University, Portland, Oregon, USA) was added at a final concentration of 0.2 µM and incubated

for a further 10 minutes. Cultures were then washed three times with 500 µl HBHBSS, before live imaging on a Zeiss Axioplan II microscope. A 60x water immersion lens, numerical aperture (NA) 0.90, was used to take images of both the mid-apical and mid-basal regions of cochlear cultures across a time range from T = 20 to T = 31 minutes post-GTTR application. Both Nomarski DIC and fluorescence images were taken. Three repeats were conducted and quantification of the intracellular GTTR fluorescence intensity was derived from selected time point images of the basal region, approximately 20% along from the basal end.

A structural comparison of gentamicin and GTTR is not presented here due to the complexity and variability of the conjugation process. Both gentamicin and GTTR come in many different varieties, as detailed in Woiwode et al., 2015.

2.4.2 Block of GTTR Loading by 24 hours Compound Incubation

For the experiments presented in Chapter 4 (4.2.5.5.1 - 4.2.5.5.3), cultures were incubated with 50 µM of selected compounds or 0.5% DMSO for 24 hours before testing the loading of GTTR into HCs. Following incubation, the cultures were placed in a Perspex viewing chamber and washed three times with 500 µl HBHBSS. GTTR was then added at a concentration of 0.2 µM and incubated for 10 minutes, after which the culture was washed with three 500 µl HBHBSS additions. Images were taken of the mid-apical and mid-basal regions of the cochlear culture on a Zeiss Axioplan II microscope with a 60x objective, across a time range from T = 20 to T = 31 minutes post-GTTR application.

2.4.3 Block of FM 1-43 Loading by 24 hours Compound Incubation

As with the 24 hours compound, GTTR live imaging experiments presented above (2.4.2), coverslips with adherent cultures that had been exposed to 50 µM of selected compounds or 0.5% DMSO for 24 hours were placed in a Perspex viewing chamber and immersed in 500 µl of HBHBSS. They were washed three times and then FM 1-43 was added to a final concentration of 0.3 µM and incubated for 10 minutes. After washing off FM 1-43 with three 500 µl HBHBSS additions to remove any unbound dye, images of the mid-apical and mid-basal regions were taken on a Zeiss Axioplan II microscope with a 60x objective at 10 and 15 minute time points post-FM 1-43 application.

2.5 Cell Culture Data Analysis

2.5.1 Protection Assay Analysis

Images of the apical and basal region were obtained using a Zeiss Axioplan II microscope with a 40x objective, with the focal plane adjusted to focus on the mechanosensory hair bundles. When two fluorescence stains were used, images were taken at the level of the hair bundles (TRITC phalloidin) and cell bodies (Alexa 488, for myosin VIIa) through separate fluorescent channels. For quantification of HC survival in otoprotection screening experiments, images from the mid-basal region were analysed. OHCs in a 300 µm-long segment of the cochlea were quantified in most instances, approximately 20% along the length of the cochlea from the basal end. The observable presence of a hair bundle was the criterion used as a marker of HC survival. Although HCs can survive without a stereociliary bundle (Gale et al., 2002; Majumder et al., 2017) their presence would be vital for sound transduction, so provide a useful marker of HC viability when screening for suitable otoprotectants.

For the purposes of the data presented in Chapter 3, OHC numbers in the mid-apical region were also quantified, as well as IHCs in both cochlear regions of interest.

2.5.2 Live Cell Imaging (GTTR and FM 1-43) Analysis

For quantification of intracellular GTTR and FM 1-43 fluorescence, images analysed were from the mid-basal region at selected time points after GTTR or FM 1-43 addition, as detailed in each chapter (between 15 and 27 minutes post-fluorescent compound application). Ten cells from the first row of OHCs central to the 160 µm-long image were analysed in Adobe Photoshop CS2 (OHC I; Figures 2.1A* and 2.2), obtaining cell cytoplasm fluorescence intensity values from a 30x30 pixel region of interest (ROI) (the square in Figure 2.1B shows the size of this ROI relative to the cell) using the Histogram tool to generate a mean grey level intensity value. Three background fluorescence intensity ROIs were measured, averaged and subtracted from each individual cell value, and the remaining grey level intensity values were then averaged as an indication of intracellular fluorescence. One background ROI was taken from non-sensory HC cellular space to account for any endocytic loading. At least three experimental replicates were conducted in every instance.

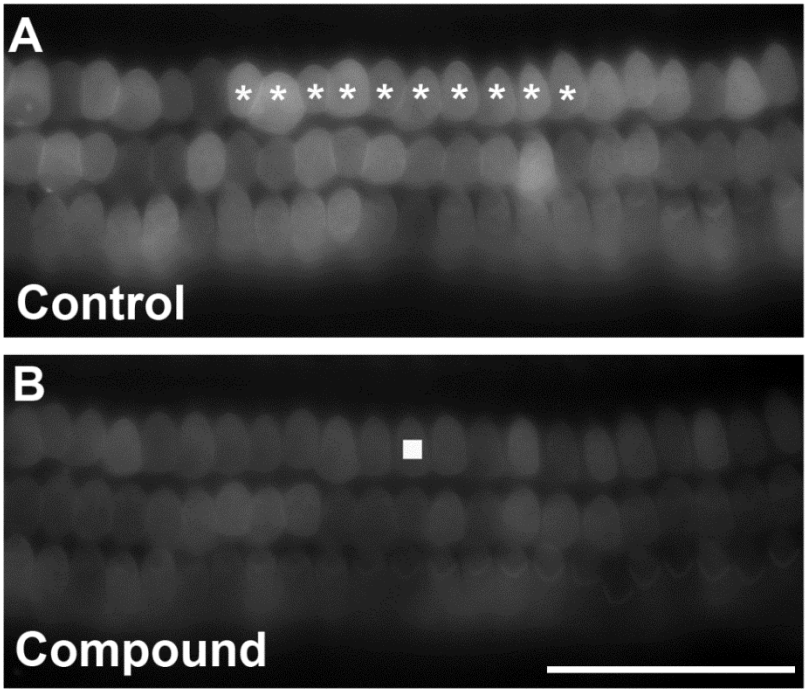

Figure 2.1: *The 10 first row (most inner) OHCs that were analysed to generate GTTR and FM 1-43 fluorescence intensity values.*

(A) The fluorescence intensity values (arbitrary units) of 10 first row OHCs (closest to the IHCs) in the centre of the image were analysed to establish whether the compounds of interest reduced the loading of the fluorescent compounds GTTR and FM 1-43 (*). **(B)** A 30x30 pixel ROI was used to generate mean intracellular fluorescence intensity values (■). Scale bar is 50 µm.

2.5.3 Statistics

GraphPad Prism 7 was used for the generation of all statistical data. All graphical representations display the mean ± S.E.M values. Numbers above bars represent the number of independent experimental replicates.

For the significance testing of zebrafish and mouse cochlear culture protection assays, 1-way analysis of variance (ANOVA) was applied followed by either Dunnett's or Tukey's post-hoc test.

For GTTR and FM 1-43 live imaging experiments, 1-way ANOVA or unpaired *t* tests were used depending on the number of experimental conditions, followed by Tukey's post hoc test if an ANOVA was used.

For the generation of the dose-response curve in Chapter 4, the percentage of OHC survival in the gentamicin plus compound conditions was compared with that in control cultures. Curves were fit to the equation:

$$OHC\ survival = \frac{B + (100 - B)[C]}{(K + [C])}$$

Where *B* is the percentage of OHCs surviving in the gentamicin alone conditions, *[C]* is the compound concentration and *K* is the concentration at which 50% protection is observed.

Significance was set at $p < 0.05$. On all graphical representations, * = $p < 0.05$, ** = $p < 0.01$, *** = $p < 0.001$.

Compounds were considered completely protective if the HC count was significantly higher than the gentamicin-treated condition but not significantly different from the control. They were considered partially protective if significantly different from both the control and gentamicin-treated conditions.

Data were tested for normality in Prism with four tests: D'Agostino & Pearson, Anderson-Darling, Shapiro-Wilk and Kolmogorov-Smirnov. The majority of data sets passed the normality tests.

2.5.4 Figure Preparation

All protection assay figures, GTTR and FM 1-43 live imaging figures were created using Photoshop CS2. When using a 40x objective, the Spot RT camera takes images at 1600 x 1200 pixels. A 1200 x 600 pixel region central to the image was extracted in every instance and used to create the final figures, correlating to a 220 µm length of the cochlear culture.

Quantification and statistical, graphical representations were created in GraphPad and imported into Photoshop. Electrophysiology figures were produced in Origin 2018.

2.6 Confocal Imaging

Confocal microscopy was used for high magnification, high resolution imaging of the mechanosensory hair bundles (Chapter 6) in order to assess any morphological disruption induced by the compounds of interest.

Slides were imaged on a Leica SP8 confocal microscope, using the 561 nm laser (at 3% intensity) and a x100 1.44 NA oil-immersion lens. Images were captured at a resolution of 736x400 (and a zoom of x 2.0 with a x4 line average), using a low detector gain (511) in order to reduce noise and improve image quality. Z-projections were created in ImageJ.

2.7 Electrophysiology

2.7.1 Equipment for Electrophysiology

The sensory HCs of cochlear cultures, adherent to collagen-coated cover slips, were visualised using an upright light microscope (Leica DM LFSA) equipped with a 63x water-immersion objective and a 15x eyepiece, using Nomarski DIC optics. Coverslips were placed in a Perspex bath chamber connected to inflow and outflow tubing, with a constant perfusion of fresh extracellular solution (ECS) over the cochlear culture. The ECS was pre-filtered before entering the bath using a Millipore Millex syringe filter unit and was perfused using a peristaltic pump (Cole-Palmer, IL, USA). To prevent the peristaltic pump from generating additional noise in the set-up, the chamber was grounded using a 63 µF capacitor, connected to the inflow tube, connected to the headstage. The recording chamber was positioned on top of a rotating stage, to allow access to HCs along the cochlear preparation from different angles. The entire setup was placed on an anti-vibration air table that was kept levitated by an air pump (JunAir), inside a Faraday cage to minimise movement and electrical noise within the system; allowing for cleaner recordings with a greater signal to noise ratio.

HC currents were recorded using a patch-clamp amplifier. The patch electrode used was a polycarbonate electrode holder with a pin headstage connector, containing a silver chloride wire for current detection. It was connected to a Cairn Optopatch headstage and an Optopatch patch-clamp amplifier. Before the signal was input to a Power1401 data acquisition interface,

it was filtered at 2.5 kHz through an 8-pole Bessel filter, which allowed for analogue to digital data conversion.

An upright glass puller (Narishige, Tokyo, Japan) was used to pull glass pipettes. Patch pipettes were pulled from soda glass capillaries. Cleaning and fluid jet pipettes were pulled from borosilicate glass capillaries. For patch pipettes, the temperature of the second pull was adjusted (~39.5 - 41.0°C) to ensure that the resistance of the pipette tip was between 2 and 3.5 MΩ - a resistance that ensured reliable patch formation. The shaft of the patch pipette was coated with a thin layer of wax (Mr Zogs SexWax), from halfway down the shaft to approximately 100 µm away from the pipette tip. This was in order to reduce the fast capacitive transients across the wall of the patch pipette, created by the pipette tip entering the bath solution.

For compound application to the cochlear cultures, a gravity-fed system was used. The system comprised of syringes (that were filled with compounds in solution), connected to fine tubing that met at a point and were bound together in an end-piece using parafilm and dental cement. The end-piece contained all solution tubes that were then funnelled into one final, relatively wide-ended tube (~200 µm) that was then placed in the bath in order to deliver the compounds of interest to the cochlear culture. The tube was placed 2 and a half turns of the focussing dial above the culture to ensure reliable, consistent compound administration and local manipulation of the external conditions. Selective solution application was achieved by having taps connected to the compound-filled syringes. When a tap was turned to the open position, solution was dispensed from the end-piece. Manual control of the taps allowed for fast, effective changes between the solutions. Control solution was initially superfused after a gigaohm (GΩ) seal had been formed, followed by the compound of interest and then the re-superfusion of the control solution to assess the washout of the compound and the reversibility of any observed block.

2.7.2 Solutions for Electrophysiology

2.7.2.1 Extracellular Solution (ECS):

Cochlear cultures were bathed in high sodium extracellular solution that mimicked perilymph composition, containing (in mM): 135 NaCl, 5.8 KCl, 1.3 $CaCl_2$, 0.9 $MgCl_2$, 0.7 NaH_2PO_4, 5.6 D-

glucose, 10 HEPES-NaOH, 2 sodium pyruvate. Eagle's minimum essential medium (MEM) amino acids solution (50X), and MEM vitamins solution (100X) were added from concentrates to a final concentration of 1X (Fisher Scientific). The pH of the solution was adjusted to 7.48 using 1M NaOH. The osmolality of the solution was 307.6 (± 0.7) mOsmol kg^{-1} (n=7).

2.7.2.2 Caesium Intracellular Solution (Cs ICS):

When recording MET currents, patch pipettes were filled with a caesium chloride-based solution. This was used in order to block potassium channels, so as to investigate MET channels independently without the interference of potassium currents. The solution contained (in mM): 137 CsCl, 2.5 $MgCl_2$, 1 EGTA-CsOH, 2.5 Na_2ATP, 10 sodium phosphocreatine, 5 HEPES-CsOH. The pH of the solution was adjusted to 7.3 using 1M CsOH. The average osmolality of the solution was 291.6 (± 0.7) mOsmol kg^{-1} (n=5), approximately 10-15 mOsm kg^{-1} below that of the extracellular solution.

2.7.2.3 Potassium Intracellular Solution (K^+ ICS):

When recording the basolateral potassium channel currents, patch pipettes were filled with a potassium-rich intracellular solution that contained (in mM): 131 KCl, 3 $MgCl_2$, 5 Na_2ATP, 1 EGTA-KOH, 5 HEPES, 10 sodium phosphocreatine. The pH of the solution was adjusted to 7.28 using 1M KOH. The average osmolality of the solution was 291 (± 0.6) mOsmol kg^{-1} (n=5).

2.7.2.4 Control ECS:

Control extracellular solution was used to dilute compounds and also as a superfusion control condition, being superfused before and after each compound application. The solution contained (in mM): 145 NaCl, 5.8 KCl, 1.3 $CaCl_2$, 0.9 $MgCl_2$, 0.7 NaH_2PO_4, 5.6 glucose, 10 HEPES-NaOH, 2 sodium pyruvate. The pH of the solution was adjusted to 7.48 with 1M NaOH. The average osmolality of the solution was 308.2 (±0.7) mOsmol kg^{-1} (n=5).

2.7.3 Whole-Cell MET and Basolateral K^+ Channel Current Recording

Both potassium and MET channel currents were recorded from the third (most outer) row of OHCs of mouse organotypic cochlear cultures, as depicted below (OHC III; Figure 2.2). All recordings were made from P2 CD-1 wildtype mice of either sex, after being maintained for 1 – 2 days *in vitro* in a 37°C, 5% CO_2 incubator. Coverslips with adherent cultures were removed from their Maximow slide assembly and placed in a Perspex microscope chamber, which was continuously perfused with ECS at an approximate rate of 14 ml/hour. All experiments were performed at room temperature (20-25°C).

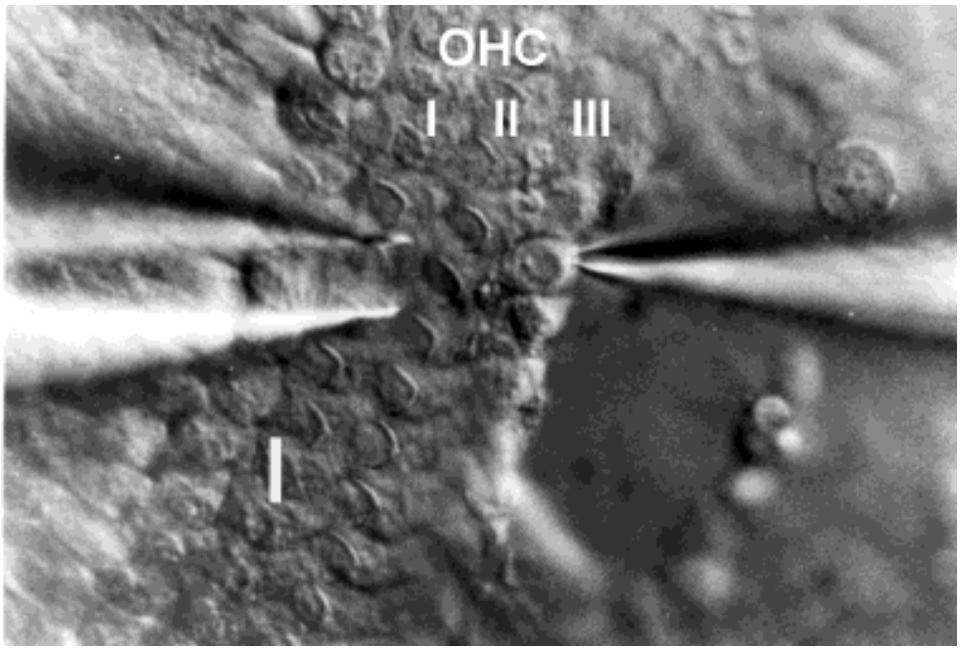

Figure 2.2: *The experimental setup used for electrophysiological recording of MET currents from mouse cochlear culture OHCs. Figure modified from Kros et al., 1992.*

The pipette entering from the left-hand side of the image is the fluid jet, used to stimulate the HC bundle and open the MET channels. The pipette entering from the right-hand side is the patch pipette, forming the seal on the HC membrane and recording the MET currents. Scale bar is 10 μm.

The location of the OHCs that were patched along the length of the coil was mostly confined to the mid-coil region. In order to expose OHC membranes, a cleaning pipette was used. This was

a glass pipette connected to a syringe system, which allowed for manual suction to occur. Support cells were removed as well as any cellular debris, exposing cell membranes and allowing patch formation.

Whole-cell patch clamp recordings were performed using an Optopatch (Cairn Research) patch-clamp amplifier. In order for MET currents to be elicited, the stereociliary hair bundle on top of the OHC was stimulated using a fluid jet from a glass pipette (tip diameter in the range of 6-12 µm), which was driven by a piezoelectric disc (Kros et al., 1992; Marcotti et al., 2005). Mechanical stimuli (filtered at 1.0 kHz, 8-pole Bessel) were applied as 45 Hz sinusoidal waves that were sufficient in order to elicit large, saturating MET currents.

To investigate the extracellular block of potassium and MET channels, compounds of interest were dissolved in a solution with a composition similar to ECS and superfused over the cochlear cultures. Control solution was superfused after a GΩ seal on the cell membrane was formed, but before the whole-cell patch configuration was achieved, and was continuously superfused during the initial control recordings. After three recordings were obtained in control solution the drug of interest was superfused over the cells, three more recordings were taken, control solution was re-superfused and three more recordings obtained. This was done in order to wash away the compound from the channels of interest and gain washout recordings – indicative of the reversibility of the channel block. A slight negative pressure was continuously applied to the tip of the fluid jet, in order for the superfused compound-containing solution to be slightly sucked into the pipette tip. This enabled the prevention of any dilution of the desired compound concentration with the extracellular bath solution expelled from the fluid jet when it was used for hair bundle stimulation.
Before recording, a note of the series resistance (Rs) and membrane capacitance (Cm) of the cell was noted, and series resistance compensation was applied, anywhere between 30-60% depending on the stability of the preparation.

2.7.4 Data Acquisition and Analysis

The acquisition of electrophysiological data was performed using Signal 4.3 software (Cambridge Electronic Design) and was stored on computer for off-line analysis. Off-line analysis was performed using Origin 2018 (Origin Lab) data analysis software. When analysing electrophysiological data, the three traces in each condition (control, during drug and

washout) were first converted from the data acquisition software Signal in to a file type readable by the data analysis software Origin (text files), where they were then averaged. This was in order to generate an average of the current sizes during each condition, thereby minimising any noise picked up in the system.

For MET channel current recordings, protocols were written in Signal in order to set the command voltages and simultaneously deliver a sine-wave stimulus from the fluid jet to the HCs. The holding potential of the cells was set to -84 mV at the beginning of recordings using an external voltage calibrator. During experiments, cells were stepped in 20 mV increments between -164 and +96 mV, whilst a sine-wave stimulus was simultaneously applied at each voltage step in order to control the piezo-driven fluid jet. The sampling rate was 10 kHz.

For the determination of MET current size, the difference between the minimum current in the inhibitory phase (the trough; the leak current) of the sinewave and the maximum steady-state current (peak) in the excitatory phase of the sinewave was calculated. There was no fixed time point for this but rather peaks and troughs were analysed manually, due to variability in the shape of the MET currents obtained. The first of the four sinewave cycles was excluded in every instance. Current-voltage (I-V) curves were created in Origin, by plotting MET current size against every membrane potential. Fractional block curves were derived by plotting the ratio of control current to current in the presence of the compound of interest, across all membrane potentials from multiple cells.

For basolateral potassium channel current analysis, protocols were written in Signal in order to set the command voltages. The holding potential of the cells was set to -84 mV at the beginning of recordings. During experiments, cells were stepped in 10 mV increments between -154 and +46 mV. Current amplitudes were measured from the steady-state current towards the end of the voltage step, before the tail currents emerged.

2.8 Compound Preparation and Storage

The parent compounds tested in this thesis are all commercially available and bought in from sources such as Tocris Biosciences, HelloBio and MilliporeSigma. Purity was ≥ 95%. Some compound derivatives were commercially bought depending on their availability; however, some specific compound modifications were synthesised in house by the chemists assigned to this project - Marco Derudas or Rosemary Huckvale at the University of Sussex.

All compounds were dissolved in DMSO at a stock concentration of 10 mM (or 50 mM for FM 1-43 derivatives). They were aliquoted and stored at -80°C. Aliquots were not used more than three times, to minimise any effect of freeze-thawing cycles.

2.9 d-Tubocurarine-Texas Red Conjugation

To a solution of d-Tubocurarine (dTC) (1.09 mg) in dimethylformamide (0.5 mL), Texas Red sulfonyl chloride (1 mg) was added and the reaction mixture was stirred at room temperature (20-25°C) in the dark for 4 hours. After this period, the solvent was removed under reduced pressure to give the desired compound which was used without any further purification.

2.10 Mitochondria

2.10.1 Isolation of Rat Liver and Kidney Mitochondria

Sprague-Dawley rats were euthanized by two methods depending on their weight, due to Home Office guidelines. If weighing less than 150 grams then cervical dislocation was used, or if over 150 grams, the rat was euthanized by 10 minutes incubation in a CO_2 chamber. No difference in the mitochondrial function under investigation was detected between the two methods of euthanasia. The liver was used due to the ease of mitochondrial isolation from this tissue type and the kidney was used because this is an organ susceptible to AG-induced (nephro)-toxicity.

The liver or kidney was dissected and transferred to ice cold Milli-Q water before being placed in buffer solution containing (in mM): 1 EGTA, 30 MOPS, 250 sucrose, 3.5 L-cysteine and 0.1% BSA, pH adjusted to 7.6 using NaOH. The tissue of interest was homogenised with 10 passes in a loose-fitting homogeniser, followed by 10 passes in a tight-fitting homogeniser. After filtering through muslin, the homogenate underwent differential centrifugation at 4°C – being spun once at 1000 g (after which the supernatant was kept and pellet discarded) and then twice at 10,000 g, each for 10 minutes, after each of which the supernatant was discarded and the mitochondrial pellet re-suspended in buffer solution. Isolated mitochondria were kept on ice

before being transferred to the Oroboros Oxygraph-2K oxygen electrode chambers upon the initiation of experimentation. Mitochondrial protein content was estimated using the Bradford method (He, 2011) using Bio-Rad protein assay dye.

2.10.2 Investigating the Electron Transport Chain (ETC) Complexes (C) I-V using an Oroboros Oxygraph-2K Oxygen Electrode

Oxygen consumption rates of isolated mitochondria were measured using an Oroboros Oxygraph-2K oxygen electrode, with the electron transport chain (ETC) complexes investigated independently with the addition of various substrates and inhibitors. Assays were performed in media containing (in mM): 200 sucrose, 25 KCl, 11 $MgCl_2$, 5 KH_2PO_4, 5 MOPS, pH adjusted to 7.4 using NaOH. Approximately 600 µg of protein from the crudely-isolated mitochondria sample was added to the chamber containing 2 ml assay media, and allowed to equilibrate for 10 minutes either in the presence or absence of selected concentrations of gentamicin. The reaction was then initiated with both 5 mM pyruvate and 2 mM malate for complex I (CI), or 10 mM succinate in the presence of rotenone for complex II (CII)-dependent respiration. Uncoupled respiration was investigated with the addition of 0.5 - 2 µM carbonyl cyanide m-chlorophenyl hydrazine (CCCP), and complex IV (CIV) respiration was investigated by addition of ascorbate (8 mM) and TMPD (4 mM). All experiments were performed at 32°C.

2.10.3 Investigating the Mitochondrial Membrane Potential (MtMP) and Reactive Oxygen Species (ROS) Production in Isolated Mitochondria using Safranin and Amplex Red

The mitochondrial membrane potential (MtMP) can be investigated with the use of Safranin, a biological stain with an excitation wavelength of 495 nm and an emission wavelength of 587 nm. An initial calibration of the safranin concentration was performed on each day of experimenting. This was achieved by performing a titration of the safranin fluorophore, between 0.1 and 2.0 µM final concentrations (Krumschnabel et al., 2014). Following calibration 2.0 µM safranin was added to the chambers followed by the MtMP effectors of interest. Most often, 10 mM succinate was added in order to generate a proton gradient and hyperpolarise the membrane, followed by serial additions of gentamicin to assess its dose-dependent effect on the MtMPs.

Mitochondrial ROS (MtROS) production can be measured using Amplex Red, a dye with a peak excitation wavelength of 563 nm and a peak emission wavelength of 587 nm. Initial calibrations were performed in both chambers by first adding Amplex (10 µM), horseradish peroxidase (HRP) (f.c. 1 U/ml) and superoxide dismutase (SOD) (f.c. 5 U/ml). Then 0.1 µM H_2O_2 was added in order to calibrate the fluorescent signal, after which endogenous ROS levels were measured by the addition of succinate (10 mM). Gentamicin addition was used to assess the effect of AGs on endogenous ROS production.

The materials used in all of the experiments detailed were purchased from Sigma.

2.10.4 Investigating MtMP Changes in Mouse Cochlear Culture HCs using Rhodmaine-123

Rhodamine-123 (1mg/ml; Vector Laboratories, USA) was diluted 1:200 in ECS. Cochlear cultures prepared from P2 CD-1 mice, and maintained for 24 hours *in vitro*, were rinsed three times in PBS and then incubated in 1 ml of the Rhodamine-123 solution for 15 minutes at 37°C. Cultures were subsequently rinsed three times in PBS and placed in the microscope chamber containing ECS. The OHCs were observed with an upright microscope (Olympus) with a 60x water-immersion objective. Fluorescence images were obtained using the Visitech VT-infinity3-based confocal system and VoxCell Scan software. Gentamicin (50mg/ml; Sigma) was added to the recording chamber to a final concentration of 5 mM. Fluorescence images were obtained at regular intervals (2 – 10 minutes). Experiments were performed at room temperature (20-22 °C).

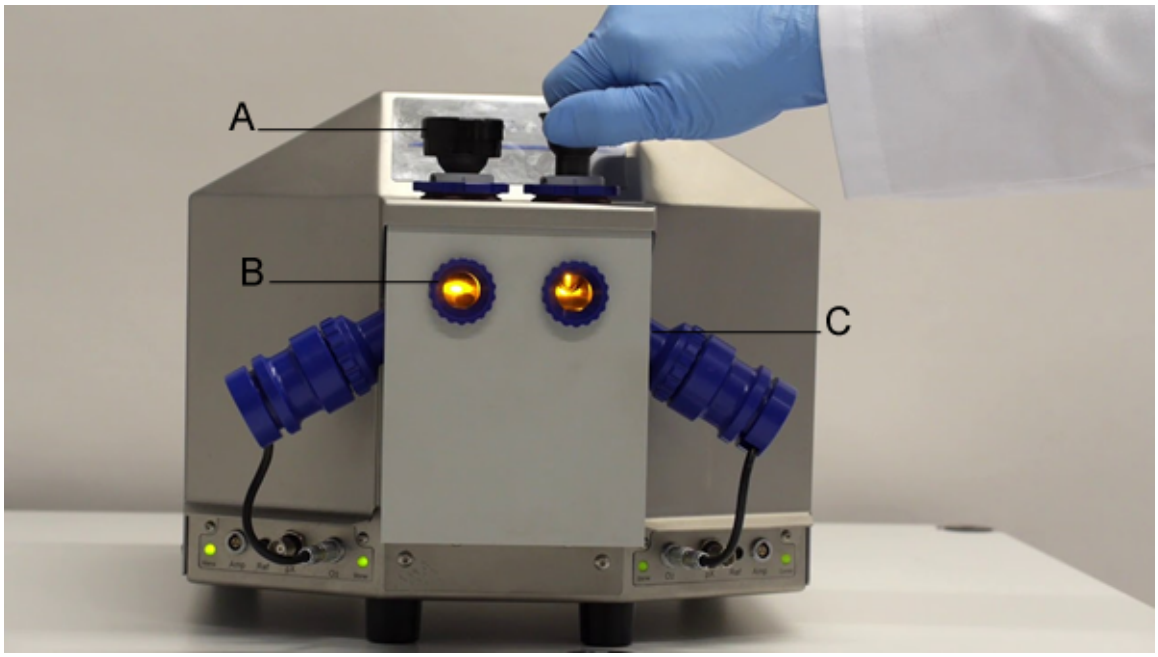

Figure 2.3: *The Oroboros Oxygraph machine used for recording oxygen consumption rates from isolated mitochondria.* Image © OROBOROS INSTRUMENTS.

Removable injection ports are located atop of the machine **(A)**, incubation chambers centrally **(B)** and the oxygen sensors on the sides **(C)**.

3 Characterising the Ototoxic Effects of Gentamicin on Mouse Cochlear Cultures

3.1 Introduction

3.1.1 Aminoglycoside Choice

Of all of the aminoglycoside antibiotics (AGs) that are Food and Drug Agency (FDA) approved for clinical use (of which there are at least nine: amikacin, gentamicin, kanamycin, neomycin, netilmicin, paromomycin, spectinomycin, streptomycin and tobramycin) (Xie et al., 2011; Jiang et al., 2017), gentamicin is the most commonly prescribed in the United Kingdom, the United States of America, and potentially worldwide (Eltahawy and Bahnassy, 1996; Gonzalez et al., 1998; Xie et al., 2011). This is due to its low cost, ease of storage and its reliability in treating a wide range of bacterial infections as a result of its broad-spectrum antimicrobial activity. For this reason, gentamicin was used in all of the experiments detailed in this thesis: in the search for clinically-relevant otoprotective compounds in mammalian models, and also in the investigation of the effect of AGs on mitochondrial function. Furthermore, the availability of a fluorescently-conjugated gentamicin analogue (gentamicin-Texas Red (GTTR)) (Steyger et al., 2003) allowed for greater ease of investigation of AG uptake into sensory HCs, so as to further elucidate the mechanisms of protection of the novel compounds that have been identified herein.

3.1.2 Aims

In this chapter the effect of gentamicin on mouse cochlear cultures will be characterised, drawing comparisons between the cochleotoxic effects induced in our *in vitro* assays and those observed in the clinic. Our standard gentamicin-kill assay used for otoprotectant detection will be described in detail and an extension of this experimental paradigm will also be provided. I aim to characterise the effects of higher gentamicin concentrations and a longer exposure time, whilst again drawing analogous comparisons with what is observed clinically.

3.2 Results

3.2.1 Standard Otoprotection Assay – 5 µM Gentamicin for 48 Hours

When used clinically, the reported hearing loss in patients treated with AGs follows a distinctive pattern, with high-frequency hearing being affected first followed by the more low-frequency ranges. This occurs in a dose and time-dependent fashion, with higher doses or prolonged exposure time leading to more severe hearing loss (Conly et al., 1994; Huth et al., 2011). The assay that was used for the assessment of otoprotection by novel compounds adhered to this pattern in an attempt to replicate and mimic real-world scenarios, with the gentamicin-induced damage confined primarily to the basal section of the cochlear cultures. Organotypic cochlear cultures (Figure 3.1A) that were incubated with 5 µM gentamicin for 48 hours showed pronounced loss of OHCs from the basal (high-frequency) region of the cochlea (Figure 3.1E) with far fewer, if any, being lost from the apical (low-frequency) region (Figure 3.1D). However, apical OHCs did often display a perturbed morphology of their characteristic V-shaped mechanosensory hair bundles when treated with this concentration of the antibiotic (Figure 3.1D).

On average, incubation with 5 µM gentamicin for 48 hours caused a loss of 88% of OHCs from the mid-basal region of the cochlear cultures, with an average of 112.9 (± 1.4) (n=68) OHCs present in a 300 µm-long segment of the controls and 14.0 (± 1.3) (n=68) in the gentamicin-treated conditions ($p < 0.001$) (Figure 3.1F). These statistics are a culmination of all of the HC counts from the otoprotection experiments conducted in Chapters 4–7, with the significance here derived from an unpaired *t* test.

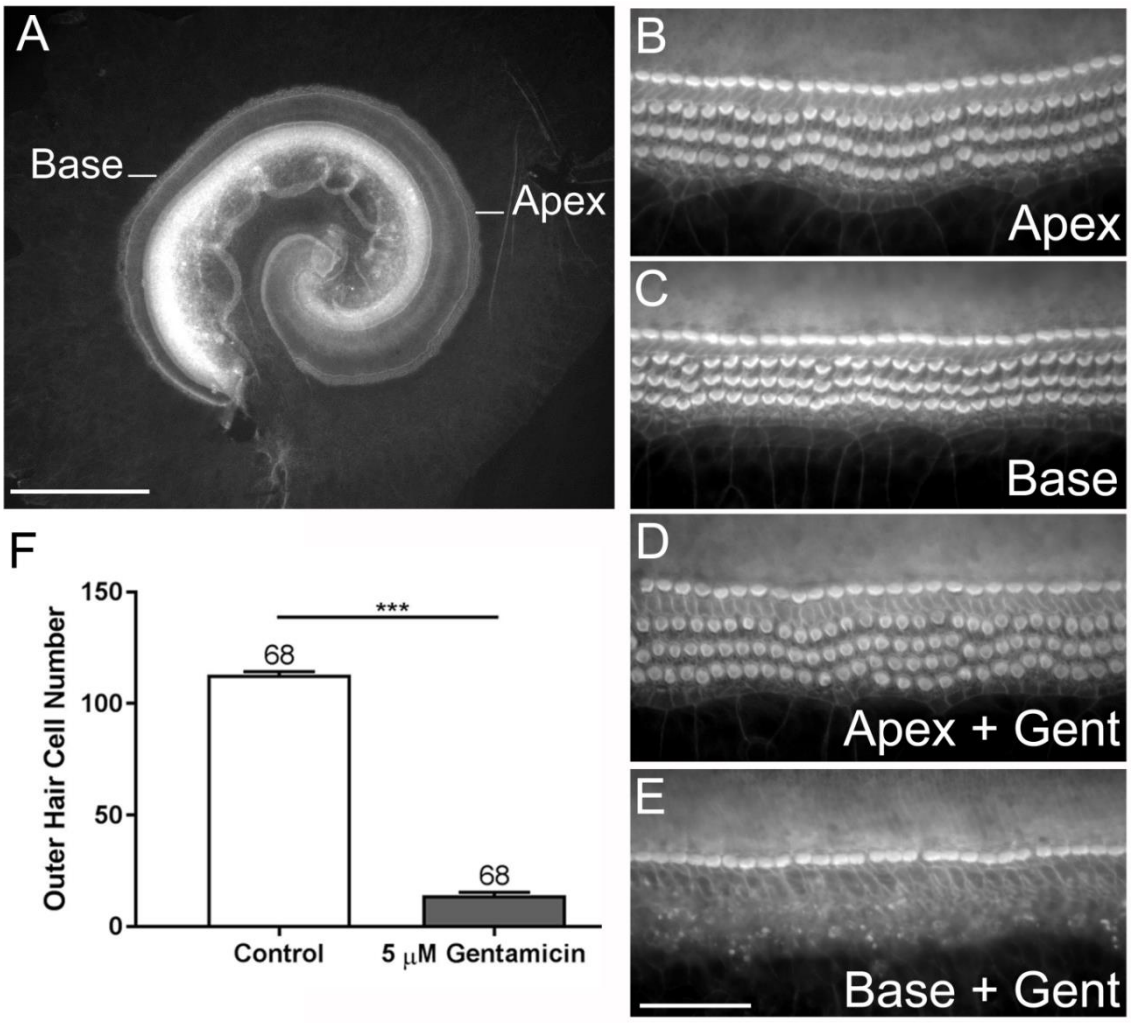

Figure 3.1: *Exposing postnatal day 2 mouse cochlear cultures to 5 μM gentamicin for 48 hours results in a significant loss of OHCs from the mid-basal region.*

(A) A whole mouse cochlea explanted onto a collagen-coated cover slip and incubated with 5 μM gentamicin for 48 hours. **(B)** The mid-apical and **(C)** the mid-basal region of a control cochlear culture. **(D)** The mid-apical and **(E)** mid-basal region of a gentamicin-treated culture. **(F)** Quantification of OHC survival in a 300 μm-long segment of the mid-basal region. Scale bar in **A** is 1 mm, and in **E** is 50 μm.

3.2.2 Assay Extension: 2.5, 5, 7.5, 10 and 12.5 µM Gentamicin for 48 Hours

Additional experiments were conducted in order to further assess the toxicity profile of gentamicin when administered to mouse cochlear explants. I first investigated the ototoxic effect of various gentamicin concentrations. The result of 48 hours incubation with a range of concentrations of gentamicin (2.5, 5, 7.5, 10 and 12.5 µM) was investigated, with the additional premise that if the otoprotective compounds identified in this thesis could protect against the higher concentrations of the antibiotic then we could eliminate the dose-limiting aspect of AG treatment (Conly et al., 1994), at least in terms of the ototoxic side-effect. This is because the dose of AGs that is given to patients is restricted due to the adverse oto- and nephro- toxic effects that they can induce. If a co-administered compound was able to prevent the undesirable side-effects, this AG dose restriction would become obsolete.

Furthermore, the concentration of gentamicin that accumulates in and around the cochlear sensory epithelium when used in a clinical setting is not fully known. At the onset of ototoxic symptoms, the AG concentration in rat endolymph has been estimated to be approximately 1 µM (Tran Ba Huy et al., 1981; Li and Steyger, 2009); however, uncertainty in the endolymphatic concentration when used clinically is due to the difficulty in accurately measuring concentrations in the endolymph due to the extremely small size of the fluid-containing compartment. Moreover, additional ambiguity arises in the clinic because of the uncertainties in the amount of the AG crossing into the endolymphatic compartment post-administration, and the numerous variables that may affect this across different patients being treated with the antibiotics. For example, those exposed to high levels of sustained noise (Li and Steyger, 2009), treated with loop diuretics (Tao et al., 2014) or with cases of inflammatory responses (Koo et al., 2015), have all been shown to have an enhanced susceptibility to AG-induced ototoxicity (Jiang et al., 2017). Each aforementioned attribute may contribute to ototoxicity by altering AG trafficking into the endolymph, potentially enhancing the endolymphatic AG concentration. Consequently, identifying compounds that can provide otoprotection against a range of AG concentrations would be desirable.

Figure 3.2A-F shows examples of the basal region of cochlear cultures exposed to increasing concentrations of gentamicin for 48 hours. Quantitative data obtained from apical and basal regions in at least 3 independent experiments is shown in Figure 3.2G-J (experimental replicate numbers range from 3 to 68). When organotypic cochlear cultures were incubated with 2.5 µM gentamicin for 48 hours, there was a sporadic loss of HCs in some experiments; however, there

was no significant difference in the number of HCs remaining when compared to the control in any of the four criteria examined (the number of OHCs or IHCs in the apical or basal coil) (Figures 3.2G-J). However, disruption of the mechanosensory hair bundle morphology (as indicated by a deviation from the characteristic V-shaped OHC hair bundle) was observed in three of the four trials (Figure 3.2B).

When incubated with 5 µM gentamicin for 48 hours, there was a loss of OHCs from the basal region, as detailed in section 3.2.1. There was no significant difference in any other measure. With 7.5 µM gentamicin for 48 hours, a similar response was seen as with 5 µM, primarily with a loss of OHCs from the basal coil of the cochlea. However, a one-way ANOVA revealed that there was also a significant loss of basal IHCs, with an average of 34.0 (± 0.5) (n=40) in control cultures, 32.9 (± 0.4) (n=43) in those treated with 5 µM gentamicin and 22.8 (± 3.9) (n=6) in those treated with 7.5 µM gentamicin ($p < 0.001$) (Figures 3.2D and H).

With 10 µM gentamicin incubation for 48 hours, the toxicity profile was markedly different. Almost all of the OHCs from the mid-basal region were lost in every experiment, with an average of 6.4 (± 2.7) (n=5) OHCs remaining compared with 14.0 (± 1.3) (n=68) in the 5 µM-treated condition. However, this difference was non-significant (Figure 3.2J). There was a 44% reduction in the number of OHCs in the mid-apical region of the cochlea, with an average of 112.3 (± 1.5) (n=60) in the control cultures and 63.8 (± 12.1) (n=4) in the 10 µM gentamicin-treated conditions (Figure 3.2I). A one-way ANOVA revealed that this difference was significant ($p < 0.001$). With IHCs, there was a reduction in numbers in both the mid-apical and mid-basal regions. In the base, IHC numbers fell from 34.03 (± 0.5) (n=43) in the control conditions to 10.8 (± 2.7) (n=5) in those treated with 10 µM gentamicin (Figure 3.2E and H). In the apex, IHC numbers fell from 33.4 (± 0.6) (n=35) to 23.6 (± 3.7) (n=5) (Figure 3.2G). Both reductions in IHC numbers were statistically significant ($p < 0.001$).

When incubated with 12.5 µM gentamicin for 48 hours, there were further reductions in all but one of the four criteria detailed above when compared to 10 µM gentamicin-treated conditions (Figures 3.2G-J). However, none of these differences were statistically significant. All statistical comparisons in this section were made using a one-way ANOVA, followed by Tukey's multiple comparisons test.

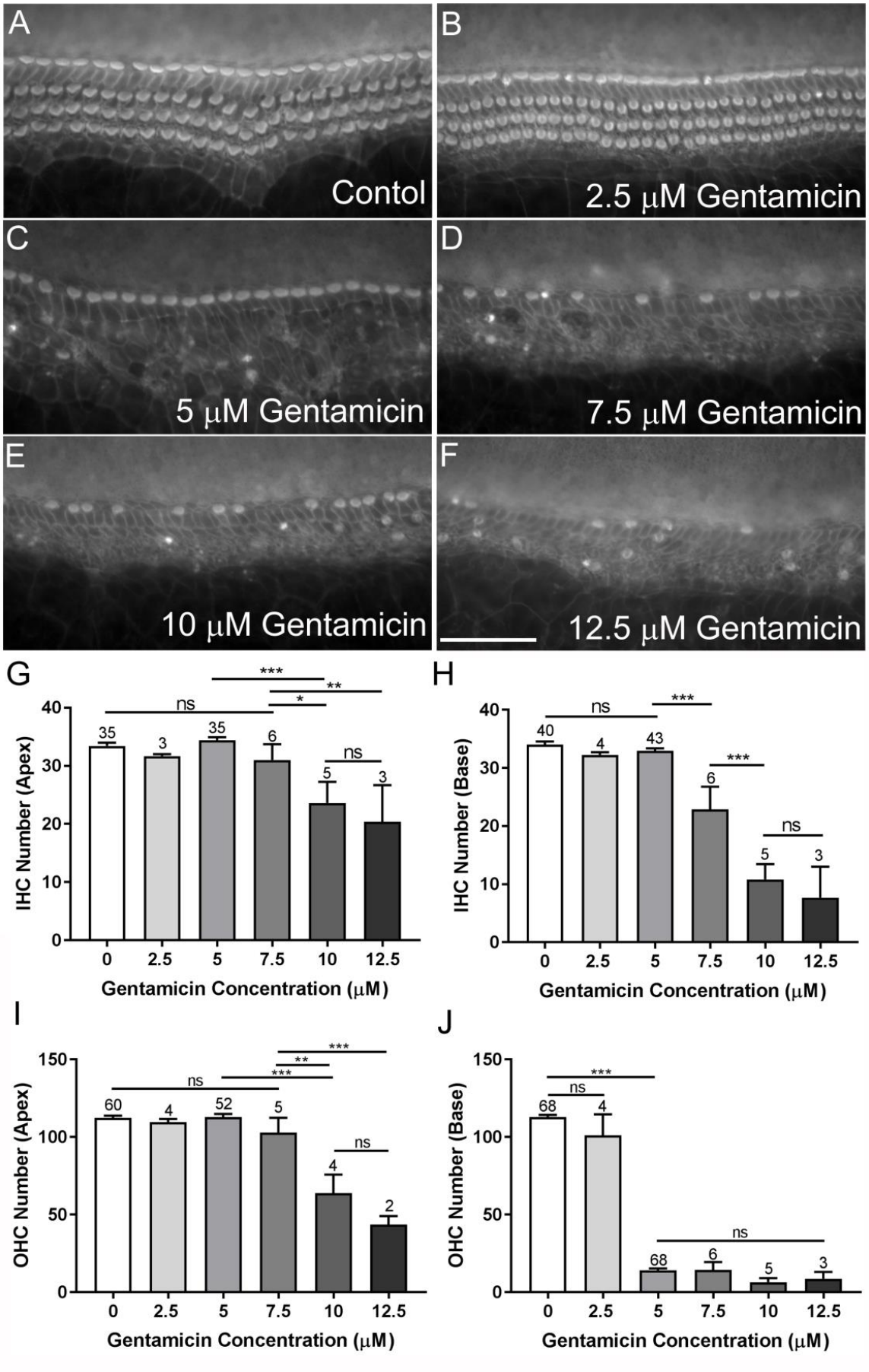
A
Contol
B
2.5 μM Gentamicin
C
5 μM Gentamicin
D
7.5 μM Gentamicin
E
10 μM Gentamicin
F
12.5 μM Gentamicin
G
IHC Number (Apex)
Gentamicin Concentration (μM)
H
IHC Number (Base)
Gentamicin Concentration (μM)
I
OHC Number (Apex)
Gentamicin Concentration (μM)
J
OHC Number (Base)
Gentamicin Concentration (μM)

Figure 3.2: *HC survival in the mid-apical and mid-basal regions of mouse cochlear cultures, treated with a range of gentamicin concentrations (2.5-12.5 µM) for 48 hours.*

(A-F) The mid-basal region of mouse cochlear cultures treated with **(A)** HBHBSS as a control or **(B)** 2.5 µM, **(C)** 5 µM, **(D)** 7.5 µM, **(E)** 10 µM or **(F)** 12.5 µM gentamicin for 48 hours. **(G-J)** Quantification of HC survival: **(G)** IHCs in the apex, **(H)** IHCs in the base, **(I)** OHCs in the apex, **(J)** OHCs in the base. Scale bar is 50 µm.

3.2.3 Assay Extension: 2.5, 5, 7.5, 10 and 12.5 µM Gentamicin for 72 Hours

When the gentamicin incubation time was extended by an additional 24 hours, to 72 hours in total, a much more severe effect was observed. Even when gentamicin was tested at 2.5 µM, there was a complete loss of all of the OHCs from the basal region, whereas IHCs mostly survived (Figure 3.3B). This result was strikingly similar to the ototoxicity pattern observed when cultures were treated with 5 µM gentamicin for 48 hours (Figure 3.2C).

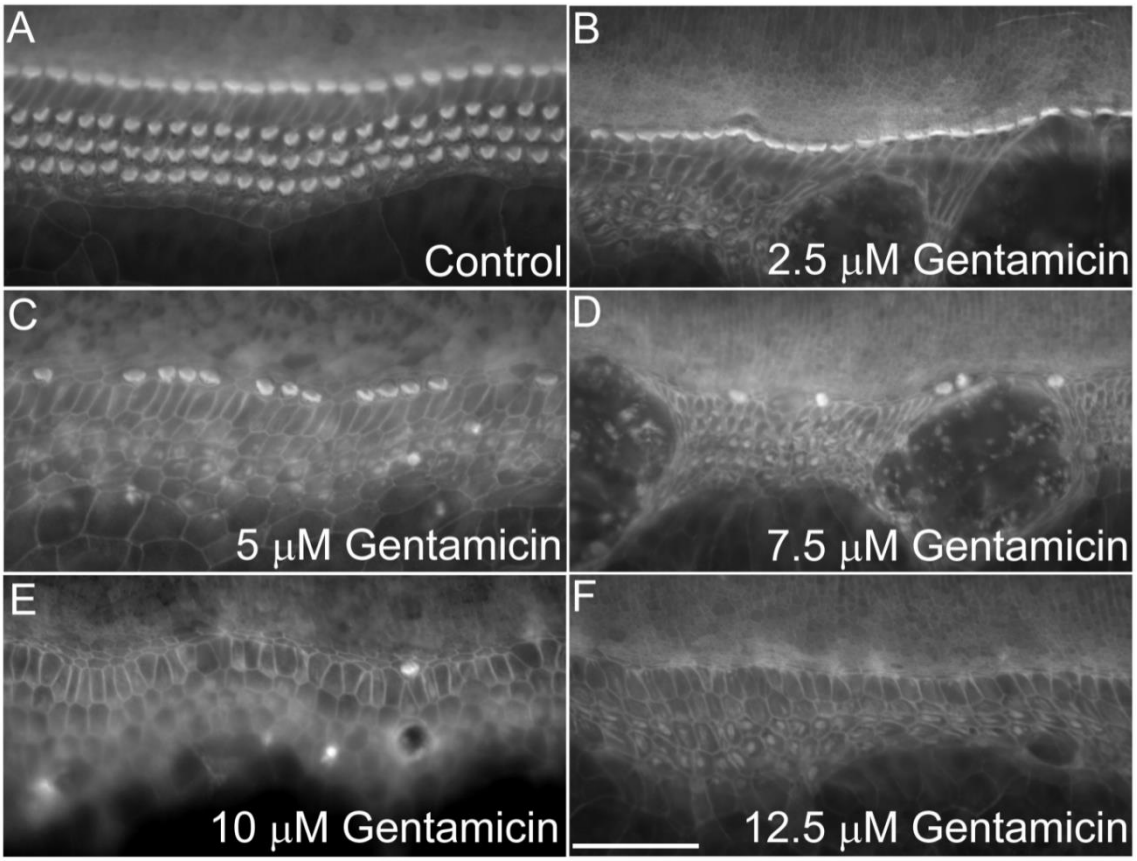

Figure 3.3: *The mid-basal region of mouse cochlear cultures treated with a range of gentamicin concentrations (2.5-12.5 µM) for 72 hours.*

(A-F) The mid-basal region of mouse cochlear cultures treated with **(A)** HBHBSS as a control or **(B)** 2.5 µM, **(C)** 5 µM, **(D)** 7.5 µM, **(E)** 10 µM or **(F)** 12.5 µM gentamicin for 72 hours. Scale bar is 50 µm.

3.3 Summary

Incubation of P2 mouse cochlear cultures with 5 µM gentamicin for 48 hours resulted in a toxicity profile remarkably similar to that observed in the clinic; with the basal, high-frequency sound-encoding sensory HCs being damaged first, followed by a progressive loss of the more apical HCs with increased dose or exposure time. This dose-dependent ototoxicity profile has been observed previously (Richardson and Russell, 1991; Forge and Richardson, 1993) and closely matches what is observed when AGs are used clinically (Chen et al., 2007; Schacht et al., 2012; Cannizzaro et al., 2014; Petersen and Rogers, 2015). In the standard gentamicin-kill assay using 5 µM gentamicin (Figure 3.1), there was an average loss of 88% of OHCs from the mid-basal region of the cochlea, whereas apical OHCs and IHCs along the length of the cochlear coil were largely preserved. As the concentration of gentamicin was increased, there was a progressively larger number of IHCs lost from the basal region, followed by OHCs from the apical region and lastly, once the concentration was doubled to ≥ 10 µM, a loss of IHCs from the apical region was also observed (Figure 3.2). A longer incubation time of 72 hours exacerbated this effect, causing an increase in the loss of each aforementioned HC type at every concentration tested (2.5 – 12.5 µM) (Figure 3.3).

3.4 Discussion

The reason for the observed pattern of OHC loss is presumably due to a number of factors that are all related to the intracellular accumulation of the antibiotics, with basal HCs accumulating gentamicin at a faster rate compared to those in the apex. Maturation of sensory HCs proceeds from the basal end upwards to the apex along a decreasing tonotopic gradient (from high to low-frequency); with MET currents present in basal HCs at birth and developing later along the apical coil (Alharazneh et al., 2011). A greater unitary conductance of the basal HC MET channels has been shown, ranging from 110 pS in the basal cells of the mouse cochlea to 62 pS in the HCs from the apical region (Beurg et al., 2014; Beurg and Fettiplace, 2017), and 300 pS versus 100 pS in the HCs of turtle cochleae (Fettiplace, 2009). Moreover, the resting open probability of the channel decreases from base to apex (Dallos et al., 1982; Johnson et al., 2011), as does the number of stereocilia on the cell's apical surface in the organ of Corti of rats (Roth and Bruns, 1992; Beurg et al., 2006). All of the aforementioned attributes will lead to a greater rate of entry of the antibiotics into basal HCs compared to those in the apex, meaning a more rapid accumulation of an intracellular concentration at which apoptotic cell-death pathways are initiated. This is a potential explanation for the clinical scenario, alongside the results of our *in vitro* assays. An alternative explanation for the disparity in apical and basal AG-induced cell death could be in the variable production of apoptosis-inducing ROS in a basal-apical gradient (Xie et al., 2011), or perhaps a combination of these factors.

IHCs are also largely preserved in the standard experimental assay detailed above and, again, this is likely due to a number of factors relating to the intracellular accumulation of the AGs. The conductance and peak amplitude of IHC MET channel currents along the tonotopic axial length of the cochlea is invariant (Beurg et al., 2006; Jia et al., 2007; Fettiplace, 2009; Kim and Fettiplace, 2013); however, IHCs are larger than their OHC counterparts, they have fewer MET channels (Jia et al., 2007), these channels have a smaller single-channel unitary conductance than basal OHCs (Beurg et al., 2006), a smaller macroscopic MET current (Kros et al., 1992) and the electrical driving force across the MET channel is reduced due to the RP of the cell being less negative in IHCs than it is in OHCs – approximately -45 mV compared to -70 mV (Russell and Sellick, 1983). This means that in the same 48 hours assay time window the intracellular accumulation of gentamicin would not reach levels as high as in OHCs, consequently not reaching a concentration at which apoptosis is triggered. With prolonged exposure time or higher concentrations of gentamicin, a loss of IHCs and apical OHCs (Figures 3.2 and 3.3) was also observed, confirming the postulation that it is the accumulation of AGs within a HC that

determines its fate, with apoptosis initiating after a certain intracellular concentration is reached.

The observed pattern of ototoxicity, both concentration and time-dependent, is due to the entry rates of the antibiotics into HCs, dictated by diffusion constants. By performing volumetric calculations of OHC size relative to the ionic concentration gradients across the MET channel, studies have shown that DHS, a semisynthetic AG, when at an endolymphatic concentration of 1 μM, can reach an intracellular concentration of 1 μM within 80 seconds (Marcotti et al., 2005) highlighting the rapid entry rates of the AGs into HCs. The underlying calculations offer explanations as to why increasing the extracellular concentration of the antibiotic, or prolonging the time of exposure, will lead to enhanced HC death – explainable by an enhanced achievement of an intracellular concentration that is sufficient to induce apoptosis in all of the aforementioned cell types and regions.

Although it is the IHCs that are directly responsible for sound transduction and information transfer to the auditory nerve, the OHCs serve as active amplifiers of the signal, fine-tuning our frequency sensitivity (Dallos and Harris, 1978; Purves et al., 2001; Dallos, 2008). Therefore, loss of OHCs alone would be sufficient to result in the loss of hearing ability, or the evident increase in hearing threshold that is frequently observed in a clinical setting when patients are treated with AGs (McRorie et al., 1989; Fausti et al., 1992; Stavroulaki et al., 2002).

4 Assessing the Otoprotective Potential of the Tocris Ion Channel Library

4.1 Introduction

4.1.1 Library Choice

The Tocris Ion Channel library (Tocriscreen Custom Collection Ion Channel Set) is a commercially-available chemical library of 160 small molecules that are known to behave as agonists or antagonists of various different ion channels.

The AGs have been shown to enter the sensory HCs of the inner ear through their MET channels (Marcotti et al., 2005; Alharazneh et al., 2011); non-selective cation channels that are capable of being blocked by numerous compounds known to interact with various other ion channels. Consequently, it was assumed that a library of ion channel interactors may provide the most suitable option for screening in the search for viable otoprotectants that could potentially block the MET channel and prevent the entry of the AGs into sensory HCs, thereby preventing their death and the unfortunate ototoxic side-effect associated with AG treatment.

4.1.2 Aims

We sought to screen the entire Tocris library in an attempt to identify novel otoprotectants *in vivo* in zebrafish and *in vitro* in mouse cochlear cultures, which could then be transferred to a mammalian *in vivo* model before potentially being taken forward to clinical trials.

We also sought to investigate the mechanism of protection of all of the protectants identified. This would inform us of several things, including, but not exclusive to: the most frequently successful mechanism of otoprotection (whether that be preventing AG entry into HCs or alternatively an intracellular protective process); how reliable zebrafish pre-screening is for this purpose; and whether we can modify compounds based on their mechanism of protection in order to generate more efficacious otoprotectants.

4.2 Results

4.2.1 Screening for Otoprotection

4.2.1.1 Zebrafish Pre-Screening

* All zebrafish research detailed in this section was conducted by Emma Kenyon, University of Sussex.

The entire set of 160 compounds was initially tested in three different zebrafish assays, as detailed in Kenyon et al., 2017. Briefly, the three assays investigated whether each Tocris compound was able to consistently:

1. Block or reduce the loading of FM 1-43FX (a dye known to permeate through sensory HC MET channels) into neuromast HCs.
2. Prevent the loading of a fluorescently-conjugated AG (neomycin-Texas Red) into neuromast HCs.
3. Prevent the neuromast HC loss caused by 1 hour incubation with neomycin.

Compounds that were successful in any of the three zebrafish assays were taken forward to mouse cochlear cultures for further screening. Additional compounds that did not hit any of the zebrafish assays were also tested in mice, as they shared a similar chemical signature to compounds that were successful in at least one of the three assays. This was in order to increase the number of possible hits whilst also assessing and reducing the number of false negatives in the initial zebrafish screen, concurrently gaining further insight regarding the usefulness and viability of preliminary zebrafish screens as a prerequisite to mammalian testing.

Of the 160 compounds screened in zebrafish, 72 were effective in at least one of the three assays. These 72, alongside 6 other structurally-related compounds, were then brought forward for additional testing in mouse cochlear cultures.

4.2.1.2 Cochlear Culture Screening

4.2.1.2.1 Protection at 50 µM

In mouse cochlear cultures, compounds that were brought forward from zebrafish screening were initially tested for their ability to provide protection against the damage caused by 5 µM gentamicin over a period of 48 hours. As previously detailed in Chapter 3, this concentration of the antibiotic caused an average loss of 88% of the OHCs from the mid-basal region of P2 mice cochleae (Figure 3.1). All of the Tocris compounds that were brought forward were initially tested at a concentration of 50 µM, to assess whether they could prevent the observed OHC loss. Any compounds that did not provide protection in this initial screen, or had any observable toxic effect, were excluded from further testing. Any compounds that did provide protection were re-tested at this concentration at least an additional two times, to ensure the reliability of their protective efficacy. The number of repeats when tested at a concentration of 50 µM ranged from 3 to 11.

Of the 78 compounds screened, 12 consistently provided complete protection against the gentamicin-induced loss of OHCs when tested at 50 µM (13087, 13097, 13104, 13142, 13143, 13150, 13154, 13170, 13190, 13196, 13218 and 13228). One compound (13222) provided partial protection, working effectively in some experiments and failing on others (protecting in 5 out of 11 trials). To note, one of these 13 compounds (13150) was not identified as being successful in the zebrafish screening procedure, but instead was selected on the basis of structural similarity to one that was successful.

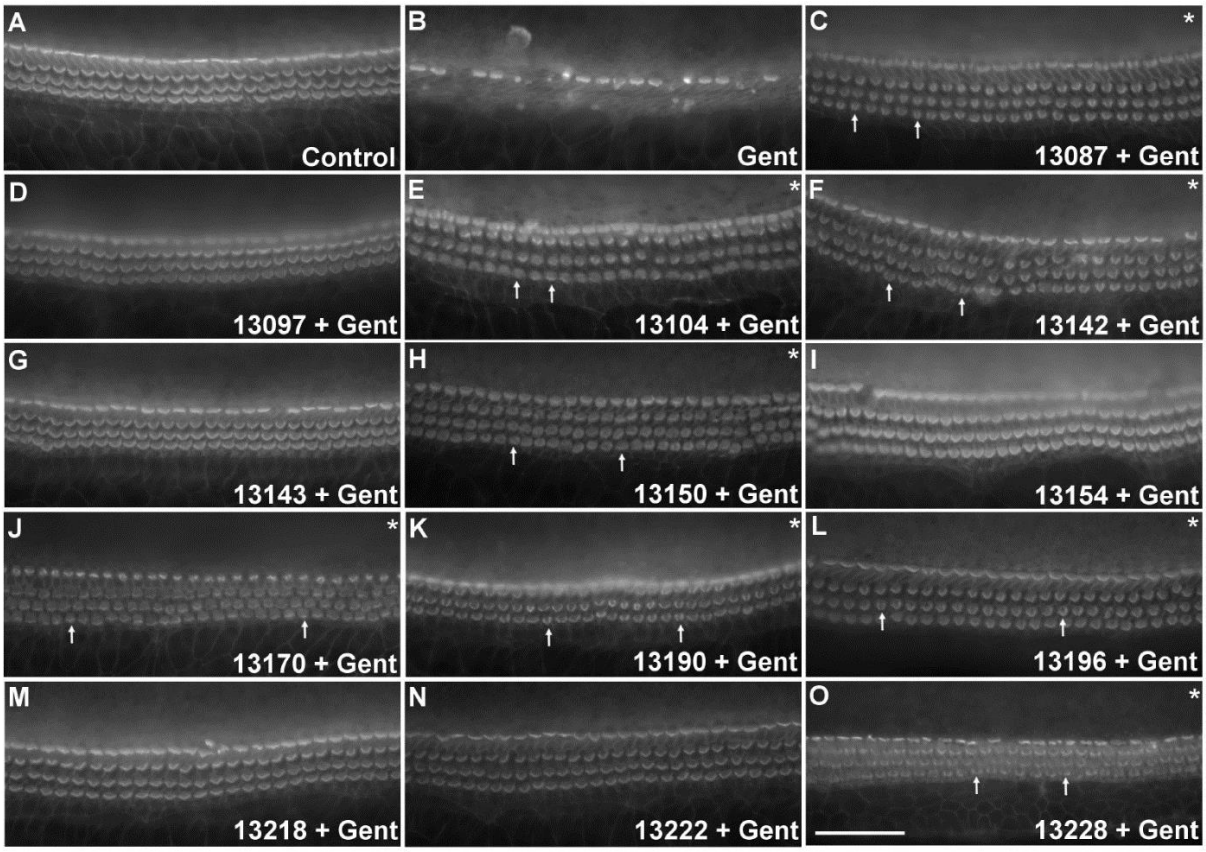

Figure 4.1: *When tested at a concentration of 50 µM, 12 of the 78 compounds consistently protected against 5 µM gentamicin damage and 1 provided partial protection.*

Cochlear cultures were treated with either **(A)** 0.5% DMSO (n=67), **(B)** 5 µM gentamicin and 0.5% DMSO (n=67), or **(C–O)** 5 µM gentamicin and 50 µM compound **(C)** 13087 (n=5), **(D)** 13097 (n=9), **(E)** 13104 (n=5), **(F)** 13142 (n=8), **(G)** 13143 (n=8), **(H)** 13150 (n=4), **(I)** 13154 (n=5), **(J)** 13170 (n=5), **(K)** 13190 (n=3), **(L)** 13196 (n=5), **(M)** 13218 (n=10), **(N)** 13222 (n=11) and **(O)** 13228 (n=4). Images in **A** and **B** are representative of 67 experiments. Images in **C–O** are representative of 3–11 experiments. A compound was considered protective if it protected in ≥ 60% of tests and partially protective if the success rate was > 20% < 60%. Asterisks identify cultures with damaged hair bundles; arrows indicate specific examples of damaged bundles. Scale bar is 50 µm. Figure taken from Kenyon et al., 2017.

4.2.1.2.2 Protection at 10 µM

All 13 compounds were then screened for their ability to protect against gentamicin damage when tested at a concentration of 10 µM, to assess the lower limit of their protective efficacy. A compound with a lower protective concentration would be preferable due to a reduction in the likelihood of it causing any unwanted, off-target side-effects following administration of the compound in a clinical setting. When tested at this concentration, 3 compounds remained consistently protective (13097, 13143 and 13170), 6 were partially protective (13104, 13142, 13154, 13196, 13222 and 13228), and 4 provided no protection (13087, 13150, 13190 and 13218). The number of repeats when tested at a concentration of 10 µM ranged from 5 to 10.

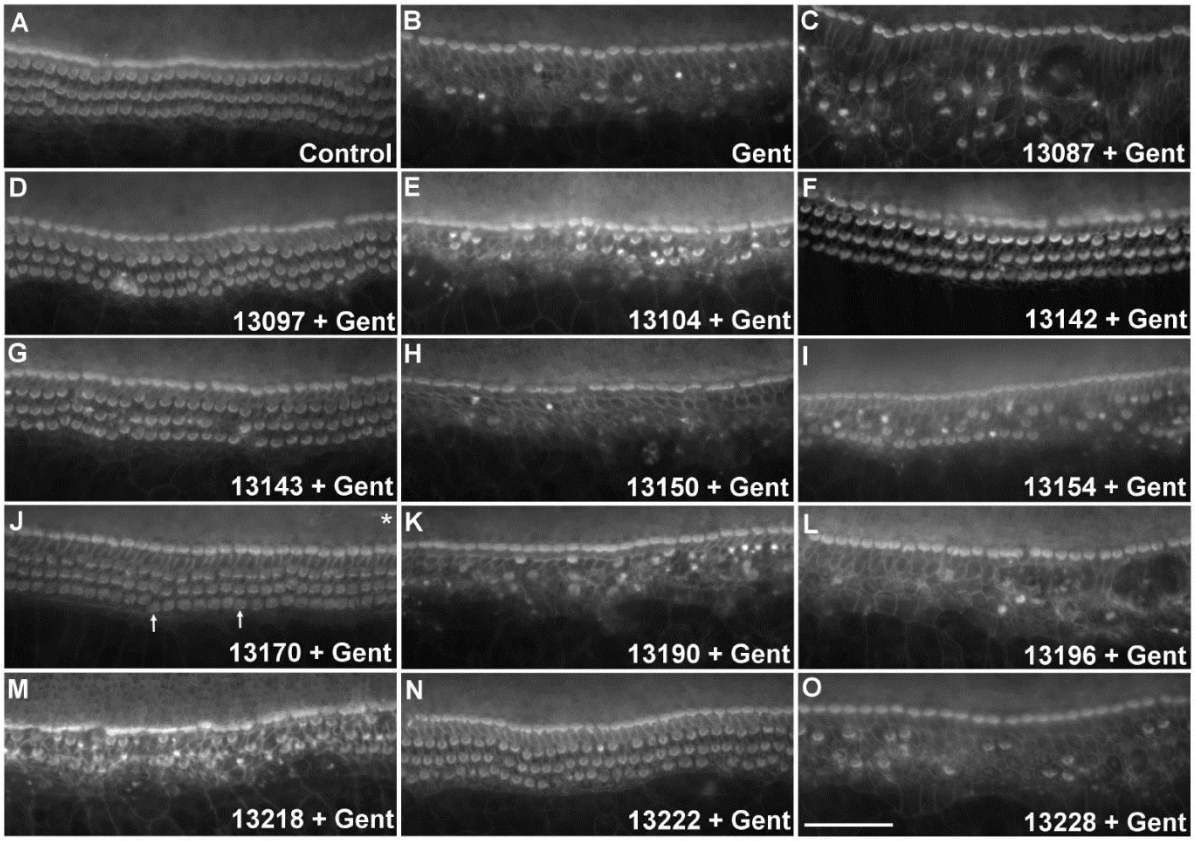

Figure 4.2: *When tested at a concentration of 10 µM, 3 of the 13 compounds protected against 5 µM gentamicin damage, 6 were partially protective and 4 provided no protection.*

Cochlear cultures were treated with either **(A)** 0.5% DMSO (n=67), **(B)** 5 µM gentamicin and 0.5% DMSO (n=67), or **(C–O)** 5 µM gentamicin and 10 µM compound **(C)** 13087 (n=6), **(D)** 13097 (n=6), **(E)** 13104 (n=7), **(F)** 13142 (n=8), **(G)** 13143 (n=8), **(H)** 13150 (n=6), **(I)** 13154 (n=5), **(J)** 13170 (n=5), **(K)** 13190 (n=6), **(L)** 13196 (n=5), **(M)** 13218 (n=7), **(N)** 13222 (n=10) and **(O)** 13228 (n=7). Images are representative. Asterisks identify compounds that damaged hair

bundles (only compound 13170 in this assay) while arrows indicate specific examples of damaged bundles. Scale bar is 50 µm. Figure taken from Kenyon et al., 2017.

4.2.1.2.3 The Effect of Otoprotectants on Sensory Hair Bundle Morphology

As a further screening precaution, all of the protective screens that had been conducted in the presence of gentamicin were analysed to assess whether any of the compounds caused any observable damage to the mechanosensory hair bundle that is located on top of sensory HCs. The hair bundle is directly responsible for auditory transduction, so any morphological disruption may lead to negative effects on hearing ability. Moreover, any compounds that did protect but caused bundle damage may have only protected due to malformation of the hair bundle to such an extent so as to render the MET channel non-functional. As this study was aimed at protecting our hearing, any observable impact on the morphology of the characteristic V-shaped OHC hair bundle led to their exclusion from being taken forward as a lead compound.

Of the 13 compounds screened in the presence of gentamicin, 8 caused some degree of disruption to the morphology of the mechanosensory hair bundle when tested at 50 µM (13087, 13104, 13142, 13150, 13170, 13190, 13196 and 13228), and 1 when tested at 10 µM (13170). Examples of morphological hair bundle disruption are indicated by the arrows in Figures 4.1 and 4.2.

4.2.1.2.4 The Intrinsic Toxicity of Otoprotectants when tested Alone in the Absence of Gentamicin

As an additional precaution all 13 compounds were also screened for their intrinsic toxicity when tested alone in the absence of gentamicin, at 50 µM and also at a higher concentration of 100 µM. Due to the uncertainty of the concentrations of these compounds when they reach the endolymphatic compartment of the cochlea, within which the sensory HCs are situated, it is essential for any potential otoprotectant to have a broad non-toxic concentration range. For this reason, all of the compounds were screened in the absence of gentamicin to assess their intrinsic toxicity at a concentration of 50 and 100 µM. When tested at 50 µM, 5 of the compounds caused some disruption to hair bundle morphology (13087, 13150, 13170, 13196 and 13228). When tested at 100 µM, 4 of the compounds were generally cytotoxic to the cochlear culture, causing a loss of the neurosensory epithelium and other supporting cells (13087, 13150, 13218 and 13228). An additional 4 compounds caused damage to the morphology of the hair bundles (13104, 13170, 13190 and 13196). Only 5 of the 13 compounds showed no adverse effects on the cochlear culture when tested at 100 µM (13097, 13142, 13143, 13154 and 13222). In Figures 4.3 and 4.4, disruption to hair bundle morphology is indicated by a singular asterisk (*) and general cytotoxicity is indicated by a double asterisk (**).

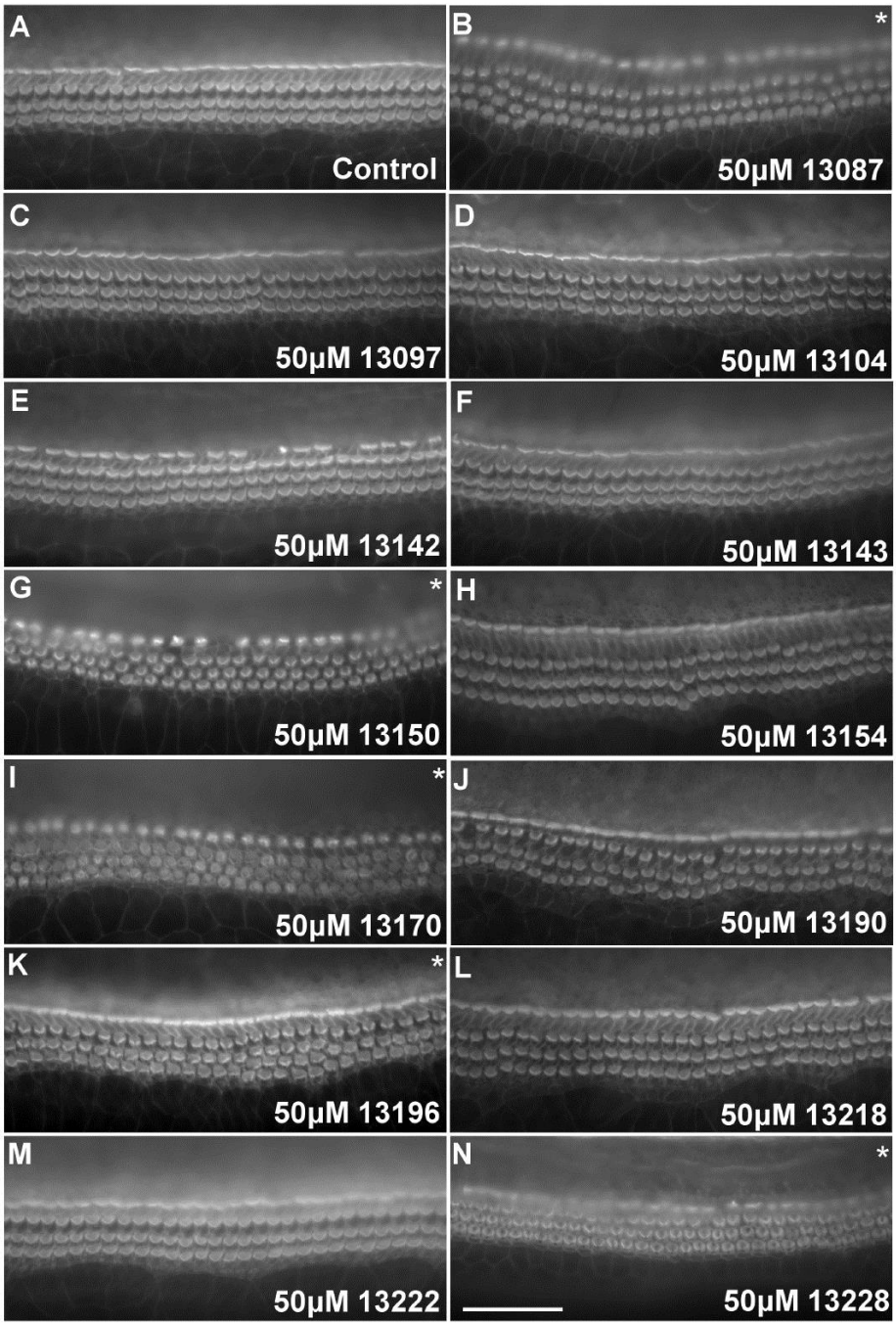

Figure 4.3: *When tested at 50 μM in the absence of gentamicin, 5 compounds caused disruption to the morphology of the mechanosensory hair bundle.*

Cochlear cultures were treated for 48 hours with either **(A)** 0.5% DMSO (n=2) or **(B-N)** 50 μM compound as indicated (n=2 for all compounds). Asterisks identify compounds that damage hair bundles. Scale bar is 50 μm. Figure taken from Kenyon et al., 2017.

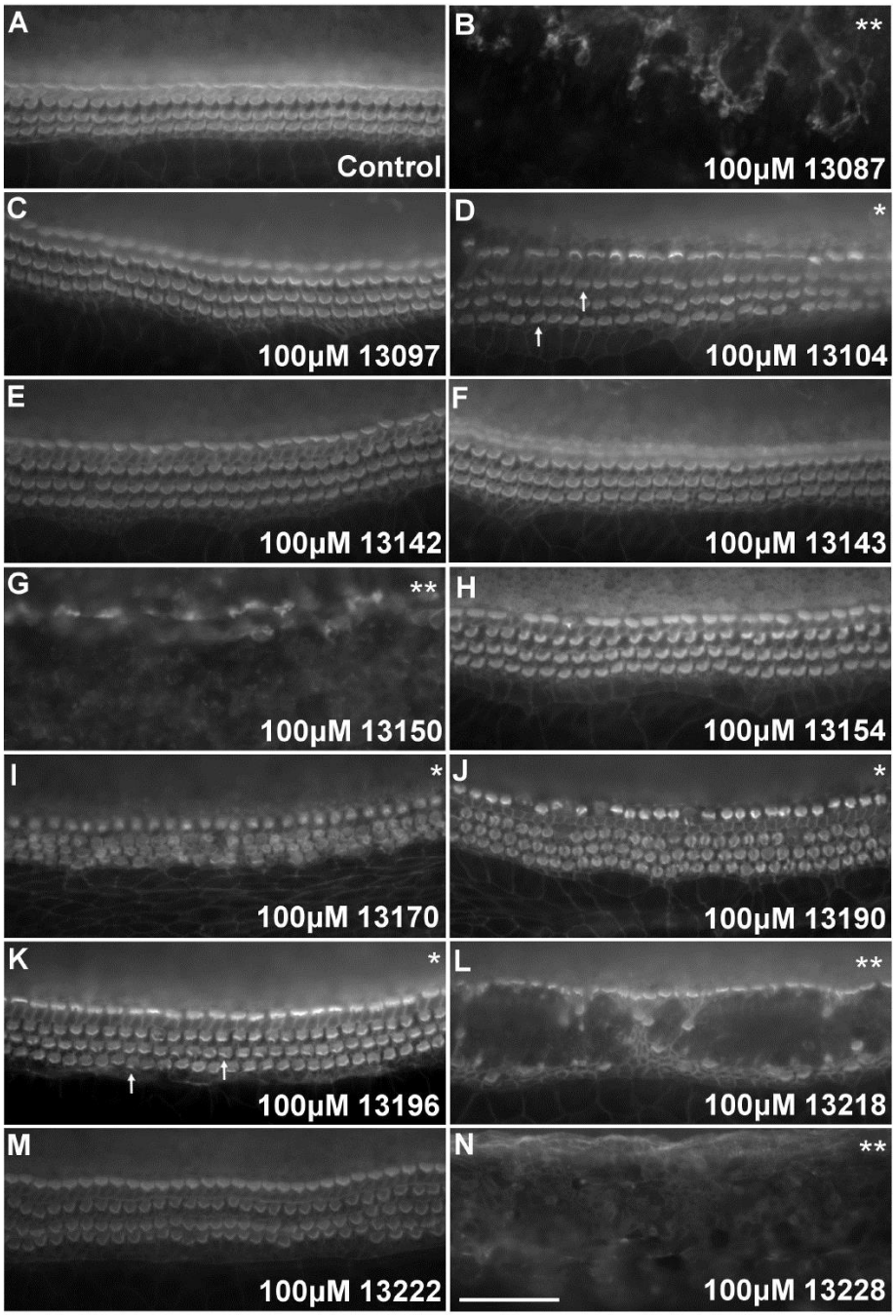

Figure 4.4: *When tested at 100 µM in the absence of gentamicin, 4 compounds were generally cytotoxic and an additional 4 caused disruption of the hair bundle morphology.*

Cochlear cultures were treated for 48 hours with either **(A)** 0.5% DMSO (n=2) or **(B-N)** 100 µM compound as indicated (n=2 for all compounds). Asterisks identify compounds that damage hair bundles, with arrows indicating examples of damaged bundles. Double asterisks identify compounds that were generally cytotoxic. Scale bar is 50 µm. Figure taken from Kenyon et al., 2017.

4.2.1.2.5 Dose-Response Experiments assessing the Minimal Protective Concentration of the Lead Compounds

After the exclusion of any compounds that had negative intrinsic characteristics, such as generalised cytotoxicity at higher concentrations or any impact on the morphology of the mechanosensory hair bundle at any concentration, just 3 compounds remained (13097, 13142 and 13143). Of these 3, only 2 provided protection against gentamicin damage when tested at 10 µM (13097 and 13143). These 2 were therefore taken as our lead compounds and dose-response experiments were conducted to assess the limit of their protective efficacy by ascertaining their minimum protective concentration. Compound 13143 (commonly known as linopirdine) was protective down to 1 µM (with a half-protecting concentration *K* of 840 nM), and a 95% CI of 210-1,480 nM. Compound 13097 (commonly known as XE 991) provided complete protection at concentrations as low as 10 nM (with a half-protecting concentration *K* of 4.9 nM), and a 95% CI of 2.2-7.7 nM. Both compounds had a remarkable protective efficacy relative to other otoprotectants previously identified both in zebrafish and mammalian systems (Ou et al., 2009; Kirkwood et al., 2017; Majumder et al., 2017), with 13097 protecting at a 1000-fold greater efficacy than any other previously identified otoprotectant reported in the literature (nM versus µM).

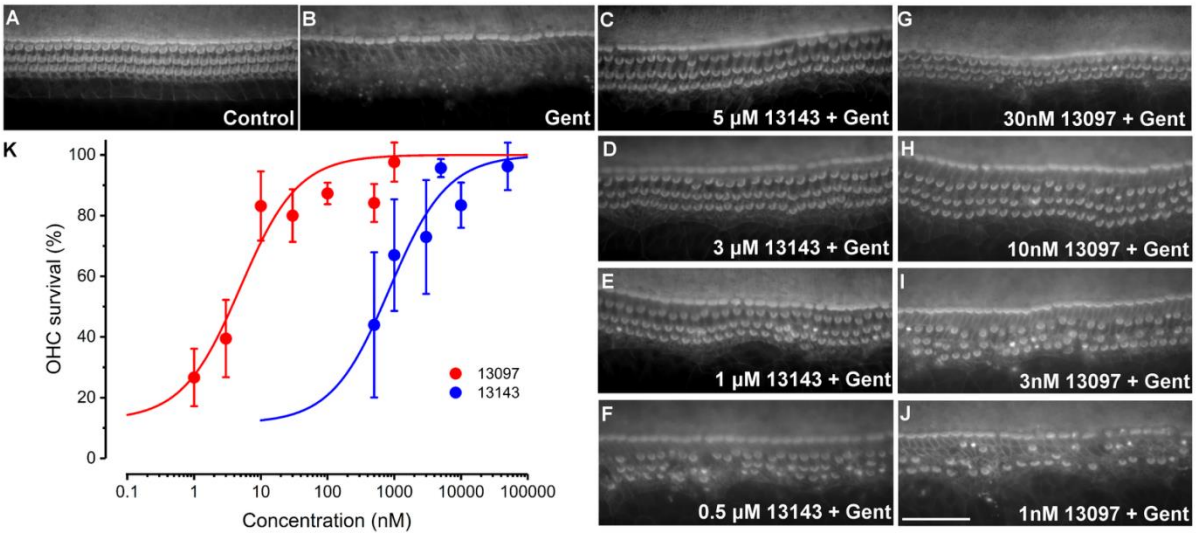

Figure 4.5: *Dose-response experiments for our two lead compounds. The half-protecting concentration for 13143 was 840 nM and for 13097 it was 4.9 nM.*

Cochlear cultures were treated with **(A)** 0.5% DMSO (n=67), **(B)** 5 µM gentamicin (n=67), 5 µM gentamicin and 13143 at **(C)** 5 µM (n=5), **(E)** 3 µM (n=5), **(G)** 1 µM (n=4), and **(I)** 0.5 µM (n=3) or 5 µM gentamicin and 13097 at **(D)** 30 nM (n=5), **(F)** 10 nM (n=5), **(H)** 3 nM (n=4), and **(J)** 1

nM (n=4). Images in **A** and **B** are representative of 67 experiments. Images in **C–J** are representative of 3–5 experiments. **(K)** Dose-response curves showing the percentage survival of basal-coil OHCs in cultures treated with gentamicin and either compound 13097 (red) or compound 13143 (blue) compared with that in control cultures. Error bars are SEM from 3–8 independent tests. Curves are fit to the equation: *OHC survival (%) = B + (100–B)[C]/(K + [C])*, where *B* is the percentage of OHCs surviving in gentamicin alone, *[C]* is the concentration of the compound, and *K* is the compound concentration at which 50% protection occurs. For 13097, *K* = 4.9 nM and B = 12.6%; for 13143, *K* = 840 nM and B = 11.5%. Scale bar is 50 µm. Figure taken from Kenyon et al., 2017.

4.2.1.2.6 Lead Compound Protection against a Higher Gentamicin Concentration or a Longer Exposure Time

I further investigated the protective ability of our most effective compound, 13097, when tested against a higher gentamicin concentration and a longer exposure time. As previously mentioned, having a broad protective range would be a desirable characteristic of an otoprotective compound. For this reason, I initially investigated the ability of 13097 to protect against the HC loss caused by 10 µM gentamicin incubation. I tested the compound at 100, 200 and 300 µM – at a high molar excess of its minimum protective concentration in the standard 5 µM protection assay. At 100 µM, no protection was seen (data not shown). At 200 µM, partial protection was observed as some HCs were protected. When tested at 300 µM, HCs were protected however the morphology of the OHC hair bundles was greatly disturbed (Figure 4.6). One cochlear culture was tested for each specified concentration.

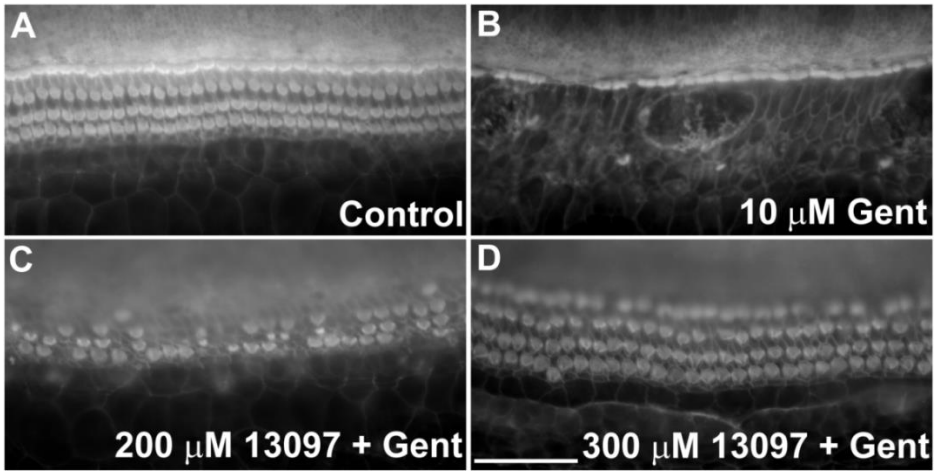

Figure 4.6: *13097 protected against 10 µM gentamicin damage when tested at 300 µM.*

Cochlear cultures were treated for 48 hours with **(A)** 0.5% DMSO, **(B)** 10 µM gentamicin and 0.5% DMSO or 10 µM gentamicin and 13097 at **(C)** 200 or **(D)** 300 µM (n=1 for all conditions). Scale bar is 50 µm.

I subsequently investigated the ability of 13097 to protect against the damage caused by 5 µM gentamicin over a longer time course of 72 hours. When tested at 1 and 50 µM, the compound showed no protection against the damaging effects of gentamicin (Figure 4.7). One cochlear culture was tested for each specified concentration.

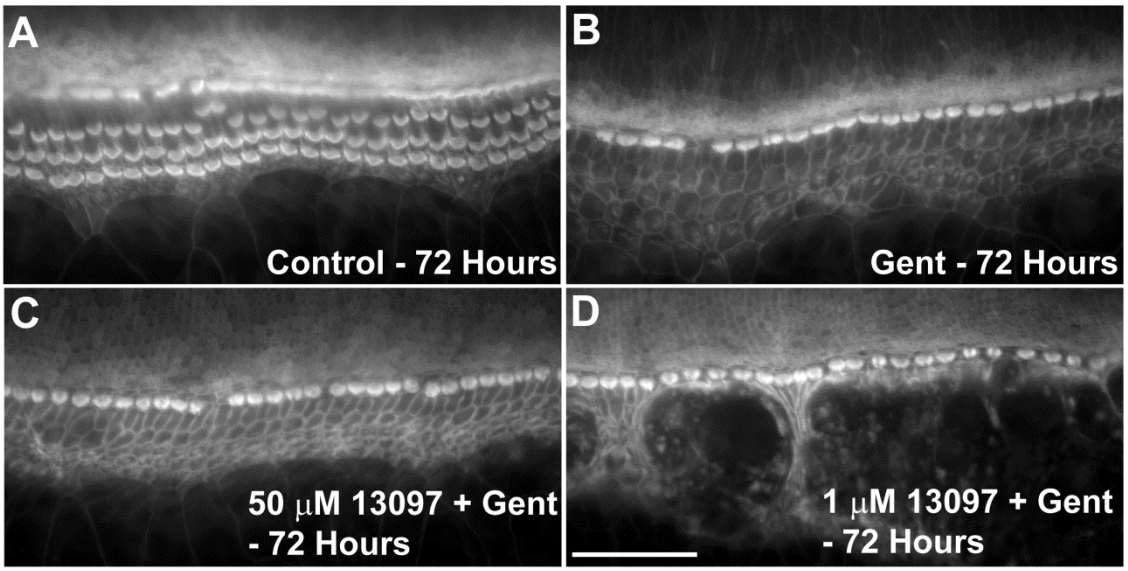

Figure 4.7: *13097 did not protect against 72 hours exposure to 5 µM gentamicin when tested at 1 or 50 µM.*

Cochlear cultures were treated for 72 hours with either **(A)** 0.5% DMSO or **(B)** 5 µM gentamicin and 0.5% DMSO or 5 µM gentamicin and 13097 at **(C)** 50 or **(D)** 1 µM (n=1 for all conditions). Scale bar is 50 µm.

4.2.2 Compound Modifications

Following our screening for mammalian otoprotectants, 2 compounds were selected for modification (13087 and 13143) in an attempt to synthesise more effective derivatives. Compound 13087 was selected due to its structural similarity to another compound that was identified as an effective mammalian otoprotectant within this thesis, which is already FDA approved for the treatment of hypertension (Carvedilol; Chapter 6). Compound 13143 was selected as it is our second most effective otoprotectant and our most effective (13097) was originally identified as an improved derivative of 13143 for use as a cognitive enhancer, with a similar chemical structure (Zaczek et al., 1998; Greene et al., 2017).

The 13087 derivatives were: 28663, 28664, 28665 and 28666. All were initially tested for their protective ability against 5 µM gentamicin when tested at a concentration of 50 µM; the limit of the parent compound's protective efficacy. Of the 4, only 1 was protective (28664) (Figure 4.8A-F). However this was the lower limit of its protective efficacy. When tested at 20 and 10 µM 28664 provided no HC protection (Figure 4.8G).

The 13143 derivatives were: 21166, 21170, 21172, 21173 and 21174. All of these compounds were tested at 10 µM, in high excess of the parent compound's minimum protective concentration. None of the derivatives provided any protection when tested at this concentration (Figure 4.8H-L), suggesting that our chemical modifications were unsuccessful at improving otoprotective efficacy.

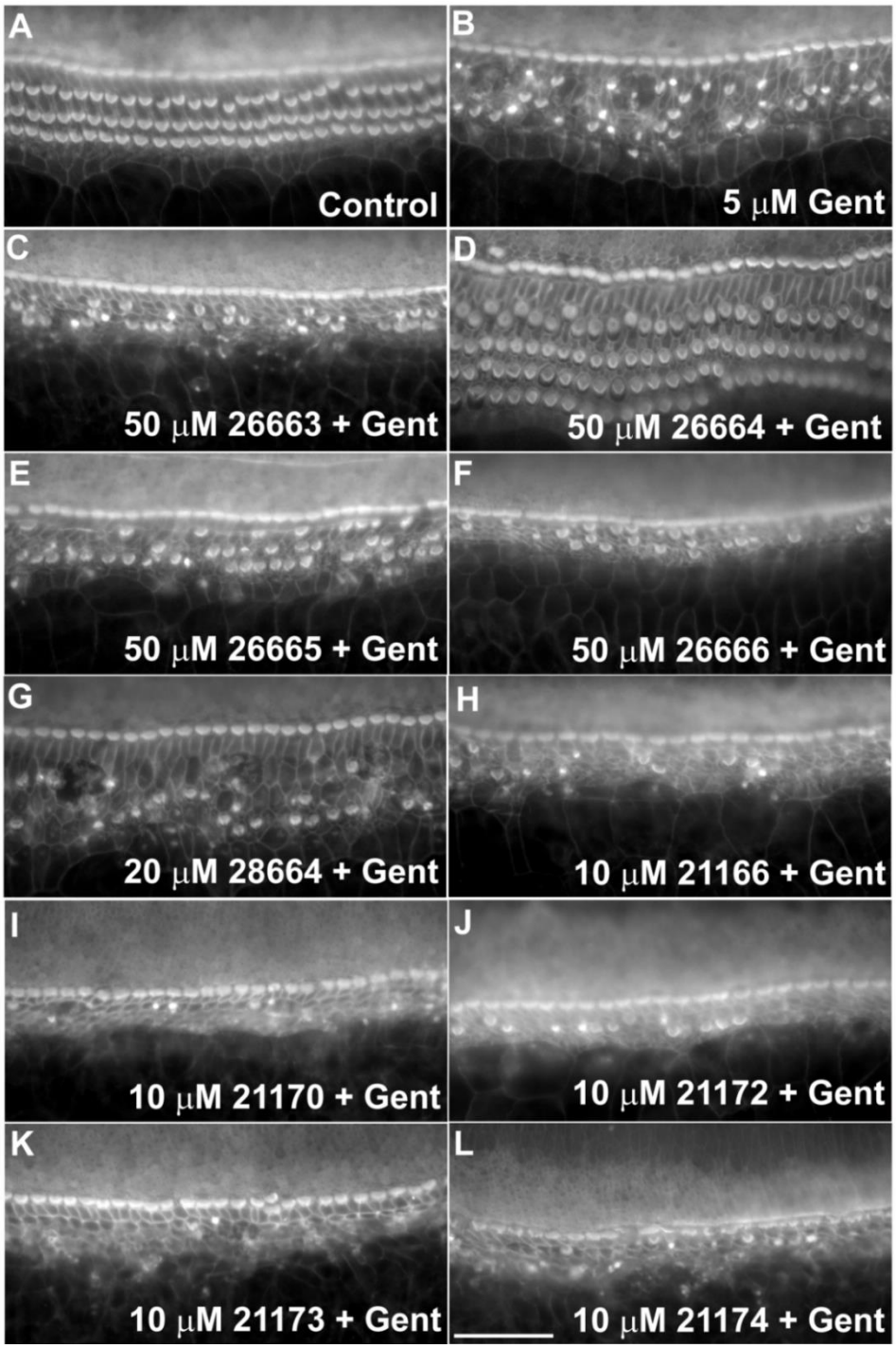

Figure 4.8: *Two Tocris compounds (13087 and 13143) were structurally modified to improve their otoprotective ability. None of the derivatives were more protective than the parent compounds.*

Cochlear cultures were treated for 48 hours with either **(A)** 0.5% DMSO, **(B)** 5 μM gentamicin and 0.5% DMSO, **(C-F)** 5 μM gentamicin and 50 μM **(C)** 28663, **(D)** 28664 (n=3), **(E)** 28665 or **(F)** 28666, **(G)** 5 μM gentamicin and 20 μM 28664 or **(H-L)** 5 μM gentamicin and 10 μM **(G)** 21166,

(H) 21170, **(I)** 21172, **(J)** 21173 or **(K)** 21174 (n=1 for all compounds unless otherwise stated). Scale bar is 50 µm.

4.2.3 The effect of Tocris Compounds on the Antimicrobial Activity of Gentamicin

All 13 compounds were tested in a bacterial cell viability assay, to ensure that they do not compromise the antimicrobial activity of gentamicin, as this would then void their usefulness as a potential otoprotectant. This research was conducted by Daire Cantillon, University of Sussex, and is thoroughly detailed in Kenyon et al., 2017. However, in brief, when co-incubated with gentamicin, 2 Tocris compounds of interest (13170 and 13228) increased gentamicin's antimicrobial effect on bacterial cell survival.

4.2.4 Candidate Otoprotectants

From all of the results detailed above, 5 compounds emerged as potential otoprotectants that should be investigated further for clinical use (13097, 13142, 13143, 13154 and 13222). These 5 are potential candidates due to their ability to protect basal OHCs against 5 µM gentamicin-induced damage when tested at 50 µM (or considerably less in some cases). They do not cause any HC death of hair bundle disruption when tested alone at 100 µM and they do not compromise the antimicrobial actions of gentamicin. Three of the 5 compounds are MET channel blockers (13142, 13154 and 13222), so may be protecting by blocking this primary entry route into HCs. All 5 compounds are blockers of the OHC potassium channel $I_{K,neo}$, so could potentially depolarise the cell membrane and in this way reduce the electrical driving force that is one determinant of AG entry into HCs.

4.2.5 Mechanisms of Protection

4.2.5.1 The Effect of Otoprotectants on MET Channel Currents

* The electrophysiology presented in this chapter was performed by Nerissa Kirkwood, University of Sussex.

The MET channel is a known entry route of the AGs into HCs (Marcotti et al., 2005; Alharazneh et al., 2011). For this reason, all of the otoprotectants that we identified were tested for their ability to block MET channel currents, on the assumption that they may be protecting HCs by blocking the channel and impeding the entry, and accumulation, of the antibiotics. MET channel currents were recorded from the third row of OHCs of P2 mouse cochleae before, during and after the superfusion of the compounds, tested at a concentration of 50 µM. Whole-cell voltage clamp experiments were conducted in order to test the effect of the compounds on the MET channel currents when the cell was stepped between membrane potentials ranging from -164 mV to +96 mV, to assess the voltage-dependency of any observed channel block.

Of the 13 compounds tested, 7 had no effect on the MET channel current size at any membrane potential tested, indicating a lack of interaction with the channel. The remaining 6 (13087, 13104, 13142, 13154, 13218 and 13222) all showed a voltage-dependent block of the channel. Shown in Figure 4.10 are two examples of MET channel current traces recorded before (black), during (red) and after (blue) the superfusion of 2 of the Tocris compounds of interest. Compound 13143 is shown in A and 13222 in B. Compound 13143 had no interaction with the channel whereas 13222 caused a reduction in the recorded current sizes, indicative of channel block. In Figure 4.10C and D, current-voltage (I-V) curves were derived by plotting the peak MET channel current amplitude at each voltage step, providing further evidence of the lack of interaction of 13143 with the MET channel (Figure 4.10C) and the reduction in MET channel current size by superfusion with 13222 (Figure 4.10D), at all membrane potentials tested. Evidently this block is reversible, as shown by the complete restoration of current size following re-superfusion of control solution (blue).

Average fractional block curves can be derived by plotting the ratio of the control MET channel current to the current in the presence of the compound against all membrane potentials; averaging the I-V curves across multiple cells. Shown in Figure 4.10E are fractional block curves for all 7 compounds that had no interaction with the channel. Shown in Figure 4.10F are all 6 compounds that interacted with the channel. All 6 compounds display a voltage-dependent

block, with all but one (13087) showing maximal block at the intermediate, slightly negative potentials. Furthermore, all of the MET channel blocking compounds showed a release of the block at the extreme depolarised and extreme hyperpolarised potentials, indicating that they all behaved as permeant blockers of the MET channel, similarly to DHS (a semisynthetic AG derived from streptomycin) (Marcotti et al., 2005) and FM 1-43 (Gale et al., 2001), a stryl dye commonly used as a marker of MET channel function.

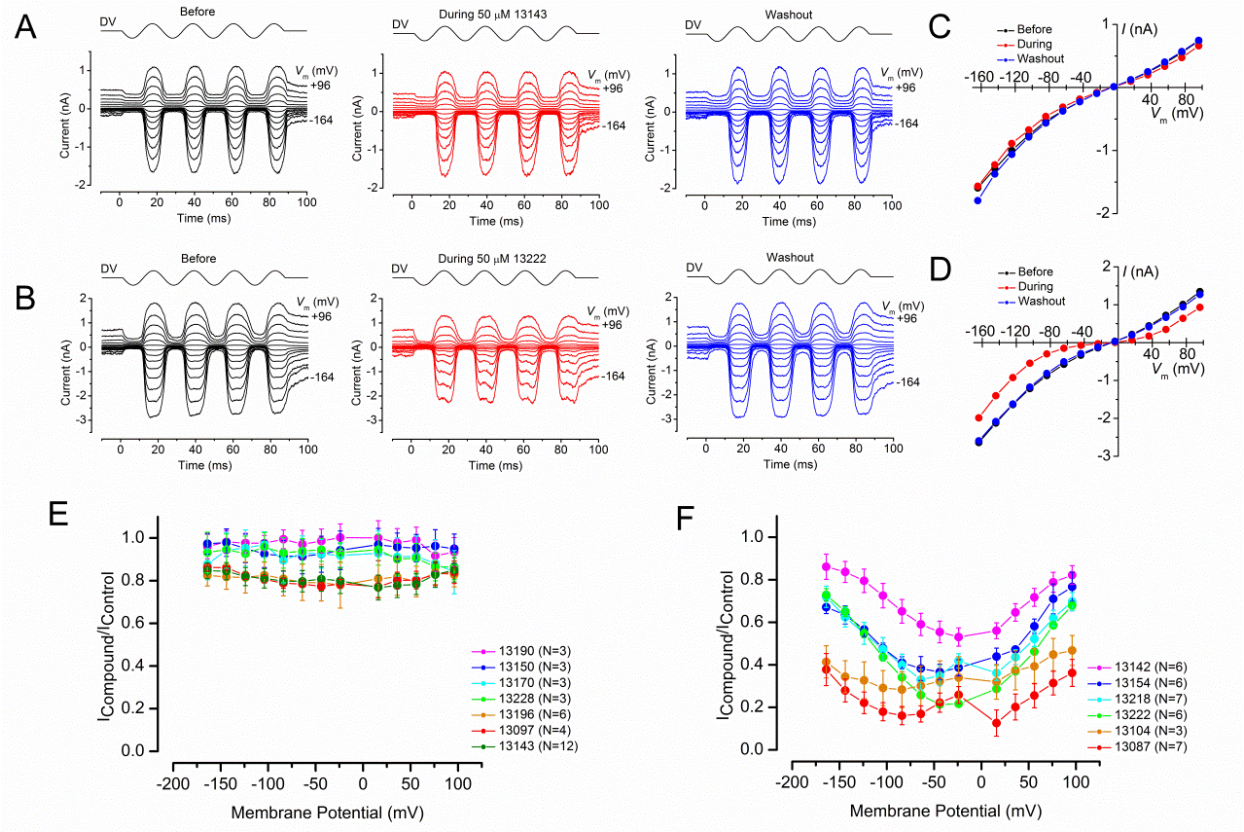

Figure 4.10: *Interactions of otoprotectants with the MET channel.*

Representative MET currents from OHCs in cultures prepared from P2 pups recorded before, during, and after exposure to **(A)** 50 µM 13143 (n=12) and **(B)** 50 µM 13222 (n=6). MET currents were recorded at membrane potentials from -164 mV to +96 mV in response to a sine-wave stimulus. Current-voltage curves for the peak MET currents derived from the recordings shown in **A** and **B** demonstrate **(C)** the lack of interaction of 13143 with the channel and **(D)** the voltage-dependence of block by 13222. **(E)** Fractional block of the MET currents at all membrane potentials reveals that 7 compounds, including 13143, do not interact with the channel. **(F)** 6 compounds, including 13222, provide a voltage-dependent block that is in most cases strongest at moderately negative potentials. Error bars are SEM. Numbers of independent tests are shown after each compound number in graphs **(E and F)**. Figure taken from Kenyon et al., 2017.

4.2.5.2 The Effect of Otoprotectants on Basolateral K^+ Channel Currents

Of the 13 compounds that provided protection against gentamicin-induced loss of OHCs, 4 of them are known to be potassium channel blockers (13087, 13097, 13143 and 13154). Two of these are K_v7 channel blockers (13097 and 13143) but do not block the MET channel, whereas the remaining two (13087 and 13154) do. We tested all 13 otoprotective compounds for their block of the potassium channels expressed by P2 mouse OHCs. In the first postnatal week, a slow outward K^+ current ($I_{K,neo}$) is expressed in OHCs which activates at potentials positive to -50 mV (Marcotti and Kros, 1999). Block of $I_{K,neo}$ may result in depolarisation of the cell membrane and in this way reduce AG entry by reducing the driving force across the MET channel, which is determined by the sum of the EP and the RP of the cell. All 13 compounds were tested for their effect on $I_{k,neo}$ at a concentration of 30 µM. K^+ currents were elicited by applying a series of hyperpolarising and depolarizing voltage steps, stepping from a holding potential of -84 mV. These results are thoroughly documented in Kenyon et al., 2017, however, in brief, of the 13 compounds tested, 11 showed some block of the K^+ current and only 2 (13170 and 13196) showed no interaction with the $I_{K,neo}$ channel.

The common effect of the compounds on both of the ion channel types expressed in OHCs that could influence AG entry into HCs suggested that our otoprotectants may be protecting by reducing the loading and intracellular accumulation of gentamicin. For this reason, we then tested our 5 lead compounds for their ability to depolarise HC membranes and also for their ability to block the loading of a fluorescently-conjugated AG (GTTR) into HCs.

4.2.5.3 The Effect of Otoprotectants on the Resting Membrane Potential

The AGs are drawn into the MET channel due to the negative charge within the channel pore and are then pulled into the HC due to the negative potential inside relative to the extracellular environment. If a compound depolarised the cell membrane there would be less of an electrical driving force pulling the AGs into the cell, so their entry rates and consequent intracellular accumulation would be reduced, perhaps providing an otoprotective effect. The 5 lead compounds (13097, 13142, 13143, 13174 and 13222) were tested for their effect on the resting membrane potential of the cell, as detailed in Kenyon et al., 2017. Briefly, none of the compounds caused any shift in cellular resting potential, eliminating membrane depolarisation as a potential mechanism of protection.

4.2.5.4 The Effect of Otoprotectants on Gentamicin-Texas Red Loading into HCs

To further assess whether any of our lead compounds may be protecting by preventing AG entry into HCs, short-term fluorescence assays were used. A fluorescently-conjugated AG is available, known as gentamicin-Texas Red (GTTR). GTTR has often been used to study the loading of AGs into HCs (Steyger et al., 2003), so we utilised this experimental technique. P2 mice cochleae were incubated with 0.2 μM GTTR for a period of 10 minutes, a concentration and time frame known to lead to HC loading. Prior to this, they were incubated for 5 minutes either with 100 μM of the Tocris compound of interest or 1% DMSO – the solvent in which the compounds were dissolved, as a control. By quantifying the intracellular GTTR florescence in the absence of presence of the compound, we were able to determine whether any of the compounds caused any reduction of AG loading into HCs.

As detailed in Kenyon et al., 2017, only 1 of our 5 lead compounds (13143) caused a significant reduction in GTTR loading, despite showing no block of the MET channel or any shift in cellular resting potential. Compound 13170, found to block TR-Neo and FM 1-43FX loading in the zebrafish assays but disregarded as a potential lead compound due to negative effects on hair bundle morphology, caused a considerable decrease in loading and was used as a positive control in this assay.

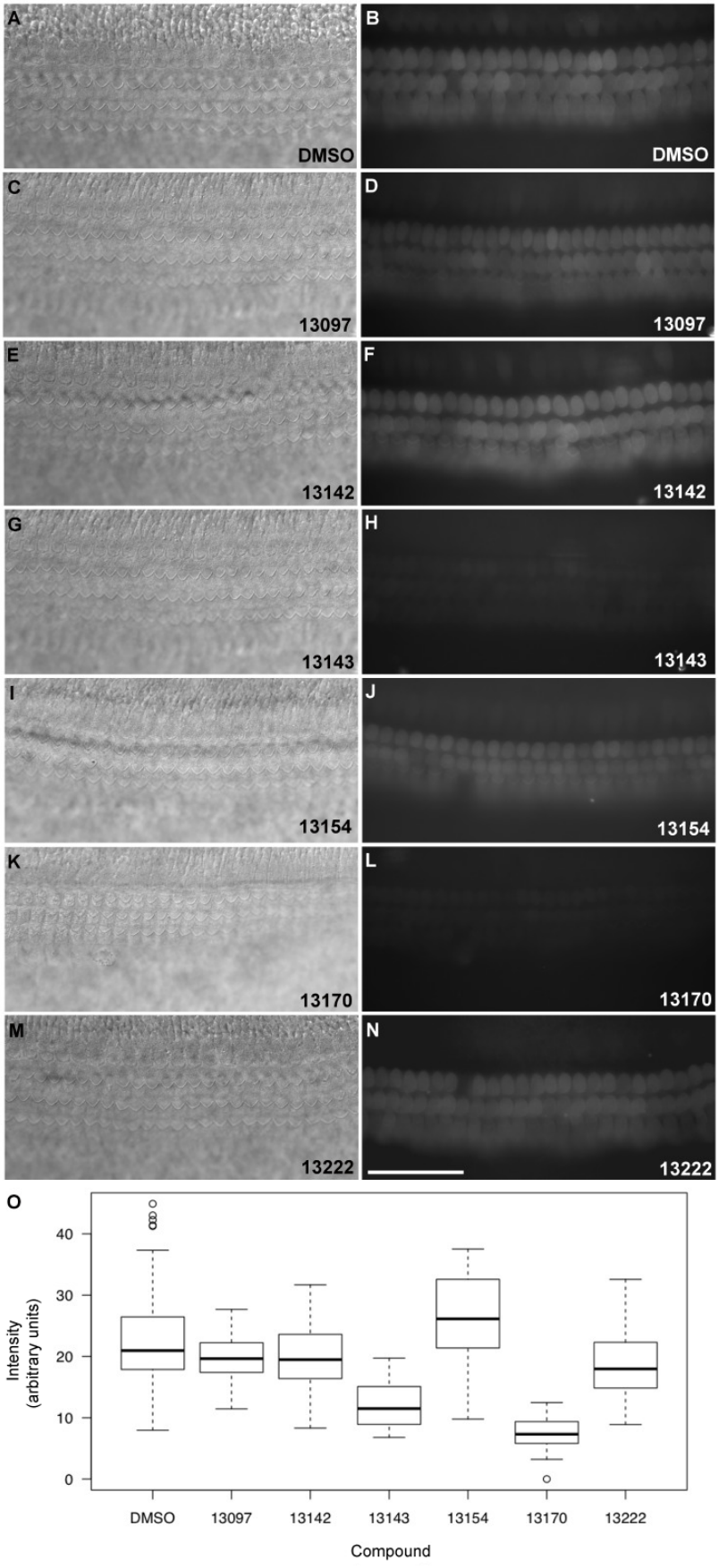
A
DMSO
B
DMSO
C
13097
D
13097
E
13142
F
13142
G
13143
H
13143
I
13154
J
13154
K
13170
L
13170
M
13222
N
13222
O
Intensity (arbitrary units)
0
10
20
30
40
DMSO
13097
13142
13143
13154
13170
13222
Compound

Figure 4.13: *Effects of lead otoprotectants on gentamicin-Texas Red (GTTR) loading in mouse cochlear cultures.*

Representative **(A, C, E, G, I, K, and M)** DIC and **(B, D, F, H, J, L, and N)** fluorescent images of cultures from P2 pups that were exposed to 0.2 µM GTTR for 10 minutes in presence of **(A and B)** 1% DMSO (n=21), **(C and D)** 100 µM 13097 (n=5), **(E and F)** 100 µM 13142 (n=6), **(G and H)** 100 µM 13143 (n=4), **(I and J)** 100 µM 13154 (n=3), **(K and L)** 100 µM 13170 (n=6), and **(M and N)** 100 µM 13222 (n=6). Scale bar is 50 µm. **(O)** Box-and-whisker plot of background-corrected intensity values for fluorescence intensity (arbitrary units) in first-row OHCs in cultures exposed to GTTR in presence of DMSO, 13097, 13142, 13143, 13154, 13170, and 13222. Thick line = median; boxes = interquartile range (IQR). Whiskers extend an additional 1.5× IQR beyond the boxes. Outliers are shown as white circles. Figure taken from Kenyon et al., 2017.

4.2.5.5 The Effect of Hair Bundle Disruption on Transduction Ability

Many of the compounds that we identified as being otoprotective were found to cause some disruption of the mechanosensory hair bundle morphology. For this reason, I investigated whether it was this bundle disruption that underlay the protectiveness of the compound, due to this effect then rendering the MET channels non-functional. In order to assess this hypothesis I developed a new experimental paradigm with several experimental conditions, to investigate whether the compounds caused the observed hair bundle damage after only 24 hours exposure time and whether if the compound was then washed away, this bundle damage was sufficient to prevent the HC loss caused by subsequent exposure to 5 µM gentamicin for 48 hours. Additionally, I investigated the loading of GTTR (and occasionally FM 1-43) into HCs from cultures treated with the compound for 24 hours, to see if AG loading was reduced by this amount of compound exposure. Of the 8 compounds that caused some disruption to bundle morphology when tested at 50 µM in the presence of gentamicin (13087, 13104, 13142, 13150, 13170, 13190, 13196 and 13228), I tested 5 in this experimental paradigm (13087, 13142, 13150, 13170 and 13196). Compounds 13104, 13190 and 13228 were not tested due to time restrictions.

4.2.5.5.1 UoS 13087 (AM 92016), 13142 ((±)-1-(1,2-Diphenylethyl) piperidine) and 13196 (m-Chlorophenylbiguanide)

Cochlear cultures treated with 0.5% DMSO for 24 hours followed by HBHBSS for 48 hours maintained control characteristics of V-shaped OHC bundles (Figure 4.14A). When treated with 0.5% DMSO for 24 hours followed by 5 µM gentamicin for 48 hours, there was a significant loss of basal OHCs (Figure 4.14B), similarly to the standard experimental paradigm presented in Chapter 3 (Figure 3.1). Following incubation with 50 µM 13087 or 13142 for 24 hours, the morphology of the mechanosensory hair bundle appeared unperturbed (Figures 4.14C and 4.15C). With 50 µM 13196, however, the morphology of the mechanosensory hair bundle appeared slightly disrupted (Figure 4.16C).

When 13087 was washed off of the cochlear culture after 24 hours (three 1 minute washes in 2 ml HBHBSS) and 5 µM gentamicin then applied for 48 hours, the compound still provided anterograde protection against the gentamicin-induced loss of OHCs (Figure 4.14D). The HCs were extremely grown out of position and the morphology of the hair bundle was disrupted but the OHCs were still present. When 13142 and 13196 were washed off of the cochlear cultures after 24 hours and 5 µM gentamicin applied for 48 hours, the compounds still provided partial anterograde protection against the gentamicin-induced loss of OHCs (Figures 4.15D and 4.16D).

Despite the hair bundle morphology appearing undisrupted by 24 hour incubation with 13087, when tested for the loading of GTTR or FM 1-43 into HCs after 24 hour exposure, there was a significant reduction in the loading of both transduction markers (Figure 4.14F-J). The average cellular fluorescence in the control condition, after 24 hour incubation in 0.5% DMSO followed by 20 minutes exposure to GTTR, was 202.0 (± 6.1) (n=10, from one animal). When treated with 13087 for 24 hours prior to GTTR exposure, the average cell fluorescence reduced by 33% to 133.3 (± 7.7) (n=10, from one animal). An unpaired *t* test revealed that this difference was statistically significant ($p < 0.001$). The average cellular fluorescence in the control condition, after 24 hour incubation in 0.5% DMSO followed by 5 minutes exposure to FM 1-43, was 244.8 (± 0.3) (n=10, from one animal). When treated with 13087 for 24 hours prior to FM 1-43 exposure, the average cell fluorescence reduced by 32% to 166.8 (± 10.3) (n=10, from one animal). An unpaired *t* test revealed that this difference was significant ($p < 0.001$).

When tested for the loading of GTTR into HCs after 24 hour exposure to 13142, there was a significant reduction in its loading. The average cellular fluorescence in the control condition,

after 24 hour incubation in 0.5% DMSO followed by 20 minutes exposure to GTTR, was 69.3 (± 2.2) (n=10, from one animal). When treated with 13142 for 24 hours prior to GTTR exposure, the average cell fluorescence reduced by 30% to 48.4 (± 1.9) (n=10, from one animal) (Figure 4.15F-H). An unpaired *t* test revealed that this difference was statistically significant ($p < 0.001$).

When tested for the loading of GTTR into HCs after 24 hour exposure to 13196, there was a significant reduction in its loading (Figure 4.16F-H). The average cellular fluorescence in the control condition, after 24 hour incubation in 0.5% DMSO for 24 hours followed by 20 minutes exposure to GTTR, was 101.2 (± 2.0) (n=10, from one animal). When treated with 13196 for 24 hours prior to GTTR exposure, the average cell fluorescence reduced by 85% to 15.2 (± 0.8) (n=10, from one animal). An unpaired *t* test revealed that this difference was statistically significant ($p < 0.001$).

Taken together, these data implied that there was some block or disruption of MET channel function after 24 hour exposure to 13087, 13142 and 1396, reducing AG entry into HCs. Furthermore, this reduction in loading was sufficient to prevent at least some degree of HC loss by delaying the accumulation and consequent onset of AG-induced HC death.

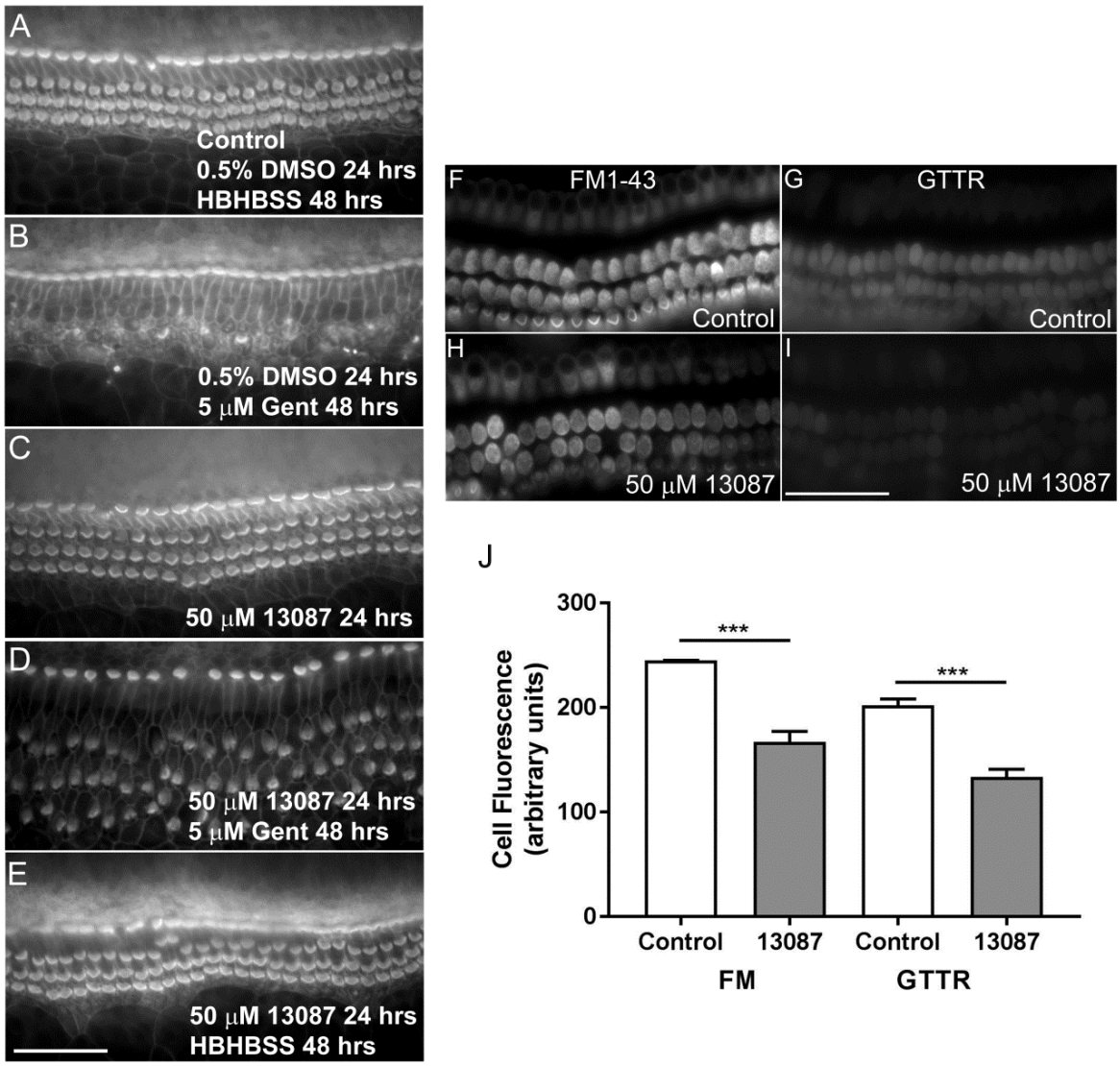

Figure 4.14: *24 hours incubation with 50 µM 13087 led to hair bundle disruption, a reduction in FM 1-43 and GTTR loading into HCs, and subsequent protection from OHC loss following washout and 48 hours, 5 µM gentamicin exposure.*

Cochlear cultures were treated with 50 µM 13087 for 24 hours. The compound was then washed off and the culture was tested for **(A-E)** protection against subsequent 5 µM gentamicin incubation for 48 hours or **(F-J)** reduction of FM 1-43 and GTTR loading. **(A-E)** Cultures incubated with **(A)** 0.5% DMSO for 24 hours followed by HBHBSS for 48 hours, **(B)** 0.5% DMSO for 24 hours followed by 5 µM gentamicin for 48 hours, **(C-E)** 50 µM 13087 for 24 hours followed by **(C)** fixation, **(D)** 5 µM gentamicin for 48 hours or **(E)** HBHBSS for 48 hours. **(F-J)** Live imaging of fluorescent dye loading into cochlear culture HCs, incubated in 0.5% DMSO or 50 µM 13087 for 24 hours. Control **(F)** FM 1-43 or **(G)** GTTR loading. 24 hour incubation with 50 µM 13087 followed by **(H)** FM 1-43 or **(I)** GTTR exposure. **(J)** Quantification of HC fluorescence. Scale bars are 50 µm.

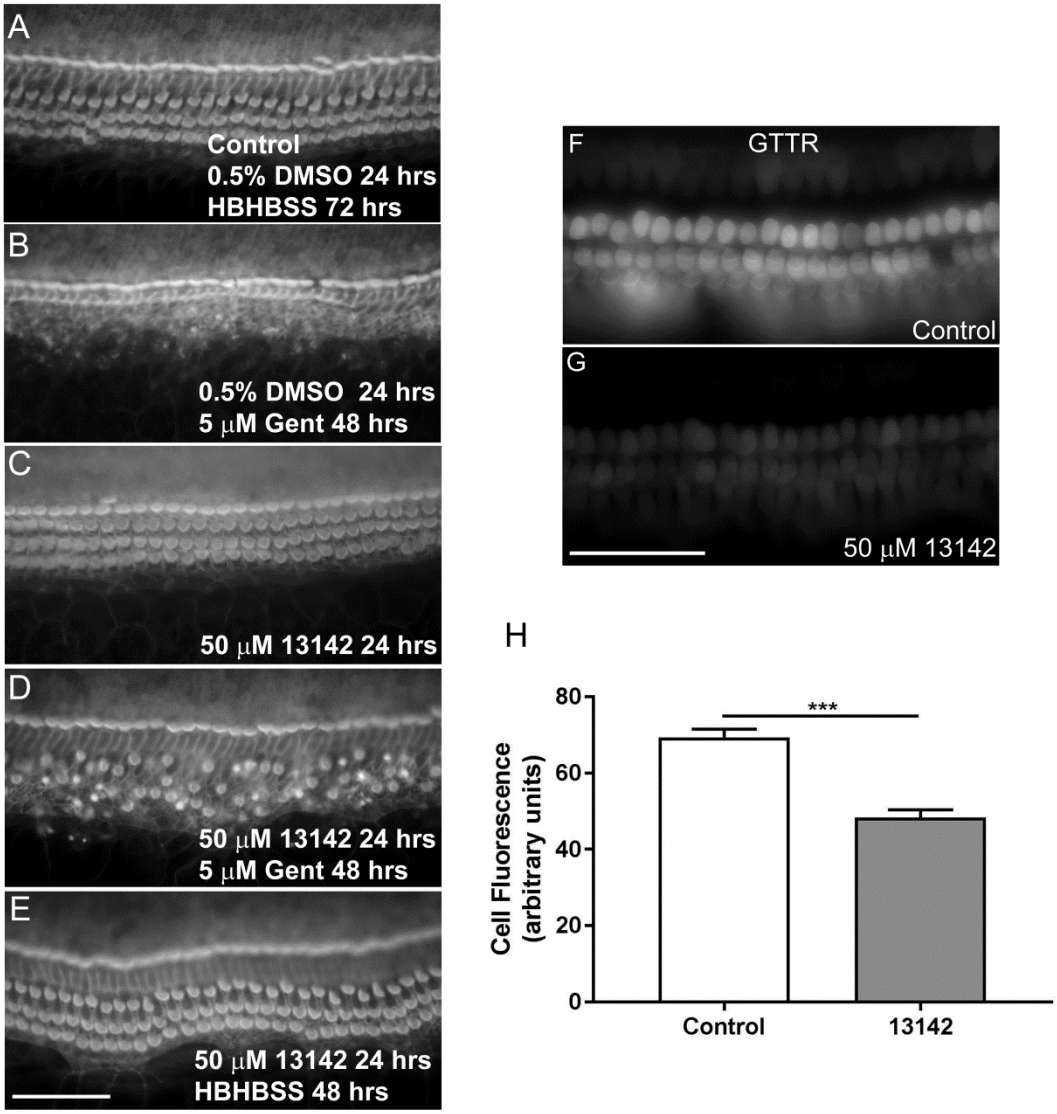

Figure 4.15: *24 hours incubation with 50 µM 13142 led to a reduction in GTTR loading into HCs despite no obvious hair bundle disruption, and subsequently partial protection from OHC loss following washout and 48 hours, 5 µM gentamicin exposure.*

Cultures were treated with 50 µM 13142 for 24 hours. The compound was then washed off and the culture was tested for **(A-E)** protection against subsequent 5 µM gentamicin incubation for 48 hours or **(F-H)** reduction of GTTR loading. **(A-E)** Cultures incubated with **(A)** 0.5% DMSO for 24 hours followed by HBHBSS for 48 hours, **(B)** 0.5% DMSO for 24 hours followed by 5 µM gentamicin for 48 hours, **(C-E)** 50 µM 13142 for 24 hours followed by **(C)** fixation or 48 hour incubation with **(D)** 5 µM gentamicin or **(E)** HBHBSS. **(F-H)** Live imaging of fluorescent dye loading into cochlear culture HCs, incubated with HBHBSS or 50 µM 13142 for 24 hours. GTTR loading into HCs following 24 hour incubation with **(F)** HBHBSS or **(G)** 50 µM 13142. **(H)** Quantification of HC fluorescence. Scale bars are 50 µm.

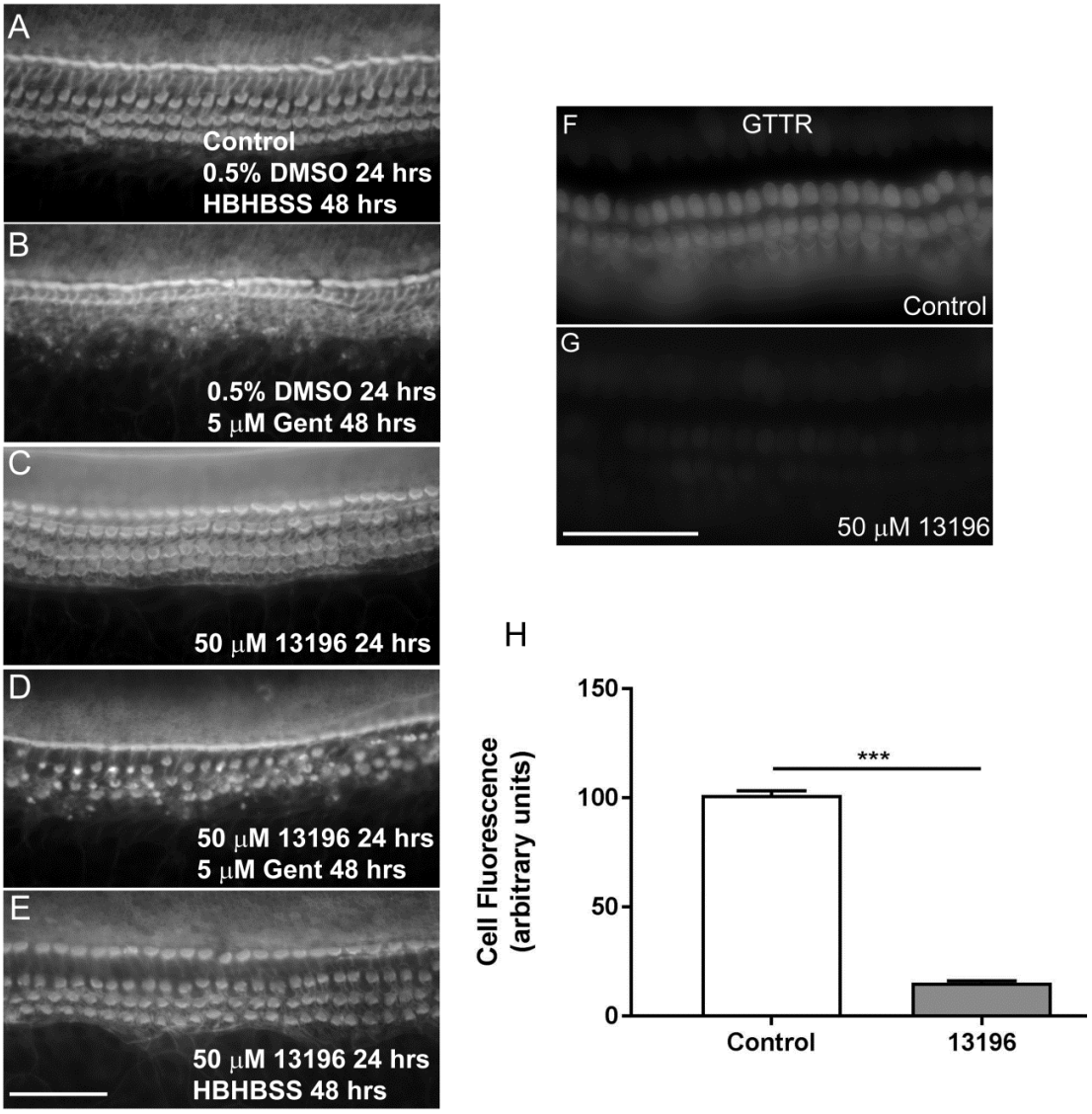

Figure 4.16: *24 hours incubation with 50 µM 13196 led to hair bundle disruption, a reduction in GTTR loading into HCs, and subsequently partial protection from OHC loss following washout and 48 hours, 5 µM gentamicin exposure.*

Cultures were treated with 50 µM 13150 for 24 hours. The compound was then washed off and the culture was tested for **(A-E)** protection against subsequent 5 µM gentamicin incubation for 48 hours or **(F-H)** reduction of GTTR loading. **(A-E)** Cultures incubated with **(A)** 0.5% DMSO for 24 hours followed by HBHBSS for 48 hours, **(B)** 0.5% DMSO for 24 hours followed by 5 µM gentamicin for 48 hours, **(C-E)** 50 µM 13150 for 24 hours followed by **(C)** fixation or 48 hour incubation with **(D)** 5 µM gentamicin or **(E)** HBHBSS. **(F-H)** Live imaging of fluorescent dye loading into cochlear culture HCs, incubated with HBHBSS or 50 µM 13150 for 24 hours. GTTR loading into HCs following 24 hour incubation with **(F)** HBHBSS or **(G)** 50 µM 13150. **(H)** Quantification of HC fluorescence. Scale bars are 50 µm.

4.2.5.5.2 UoS 13150 - FPL 64176

When treated with 50 µM 13150 for 24 hours, the morphology of the mechanosensory hair bundle was greatly disrupted, with no evidence of the characteristic V-shaped OHC bundles along the entirety of the cochlear coil (Figure 4.17C). When 13150 was then washed off of the cochlear culture and 5 µM gentamicin applied for 48 hours, the compound still provided complete protection against the gentamicin-induced loss of OHCs (Figure 4.17D). Interestingly, when 13150 was washed off of the cochlear culture and HBHBSS applied for 48 hours, there was a loss of IHCs (Figure 4.17E), dissimilarly to what was observed following the application of gentamicin (Figure 4.17D). This result is likely explained by the fact that 13150 is a calcium channel agonist. As IHCs have a larger number of voltage-gated calcium channels than OHCs, the IHCs presumably loaded with a large intracellular calcium concentration over 24 hours. Following compound washout and gentamicin application, calcium loading into IHCs was reduced due to competition for entry through the MET channel, whereas when HBHBSS was applied calcium loading was not inhibited. This postulation is supported by the comparison of IHC loss when cochlear cultures were treated with 50 µM 13150 alone (Figure 4.3) and the preservation of IHCs when co-incubated with gentamicin (Figure 4.1).

When tested for the loading of GTTR into HCs after 24 hour exposure to 13150, there was a complete block of its loading (Figure 4.17F-H). The average cellular fluorescence in the control condition, after 24 hour incubation in 0.5% DMSO followed by 20 minutes exposure to GTTR, was 113.3 (± 2.6) (n=10, from one animal). When treated with 13150 for 24 hours prior to GTTR exposure, the average cell fluorescence reduced by 97% to 3.1 (± 0.2) (n=10, from one animal). An unpaired *t* test revealed that this difference was statistically significant ($p < 0.001$).

Taken together, these data imply that there was full inhibition of MET channel function after 24 hour exposure to the compound and that this is what underlay the protective ability of the compound.

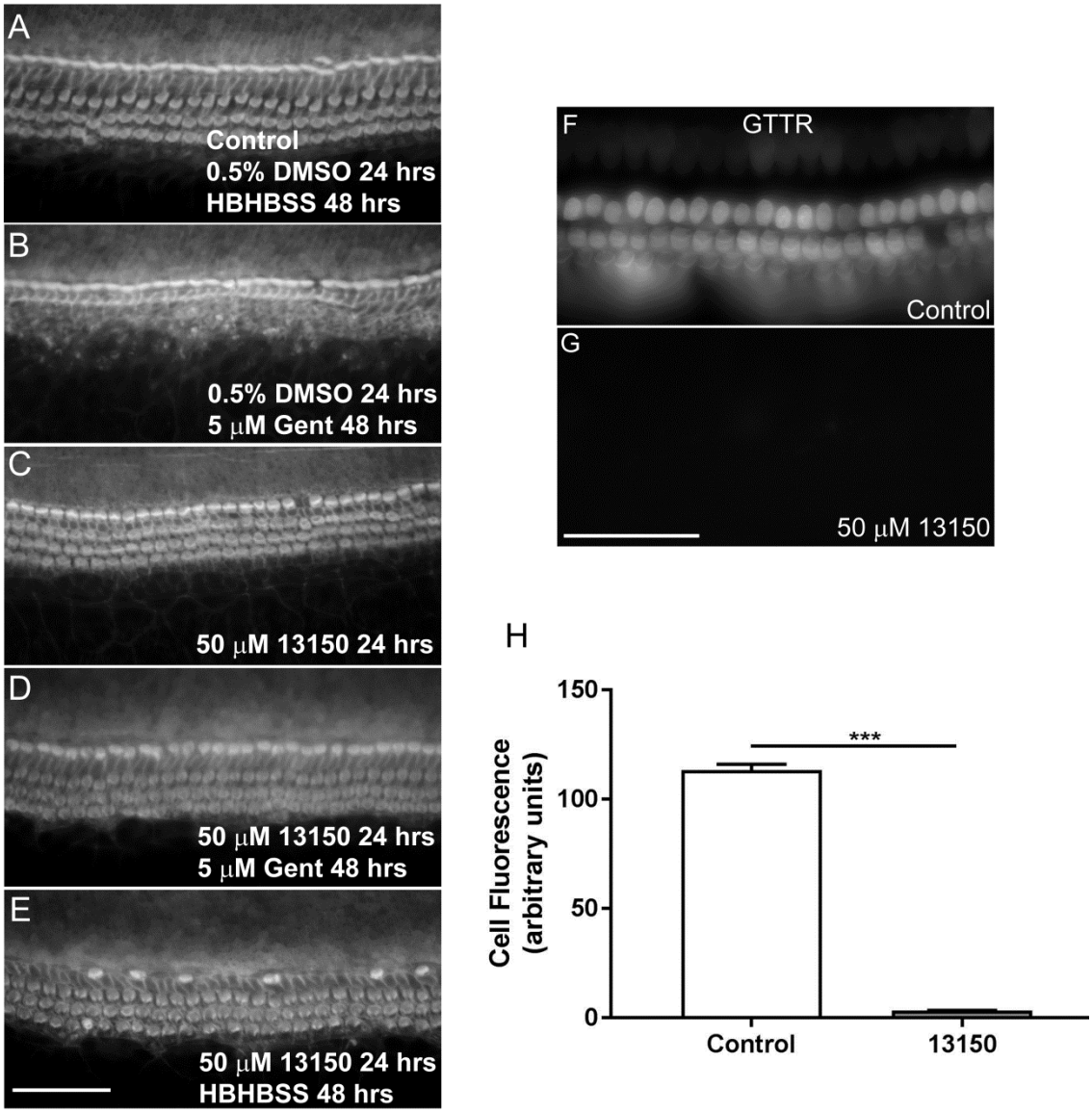

Figure 4.17: *24 hour incubation with 50 µM 13150 led to hair bundle disruption, a reduction in GTTR loading into HCs, and subsequent complete protection from OHC loss following washout and 48 hours, 5 µM gentamicin exposure.*

Cultures were treated with 50 µM 13150 for 24 hours. The compound was then washed off and the culture was tested for **(A-E)** protection against subsequent 5 µM gentamicin incubation for 48 hours or **(F-H)** reduction of GTTR loading. **(A-E)** Cultures incubated with **(A)** 0.5% DMSO for 24 hours followed by HBHBSS for 48 hours, **(B)** 0.5% DMSO for 24 hours followed by 5 µM gentamicin for 48 hours, **(C-E)** 50 µM 13150 for 24 hours followed by **(C)** fixation or 48 hour incubation with **(D)** 5 µM gentamicin or **(E)** HBHBSS. **(F-H)** Live imaging of fluorescent dye loading into cochlear culture HCs, incubated with HBHBSS or 50 µM 13150 for 24 hours. GTTR loading into HCs following 24 hour incubation with **(F)** HBHBSS or **(G)** 50 µM 13150. **(H)** Quantification of HC fluorescence. Scale bars are 50 µm.

4.2.5.5.3 UoS 13170 - ZK 93423 HCl

When treated with 50 µM 13170 for 24 hours, the morphology of the mechanosensory hair bundle was greatly disrupted, with no evidence of the characteristic V-shaped OHC bundles along the length of the cochlear culture (Figure 4.18C). When 13170 was washed off of the cochlear culture after 24 hours and 5 µM gentamicin applied for 48 hours, the compound provided no protection against the gentamicin-induced loss of OHCs, but rather exacerbated the damage, leading to IHC loss as well as the characteristic OHC loss (Figure 4.18D). This also occurred when the compound was washed off after 24 hours and then HBHBSS (a control saline solution in which gentamicin is dissolved) was incubated for 48 hours.

When tested for the loading of GTTR or FM 1-43 into HCs after 24 hour exposure, there was a complete block of the loading of both fluorescent compounds (Figure 4.18F-J). The average cellular fluorescence in the control condition, after 24 hour incubation in 0.5% DMSO followed by 20 minutes exposure to GTTR, was 70.94 (± 3.1) (n=10, from one animal). When treated with 13170 for 24 hours prior to GTTR exposure, the average cell fluorescence reduced by 99% to 0.7 (± 0.2) (n=10, from one animal). An unpaired *t* test revealed that this difference was statistically significant ($p < 0.001$). The average cellular fluorescence in the control condition, after 24 hour incubation in 0.5% DMSO followed by 15 minutes exposure to FM 1-43, was 101.4 (± 4.7) (n=10, from one animal). When treated with 13170 for 24 hours prior to FM 1-43 exposure, the average cell fluorescence reduced by 96% to 3.6 (± 0.6) (n=10, from one animal). Again, an unpaired *t* test revealed that this difference was significant ($p < 0.001$).

Taken together, these data imply that 13170 caused dysfunction of the MET channel after 24 hours incubation, and over time, even in the absence of the compound or gentamicin, caused HC toxicity.

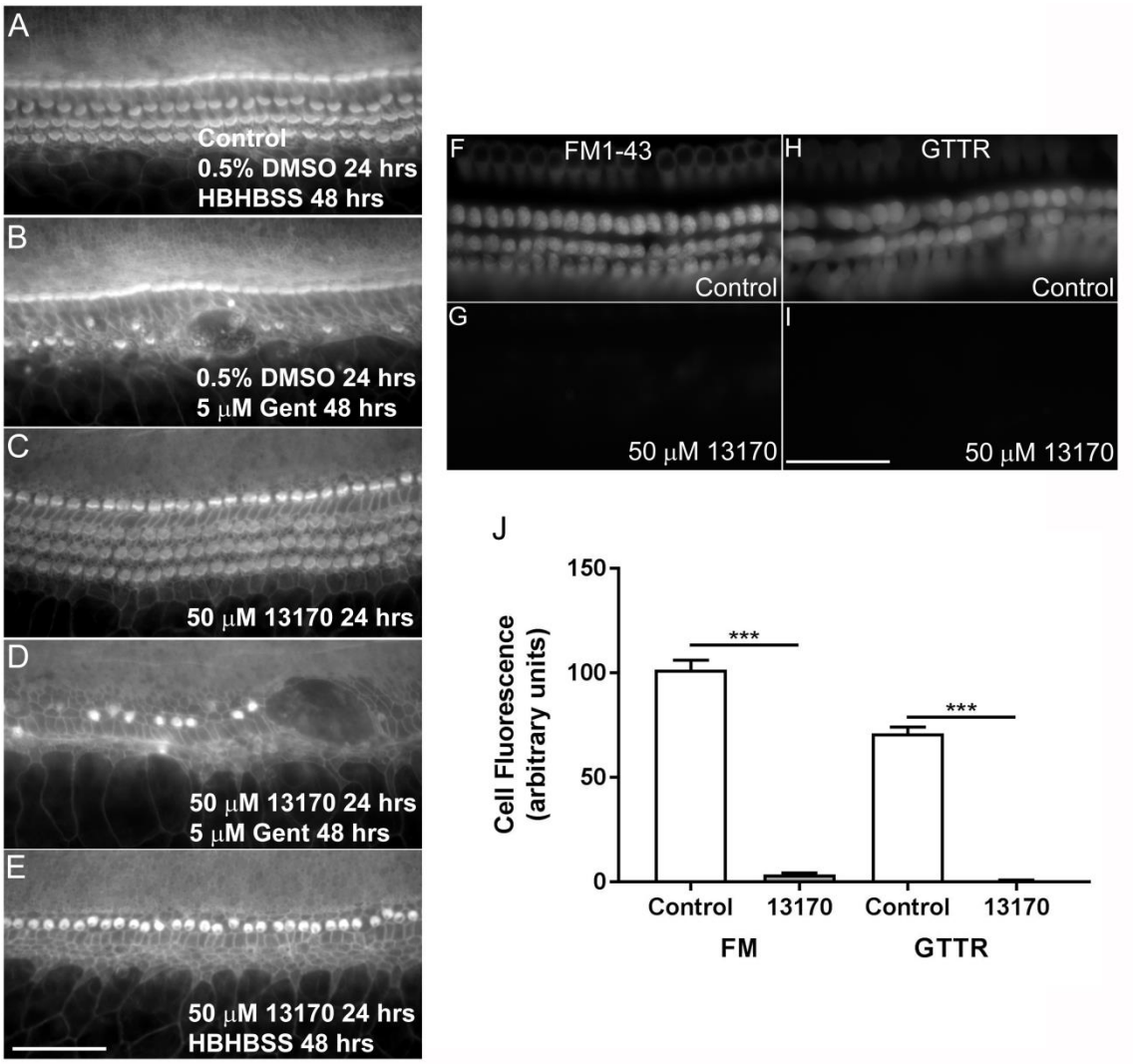

Figure 4.18: *24 hour incubation with 50 µM 13170 led to hair bundle disruption and a reduction of FM 1-43 and GTTR loading into HCs. However, no protection from OHC loss was observed following washout and 48 hours, 5 µM gentamicin exposure.*

Cultures were treated with 50 µM 13170 for 24 hours. The compound was then washed off and the culture was tested for **(A-E)** protection against 5 µM gentamicin incubation for 48 hours or **(F-J)** reduction of FM 1-43 or GTTR loading. **(A-E)** Cultures incubated with **(A)** 0.5% DMSO for 24 hours followed by HBHBSS for 48 hours, **(B)** 0.5% DMSO for 24 hours followed by 5 µM gentamicin for 48 hours, **(C-E)** 50 µM 13170 for 24 hours followed by **(C)** fixation or 48 hour incubation with **(D)** 5 µM gentamicin or **(E)** HBHBSS. **(F-J)** Live imaging of fluorescent dye loading into cochlear culture HCs, incubated with HBHBSS or 50 µM 13170 for 24 hours. Control **(F)** FM 1-43 or **(H)** GTTR loading. 24 hours incubation with 50 µM 13170 followed by **(G)** FM 1-43 or **(I)** GTTR exposure. **(J)** Quantification of HC fluorescence. Scale bars are 50 µm.

4.3 Summary

Screening of the Tocris Ion Channel library has led to the identification of several novel otoprotectants. Of the 160 compounds tested in zebrafish, 78 were taken forward to mouse cochlear cultures. Of these 78, 13 provided protection against the 48 hours, 5 μM gentamicin-induced loss of HCs when tested at 50 μM, and 3 of these were still protective at 10 μM. When tested at 50 μM in the presence of 5 μM gentamicin, 8 caused disruption to sensory hair bundle morphology, and 1 when tested at 10 μM. When tested alone at 50 μM in the absence of gentamicin, 5 caused hair bundle disruption; alone at 100 μM, 4 were generally cytotoxic and 4 caused bundle disruption. Our 2 most effective otoprotectants both provided half-protection in the nanomolar range. Our most effective compound (13097) was protective when tested at a high concentration (300 μM) against 10 μM gentamicin for 48 hours; however, when tested (≤ 50 μM) against 5 μM gentamicin for 72 hours, it failed to protect. Modification of 2 Tocris compounds of interest failed to yield more effective otoprotectants.

After the exclusion of any compounds that caused adverse effects on the morphology of the mechanosensory hair bundle or displayed any intrinsic toxicity, 5 potential otoprotectants remained. When all 13 compounds were tested for their effect on MET channel currents 6 compounds showed an interaction with the channel, all displaying voltage-dependent, permeant blocking characteristics. When tested for their effect on the basolateral potassium channel currents, 11 showed block of the channel, with varying degrees of current inhibition. Despite the potassium channel block, none of the 5 lead compounds caused any shift in the resting membrane potential of HCs. When tested for their ability to block GTTR loading into HCs in a short time assay, only 1 compound reduced its loading.

Five of the 8 compounds that caused hair bundle damage when tested at 50 μM in the presence of gentamicin were tested to see if they caused a reduction in GTTR loading 24 hours after the onset of application, and if such pre-treatment provided anterograde protection to subsequent gentamicin exposure. After 24 hours, all 5 compounds significantly reduced GTTR loading to varying degrees, and all but 1 provided some level of anterograde HC protection.

4.4 Discussion

Our screening of the Tocris Ion Channel library has further reinforced the usefulness and viability of zebrafish pre-screening when conducting large otoprotectant drug screening projects. By using zebrafish as a preliminary screening tool we have more than doubled the number of mammalian otoprotectants previously identified using this approach (Chiu et al., 2008; Owens et al., 2008; Ou et al., 2009, 2012; Vlasits et al., 2012; Thomas et al., 2015; Hirose et al., 2016; Kruger et al., 2016). Furthermore, we have identified 2 compounds that protect in a mammalian system in the nanomolar range - an unparalleled protective efficacy reported to date. Due to the restrictions on the number of viable cochlear cultures that can be produced on a regular basis, we would not have been able to achieve these results with mammalian system screening alone. By comparing the number of compounds that were protective in each different zebrafish screen and subsequently found to also be protective in cochlear cultures, the zebrafish screening process has the potential to be refined to have a greater transferable efficiency to mammalian systems. Of the three zebrafish screens, the assay that tested protection against neomycin-induced HC damage yielded the highest number of compounds that were also protective in mouse cochlear cultures. Ten of the 13 compounds were protective in this assay, relative to 2 that reduced FM 1-43FX loading and 5 that reduced the loading of neomycin-Texas Red. Only 1 of the 19 compounds that were successful in each of the three zebrafish assays was protective in mouse cochlear cultures. Ten of the 13 compounds would have been identified in the neomycin protection assay alone, so the added value of the FM 1-43FX and neomycin-Texas Red loading assays in these large-scale screens is questionable.

Despite the usefulness of zebrafish pre-screening, caution must be executed when relying solely on zebrafish protection assays to determine which compounds are selected for further screening in mammalian systems. Of the 72 that were protective in zebrafish, 12 were consistently protective in mouse cochlear cultures. This signifies a 17% transferrable efficacy. Of the 6 compounds that were selected that did not protect in zebrafish, but had a similar chemical structure to some of those that did, 1 was consistently protective. This again signifies a 17% transferable efficacy. Although these numbers are small, it is evident that zebrafish screening alone would lead to a number of false negatives, with potentially effective mammalian otoprotectants being missed in this screening process. One way to avoid this issue is to refine and improve the procedure, by identifying the most effective zebrafish assay in terms of transferable efficacy and primarily using the results of this assay to select structurally similar compounds for mammalian screening.

The cochlear culture screening conducted in this chapter revealed the need for an extensive screening procedure in mammalian systems. When the 12 compounds that consistently protected HCs were put through rigorous additional screening for adverse effects on bundle morphology or any intrinsic toxicity at higher concentrations, only 3 remained (compounds 13097, 13142 and 13143). This means that the majority of identified protectants had the potential to cause adverse effects in the cochlea if transferred directly to an *in vivo* model, reinforcing the notion that a thorough screening regime should be adhered to when searching for clinically-viable compounds. It is vital that compounds are assessed for any adverse effect on bundle morphology, especially due to the disruptive effect this may have on auditory transduction and consequent hearing ability.

Of the 13 compounds that provided protection, almost half blocked the MET channel. We therefore assumed that they were providing protection against AG damage by preventing antibiotic entry into the HCs. However, when half of the MET channel blockers were tested for their ability to block the entry of GTTR into HCs, all failed to reduce its loading. Noteworthy here is that native (un-tagged) gentamicin was also unable to reduce GTTR loading (data not shown). Several conclusions can be made from this observation. Firstly, evident interaction with the MET channel current is not indicative of the compound's ability to prevent AG entry through this ion channel. Secondly, precaution should be taken when using GTTR as a surrogate for gentamicin trafficking through the cochlea and into HCs, despite its ongoing use for this purpose (Steyger et al., 2003). The MET channel-blocking compounds may prevent the entry of native gentamicin into HCs, however it could be that GTTR has a higher affinity for the channel and is therefore able to compete for entry more efficiently, reducing the likelihood of compounds being able to prevent its loading. To note here, all of the Tocris compounds showed maximal block at the intermediate potentials and displayed a release of block at both extremes of depolarisation and hyperpolarisation, indicative of them behaving as permeant blockers. The fact that they are readily reversible and do not remain in the channel to block it continuously could explain the somewhat surprising GTTR result.

Interestingly, the two most effective otoprotectants identified in this chapter (13097 and 13143) have both been identified in the literature as K_v7 potassium channel inhibitors. The $K_v7.4$ potassium channel subunit is encoded by the KCNQ4 gene and is known to play a role in the regulation of neuronal excitability, particularly in the sensory cells of the cochlea. For this reason we hypothesised that these two compounds may be protecting by blocking the outward potassium channels in the OHCs of our cochlear cultures, thereby depolarising the cell and reducing the entry of the positively charged AGs. However, when tested for their influence

on the resting membrane potential both had no effect, thereby eliminating depolarisation, at least in the short term, as a potential mechanism of protection. In this study 13143 was shown to reduce GTTR loading however it displayed no interaction with the MET channel and did not shift the resting potential of the cell, implying that its block of GTTR loading was irrespective of its mechanism of protection. Later chapters in this thesis also elucidate an effect of 13143 on AG-induced mitochondrial dysfunction. However this will be discussed later, in Chapter 8.

The issue with our lead compounds being K_v7 channel blockers arises from our use of postnatal day 2 mouse cochlear cultures. Around postnatal day 8, a mature OHC K^+ current starts to be expressed ($I_{K,n}$) and this coincides with a decrease of $I_{k,neo}$ (Marcotti and Kros, 1999) – the potassium current that we investigated in our experiments. If we had tested our compounds on cultures made from a later developmental stage (> postnatal day 8), our lead compounds may have caused a block of the more mature potassium channels and consequent damage to HCs as a result of continuous depolarisation (Oliver et al., 2003), due to the strong influence of plasma membrane K^+ efflux channels in the regulation of apoptosis (Kondratskyi et al., 2015). For this reason, we should have tested them at a later developmental stage. However, dissecting the cochlea from > P8 mice and keeping the basal coil intact is notoriously difficult. As we are trying to replicate the clinical manifestation of AG ototoxicity, with HC loss primarily from the basal section, it is important to experiment on this cochlear region. We therefore had to compromise between the cochlear region of interest and the developmental expression of relevant ion channels. However, the concentration at which our lead compound (13097) protects 50% of basal-coil HCs from 5 μM gentamicin is an order of magnitude below its IC_{50} for KCNQ4-encoded K^+ channels (Oliver et al., 2003), so channel block may not be an issue. We are now awaiting in vivo confirmation of the otoprotective ability of 13097.

Somewhat surprisingly, our most effective compound (13097), protective at nanomolar concentrations, was unable to provide any protection when tested against a longer time exposure to gentamicin. Furthermore, it was only protective against a higher gentamicin concentration when tested at a high molar excess of its minimum protective concentration in our standard protection assay, and even then it did not protect against AG-induced bundle damage. This highlights the complexity of the AG-induced cell-death process and also adds ambiguity to the mechanism by which the compound is protecting. Ideally, 13097 should have been tested at a higher concentration in the 72 hour assay however this was not possible due to stock limitations.

Lastly, experiments assessing the effect of hair bundle morphological disruption on GTTR loading and consequent protection provided some interesting results. All of the compounds that were incubated for 24 hours caused a significant reduction in GTTR loading, even if there was no obvious damage to the morphology of the hair bundle. Four of the 5 compounds then provided anterograde protection from subsequent gentamicin exposure, to varying degrees. The fifth compound caused generalised cytotoxicity after 72 hours even in the absence of gentamicin, so conclusions cannot be made regarding its subsequent protective ability. These results suggest that in our protection assay, any compounds that do cause an observable disruption to hair bundle morphology after 48 hours should be excluded from further screening, as they render the function of the MET channel compromised to some degree and this potentially underlies at least part of its protective ability. Moreover, high-resolution microscopy should be used to ascertain the effect of these compounds on hair bundle morphology, due to the limitations of detection with lower-resolution imaging. Preserving MET channel function is a vital task when searching for otoprotectants, so this part of the screening procedure should be considered imperative.

5 Assessing the Otoprotective Potential of d-Tubocurarine and Berbamine

5.1 Introduction

5.1.1 Compound Choice

Historically, d-Tubocurarine (dTC) is known to be the main active ingredient of the arrow poison curare. It is an alkaloid that can be obtained from the bark of the plant *Chondrodendron tomentosum* (Perotti, 1977). Characterised as a nicotinic antagonist, studies have shown that it blocks the acetylcholine receptor response in guinea-pig OHCs (Housley and Ashmore, 1991; Eróstegui et al., 1994) and also MET channels in the cochlear HCs of neonatal mice (Glowatzki et al., 1997). A study investigating the MET channel pore identified curare as being a non-permeant blocker of these channels in turtle sensory HCs (Farris et al., 2004); a quality that we sought to identify in a potential otoprotectant throughout this project. Other studies have shown that 1 mM curare can block 3 µM GTTR loading into HCs and that co-incubation of 1 mM curare and 0.1 mM gentamicin prevents AG-induced HC death (Alharazneh et al., 2011), suggesting a MET channel-blocking mechanism of protection. These characteristics rendered dTC an interesting compound to investigate in our search for otoprotectants, as a potential candidate for compound modification.

In the search for other MET channel-blocking compounds we identified berbamine, another naturally occurring alkaloid present in many plant species of the *Berberidaceae* family (Rahmatullah et al., 2014). Berbamine has an extremely similar chemical structure to dTC (Kirkwood et al., 2017). In Eastern medicine it has been used for centuries and is still of current interest due to its potential anti-cancer properties (Ji et al., 2009; Meng et al., 2013; Zhao et al., 2016). Zebrafish lateral line studies have revealed that 25 µM berbamine can protect neuromast HCs from the damage induced by both neomycin and gentamicin, tested at a concentration range of 50-400 µM (Kruger et al., 2016). This study also revealed that berbamine was able to block the loading of GTTR and FM 1-43 into zebrafish lateral line HCs, leading to the conclusion that berbamine protects similarly by acting as a competitive blocker of the MET channel, thereby preventing AG entry into HCs.

5.1.2 Aims

We investigated both dTC and berbamine for their otoprotective abilities in zebrafish and mouse cochlear cultures, assessing whether dTC also provides protection in zebrafish models

and whether berbamine is able to provide protection in mammalian systems. Comparing compound protection of neuromast and cochlear HCs provides further evidence of the viability of zebrafish pre-screening when searching for mammalian otoprotectants. We also provided full characterisation of the interaction of both compounds with the MET channel by performing electrophysiological experiments on mouse cochlear culture HCs. Comparative studies like this allow us to further ascertain what characteristics of a compound determine their otoprotective, MET channel-blocking abilities, thereby informing future studies and the design of potential otoprotectants.

5.2 Results

5.2.1 Screening for Otoprotection

5.2.1.1 Zebrafish Pre-Screening

*The zebrafish research presented in this section was collected by Emma Kenyon, University of Sussex. I performed the statistical analysis of the data.

The protective abilities of dTC and berbamine were initially assessed using a zebrafish lateral line protection assay, investigating whether the two compounds of interest could prevent the loss of neuromast HCs caused by exposure to either neomycin or gentamicin. These results are thoroughly documented in Kirkwood et al., 2017, however, in brief: dTC was found to provide complete protection against the damage induced by 1 hour exposure to 6.25 μM neomycin at concentrations ≥ 12.5 μM, with partial protection observed at 6.25 μM. Full protection against the damage induced by 6 hour exposure to 10 μM gentamicin was only observed at dTC concentrations ≥ 50 μM, with partial protection at 25 μM. Berbamine consistently provided protection at lower concentrations against both AGs. It provided full protection against the neomycin-induced neuromast damage at concentrations ≥ 12.5 μM, with partial protection even down to 1.55 μM, the lowest concentration tested. Berbamine offered full protection against 10 μM gentamicin damage at ≥ 25 μM, with partial protection at 12.5 μM. Noteworthy, no signs of toxicity due to either compound were observed at the highest concentration tested (200 μM).

5.2.1.2 Cochlear Culture Screening

dTC and berbamine were subsequently screened in mouse cochlear cultures to test if they would protect mammalian cochlear HCs from the damage induced by exposure to 5 μM gentamicin for 48 hours (Figure 5.1A–D). Such treatment results in the average loss of 88% of OHCs from the mid-basal region of the cochlea, with little effect if any on the survival of IHCs and apical OHCs (see Chapter 3). dTC and berbamine were found to be protective against the gentamicin-induced loss of OHCs (Figure 5.1A and B) at minimum concentrations of 25 μM and 20 μM respectively (Figure 5.1C and D), as quantified in Figure 5.1G and H, which show graphs of OHC counts from a 220 μm-long segment of the mid-basal region of mouse cochlear cultures.

As a further criterion to assess the suitability of a compound for use as an otoprotectant we examined the hair bundle morphology. No hair bundle damage was observed during exposure to either compound (Figure 5.1C and D). To determine if either compound had any adverse effects on HCs in the absence of gentamicin, they were tested alone at a higher concentration of 50 μM. Berbamine was found to be generally cytotoxic and killed all cell types in the cochlear culture (Figure 5.1H), whereas dTC had no adverse effect at this concentration (Figure 5.1E and G). Berbamine was tested alone at the lower concentrations of 20 and 30 μM and found to be equally toxic at 30 μM as it was at 50 μM but not at 20 μM, the concentration at which it showed protection (Figure 5.1F and H). When 30 μM berbamine was tested together with 5 μM gentamicin the same cytotoxic effect was observed as with 30μM berbamine alone (Figure 5.1H), highlighting the extremely narrow protective concentration range of this compound in cochlear cultures.

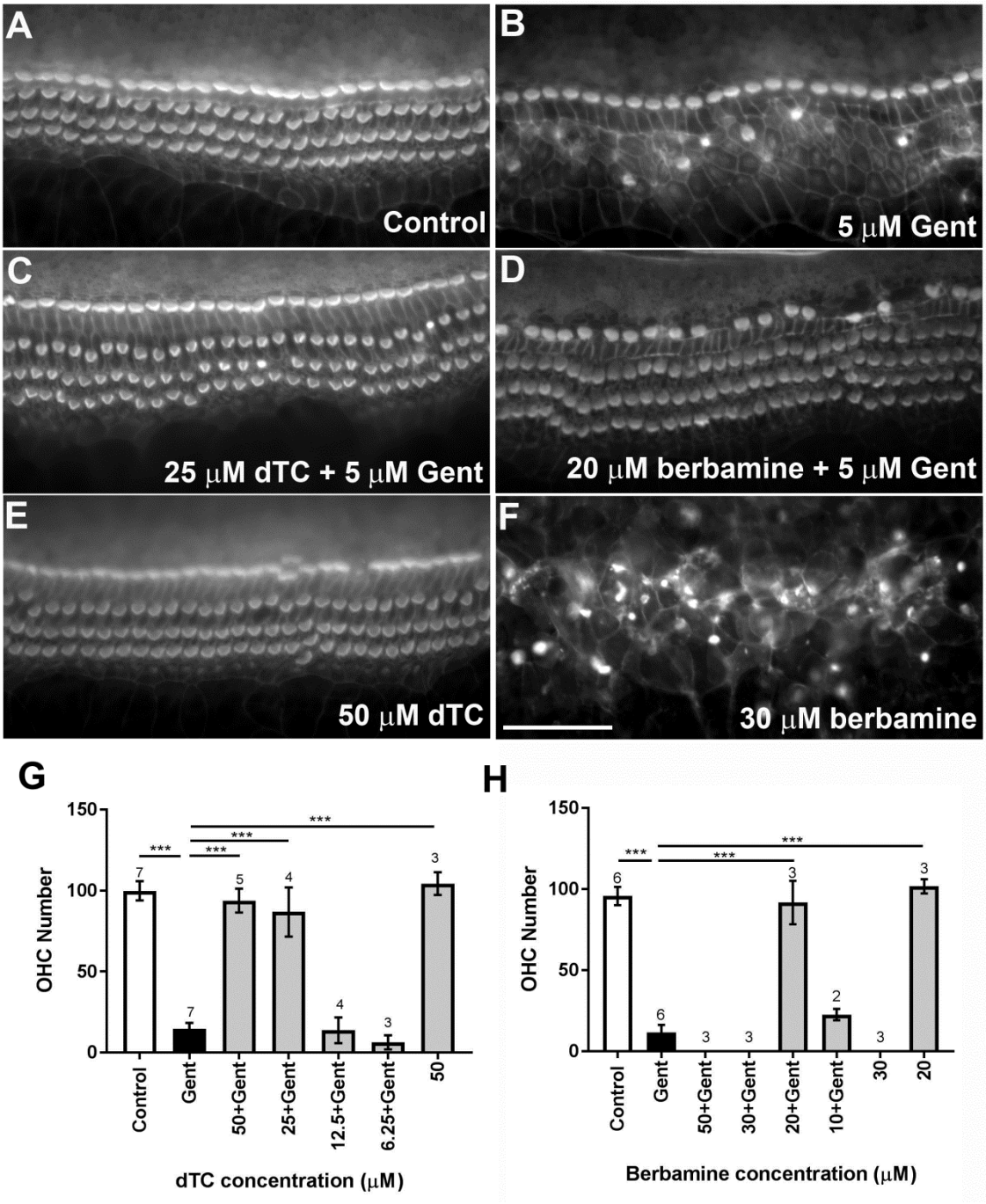

Figure 5.1: *d-Tubocurarine and berbamine protect mouse OHCs from gentamicin damage.*

(A) A control culture incubated for 48 hours in the presence of 0.5% DMSO. The sensory HC loss shown in **(B)**, caused by 48 hours incubation with 5 μM gentamicin and 0.5% DMSO can be prevented by co-incubation with 25 μM dTC **(C)** or 20 μM berbamine **(D)**. Cells incubated in 50 μM dTC in the absence of gentamicin were not damaged **(E)**, whereas 30 μM berbamine resulted in widespread loss of all cell types **(F)**. Scale bar is 50 μm. **(G-H)** Quantification of OHC survival in the control, 5 μM gentamicin, 5 μM gentamicin plus different concentrations of compounds and in compound alone-treated conditions.

5.2.2 Mechanism of Protection

5.2.2.1 The Effect of dTC and Berbamine on MET Channel Currents

* The electrophysiology presented in Figures 5.2E, 5.3 and 5.6G was performed by Nerissa Kirkwood, University of Sussex.

To ascertain whether the otoprotective nature of dTC and berbamine may be a result of their MET channel-blocking abilities, due to the consequent impedance of AG entry into HCs, we investigated their interaction with the MET channel using P2 mouse cochlear cultures. All recordings were performed on basal-coil HCs; the cells most susceptible to AG damage. dTC had previously been reported to behave as a MET channel blocker (Glowatski et al., 1997; Farris et al., 2004), however no such study had been conducted for berbamine. MET currents were recorded from OHCs as their membrane potential was stepped from -164 to +96 mV, before, during and after the local superfusion of dTC or berbamine, tested at concentrations ranging from 300 nM to 100 µM (dTC) or 1 to 30 µM (berbamine). When exposed to either compound, there was a reduction in MET current size when the cell was stepped to hyperpolarised potentials. At depolarised potentials this reduction was less pronounced and was dependent on the concentration of the compound. Examples of MET channel block by 30 µM dTC and berbamine can be seen in Figures 5.2A-C and 5.3A-C respectively. During superfusion of the compounds when the cell was held at negative potentials, on each cycle of the sine-wave there was an initial inward current peak, after which the current rapidly declined. This characteristic is indicative of an open-channel mechanism of block, as the compounds can only block the channel and reduce the current size once it is in the open conformation. This is a postulation further supported by investigation of MET current size in response to large step stimuli, which revealed an adaptation-like decline in the current sizes when exposed to the compounds; a response not observed in the controls, as detailed in Kirkwood et al., 2017. MET channel block and subsequent washout were very rapid, with current sizes making a complete recovery following re-superfusion of the control solution, suggesting that the block by both of these compounds is completely reversible.

The current-voltage curves displayed in Figure 5.2D and 5.3D, generated from the raw data in A-C, highlight the voltage-dependency of MET channel block by both compounds. Fractional block curves were generated from the extracellular block of the MET channel by both dTC and berbamine across a range of concentrations (Figures 5.2E and 5.3E). These graphs serve to

further highlight the voltage and concentration-dependency of MET channel block by both of the compounds. Furthermore, the block of the channels is released at both extreme hyperpolarised and depolarised potentials, indicative of dTC and berbamine acting as permeant blockers of the channel. Release of block at hyperpolarised potentials was more pronounced for berbamine than it was for dTC, suggesting that berbamine would more readily permeate through the channel and enter into the cell cytoplasm. Maximal block was seen at a membrane potential of -118 mV for dTC and -94 mV for berbamine.

Further investigation revealed that the half-blocking concentration, K_D, of the MET channel is extremely similar for both compounds, found to be 2.2 μM for dTC and 2.8 μM for berbamine (Kirkwood et al., 2017). Investigation of the intracellular block of the channel, established by including the compounds in the patch pipette-filling solution, revealed that berbamine caused no block of the channel when tested at ≤ 300 μM. When tested at a much higher concentration of 1 mM, berbamine had an adverse effect on the cells and their ability to be patched. With intracellular dTC, however, when tested at concentrations ranging from 100 μM to 1 mM we observed current reduction when cells were stepped to depolarised, but not hyperpolarised, membrane potentials. Again this block was both voltage and concentration-dependent, as detailed in Kirkwood et al., 2017.

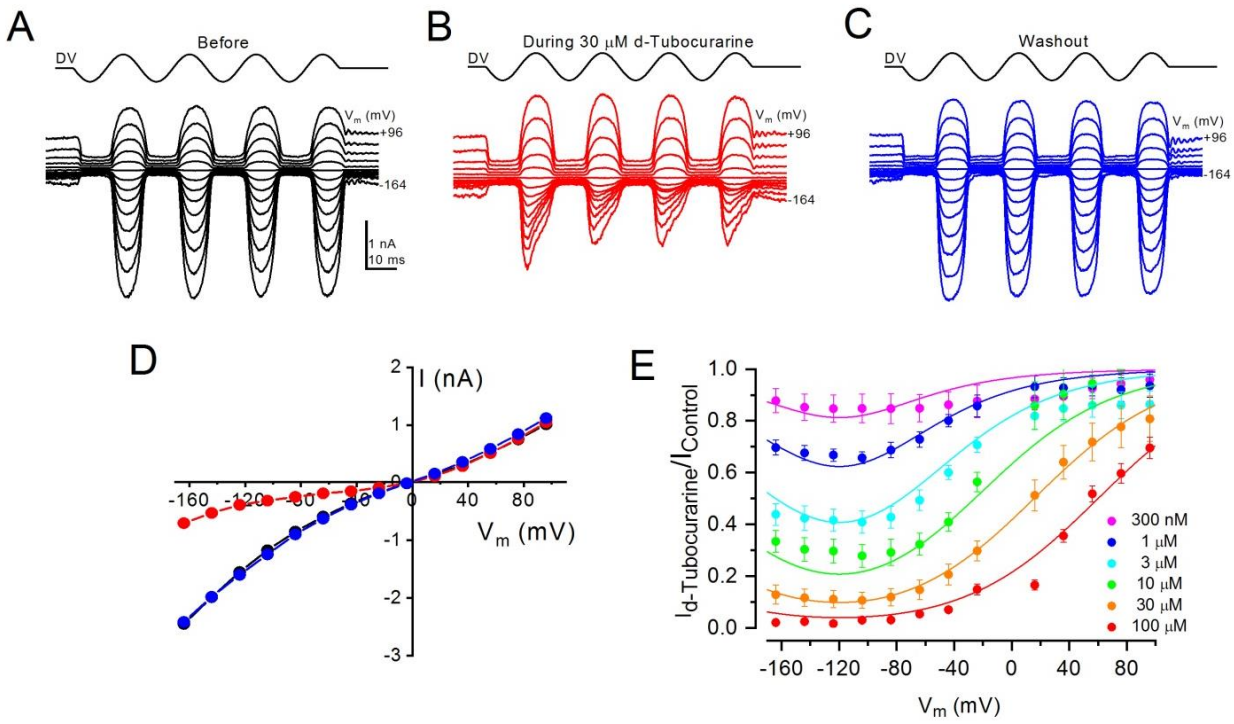

Figure 5.2: *The interaction of d-Tubocurarine with the MET channel.*

(A-C) Representative MET currents from OHCs in cultures prepared from P2 pups recorded before, during, and after exposure to 30 μM dTC. MET currents were recorded at membrane potentials from -164 mV to +96 mV in response to a sine-wave stimulus. **(D)** Current-voltage curve for the peak MET currents derived from the recordings shown in **A-C** demonstrates the voltage-dependency of the block by dTC. **(E)** Fractional block of the MET currents at all membrane potentials revealed that block is strongest at negative potentials and is released at the extremes, at every concentration tested. Data in **E** obtained from Nerissa Kirkwood.

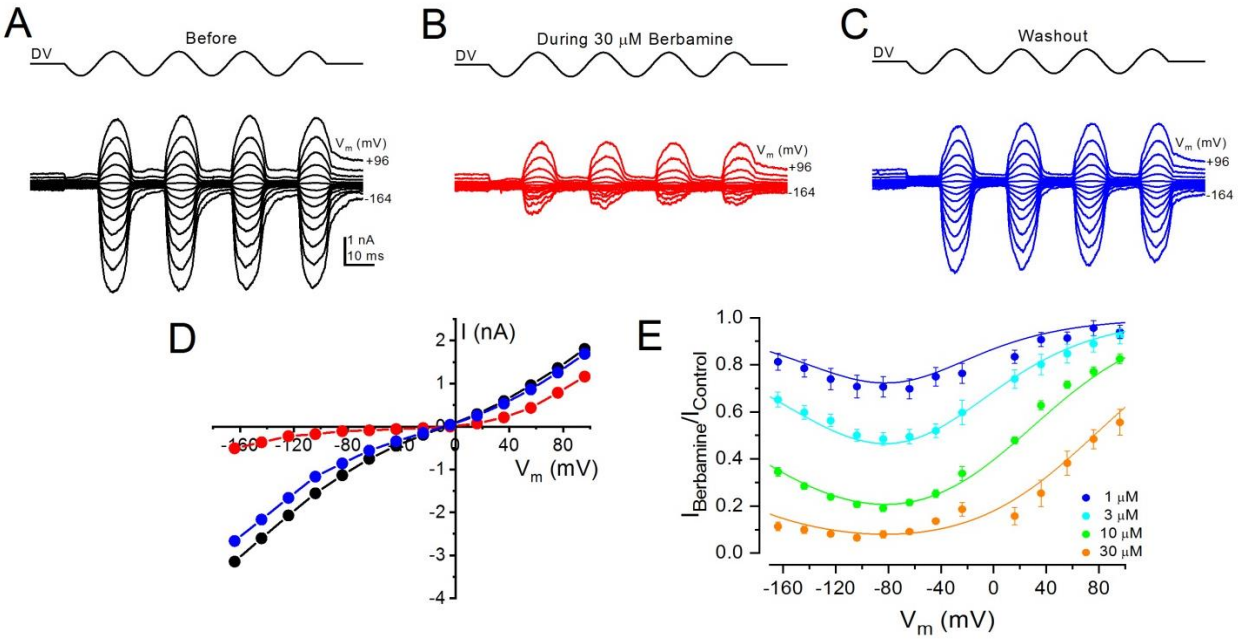

Figure 5.3: *The interaction of berbamine with the MET channel.*

(A-C) Representative MET currents from OHCs in cultures prepared from P2 pups recorded before, during, and after exposure to 30 µM berbamine. MET currents were recorded at membrane potentials from -164 mV to +96 mV in response to a sine-wave stimulus. **(D)** Current-voltage curve for the peak MET currents derived from the recordings shown in **A-C** demonstrates the voltage-dependency of the block by berbamine. **(E)** Fractional block of the MET currents at all membrane potentials revealed that block is strongest at negative potentials and is released at the extremes, at every concentration tested. Data obtained from Nerissa Kirkwood, figure prepared by myself.

5.2.2.2 The Effect of dTC and Berbamine on K^+ Channel Currents and the Resting Potential of the Cell

dTC has been shown to block a number of potassium channels, including neuronal apamin-sensitive potassium currents (Goh and Pennefather, 1987) and various calcium-dependent potassium channels in other cell types (Ishii et al., 1997; Vacher et al., 1998). During the first postnatal week, cochlear OHCs express a slow outward K^+ current ($I_{K,neo}$), as detailed in chapter 4 (section 4.2.5.2) (Marcotti and Kros, 1999). We therefore tested whether dTC and berbamine had any interaction with this channel. In addition to MET channel block, the compounds could inhibit this current and thereby potentially depolarise the resting cell membrane potential. This would lead to a further reduction in AG entry due to a reduction in the electrical driving force pulling the positively charged AGs into the cell, thereby providing an additional mechanism of protection. The results of these experiments are thoroughly documented in Kirkwood et al., 2017, however will be described here in brief.

Basolateral K^+ channels were investigated in whole-cell voltage clamp mode, with currents elicited by applying a series of hyperpolarising and depolarising voltage steps from a holding potential of -84 mV. Currents were recorded before, during and after the superfusion of 30 µM dTC or berbamine. At this concentration berbamine caused a large reduction in K^+ current size, however dTC had no effect. The effect on the resting membrane potential was subsequently investigated in current-clamp mode. Neither compound caused a depolarisation in the resting membrane potential when tested at 30 µM. Conversely, both berbamine and dTC caused a hyperpolarisation of the resting membrane potential. This hyperpolarisation would increase AG entry rates into HCs due to the increased electrical driving force, thus eliminating membrane depolarisation as a potential mechanism of protection.

5.2.2.3 The Effect of dTC and Berbamine on GTTR Loading into HCs

In order to test whether dTC and berbamine reduced the accumulation of gentamicin into OHCs by blocking the MET channel, mouse cochlear cultures were exposed to a low concentration (0.2 µM) of GTTR in the presence of a large molar excess (100 µM) of each compound for a short period of time to enable a quantification of AG uptake into HCs (Steyger

et al., 2003). For a negative control, cultures were incubated in 0.2 µM GTTR and 1% DMSO alone – the solvent in which the compounds were dissolved. Following 5 minutes pre-incubation with dTC, berbamine or DMSO and subsequently 10 minutes co-incubation with 0.2 µM GTTR, a one-way ANOVA revealed that a significant decrease in GTTR loading was seen in OHCs that were pre-exposed to either dTC (p = 0.001) or berbamine (p < 0.001) compared to the DMSO vehicle controls (Figures 5.4A–D). The reduction in GTTR labelling observed with the two compounds was very similar and not significantly different. In the control, the average intracellular fluorescence 12 minutes after GTTR washout was 75.5 (± 3.7) (arbitrary units) (n=30). In the dTC treated condition it was 36.8 (± 4.6) (n=30, from 3 animals) and in the berbamine treated condition it was 32.4 (± 3.2) (n=30, from 3 animals).

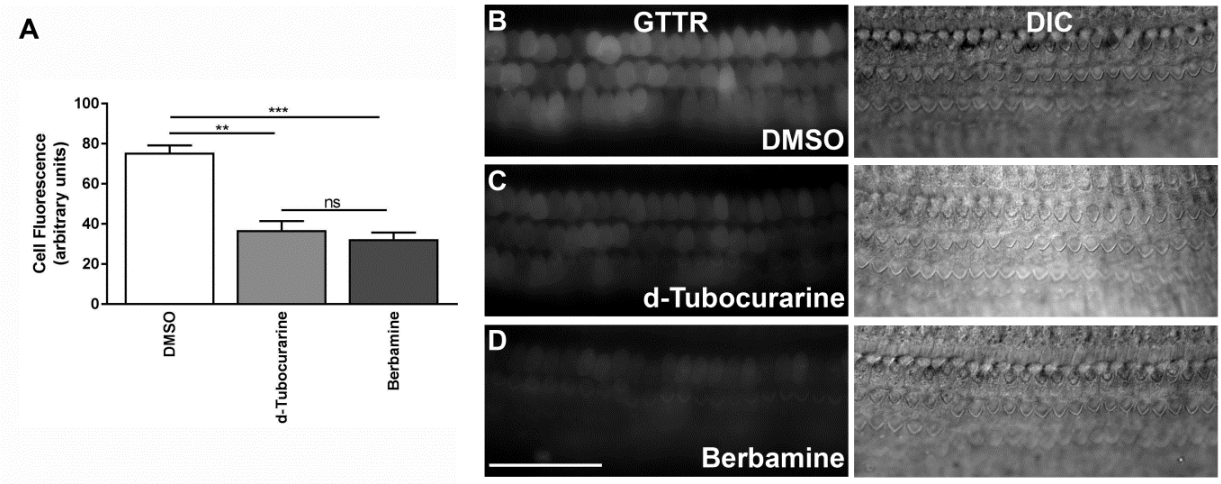

Figure 5.4: *d-Tubocurarine and berbamine reduce the loading of GTTR into HCs.*

(A) Quantification of intracellular fluorescence in cochlear culture HCs pre-treated for 5 minutes with 100 µM dTC, berbamine or 1% DMSO, followed by 10 minutes co-incubation with 0.2 µM GTTR. **(B–D)** Representative images captured 12 minutes after GTTR washout. **(C)** dTC (**p = 0.001) and **(D)** berbamine (***p < 0.001) significantly reduced the intracellular fluorescence intensity of GTTR compared to the DMSO vehicle controls. No significant difference was observed between the reduction caused by dTC and berbamine. Scale bar is 50 µm.

5.2.3 Compound Modification

5.2.3.1 dTC-related Compounds

Following the success of the screening procedure, reinforcing that both dTC and berbamine protect against AG ototoxicity by blocking the MET channel, compounds that share a similar mechanism of action to dTC (other neuromuscular blockers) were bought for testing. This was in an attempt to identify a compound with similar otoprotective abilities - maintaining, and ideally enhancing, the desirable characteristics of MET channel block and otoprotection, whilst also reducing the concurrent permeation properties. This investigation would inform us of what parts of the dTC molecule are integral to its interaction with the MET channel, enhancing our knowledge and informing the future design of otoprotectants.

Four compounds were commercially available (14916, 16297, 16298 and 16299) that share the same mechanism of action of dTC but differ slightly chemically. Compound 14916 is the dTC molecule cut in half. Compounds 16297 and 16298 are structurally identical but 16297 has two fixed positive charges (quaternary nitrogens) whilst 16298 has only one fixed positive charge and one that is pH-dependent. Compound 16299 consists of two 14916 linked together via a chemical linker and has two fixed positive charges.

Shown in Figure 5.6A-F is the cochlear culture protection assay displaying the protective efficacy of each compound. Figure 5.6G shows their interaction with the MET channel. When tested at 50 µM, only one of the four compounds provided protection against the AG-induced OHC loss (16297), two showed no protection (14916 and 16298) and one displayed a toxic effect on the sensory epithelium (16299), causing an enlargement of the apical surface of all OHCs and a deformity of the hair bundle along the entire length of the cochlear coil (Figure 5.6A-F). When tested at lower concentrations (25 and 12.5 µM) 16297 failed to protect, suggesting that there was no improvement of the protective efficacy compared to dTC itself (data not shown). Moreover, when tested electrophysiologically all but one compound retained the MET channel blocking ability, however none blocked as strongly as dTC (Figure 5.6G). The one compound that had no interaction with the channel (14916) was the dTC structure that was cut in half, so it was perhaps not surprising that it did not show any block of the channel.

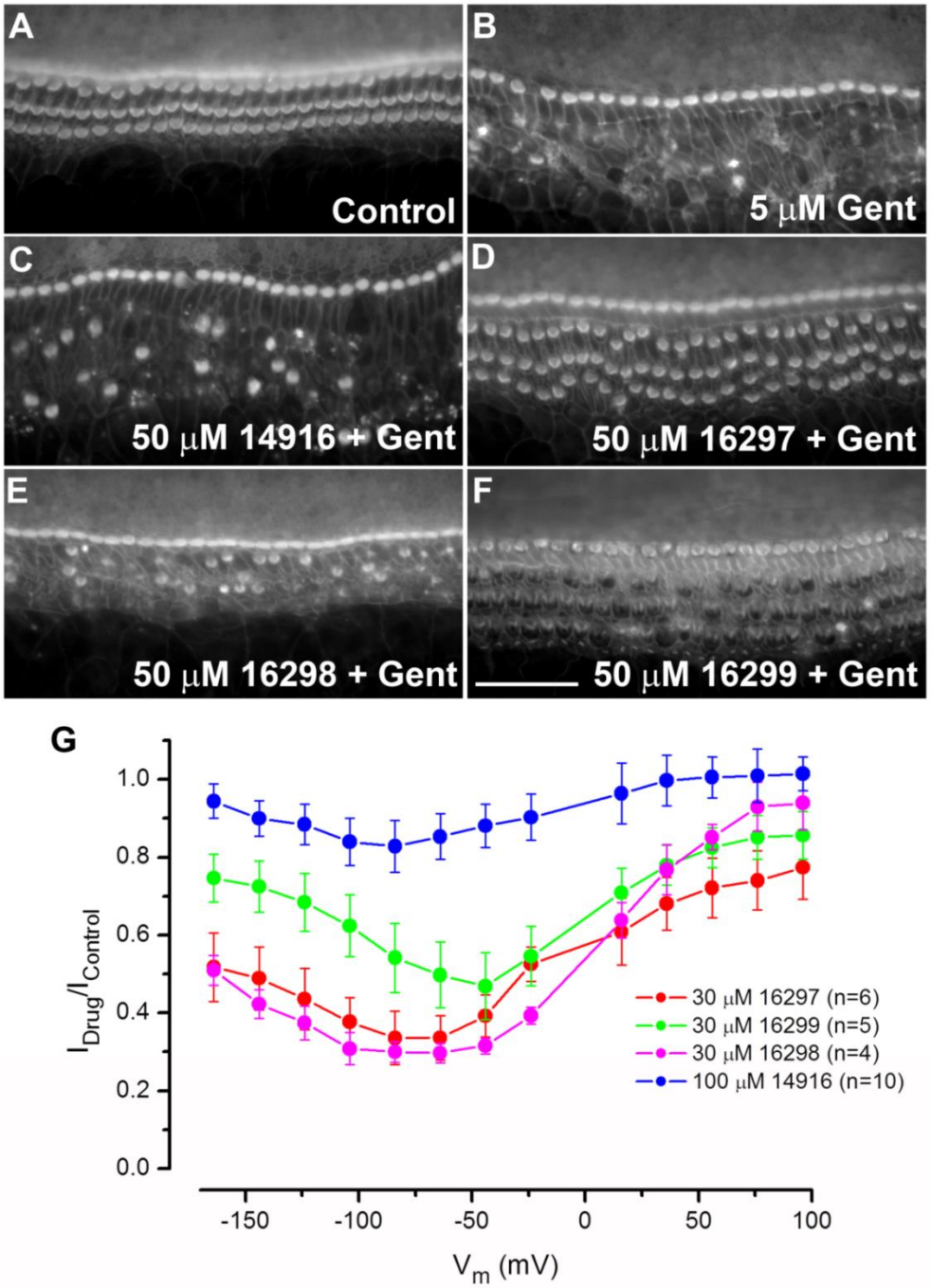

Figure 5.6: *One of the four d-Tubocurarine-related compounds protected against gentamicin damage and three showed a voltage-dependent block of the MET channel.*

(A-F) Cochlear culture protection assay. **(A)** A control culture incubated for 48 hours in the presence of 0.5% DMSO. The sensory HC loss shown in **(B)**, caused by 48 hours incubation with 5 μM gentamicin and 0.5% DMSO can be prevented by co-incubation with 50 μM 16297 (n=3) **(D)**, but not with 14916 (n=1) **(C)** or 16298 (n=1) **(E)**. Cells incubated with 50 μM 16299 (n=1) showed toxicity symptoms **(F)**. Scale bar is 50 μm. **(G)** The average fractional block curves

reveal that all but one compound (14916) display a voltage-dependent, permeant block of the MET channel, similar to dTC. Data in **G** obtained from Nerissa Kirkwood.

5.2.3.2 d-Tubocurarine-Texas Red

A previous study into the MET channel interacting properties of dTC revealed that it is a non-permeant blocker, however here we have found evidence to contradict this. Electrophysiological recordings revealed a release of channel block at extreme hyperpolarised potentials (Figure 5.2), indicative of the dTC molecule being drawn into the HC. To further assess this postulation we conjugated dTC to a fluorescent dye, Texas Red, and investigated its loading into HCs using live cell imaging. I incubated cochlear cultures with 50 nM of either Texas Red or dTC-Texas Red (dTC-TR) for 4 hours, washed the compound away with three 1 minute washes in HBHBSS and then performed live imaging of HC fluorescence. By comparing the intracellular fluorescence of Texas Red, a dye that would not selectively enter HCs over this time course (Steyger et al., 2003; Wang and Steyger, 2009; Alharazneh et al., 2011), with the loading of dTC-TR, comparisons can be made as to whether dTC enhances its specific loading into HCs.

As shown in Figure 5.7A, Texas Red alone does not enter HCs over a 4 hour time course when tested at 50 nM. When conjugated with dTC, however, selective HC loading is observed (Figure 5.7B). The average HC fluorescence in the Texas Red-treated culture was 6.5 (±0.7) (n=10, from one animal) and in the dTC-Texas Red culture it was 64.7 (±1.7) (n=10, from one animal) (Figure 5.7C). A two-tailed *t* test revealed that this difference was significant ($p < 0.001$). This provides additional evidence in support of our hypothesis that dTC is a permeant MET channel blocker and does enter HCs following its block of the channel, consistent with the electrophysiological evidence presented in this chapter.

Additionally, I performed a cochlear culture protection assay to ascertain whether dTC-TR retained the same protective ability of the parent compound. As seen in Figure 5.7D-G, myosin VIIa staining of HC bodies reveals that both compounds protect HCs similarly when tested at 50 µM (Figure 5.7F and G), suggesting that the conjugation of the fluorophore did not cause a change in the otoprotective characteristics of dTC.

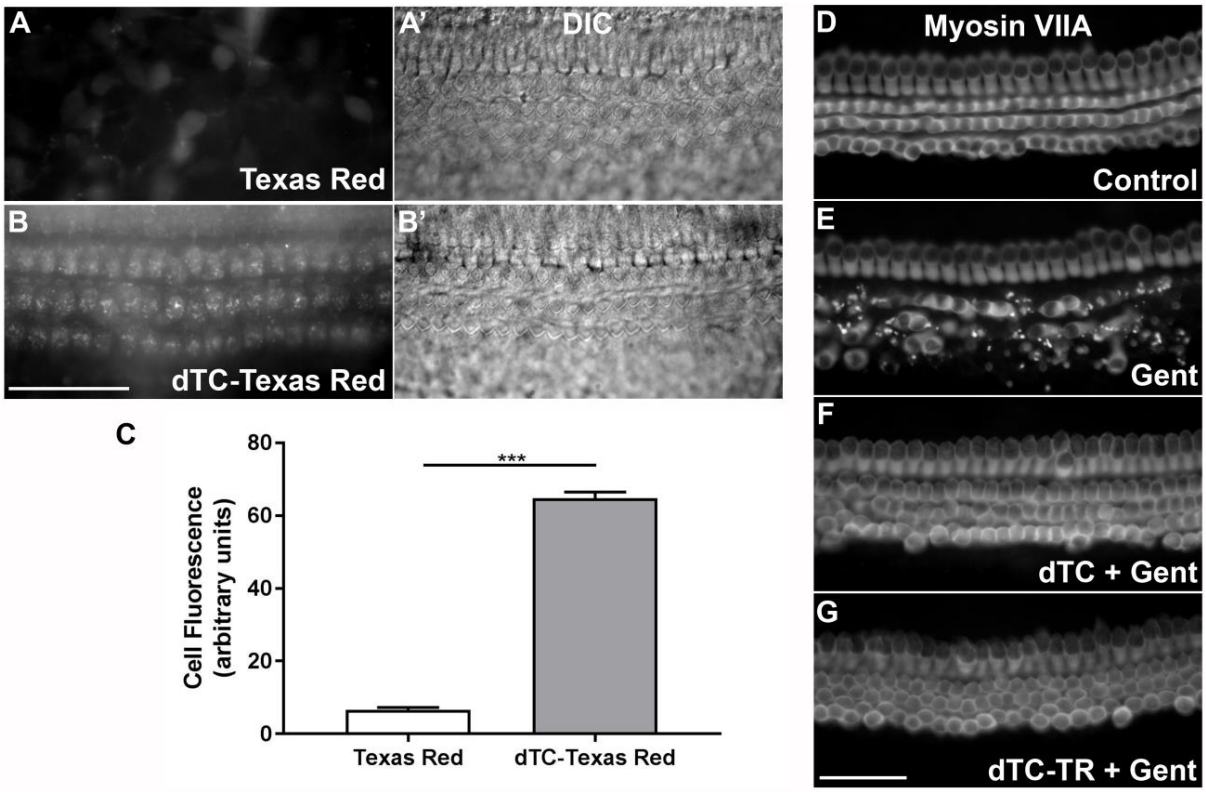

Figure 5.7: *d-Tubocurarine-Texas Red loads into HCs specifically over a 4 hour time period, and protects cochlear HCs similarly to dTC.*

(A-C) Live cell imaging of OHC fluorescence. Cultures incubated with 50 nM Texas Red for 4 hours **(A)** displayed no specific labelling, whereas those incubated with dTC-TR **(B)** showed granular fluorescence labelling within HCs specifically. **(C)** Quantification shows that the difference in cytoplasmic fluorescence is statistically significant ($p < 0.001$). **(D-G)** Cochlear culture protection assay, stained with myosin VIIa primary antibody. **(D)** A control culture incubated for 48 hours in the presence of 0.5% DMSO. The sensory HC loss shown in **(E)**, caused by 48 hour incubation with 5 µM gentamicin and 0.5% DMSO, can be completely prevented by co-incubation with 50 µM d-TC **(F)** or dTC-TR **(G)**. Scale bars are 50 µm.

5.3 Summary

Our screening of the structurally-related compounds dTC and berbamine has further highlighted their otoprotective similarities. Here we show that dTC also protects against neomycin and gentamicin damage in zebrafish neuromasts and that berbamine also protects against gentamicin damage in mouse cochlear cultures. In cochlear cultures, we show that the protective range of berbamine is extremely narrow; it provides protection against 5 μM gentamicin damage when tested at 20 μM, however when tested at ≥ 30 μM both alone and in the presence of gentamicin, cytotoxicity and a complete loss of all cell types in the cochlear culture is observed. dTC does not share these toxicity characteristics when tested ≤ 50 μM.

Characterisation of their MET channel-blocking abilities shows that they both interact with the channel in an extremely similar way. Both display a voltage-dependent, permeant block of the channel, with maximum block at negative potentials around -80 mV and release of block at the extreme hyperpolarised and depolarised potentials. dTC and berbamine have a similar half-blocking K_D, 2.2 and 2.8 μM respectively (Kirkwood et al., 2017), showing that they have a similar affinity for the channel. Their block of basolateral potassium channels is different, however, in that berbamine blocks these channels whereas dTC does not. Neither causes a positive shift in the resting cell membrane potential, eliminating depolarisation as a potential, additional mechanism of protection.

The postulation that the compounds may be protecting by blocking MET channels and impeding AG entry is further supported by our evidence of the reduction of GTTR loading into HCs, both by dTC and berbamine, consistent with the results published by other researchers (Alharazneh et al., 2011; Kruger et al., 2016). Contrary to what is found in the literature (Farris et al., 2004), however, here we show that dTC is itself a permeant blocker of the MET channel. This is evident from electrophysiological recordings showing release of MET channel block at extreme hyperpolarised potentials, and is further supported by my investigation of the loading of dTC-TR into HCs. Over a 4 hour time course dTC-TR selectively enters sensory HCs, whereas Texas Red alone does not.

Lastly, of the 4 compounds with a similar mechanism of action to dTC that were commercially available, only one provided protection and this was at a reduced efficacy compared to dTC itself. Furthermore, all 3 that blocked the MET channel retained the undesirable characteristic of channel permeation.

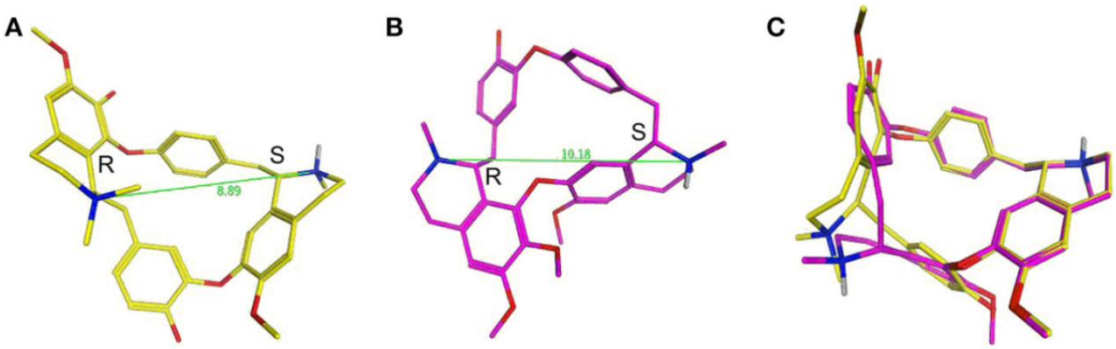

Figure 5.8: *d-Tubocurarine and berbamine share similar chemical structures.*

(A-B) Energy-minimized structures showing the distance between the positive charges for dTC (8.89 Å; yellow) **(A)** and berbamine (10.18 Å; magenta) **(B)** respectively. **(C)** A flexible alignment with the structures not minimized reveals dTC and berbamine share striking structural similarities. Figure taken from Kirkwood et al., 2017.

5.4 Discussion

The research conducted in this chapter, into the protective and mechanistic characterisation of dTC and berbamine, has further reinforced the usefulness of zebrafish pre-screening in the search for clinically-relevant otoprotectants. If these compounds had been blindly screened in the zebrafish assays they would have been selected and taken forward to mouse cochlear cultures for additional screening. This again suggests that zebrafish provide a useful pre-screening tool in the search for mammalian otoprotectants.

From the cochlear culture screening section of this chapter, we have gained further evidence of the importance of a thorough, comprehensive screening procedure. Berbamine was found to be protective at 20 µM but extremely toxic when tested ≥ 30 µM. Evidently, it is vital to screen compounds at a series of concentrations outside of their protective range, to ensure no adverse effects at higher concentrations. Furthermore, it is vital that this thorough screening is conducted in mammalian systems as berbamine showed no signs of toxicity when tested against either AG in the zebrafish assays, even at the highest concentration tested (200 µM). Consequently, any compound put forward as a potential otoprotectant to be used in a clinical setting should be screened thoroughly in mammalian models to ensure a broad protective, non-toxic range and also no inherent intrinsic toxicity when tested alone. To this end, the

current use of berbamine for this very purpose should be exercised with some caution, as it has been identified as an otoprotectant in the literature (Kruger et al., 2016; Neveux et al., 2017) and reported to protect against a range of other ailments (Zhnag et al., 2012; Wang et al., 2016; Jia et al., 2017) however reports of its striking toxicity profile are lacking.

Our electrophysiological investigation of MET channel interaction revealed that dTC is a permeant blocker of the channel, contrary to what has been reported elsewhere (Farris et al., 2004). This is further supported by my live imaging of the loading of a fluorescently-tagged version of dTC (dTC-TR) into HCs specifically. This literature-contradicting evidence highlights that when investigating compounds electrophysiologically for their permeation properties the cell membrane should be stepped to all possible physiologically-relevant potentials, to ensure any potential permeation is detected.

Investigation of the dTC-related compounds informed us that it is not sufficient for a compound to interact with the MET channel in order for it to provide protection from AG-induced ototoxicity. Although all but one of the derivatives interacted with the MET channel similarly to dTC, only one conferred any protection against gentamicin damage. Alongside channel interaction, other factors underlying a compound's ability to block AG entry through the MET channel include: the compound's affinity for the channel, dictating the force of its binding within the channel pore; the permeation properties of the compound, determining how easily the compound is drawn into the HC and the duration of time it spends bound inside the vestibule; and lastly the structure, determining whether the compound is bulky enough to prevent AG entry or compact enough to allow AGs to pass through.

What can be concluded from the dTC-related compounds is that in this case, two fixed positive charges are necessary for otoprotection. The compound that protected (16297) and one compound that did not (16298) were structurally identical, aside from 16297 having a fixed and 16298 having a pH-dependent positive charge. For this set of compounds, the two fixed positive charges may be vital to the compound's protective ability – potentially due to the electrically expelling force this would have on any AGs encountering the MET channel.

Another issue for consideration, as a result of the channel-blocking nature of dTC's mechanism of protection, is in regards to the lack of effect on stereociliary morphology. After 48 hours incubation with dTC, known to block HC MET channels, the morphology of the stereociliary hair bundle appeared unperturbed; at least through the low-resolution microscopy that we used for our screening procedures. A study investigating the effect of the MET current on the dynamic control of stereocilial morphology (Vélez-Ortega et al., 2017) highlighted that MET

channel blockers can alter the shape and height of the sterociliary rows, shortening the second and third rows specifically, and that this effect can be reversed following washout of the MET blocker. This suggests that any prolonged block of the MET channel will lead to bundle disfiguration, and that there may be a morphological difference in the cultures treated with MET blockers that we are not detecting in our low-resolution microscopy.

Lastly, the evidence collected in regards to the HC loading of dTC-TR poses several questions. The evident granular nature of the fluorescence within the HCs would suggest an endocytosis-driven, vesicle-bound intracellular accumulation of the dye. If the Texas Red was simply funnelling through the MET channel when conjugated to dTC then we would expect an equally-dispersed fluorescence signal within the cell. However, if this were the case and the compound was being brought into the cell via endocytic mechanisms then we would also expect to see the same pattern of granular fluorescence in the HCs exposed to Texas Red alone, which is not what we observed. An alternative explanation of the granular labelling is that once inside the cell, the fluorescently-tagged dTC is being internalised by other intracellular structures such as lysosomes or mitochondria, leading to the punctate fluorescence signal that we observed. In order to test this we could incubate for a reduced time frame in order to see if the fluorescence is intracellularly dispersed before aggregating into punctate clusters. Another way in which we could test this hypothesis is by using myosin VIIa mouse mutants *(Myo7a*^{Sh6J} mice) - mice with a mutation in a protein that is crucial to MET channel function (Richardson et al., 1997; Kros et al., 2002) and renders all MET channels closed at rest. Consequently, if we tested dTC-TR loading in these mutants and did not observe the same punctate fluorescence within the cell, this would provide compelling evidence that dTC does enter HCs through the MET channel.

6 Assessing the Otoprotective Potential of Carvedilol, an FDA-Approved Drug used to treat Hypertension

6.1 Introduction

6.1.1 Compound Choice

Carvedilol is an FDA-approved beta-2 adrenergic blocker, used clinically for the treatment of hypertension, angina and symptomatic chronic heart failure (Al-Ghamdi, 2011; Akbar and Alorainy, 2014). Carvedilol had previously been reported to protect against neomycin damage in zebrafish, when tested at 10-100 µM against 200 µM neomycin (Ou et al., 2009). This study also reported its block of GTTR loading into zebrafish neuromast HCs. However, its protective abilities in mammalian systems had not yet been documented. For this reason, I sought to characterise the protective efficacy of carvedilol in mouse cochlear cultures, whilst also establishing the mechanism by which it protects through use of electrophysiology and fluorescence imaging studies.

6.1.2 Aims

In this chapter I aimed to assess whether carvedilol also protected zebrafish lateral line HCs against gentamicin damage and whether it behaved as an otoprotectant when tested in mouse cochlear cultures. This would provide further evidence of the similarity between zebrafish and mammalian models and further highlight the transferable efficacy from zebrafish pre-screening into mammalian systems.

As carvedilol is already FDA-approved, the transition from scientific screening to use in a clinical setting would be greatly reduced, depending on the method of administration. If the administrative procedure when the drug is used to treat hypertension (usually oral administration (Stafylas and Sarafidis, 2008)) was suitable for its additional use as an otoprotectant, it is possible that no additional testing would be necessary. Carvedilol has been shown to cross the blood brain barrier, so this is a possibility (Elsinga et al., 2004).

I also aimed to assess carvedilol's mechanism of protection - investigating whether it had a MET channel-blocking mechanism of protection or otherwise. Lastly, derivatives of carvedilol were designed and synthesised in order to further assess structure-activity relationships and potentially synthesise a more effective otoprotectant than the parent compound. Testing these derivatives electrophysiologically would provide additional information concerning which aspects of a compound's chemical composition are vital to enabling MET channel interaction.

6.2 Results

6.2.1 Screening for Otoprotection

6.2.1.1 Zebrafish Pre-Screening

*The zebrafish research presented in this section was collected by Emma Kenyon, University of Sussex. I performed the statistical analysis of the data.

In order to assess the protective capability of carvedilol against AG damage, an initial protection assay was performed using the sensory HCs of the lateral line organs of zebrafish larvae at 4 dpf, a time point that ensures the reliable loading of Yo-Pro 1 (Santos et al., 2006; Kindt et al., 2012).

Carvedilol was found to provide complete protection against the damage induced by 6.25 μM neomycin over the course of 1 hour when tested at concentrations ≥ 6.25 μM (Figures 6.1A-G and graph O). Complete protection against the damage induced by 10 μM gentamicin over the course of 6 hours was only observed at concentrations ≥ 25 μM, with partial protection at 12.5 μM (Figures 6.1H-N, graph P). Complete protection is defined here as the HC counts from the carvedilol-treated conditions being significantly higher than the AG-alone treatments and also not significantly different from the control. Partial protection is defined here as being significantly different to both the control and the AG-treated conditions.

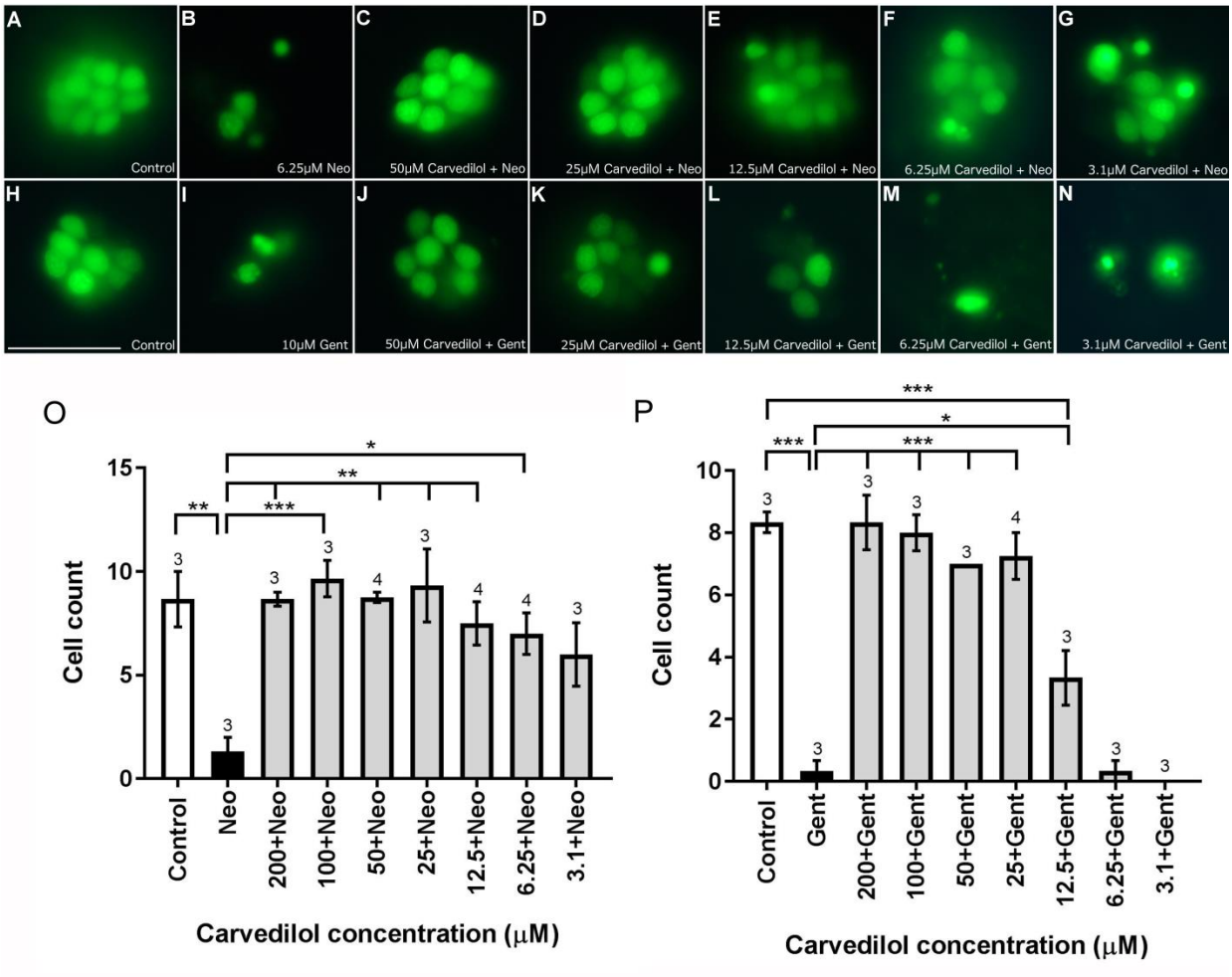

Figure 6.1*: Carvedilol protects zebrafish lateral line HCs against 6.25 µM neomycin and 10 µM gentamicin when tested at a concentration of 6.25 and 25 µM respectively.*

Zebrafish were treated with: **(A, H)** E3 alone **(B)** 6.25 µM neomycin, or **(C-G)** 50 µM, 25 µM, 12.5 µM, 6.25 µM, or 3.1 µM of carvedilol plus 6.25 µM neomycin for 1 hour, **(I)** 10 µM gentamicin, **(J-N)** 50 µM, 25 µM, 12.5 µM, 6.25 µM, or 3.1 µM of carvedilol plus 10 µM gentamicin for 6 hours. Neuromasts were pre-stained with 3 µM Yo-Pro1. n=3 independent experiments with at least 3 fish per well. Images were obtained with a 40x objective. Scale bar is 25 µm. **(O-P)** Quantification of neuromast HC survival when exposed to **(O)** neomycin or **(P)** gentamicin together with selected concentrations of carvedilol. Numbers above bars are the number of experimental replicates.

6.2.1.2 Cochlear Culture Screening

Following zebrafish trials, mouse cochlear cultures were used to assess whether carvedilol could protect against the HC death caused by exposure to 5 µM gentamicin over a 48 hour time course. As detailed in Chapter 3, incubation with 5 µM gentamicin alone caused a loss of 88% of OHCs from the mid-basal region of mouse cochlear cultures (Figures 3.1, 6.2A and B). When co-incubated together with gentamicin, 5 µM carvedilol provided partial protection, with OHC survival being significantly different from both the control and gentamicin-treated cultures ($p < 0.001$ in both cases) (Figure 6.2C). The average number of HCs in a 300 µm-long segment of the mid-basal region of the control was 109.8 (± 2.2) (26), in the gentamicin-treated condition it was 15.3 (± 2.2) (n=26) and in the 5 µM carvedilol condition it was 69.7 (± 12.9) (n=7). This highlights the partial protectiveness at this concentration, suggesting that this is the lower limit of carvedilol's protective efficacy. Consistently complete protection against the gentamicin-induced loss of OHCs was observed with both 10 µM and 20 µM carvedilol ($p < 0.001$) (Figures 6.2D and E). Higher concentrations of carvedilol, from 30 to 50 µM, proved to be generally cytotoxic to cochlear cultures, causing widespread, non-specific cell death (Figure 6.2F and G).

When carvedilol was tested alone no OHC death was observed at either 10 µM or 20 µM, similar to control conditions (Figure 6.3C and D). However when tested both alone at 20 µM and alongside 5 µM gentamicin, some degree of IHC damage and disruption to hair bundle morphology in both IHCs and OHCs can be observed (Figure 6.2E, Figure 6.3D-F). Figure 6.3E and F shows confocal images of IHC stereocilia bundles in both control conditions (Figure 6.3E) and during exposure to 20 µM carvedilol (Figure 6.3F), revealing the damage caused to the hair bundle morphology by carvedilol exposure. When used in a clinical setting carvedilol is known to cause hearing loss in a small percentage of treated patients (eHealthMe, 2017). The sporadic toxicity to IHCs could potentially underlie this finding, with the incidence explained by the individual differences in carvedilol's accumulation within the endolymphatic compartment of the inner ear. At concentrations ≥ 30 µM, carvedilol is generally cytotoxic to all cell types in the cochlear culture, both alone and in the presence of 5 µM gentamicin (Figure 6.2F and G, Figure 6.3G and H).

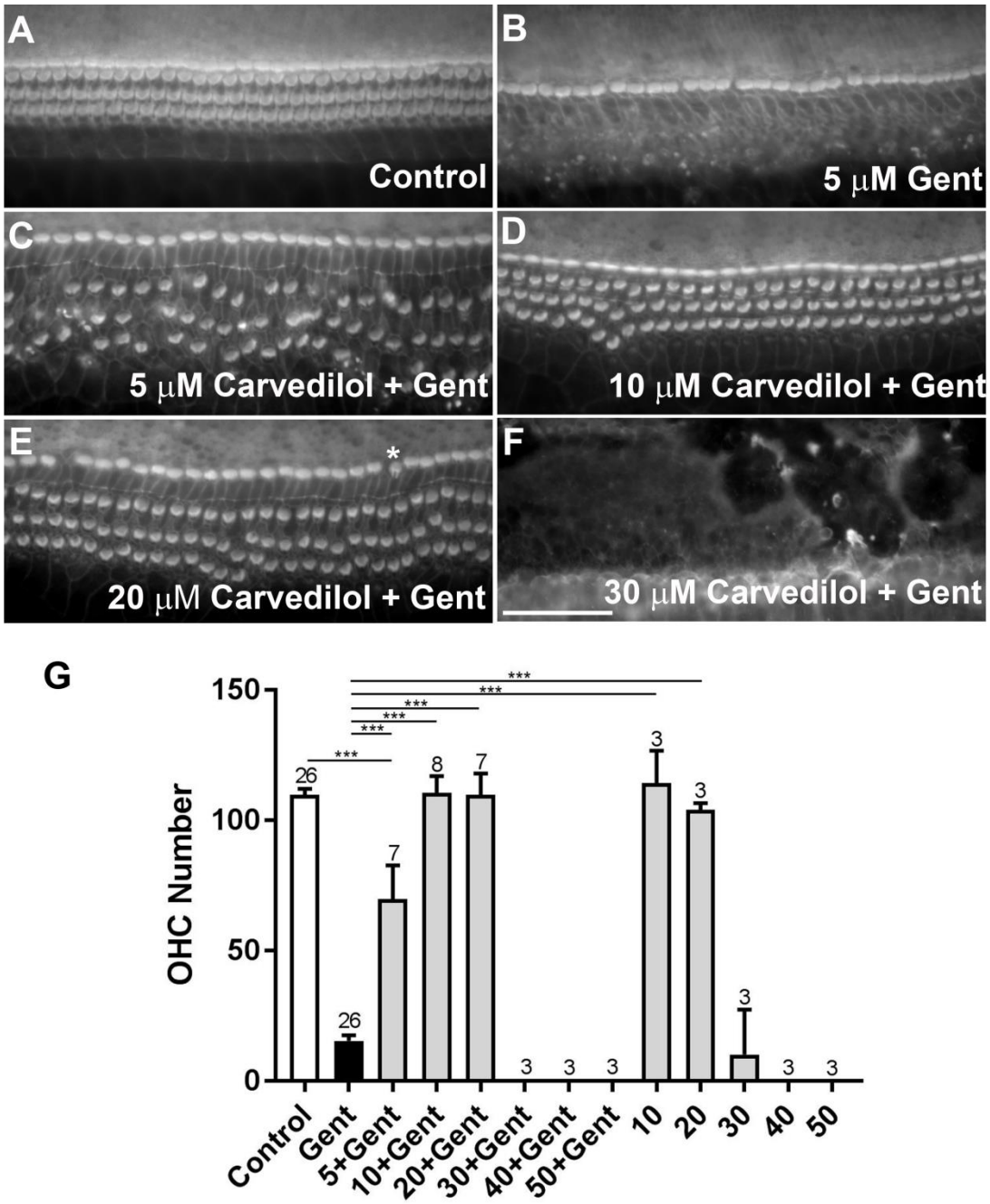

Figure 6.2: *When exposed to 5 µM gentamicin for 48 hours, co-incubation with 10 or 20 µM carvedilol completely protects against OHC loss. 5 µM provides partial protection. ≥ 30 µM carvedilol is generally cytotoxic.*

(A) A control culture exposed to 0.5% DMSO for 48 hours. **(B)** A culture exposed to 5 µM gentamicin and 0.5% DMSO for 48 hours. **(C-F)** A culture exposed to 5 µM gentamicin for 48 hours plus **(C)** 5 µM, **(D)** 10 µM, **(E)** 20 µM or **(F)** 30 µM carvedilol. The asterisk in **(E)** shows an example of IHC disruption. Scale bar is 50 µm. **(G)** Quantification of HC survival in a 300 µm-long segment of the mid-basal region of cochlear cultures treated with 5 µM gentamicin alone, 5 µM gentamicin together with carvedilol (5 – 50 µM) or carvedilol alone (10 – 50 µM).

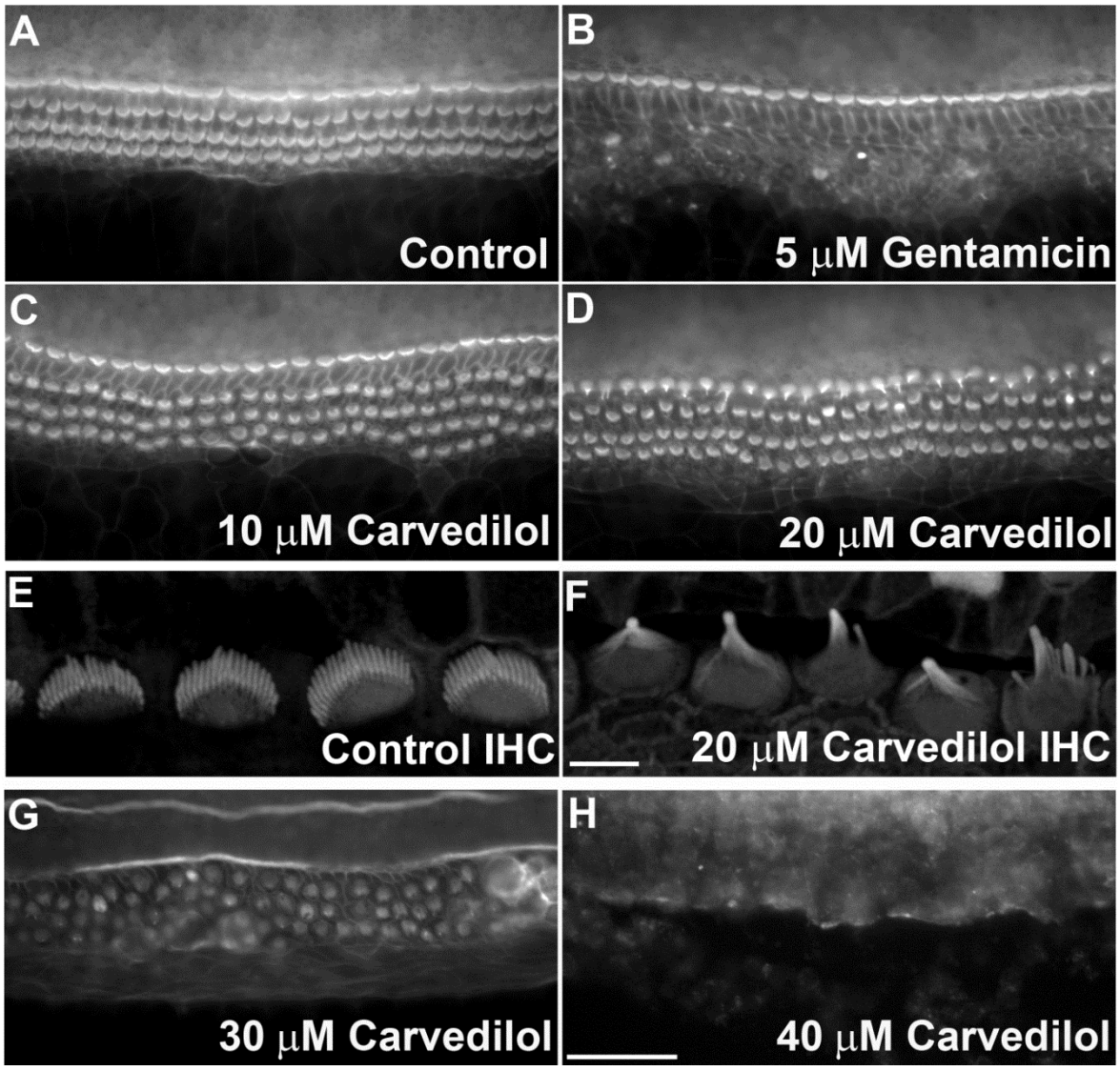

Figure 6.3: *When tested in the absence of gentamicin carvedilol is selectively toxic to mechanosensory hair bundles at 20 μM and generally cytotoxic at ≥ 30 μM.*

(A) A control culture exposed to 0.5% DMSO for 48 hours. **(B)** A culture exposed to 5 μM gentamicin and 0.5% DMSO for 48 hours. **(C-D)** Cultures exposed to **(C)** 10 or **(D)** 20 μM carvedilol in the absence of gentamicin for 48 hours. **(E-F)** Magnification of a region of IHCs in **(E)** a control culture or **(F)** a culture treated with 20 μM carvedilol. **(G-H)** Cultures exposed to **(G)** 30 or **(H)** 40 μM carvedilol 48 hours. Scale bar in **(F)** is 5 μm, scale bar in **(H)** is 50 μm.

6.2.2 Mechanism of Protection

6.2.2.1 The Effect of Carvedilol on MET Channel Currents

* The electrophysiology presented in Figures 6.5, 6.7 and 6.9 was performed by Nerissa Kirkwood, University of Sussex.

In order to assess whether carvedilol provides otoprotection by blocking MET channels and preventing AG entry into HCs, we investigated its effect on OHC MET currents in P2 mouse cochlear cultures. Whole-cell voltage clamp procedures were used to step the cell membrane between potentials ranging from -164 to +96 mV, whilst MET currents were elicited by a sine-wave stimulus and recorded before, during and after the extracellular superfusion of 1, 3 and 10 µM carvedilol. Shown in Figure 6.4 (A-C) is an example of MET channel block by 3 µM carvedilol. Carvedilol reduces MET current sizes at all membrane potentials tested. Current-voltage (Figure 6.4D) and fractional block curves (Figure 6.4E) revealed that the reduction in current size is voltage-dependent, with maximal block at the intermediate and depolarised potentials (maximum block is seen at +16 mV). Following re-superfusion of control solution I observed full recovery of the MET channel current (Figure 6.4C), suggesting that the block of the channels is completely reversible.

Averaged current-voltage curves from multiple cells (Figure 6.5A) highlight the concentration-dependency of the block, with increasing carvedilol concentrations leading to stronger block of the channel at all membrane potentials tested. Fractional block curves showing the current recorded during carvedilol superfusion relative to that during control solution (Figure 6.5B) reveal that there is a modest release of the channel block at the extreme depolarised potentials and a large release of block at the extreme hyperpolarised potentials. This is a characteristic of a permeant MET channel blocker, with the release of block evident at hyperpolarised potentials being due to the compound entering into the cell driven by the electrical potential present across the MET channel.

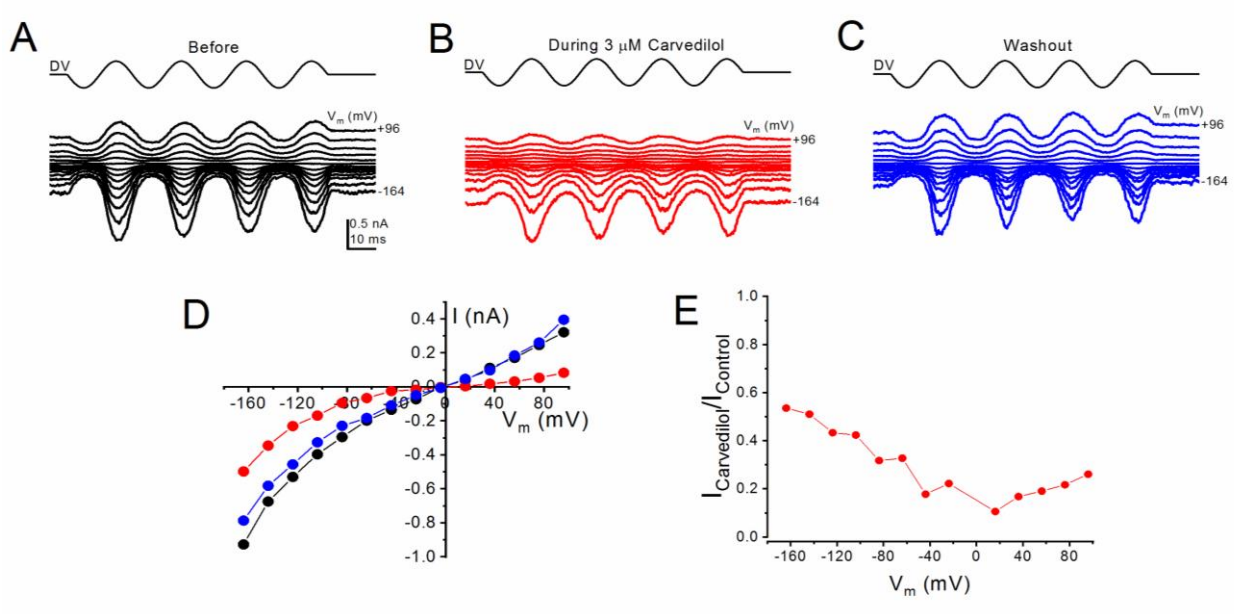

Figure 6.4: *Extracellular exposure to 3 μM carvedilol reduces OHC MET currents at all potentials, with the reduction most pronounced at intermediate and depolarized potentials.*

(A-C) MET currents recorded from a P2 basal OHC between -164 and +96 mV in response to a sine-wave stimulus delivered by a fluid jet (45 Hz sinusoid, ± 40V driver voltage, DV shown above each trace), before, during and after exposure to 3 μM carvedilol. Carvedilol reduces the current size at all potentials. Full recovery is seen following re-exposure to the control solution. **(D)** Current-voltage curves of the currents shown in **(A-C)** reveal the current block at all potentials during carvedilol exposure and the reversibility of the block following washout. **(E)** Fractional block of the MET currents at all membrane potentials reveals that block is strongest at the intermediate and depolarised potentials and is released at the extremes.

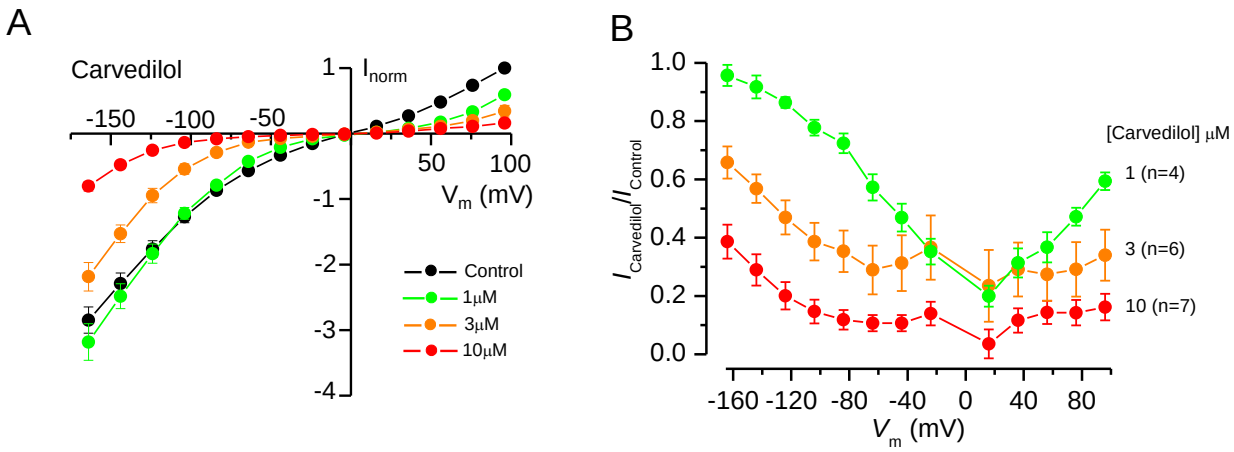

Figure 6.5: *Carvedilol acts as a voltage-dependent, permeant blocker of the MET channel with maximum block observed at +16 mV.*

(A) Average normalized current-voltage curves for the peak MET currents recorded before and during exposure to 1, 3 and 10 µM carvedilol. Currents for each cell were normalized to the peak control current measured at +96 mV. The block is strongest at the intermediate and depolarized potentials and the level of block increases with increasing carvedilol concentration. Number of cells; Control: 17, 1 µM: 4, 3 µM: 6, 10 µM: 7. **(B)** Fractional block curves of the current during carvedilol exposure (1-10 µM) relative to the control current at each membrane potential demonstrate a release of the block at the extreme hyperpolarized potentials, indicative of a permeant blocker. Data collected by Nerissa Kirkwood.

Electrophysiological evidence of MET channel block suggested this to be the mechanism of protection of carvedilol, by way of preventing AG entry into HCs. GTTR studies were conducted to further investigate this postulation; however, this will be detailed in a later section of this chapter (6.2.4).

6.2.3 Compound Modification

6.2.3.1 Carvedilol Derivatives: Protective Abilities and MET Channel Block

Our results demonstrated that carvedilol is a voltage-dependent blocker of the MET channel and consistently protects OHCs from AG damage at 10 and 20 μM; however, it is toxic at higher concentrations and is itself a permeant blocker, entering the HCs via their MET channels once the cell is stepped to a sufficiently negative potential. In an attempt to identify a compound with reduced toxicity and improved blocking and protective properties, 7 carvedilol derivatives were initially synthesised (14953, 14958, 14970, 14971, 14972, 15173 and 15174). Each derivative was screened at 20 μM to assess its protective ability against 5 μM gentamicin with each screen repeated ≥ 3 times. At this concentration 1 of the derivatives was generally cytotoxic (14971), 3 provided no protection (14953, 14958 and 15173), 1 showed partial protection (14970) and 2 of the 7 derivatives consistently protected against OHC loss (14972 and 15174) (Figure 6.6 A-J). Both 14972 and 15174 caused disruption of the mechanosensory hair bundle morphology when tested at this concentration together with gentamicin.

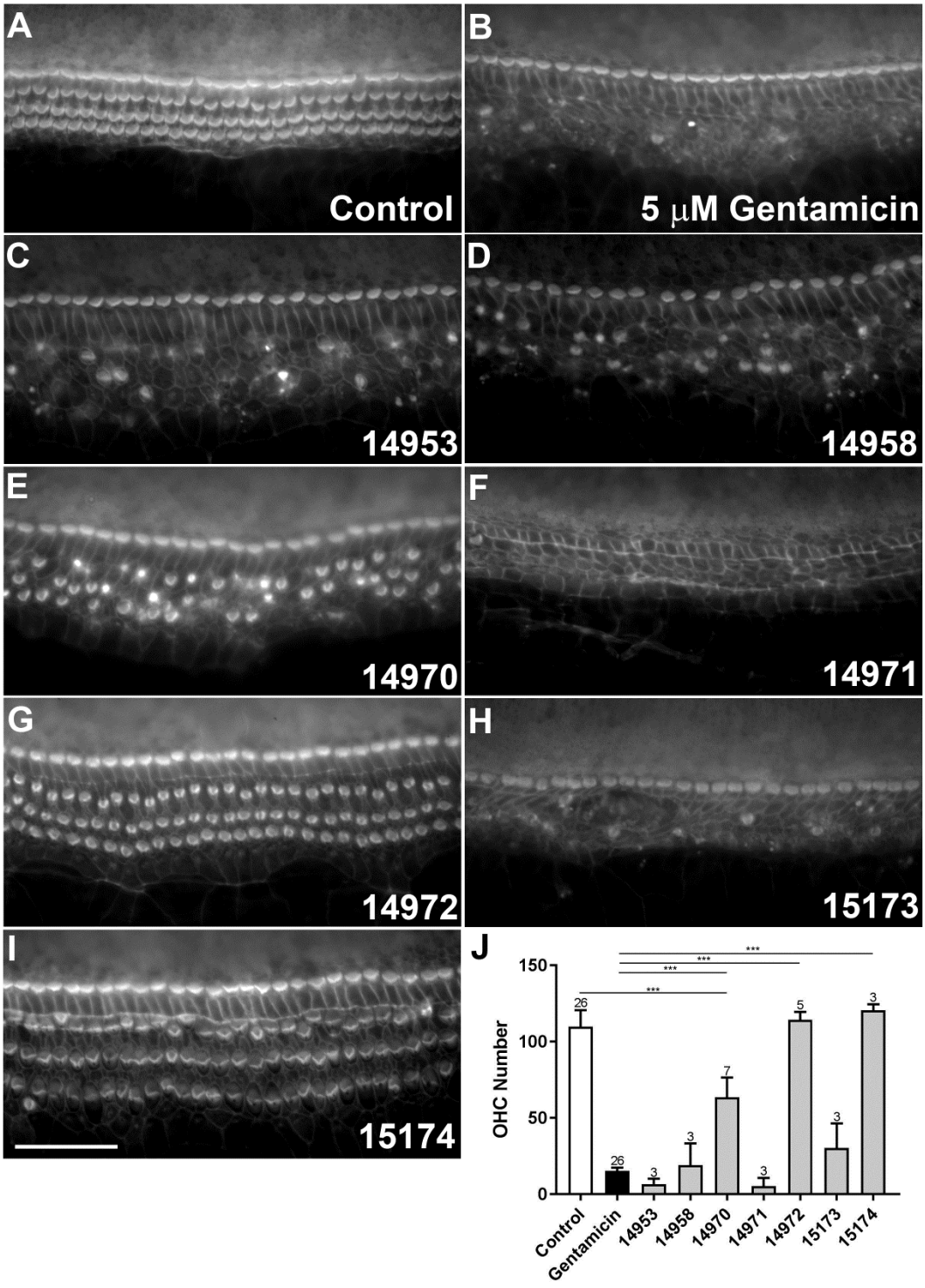

Figure 6.6: *When exposed to 5 μM gentamicin for 48 hours, co-incubation with certain carvedilol derivatives can prevent the mid-basal OHC loss. At 20 μM, 2 out of the 7 derivatives protected and 1 derivative showed partial protection.*

(A) A control culture exposed to 0.5% DMSO for 48 hours. **(B)** A culture exposed to 5 μM gentamicin and 0.5% DMSO for 48 hours. **(C-I)** Cultures exposed to 5 μM gentamicin for 48 hours plus 20 μM: **(C)** 14953, **(D)** 14958, **(E)** 14970, **(F)** 14971, **(G)** 14972, **(H)** 15173, **(I)** 15174.

Scale bar is 50 µm. **(J)** Quantification of HC survival revealed that 2 derivatives protected at 20 µM against 5 µM gentamicin (14972 and 15174) and 1 derivative offered partial protection (14970), with the HC survival significantly different from both the control and gentamicin exposed cultures ($p < 0.001$ in both cases).

The three derivatives that showed partial or full protection at 20 µM were subsequently tested against 5 µM gentamicin at 10 and 5 µM. At these concentrations, only 14972 remained protective, providing full protection at 5 µM in 6 out of 7 screens. Carvedilol itself showed full protection at 5 µM in 4 out of 8 screens, suggesting that 14972 had slightly improved protective properties (Figure 6.7). The average HC number in the control conditions was 109.8 (± 2.2) (n=24) and in the gentamicin-treated conditions it was 15.3 (± 2.2) (n=26). When gentamicin was co-incubated with 5 µM carvedilol the HC count was 66.1 (± 12.4) (n=7), and when co-incubated with 14972 it was 98.9 (± 8.2) (n=7). A one-way ANOVA followed by Tukey's multiple comparisons test revealed that the difference in HC survival between the carvedilol and 14972-treated cultures was significant ($p = 0.0016$) (Figure 6.7).

When tested alone 14972 showed similar toxicity characteristics to carvedilol, proving toxic to OHCs at concentrations ≥ 30 µM and affecting the IHC and OHC bundle morphology at 20 µM. Unlike carvedilol, however, 14972 was not toxic at 30 µM when tested together with 5 µM gentamicin. At this concentration 14972 provided protection but did affect IHC and OHC bundle morphology (data not shown).

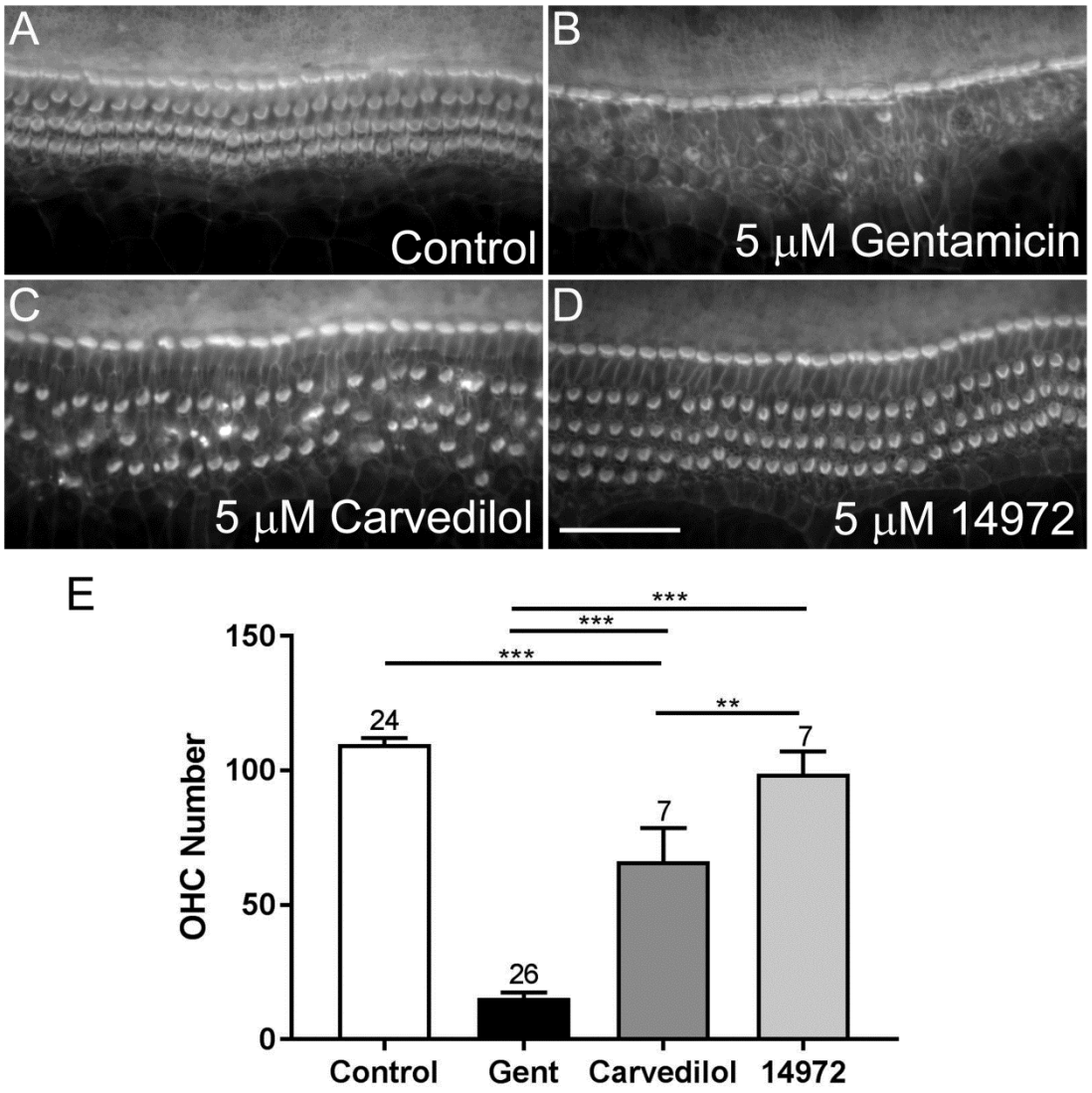

Figure 6.7: *When exposed to 5 μM gentamicin for 48 hours, co-incubation with 5 μM 14972 was more effective at preventing OHC loss than co-incubation with 5 μM carvedilol.*

(A) A control culture exposed to 0.5% DMSO for 48 hours. **(B)** A culture exposed to 5 μM gentamicin and 0.5% DMSO for 48 hours. **(C-D)** Cultures exposed to 5 μM gentamicin for 48 hours plus 5 μM: **(C)** carvedilol or **(D)** 14972. Scale bar is 50 μm. **(J)** Quantification of HC survival reveals that 14972 is completely protective when tested at 5 μM however carvedilol is only partially protective, with HC survival significantly different from both the control and gentamicin exposed cultures ($p < 0.001$ in both cases).

In conjunction with assessing the protective abilities of the 7 carvedilol derivatives, potential interactions with the MET channel were investigated by recording MET currents from OHCs before and during exposure to 10 µM of each compound. Fractional block curves of the currents during compound exposure relative to the control currents at each membrane potential show that 2 of the derivatives have limited interaction with the channel at this concentration (14958 and 15173; Figure 6.8). These derivatives were among the three that showed no protection at 20 µM, providing further evidence that the protection offered by carvedilol is a result of MET channel block. The third derivative showing no protection at 20 µM (14953) did reduce the MET currents across all membrane potentials; however, the level of block was greatly reduced compared to carvedilol suggesting that this derivative has a far lower affinity for the channel (Figure 6.8). Similar levels of block to 14953 were observed with 14970 (Figure 6.8), with no release of the block at extreme hyperpolarized potentials suggesting this compound is non-permeant. However, this derivative only offered partial protection against 5 µM gentamicin, possibly due to its lower affinity for the channel. Three of the derivatives were strong MET channel blockers at 10 µM (14971, 14972 and 15174; Figure 6.8). Compound 14971 was generally cytotoxic at 20 µM, however 14972 and 15174 offered consistent protection, with 14972 protecting OHCs from gentamicin damage at concentrations down to 5 µM. This result again suggests that the protection observed is brought about by a block of the MET channels, reducing the entry and accumulation of gentamicin into the cells. Both 15174 and 14972 appeared to be permeant blockers of the MET channel, indicated by the release of the block at the extreme hyperpolarized potentials (Figure 6.8).

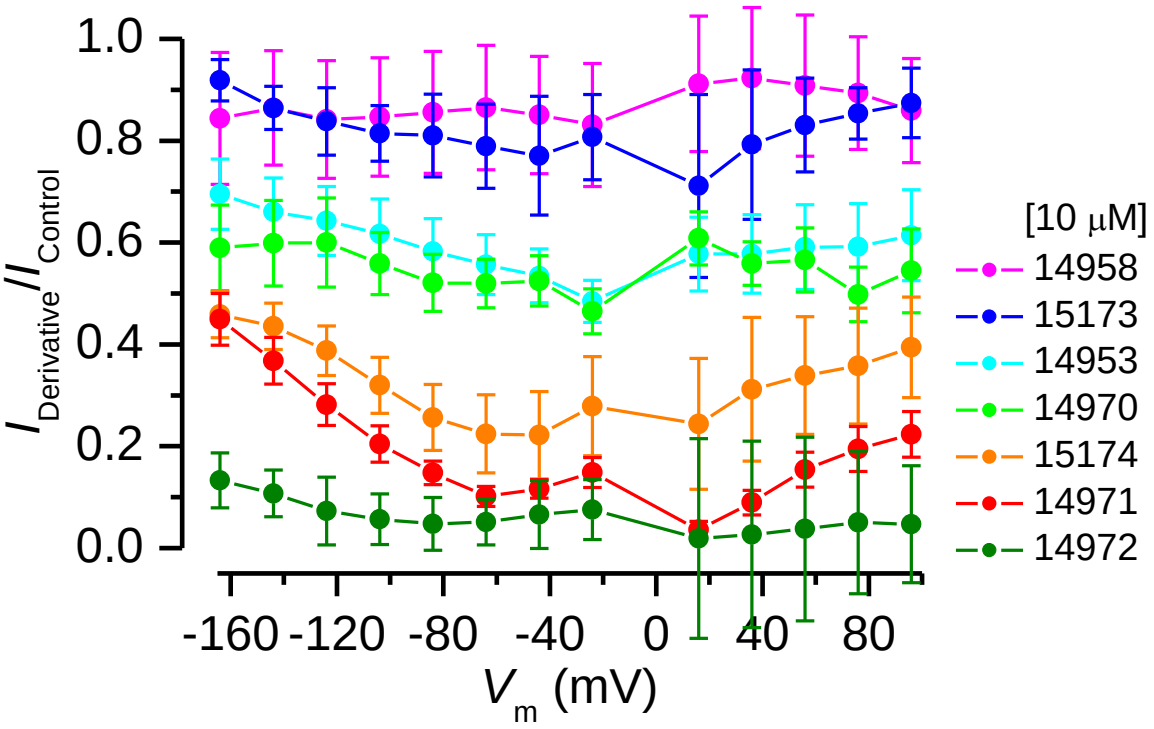

Figure 6.8: *Fractional block curves revealed varying degrees of interaction between the 7 carvedilol derivatives and the MET channel.*

Fractional block curves of the currents recorded during 10 µM derivative exposure relative to the control currents at each membrane potential (between -164 and +96 mV). Two of the derivatives showed limited interaction with the channel (14958 and 15173), two showed a partial block of the currents (14953 and 14970) and three acted as strong MET channel blockers (14971, 14972 and 15174). Number of cells; 14970: 3, 14971: 5, 14972: 2, 14953: 8, 14958: 5, 15173: 2, 15174: 4. Data collected by Nerissa Kirkwood.

Combining the desired characteristics of a non-permeant MET channel blocker (14970) and a higher-affinity blocker (14972) a further derivative was synthesised (31036) and the protective and channel-blocking abilities determined. Compound 31036 showed limited interaction with the MET channel at both 3 and 10 µM (data not shown). It protected against 5 µM gentamicin in only one out of three trials when tested at 20 µM (Figure 6.9A-C) and provided no protection at 10 µM (3 repeats; data not shown). However solubility problems were identified with this derivative hindering any meaningful interpretation of the results.

A further 6 derivatives were synthesised in an attempt to improve the protective abilities and eliminate the solubility problems of previous compounds (31833, 32528, 32536, 32546, 32639

and 32663). Of these derivatives, 2 were generally cytotoxic when tested at 20 µM against 5 µM gentamicin (32639 and 32633) for 48 hours, 2 offered no protection (32528 and 32546) 1 showed partial protection (31833) and 1 was consistently protective (32536) (Figure 6.9D-J). When tested at 10 µM, 31833 no longer offered any protection and 32536 was protective in 2 out of 4 screens but offered no protection at 5 µM (data not shown).

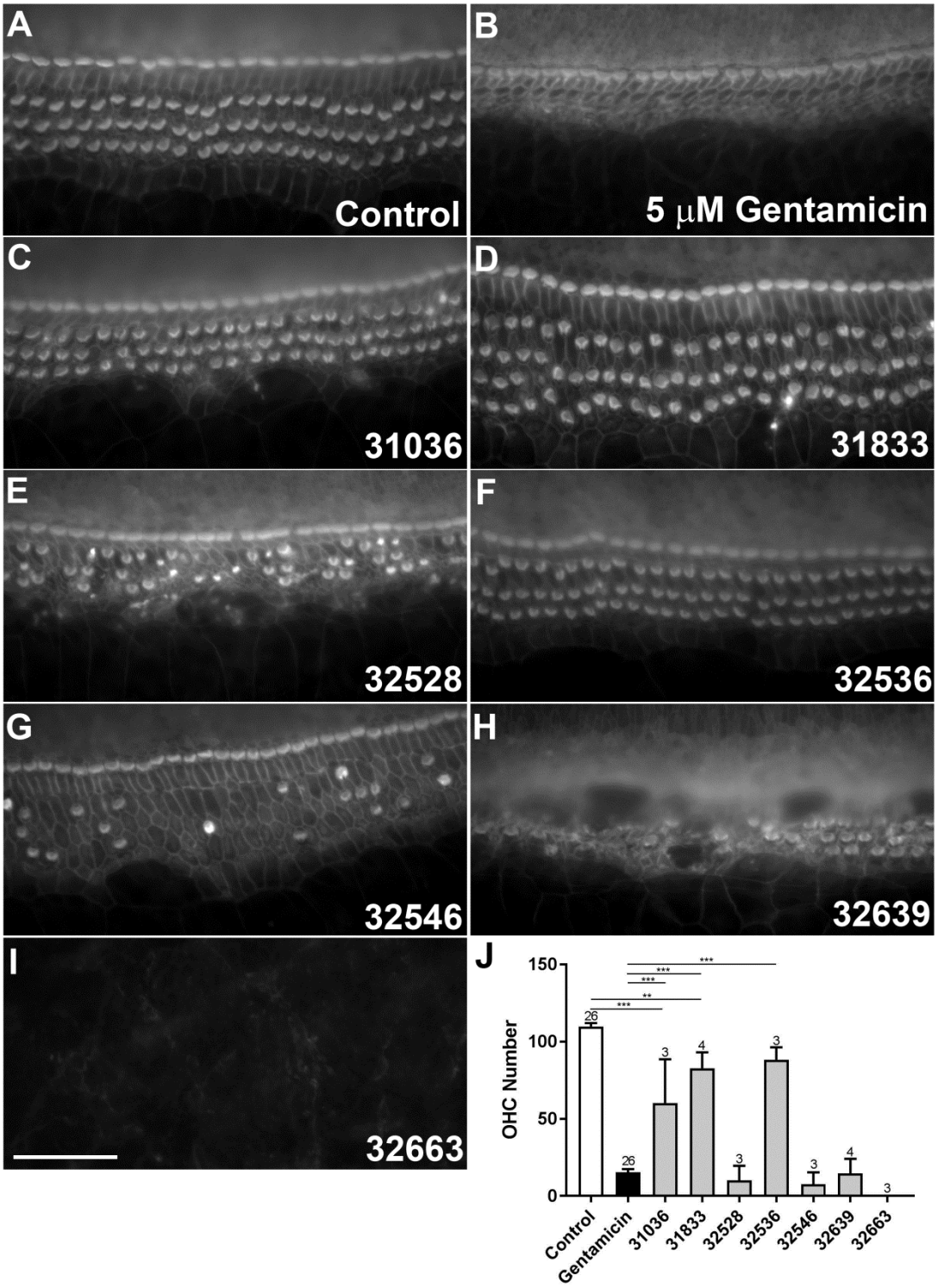

Figure 6.9: *When exposed to 5 μM gentamicin for 48 hours, co-incubation with certain carvedilol derivatives can prevent mid-basal OHC loss. At 20 μM, 1 out of the 7 derivatives protected and 2 showed partial protection. At 10 μM, none maintained their protective ability (data not shown).*

(A) A control culture exposed to 0.5% DMSO for 48 hours. **(B)** A culture exposed to 5 µM gentamicin and 0.5% DMSO for 48 hours. **(C-I)** Cultures exposed to 5 µM gentamicin for 48 hours + 20 µM: **(C)** 31036, **(D)** 31833, **(E)** 32528, **(F)** 32536, **(G)** 32546, **(H)** 32639 or **(I)** 32663. Scale bar is 50 µm. **(J)** Quantification of HC survival reveals one derivative protects at 20 µM against 5 µM gentamicin (32536) and two derivatives offer partial protection (31036 and 31833) with the HC survival significantly different from both the control ($p < 0.001$ and p = 0.0087, respectively) and gentamicin exposed cultures ($p < 0.001$).

MET channel interactions were investigated for the two derivatives that showed protection or partial protection at 20 µM (31833 and 32536). Fractional block curves revealed that both compounds, at a concentration of 10 µM, blocked the MET channel at all membrane potentials, however the degree of block was far less than for both carvedilol and 14972 (Figure 6.10) suggesting these derivatives had a reduced affinity for the channel.

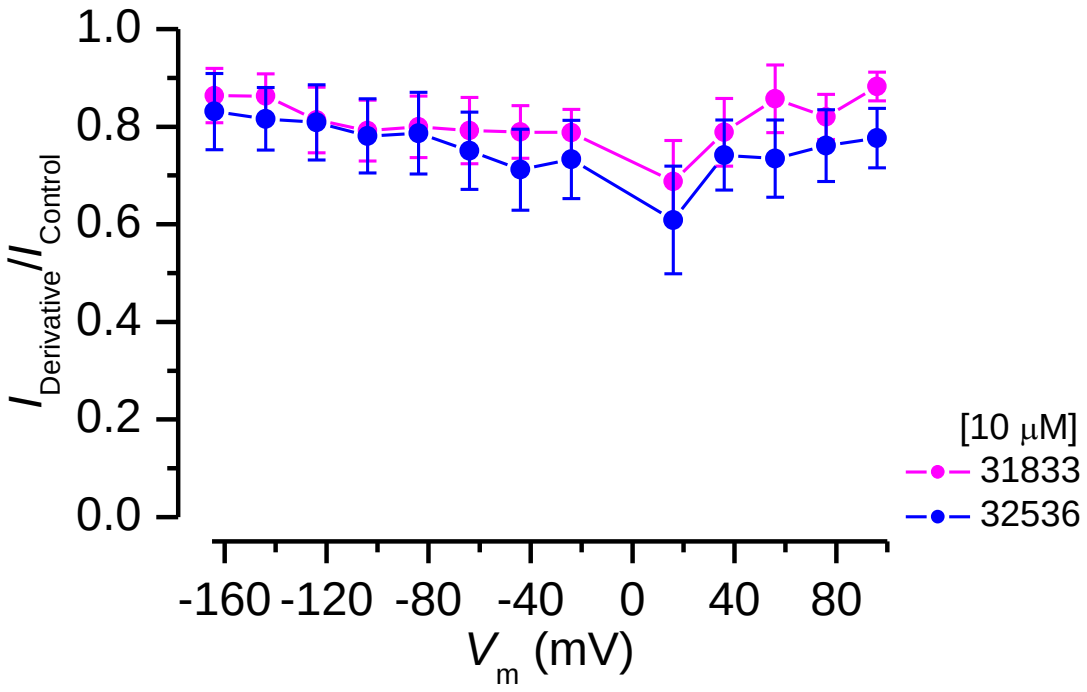

Figure 6.10: *Fractional block curves revealed that the carvedilol derivatives 31833 and 32536 had a far lower affinity for the MET channel than carvedilol itself.*

Fractional block curves of the currents recorded during 10 µM derivative exposure relative to the control currents at each membrane potential (between -164 and +96 mV). Both 31833 and 32536 show a limited interaction with the MET channel across all membrane potentials. Number of cells; 31833: 5, 32536: 5. Data collected by Nerissa Kirkwood.

6.2.4 Mechanism of Protection (continued)

To further assess whether carvedilol and the most protective derivative 14972 protected sensory HCs against AG damage by blocking the MET channel and thereby preventing the entry of the antibiotics into the cells, a fluorescent gentamicin analogue (GTTR) was used to quantify gentamicin uptake (Steyger et al., 2003). Pre-incubation with either 1% DMSO, 100 µM carvedilol or 100 µM 14972 for 5 minutes prior to 0.2 µM GTTR application resulted in significantly reduced loading of GTTR in the presence of both carvedilol and 14972 relative to the DMSO control ($p < 0.001$ in both cases) (Figure 6.11). No significant difference was observed between the GTTR loading in the presence of carvedilol or 14972. These findings further suggested that both carvedilol and 14972 protected against AG damage by competitively blocking the MET channel and thereby preventing AG entry into HCs, minimising accumulation and consequent apoptosis induction.

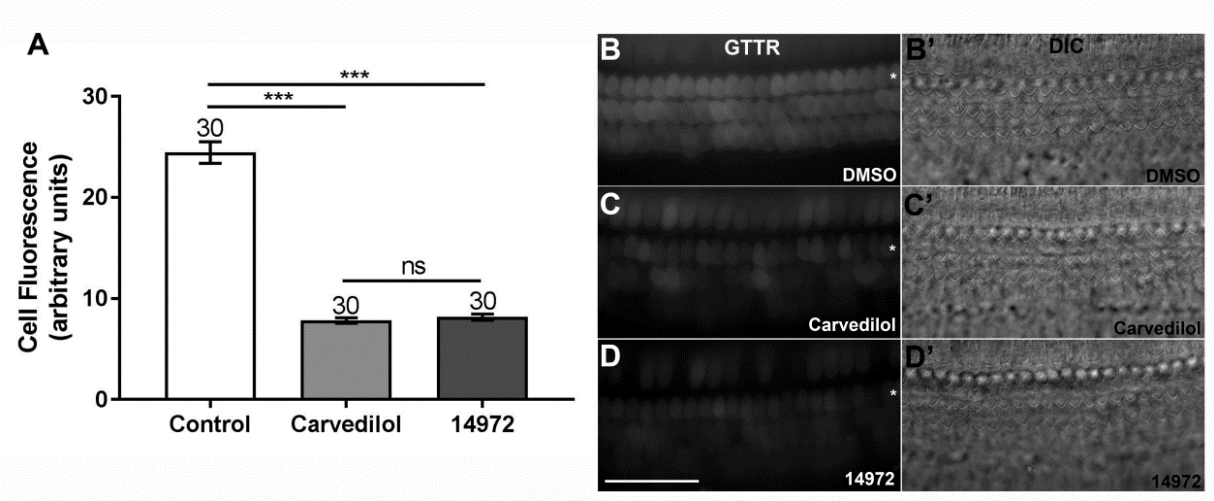

Figure 6.11: *Carvedilol and 14972 significantly block the entry of GTTR into mouse cochlear culture HCs.*

(A) Quantification of GTTR fluorescence intensity in a control culture pre-treated with 1% DMSO before the addition of 0.2 µM GTTR, compared to cultures pre-treated with 100 µM carvedilol or 14972. Both compounds significantly reduced GTTR loading ($p < 0.001$). No significant difference in reduction was seen between the two compounds. **(B-D)** A representative fluorescence image from which intensity values were measured and a DIC image for: **(B and B')** the control **(C and C')** carvedilol and **(D and D')** 14972. Asterisks indicate the first row of OHCs, from which fluorescence intensity values were taken. Scale bar is 50 µm.

6.3 Summary

The screening process detailed in this chapter has enabled a full characterisation of carvedilol's otoprotective profile, both in terms of its protective ability and also its mechanism of protection. Here we confirm that it is protective against neomycin damage to the HCs of the zebrafish lateral line (Ou et al., 2009) and we extended this knowledge to show that it also protects neuromast HCs against 10 μM gentamicin damage when tested at ≥ 25 μM. We also provided evidence of its protection against 5 μM gentamicin damage in mouse cochlear cultures when tested at 10 and 20 μM. Extensive screening and confocal imaging revealed that at 20 μM, carvedilol caused selective damage to the IHC mechanosensory hair bundles in cochlear cultures, both when tested alone and in the presence of gentamicin. Furthermore, when tested at ≥ 30 μM both in the absence and presence of gentamicin, carvedilol is generally cytotoxic to all cell types in cochlear cultures.

Electrophysiological recordings revealed that carvedilol is a relatively high-affinity blocker of the MET channel (K_D = 1.5 μM at +96 mV; data not shown), displaying a voltage-dependent, permeant block of the channel similarly to the compounds previously identified in Chapters 4 and 5. Block of the channel was strongest at intermediate and depolarised potentials, was released at both extremes of depolarisation and hyperpolarisation, and was completely reversible.

We synthesised 7 carvedilol derivatives, 2 of which provided complete protection against gentamicin damage in cochlear cultures when tested at 20 μM. Both of these were found to be strong MET channel blockers. We then synthesised 6 more derivatives, only one of which was protective. Although it did block the MET channel, it was with a much lower affinity than carvedilol. Of all of the synthesised derivatives only one (14972) showed improved protection characteristics relative to carvedilol, more frequently providing protection when tested at a concentration of 5 μM.

As a final confirmation of the relation between MET block and protective ability, GTTR experiments were conducted to assess if carvedilol and 14972 blocked GTTR uptake into HCs. Both significantly reduced its loading, adding further confirmation to the identified mechanism of protection.

6.4 Discussion

Within this chapter, evidence is provided of the otoprotective profile of carvedilol, for both zebrafish lateral line and mouse cochlear culture HCs. We have clearly demonstrated the mechanism of protection of the compound, linking carvedilol's protective nature to its ability to block the MET channel and thereby reduce AG entry and consequent accumulation within sensory HCs. This screening process has further highlighted the usefulness and applicability of zebrafish pre-screening in the search for mammalian otoprotectants. If blindly screened in our zebrafish assay, carvedilol would have been taken forward to mouse cochlear cultures for additional testing – thus reinforcing the viability of our two-model screening procedure.

The results of the cochlear culture screening process detailed in this chapter have again reinforced the proposition that we need to adhere to a thorough screening procedure in mammalian systems when searching for potential clinically-viable otoprotectants. Despite being protective at 10 and 20 μM, carvedilol caused severe IHC bundle disruption at 20 μM and was generally cytotoxic when tested ≥ 30 μM, both in the presence and absence of gentamicin. Similarly to the extremely narrow protective range that was found for the alkaloid berbamine (Chapter 5), these toxicity characteristics had not been picked up on when previously screened in zebrafish alone (Ou et al., 2009). However, it is possible that compounds that would not be toxic *in vivo* may appear toxic *in vitro* due to the experimental assay conditions. Consequently, this criterion should not be used to eliminate compounds as this could result in the rejection of possibly useful drugs. Mammalian *in vivo* screening is necessary to address this concern.

The screening of carvedilol derivatives offered further confirmation that the otoprotective nature of the compound is attributable to its block of the MET channel, as the three compounds that did protect all displayed a voltage-dependent block of the channel, similarly to the parent compound. Interestingly, the one compound that did strongly block the MET channel but did not protect (14971; shown to be toxic at 20 μM (Figure 6.8)), was also the most permeant of all of the compounds tested, displaying a large release of the block once the cell was stepped to -84 mV or below, indicative of the compound being drawn into the cell. This result suggests that the permeation and accumulation of the compound may underlie its evident toxicity, similarly to the AGs themselves. Although toxic to the basal section, 14971 caused no toxicity to the HCs in the apical region (data not shown); adding further confirmation to this postulation. This idea of permeation underlying toxicity could also underlie the disparity in the dTC and berbamine toxicity profiles, with berbamine found to be toxic at higher concentrations whereas dTC was not. As berbamine is a more permeant blocker

of the MET channel, it would enter the HCs more readily. This greater permeation would lead to greater intracellular accumulation and consequently a greater likelihood of initiating intracellular apoptotic pathways.

The improved protective ability of one compound (14972) relative to carvedilol itself suggests that we are capable of modifying compounds based on their mechanism of protection in order to improve their protective efficacy. Although a labour-intensive procedure, here we have shown that modifying compounds based on structure-activity relationships is a viable method for the generation of otoprotectants.

7 Assessing the Otoprotective Potential and MET Channel Interaction Abilities of FM 1-43 and its Derivatives

7.1 Introduction

7.1.1 Compound Choice

The styryl dye FM 1-43 is a water-soluble, cationic dye that has classically been a useful tool for the study of endo- and exo- cytosis (Betz et al., 1996; Amaral et al., 2011). It has been shown to behave as a permeant blocker of the MET channels in cochlear sensory HCs (Gale et al., 2001) and also in neurons (Drew and Wood, 2007). The dye rapidly loads into HCs via the apical surface, exhibits a voltage-dependent block of the MET channel and its loading is reduced by increasing the extracellular calcium concentration (leading to greater adaptation in the HC tip links). These data suggest that FM 1-43 primarily enters HCs in the same way as the AGs – through the MET channel. This postulation is further supported by the evidence that FM 1-43 co-administration alongside AG exposure reduced the ototoxic effects of the antibiotics (Gale et al., 2001), implying a common, competitive mode of entry into cells. The dye therefore provides a useful marker of MET channel function in the sensory HCs of the cochlea.

7.1.2 Aims

Due to its obvious interaction with the MET channel we chose to investigate this compound further, chemically synthesising 15 derivatives in order to assess the structure-activity relationships and gain a better understanding of which moieties of the compound are integral to its interaction with the MET channel and also its otoprotective abilities. This work is done on the premise that understanding what is required to block the MET channel will help with the future design of otoprotective compounds capable of blocking the channel and preventing AG entry and the associated ototoxicity. All derivatives were tested for their ability to protect against gentamicin damage in mouse cochlear cultures. They were also tested for their ability to load into the neuromast HCs of the zebrafish lateral line in a short time assay. Their block of the MET channel was subsequently investigated electrophysiologically as the focus of this study. The overarching aim was to better understand the components of the FM 1-43 molecule that enable it to behave as a permeant blocker of the MET channel, whilst also attempting to synthesise a non-permeant MET channel blocker.

7.2 Results

7.2.1 The Structural Modifications made to FM 1-43 in the Synthesising of Derivatives

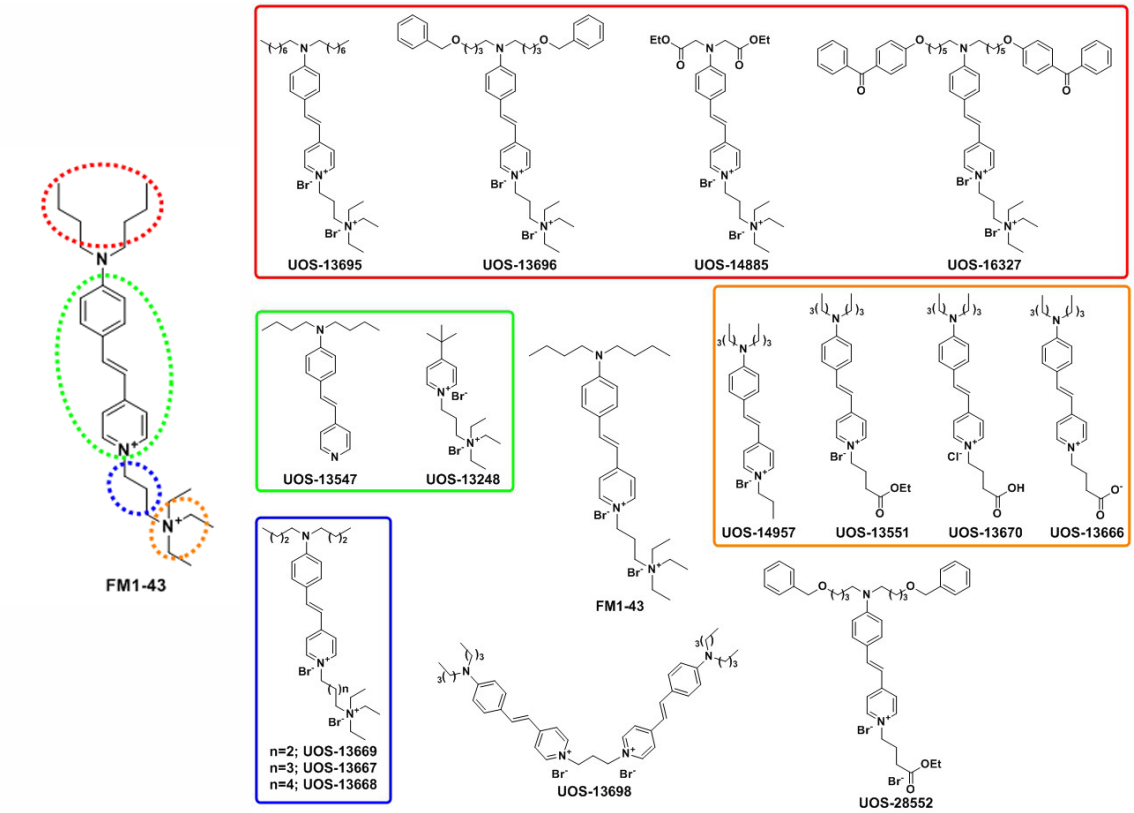

Figure 7.1: *The structure of FM 1-43 and the 15 derivative modifications synthesised in house.*

FM 1-43 has three distinct moieties: a lipophilic tail (red), a central core (green) and a hydrophilic head (orange and blue). Modifications were made to each moiety, as depicted.

The FM 1-43 molecule has a chemical structure consisting of three distinct moieties, as depicted in Figure 7.1. These are: a lipophilic tail (red circle), exemplified by two linear alkyl chains; a central core consisting of a pyridine ring conjugated via a double bond linker to a phenyl ring (green circle); and a hydrophilic head usually consisting of a quaternary nitrogen (orange circle) linked to the piridinium nitrogen via an alkyl chain (blue circle).

Chemical modifications were made to each of these three separate moieties to produce 15 FM 1-43 derivatives (13248, 13547, 13551, 13666, 13667, 13668, 13669, 13670, 13695, 13696, 13698, 14885, 14957, 16327 and 28552), with their structures as depicted in Figure 7.1.

7.2.2 Screening for Otoprotection in Mouse Cochlear Cultures

7.2.2.1 Protection at 5 μM

For the purposes of the experiments detailed in this chapter, FM 1-43 is denoted on graphical representations as 13550 – made in house by the chemist assigned to this project (Marco Derudas, University of Sussex). When tested at a concentration of 5 μM for their ability to protect against 48 hours exposure to 5 μM gentamicin, 9 of the FM 1-43 derivatives were found to be generally cytotoxic to the entire cochlear culture (13551, 13667, 13668, 13669, 13696, 14885, 14957, 16327 and 28552), killing not only the sensory HCs but also the other supporting cell types in the cochlear explant, similar to what I observed with FM 1-43 (13550) itself (Figure 7.2). Previously, FM 1-43 had been reported to be only mildly toxic when tested on mouse cochlear cultures at 30 μM, causing blebbing, or membrane externalisation, of the apical surface of basal-coil HCs (Gale et al., 2001; Chung et al., 2007). However, this was when tested in a relatively short 70 minutes exposure assay, much shorter than our 48 hours incubation assay. Two of the derivatives were not protective (13248 and 13547), 3 provided full protection from the gentamicin-induced loss of OHCs (13666, 13670 and 13695) and 1 (13698) provided partial protection in this initial trial. The 4 that provided at least some degree of protection were re-screened to confirm their protective abilities. Compounds 13666 and 13695 failed on these subsequent trials however 13670 and 13698 were successful, providing complete protection across three independent trials (Figure 7.2).

In terms of disruption to the morphology of the mechanosensory hair bundle, when tested at 5 μM the 2 derivatives that were consistently protective (13670 and 13698) both caused some degree of bundle disruption in all 3 independent trials. However, this could be due to the gentamicin as opposed to the derivatives. Compounds should be tested alone in the absence of gentamicin to further investigate this.

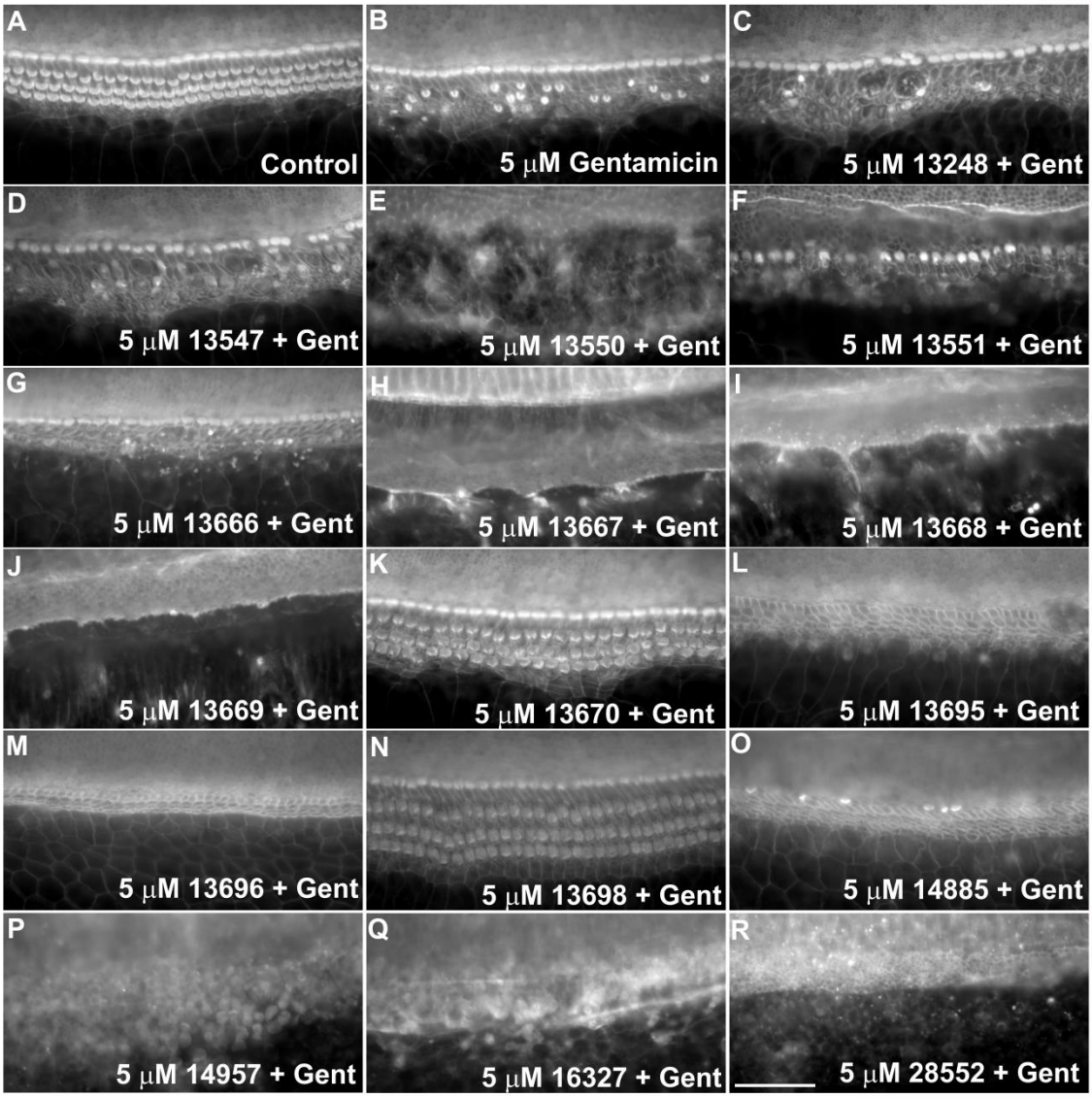

Figure 7.2: *When tested at 5 μM against 5 μM gentamicin for 48 hours, FM 1-43 and 9 of its derivatives were cytotoxic to mouse cochlear cultures, 4 were not protective and 2 were consistently protective*.

Cochlear cultures were treated with either **(A)** 0.5% DMSO, **(B)** 5 μM gentamicin and 0.5% DMSO, or **(C–O)** 5 μM gentamicin and 5 μM compound: **(C)** 13248 (n=1), **(D)** 13547(n=1), **(E)** 13550 (n=1), **(F)** 13551 (n=1), **(G)** 13666 (n=3), **(H)** 13667 (n=1), **(I)** 13668 (n=1), **(J)** 13669 (n=1), **(K)** 13670 (n=3), **(L)** 13695 (n=3), **(M)** 13696 (n=1), **(N)** 13698 (n=4), **(O)** 14885 (n=1), **(P)** 14957 (n=1), **(Q)** 16327 (n=1) or **(R)** 28552 (n=1) for 48 hours. Images in **A** and **B** are representative of 17 experiments. Images in **C–R** are representative of 1-4 experiments each. Scale bar is 50 μm.

7.2.2.2 Protection at 0.5 µM

When the compound concentration was reduced to 0.5 µM, still in the presence of 5 µM gentamicin, no toxicity was observed with any of the 15 derivatives or from the parent compound, 13550. In the initial trial, 10 were not protective (13248, 13547, 13550, 13666, 13667, 13668, 13669, 13695, 13696 and 14885), 2 were partially protective (13698 and 14957) and 4 were found to be protective (13551, 13670, 16327 and 28552); however, 2 of these (13670 and 16327) then failed to provide protection on subsequent trials, and only 2 (13551 and 28552) consistently provided complete protection across 3 independent trials (Figure 7.3). No compound was consistently protective when tested at 0.1 µM (only one, 16327, protected on 1 of 3 occasions (data not shown)).

When tested at 0.5 µM, the 2 derivatives that were protective (13551 and 28552) both caused some degree of bundle disruption in all three independent trials. Again, however, this could be due to the gentamicin as opposed to the derivatives. Compounds should be tested alone in the absence of gentamicin to further investigate this.

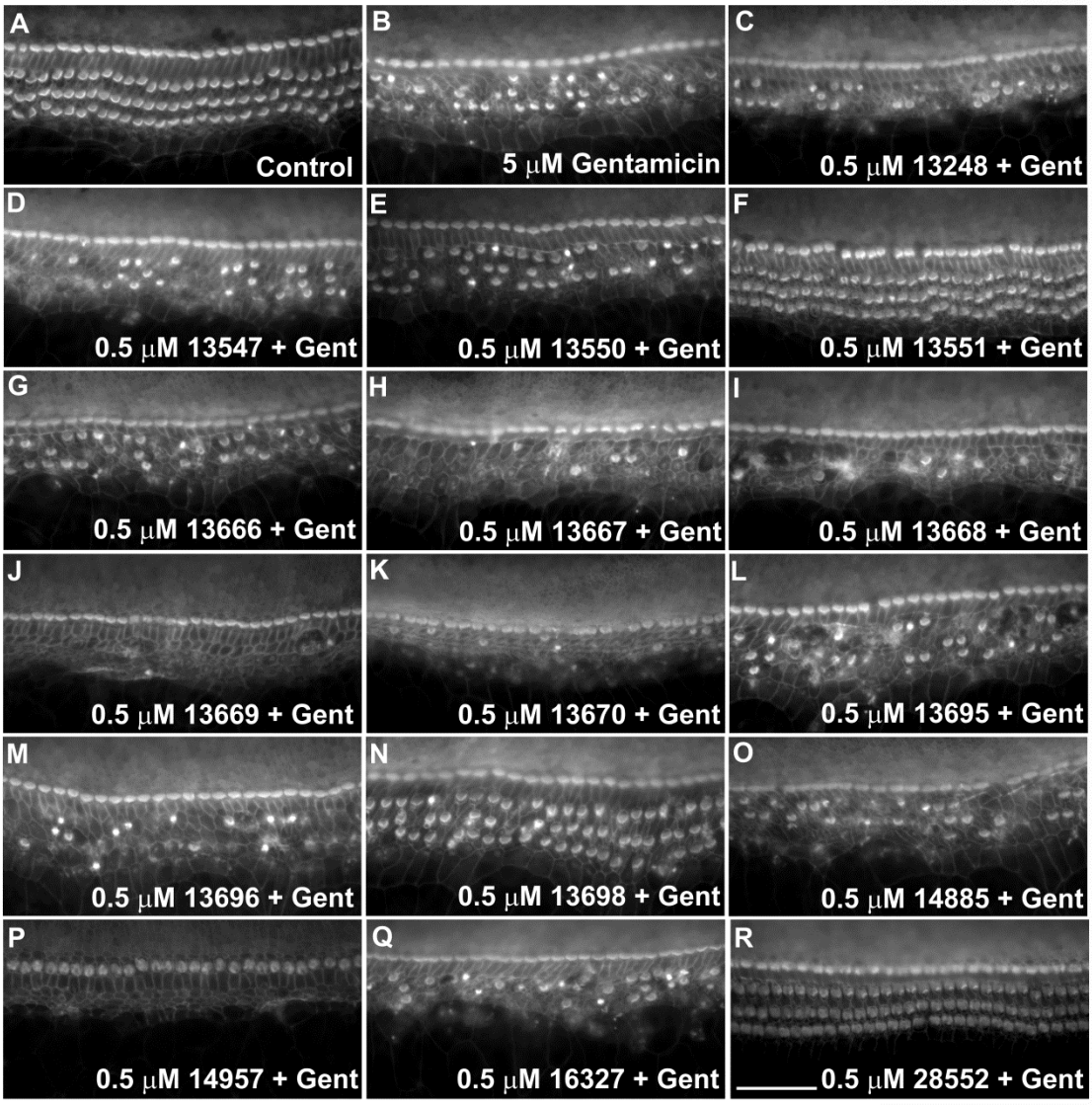

Figure 7.3: *When tested at 0.5 μM against 5 μM gentamicin for 48 hours, 2 FM 1-43 derivatives were consistently protective whilst the remaining 13 and FM 1-43 itself were not protective.*

Cochlear cultures were treated with either **(A)** 0.5% DMSO, **(B)** 5 μM gentamicin and 0.5% DMSO, or **(C–O)** 5 μM gentamicin and 0.5 μM compound: **(C)** 13248 (n=1), **(D)** 13547 (n=1), **(E)** 13550 (n=1), **(F)** 13551 (n=3), **(G)** 13666 (n=1), **(H)** 13667 (n=1), **(I)** 13668 (n=1), **(J)** 13669 (n=1), **(K)** 13670 (n=3), **(L)** 13695 (n=1), **(M)** 13696 (n=1), **(N)** 13698 (n=1), **(O)** 14885 (n=2), **(P)** 14957 (n=1), **(Q)** 16327 (n=3) or **(R)** 28552 (n=3) for 48 hours. Images in **A** and **B** are representative of 17 experiments. Images in **C–R** are representative of 1-3 experiments. Scale bar is 50 μm.

7.2.3 Assessing MET Channel Interaction

7.2.3.1 Zebrafish Loading Assay

*The zebrafish research presented in this section was collected by Emma Kenyon, University of Sussex.

All derivatives were initially screened for their ability to load into the HCs of zebrafish lateral line neuromasts. This gave an initial indication of whether the compounds still behaved as permeant MET channel blockers and entered into sensory HCs, similar to FM 1-43 itself. Compounds were tested at a range of concentrations: 300 nM, 1 µM, 3 µM or 10 µM and images were taken at a range of time intervals: 1, 2.5, 5 or 10 minutes.

Only one compound (14885) did not load into neuromast HCs at any concentration, over any time period. Compound 13666 showed extremely weak loading into HCs, however some slight loading was detected after 10 minutes incubation at 10 µM, potentially as a result of endocytic processes as opposed to MET channel permeation (Figure 7.4).

Of the remaining 13 derivatives, in comparison to the parent compound (13550), 4 showed a greatly reduced loading pattern (13547, 13667, 13669, and 13670), 2 showed a moderately reduced loading pattern (13698 and 16327), 4 showed a similar level of loading (13551, 13695, 13696 and 28552) and 2 showed enhanced loading into neuromast HCs (13668 and 14957) (Figure 7.4). Compound 13248 was not tested for its loading ability as it does not bear any chromophore so cannot be seen in these assays.

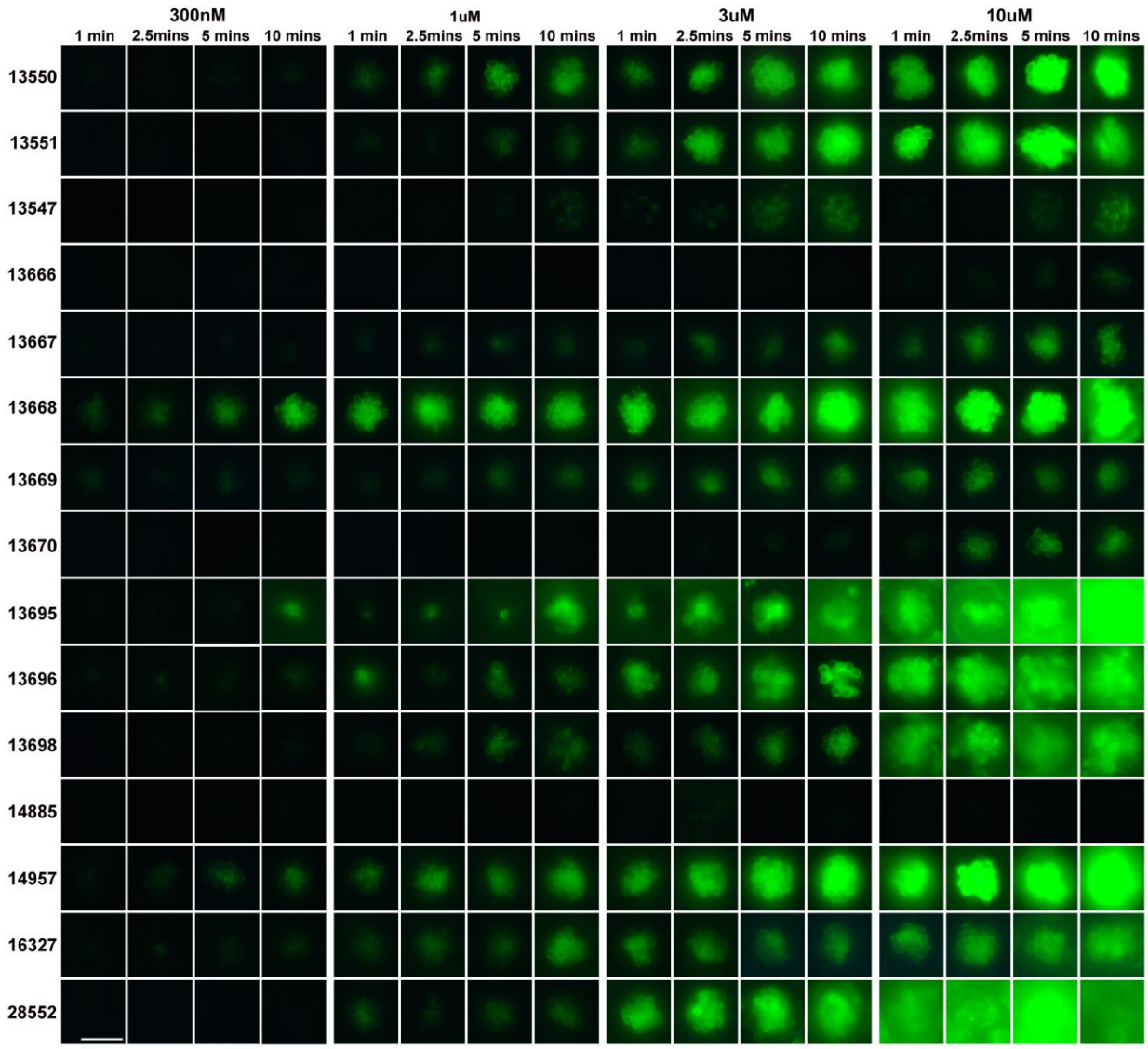

Figure 7.4: *Comparison of loading of FM 1-43 derivatives into zebrafish lateral line HCs.*

4 days post fertilisation zebrafish embryos were treated with FM 1-43 derivatives at a concentration of 300 nM, 1 µM, 3 µM or 10 µM for either 1 minute, 2.5 minutes, 5 minutes or 10 minutes before washing and imaging. Derivative loading is compared to that of the parent compound, 13550. Neuromast 4 was imaged in every instance. Scale bar is 25 µm.

7.2.3.2 Electrophysiological Recordings of MET Channel Currents

* The electrophysiology presented in Figure 7.6 was performed by Nerissa Kirkwood, University of Sussex.

7.2.3.2.1 FM 1-43 (13550)

FM 1-43 and all of its derivatives were tested for their ability to block the OHC MET channels of P2 mouse cochlear cultures. MET channel currents were recorded in whole-cell voltage clamp mode before, during and after the superfusion of each compound, tested at 10 µM. The cell was clamped at a holding potential of -84 mV and stepped to hyperpolarising voltages down to -164 mV and up to depolarising voltages of +96 mV, in 20 mV increments, in order to assess the voltage-dependency of any observed channel block.

Shown in Figure 7.5A-C is an example of the MET current recordings from a third row OHC, before (black), during (red) and after (blue) the superfusion of 10 µM 13550. Also shown is the current-voltage curve derived from the traces in A-C (Figure 7.5D) and the fractional block curve generated from 3 different cells (Figure 7.5E). The transformed data highlights the voltage-dependency of the observed MET channel block. Block of the MET channel by 13550 is strongest at slightly depolarised potentials (+16 mV). The block of the channel is released at the extreme depolarised and hyperpolarised potentials, which is indicative of 13550 behaving as a permeant blocker of the MET channel, as has been reported elsewhere (Gale et al., 2001). This notion is further supported by the zebrafish loading assay presented herein (Figure 7.4), which showed the loading of 13550 into neuromast HCs after 1 minute at 3 of the 4 concentrations tested.

Interestingly, FM 1-43 had previously been reported to have otoprotective abilities against neomycin-induced HC damage in mouse cochlear cultures when tested in a short-time assay (Gale et al., 2001), and the mechanism of protection was assumed to be due to MET channel block. Here, however, I found that despite the observed channel block, in the 48 hours cochlear culture protection assay FM 1-43 provided no protection when tested at 0.5 µM (Figure 7.3E) and was generally cytotoxic when tested at 5 µM (Figure 7.2E). Gale et al. (2001) did report a blebbing effect on the apical membranes of cochlear HCs after 70 minutes of prolonged exposure to FM 1-43, so this result is perhaps not surprising.

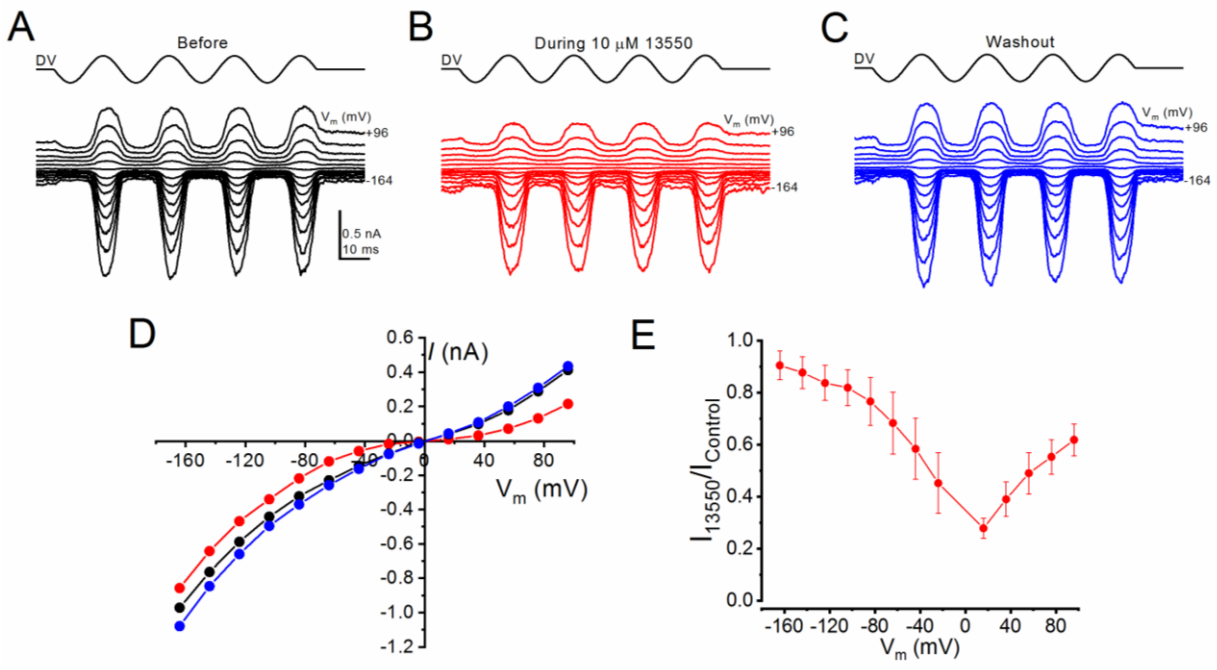

Figure 7.5: *Extracellular exposure to 10 µM FM 1-43 (13550) reduced OHC MET currents at all membrane potentials, with the reduction most pronounced at slightly depolarised potentials.*

(A-C) MET currents recorded from a P2 basal OHC between -164 and +96 mV in response to a sine-wave stimulus delivered by a fluid jet (45 Hz sinusoid, ±40V driver voltage, DV) shown above each trace, before (black), during (red) and after (blue) exposure to 10 µM 13550. Compound 13550 caused a reduction of the current size at all potentials. Full recovery is seen following re-exposure to the control solution. **(D)** Current-voltage curves of the currents shown in **(A-C)** reveal the current block at all potentials during 13550 exposure and the reversibility of the block following washout. **(E)** Fractional block curve reveals the voltage-dependency of the block, with maximal block observed at slightly depolarised potentials (n=3 OHCs).

7.2.3.2.2 Derivatives with Lipophilic Tail Modifications - 13695, 13696 and 14885

Lipophilic tail alterations were made to the FM 1-43 molecule based on the assumption that we could potentially design a compound that did not permeate the MET channel following its block, due to the altered size of the lipophilic tail moiety. This is because, in theory, the positively charged head moiety of the molecule would interact with the MET channel as usual however the lipophilic tail moiety might be too big to permeate into the HC, thereby creating a non-permeant blocker of the channel.

Three derivatives were designed with lipophilic tail modifications (13695, 13696 and 14885) and investigated for their interaction with the channel: compounds 13695 (a C-8 derivative), 13696 (a C-4 Obenzyl derivative, with the introduction of oxygen assumed to increase solubility) and 14885 (ethyl acetate), which shares the same moiety as the calcium chelator BAPTA, known to abolish mechano-electrical transduction by way of tip-link degeneration (Assad et al., 1991; Goodyear and Richardson, 2003; Marcotti et al., 2014).

When tested electrophysiologically, there was a mixture of MET channel interactions. Compound 13695 gave a moderate block of the channel, as shown by the exemplar MET current traces in Figure 7.6, showing the currents recorded before (black), during (red) and after (blue) 10 µM 13695 superfusion (Figure 7.6A-C). A current-voltage curve is shown in Figure 7.6D and the average fractional block curve from 3 cells is shown in Figure 7.6E, further highlighting the voltage-dependency of the observed channel block. Compound 13696 was not tested at 10 µM due to time limitations, however when tested at 3 µM it displayed a strong, voltage-dependent block of the MET channel, as shown by the fractional block curve presented in Figure 7.6F (n=2 OHCs). Compound 14885 displayed no interaction with the channel. Its average fractional block is presented later, in Figure 7.11B. Compound 14885's lack of interaction is perhaps not surprising following the result of the zebrafish loading assay (Figure 7.4), which showed that this compound did not load into neuromast HCs at any concentration over any time course tested. Both 13695 and 13696 loaded similarly into neuromast HCs when tested in the zebrafish assay, confirming that they still behave as permeant blockers of the channel (Figure 7.4).

Interestingly, all 3 compounds were toxic when tested in cochlear cultures at 5 µM (Figure 7.2) and none of the compounds provided any protection against the gentamicin-induced loss of OHCs when tested at 0.5 µM (Figure 7.3), similarly to FM 1-43 itself.

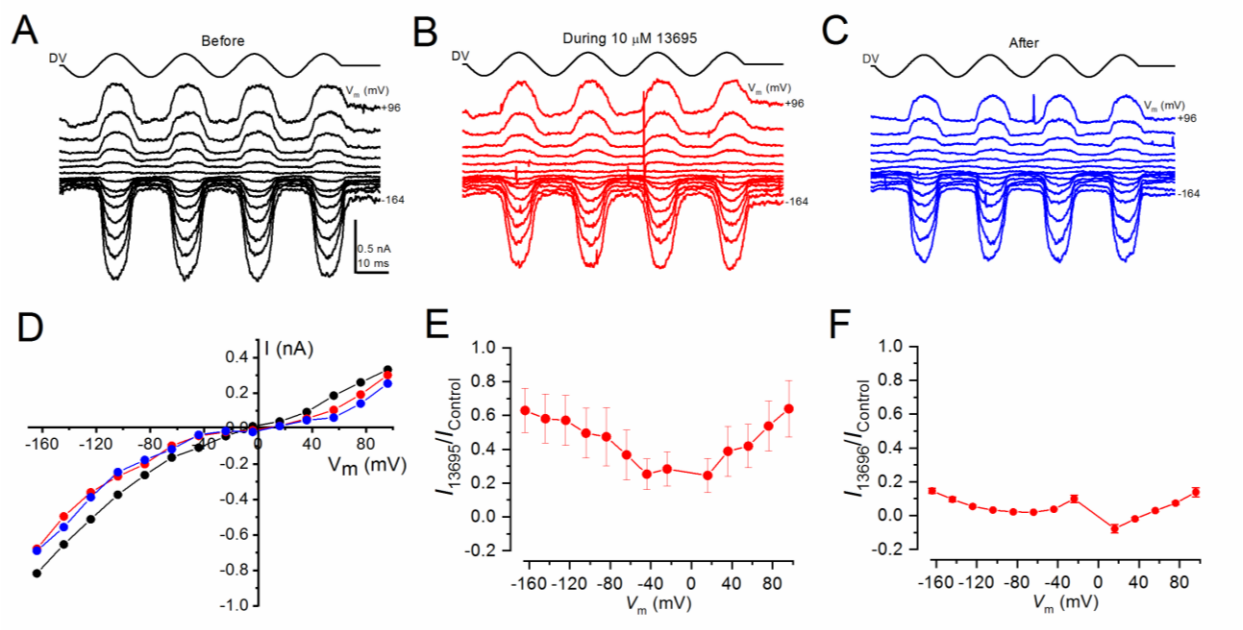

Figure 7.6: *Extracellular exposure to 10 µM 13695 and 3 µM 13696, two of the three FM 1-43 derivatives with lipophilic tail modifications.*

(A-C) MET currents recorded from a P2 basal OHC between -164 and +96 mV in response to a sinewave stimulus delivered by a fluid jet (45 Hz sinusoid, ±40V driver voltage, DV) shown above each trace, before (black), during (red) and after (blue) exposure to 10 µM 13695. Compound 13695 caused a reduction of the current size at all membrane potentials. No recovery is seen following re-exposure to the control solution. **(D)** Current-voltage curves of the currents shown in **(A-C)** reveal the current block at all potentials during 13695 exposure and the irreversibility of the block following washout. **(E)** Fractional block curve reveals the voltage-dependency of the block, with maximal block observed at slightly depolarised potentials (n=3 OHCs). **(F)** Fractional block curve for 3 µM 13696 shows the strong, voltage-dependent block of the MET channel (n=2 OHCs). Data obtained from Nerissa Kirkwood, figure prepared by myself.

7.2.3.2.3 Derivatives with Central Core Modifications – 13248 and 13547

The 2 compounds synthesised with alterations to their central core were compounds 13248 and 13547. The FM 1-43 parent molecule was cut into two halves, with the positive charges contained in one molecule (13248) and the lipophilic moiety in the other (13547). Due to the lack of positive charges in the lipophilic compound 13547, it was not expected to interact with the MET channel. Compound 13248 was expected to show an interaction due to the existence of two positive charges contained within the molecule.

When tested electrophysiologically, neither compound blocked the MET current at any membrane potential (-164 to +96 mV) when tested at 10 µM, indicating no interaction with the channel. Shown in Figure 7.7A-C is an example of the MET currents obtained from a third row OHC before (black), during (red) and after (blue) the superfusion of 10 µM 13547. The current-voltage (Figure 7.7D) and fractional block curves (figure 7.7E) generated from the raw data further highlight the lack of interaction of the compound with the MET channel. The average fractional block curve for 13248 is presented later, in Figure 7.11B.

When tested in zebrafish, 13547 did display some loading into neuromast HCs after approximately 5 minutes at the higher concentrations tested; however this could potentially be due to endocytic processes. Compound 13248 was not tested in the zebrafish loading assay due to it not bearing any chromophore.

Interestingly, neither compound with central core modifications provided any protection against the gentamicin-induced OHC loss when screened in cochlear culture assays (Figures 7.2 and 7.3), reinforcing the notion that the mechanism of otoprotection of FM 1-43 is due to its block of the MET channel. Furthermore, they also showed no toxicity at either concentration tested, implying that FM 1-43's toxic properties are due to its block of the MET channel and subsequent permeation into HCs. These data reveal that the central core and lipophilic moiety of the FM 1-43 molecule are integral to MET channel block and consequent otoprotection.

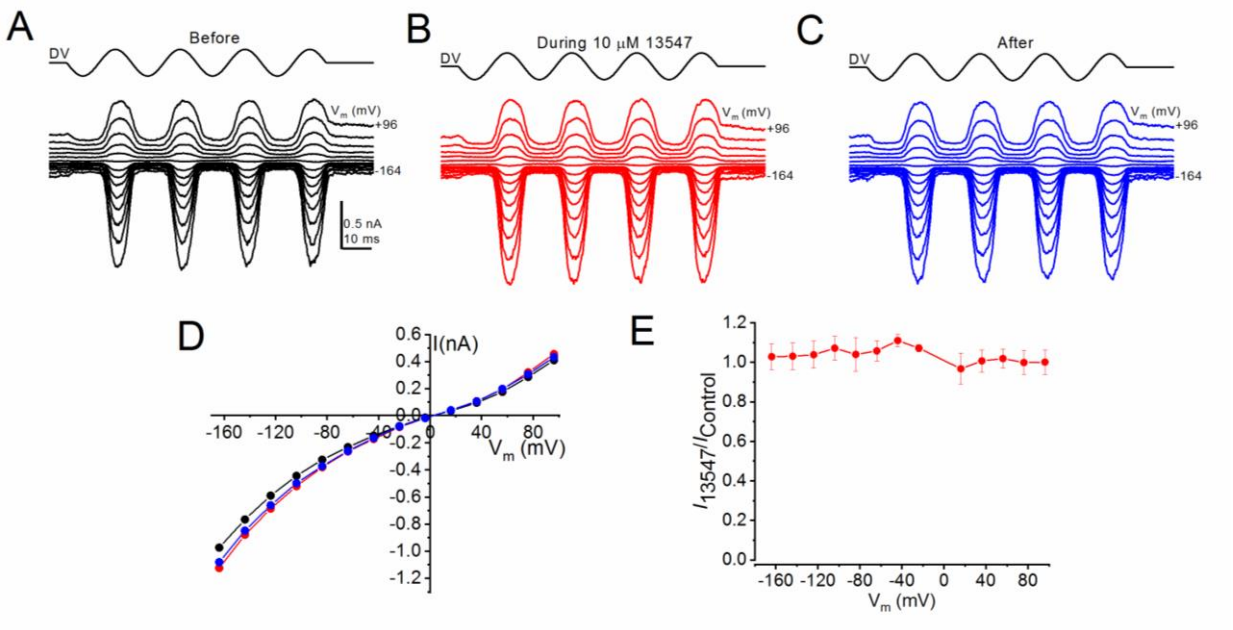

Figure 7.7: *Extracellular exposure to 10 µM compound 13547, one of the two FM 1-43 derivatives with central core modifications.*

(A-C) MET currents recorded from a P2 basal OHC between -164 and +96 mV in response to a sinewave stimulus delivered by a fluid jet (45 Hz sinusoid, ±40V driver voltage, DV) shown above each trace, before (black), during (red) and after (blue) exposure to 10 µM 13547. Compound 13547 caused no reduction in MET current size at any membrane potential tested. **(D)** The current-voltage and **(E)** fractional block curves further highlight the lack of interaction of 13547 with the MET channel (n=3 OHCs).

7.2.3.2.4 Derivatives with Hydrophilic Head, Quaternary Nitrogen Modifications – 13551, 13670 and 14957

Three derivatives were designed with altered hydrophilic heads based on quaternary nitrogen modifications (13551, 13670 and 14957). With compounds 13551 and 14957, one of the two positive charges was substituted for a neutral moiety to test if two positive charges are required for MET channel interaction. Compound 13670 had a substitution of the terminal positive charge with a negative moiety (free acid).

The 3 compounds were tested for their MET channel blocking abilities. All 3 blocked the MET channel to varying degrees. Compounds 13551 and 14957 showed strong block of the channel whereas 13670 showed a modest block. Shown in Figure 7.8A-C is an example of the currents obtained from a third row OHC before (black), during (red) and after (blue) the superfusion of 10 µM 14957. The current-voltage (Figure 7.8D) and fractional block curves (Figure 7.8E) generated from the raw data highlight the voltage-dependency of the observed channel block. The strongest block of the MET channel by 10 µM 14957 was observed at slightly depolarised potentials (+16 mV). Release of the block occurred at the extreme hyperpolarised potentials and slightly at the extreme depolarised potentials, indicating that the compound still behaved as a permeant blocker of the MET channel. The average fractional block curves for 13551 and 13670 are presented later, in Figure 7.11D and C respectively.

The electrophysiological data correlates well with what was observed in the zebrafish loading assay – both 13551 and 14957 loaded strongly into neuromast HCs, whereas 13670 displayed a much weaker pattern of loading (Figure 7.4).

Of the 3 compounds, 2 were protective in the cochlear culture assays. Compound 13551 protected against the gentamicin-induced loss of OHCs when tested at 0.5 µM (Figure 7.3) and 13670 when tested at 5 µM (Figure 7.2). The difference in protective concentration could be directly correlated with their MET channel blocking abilities – with 13551 acting as a strong MET channel blocker whereas 13670 displayed only modest block. The third compound, 14957, was highly toxic to cochlear cultures so comparisons of MET channel block and otoprotection cannot be made (Figures 7.2 and 7.3). Convincingly, we can confirm that only one positive charge is needed for MET channel block by the FM 1-43 compound, and substitution of a positive for a negative charge unsurprisingly reduced the observed channel interaction.

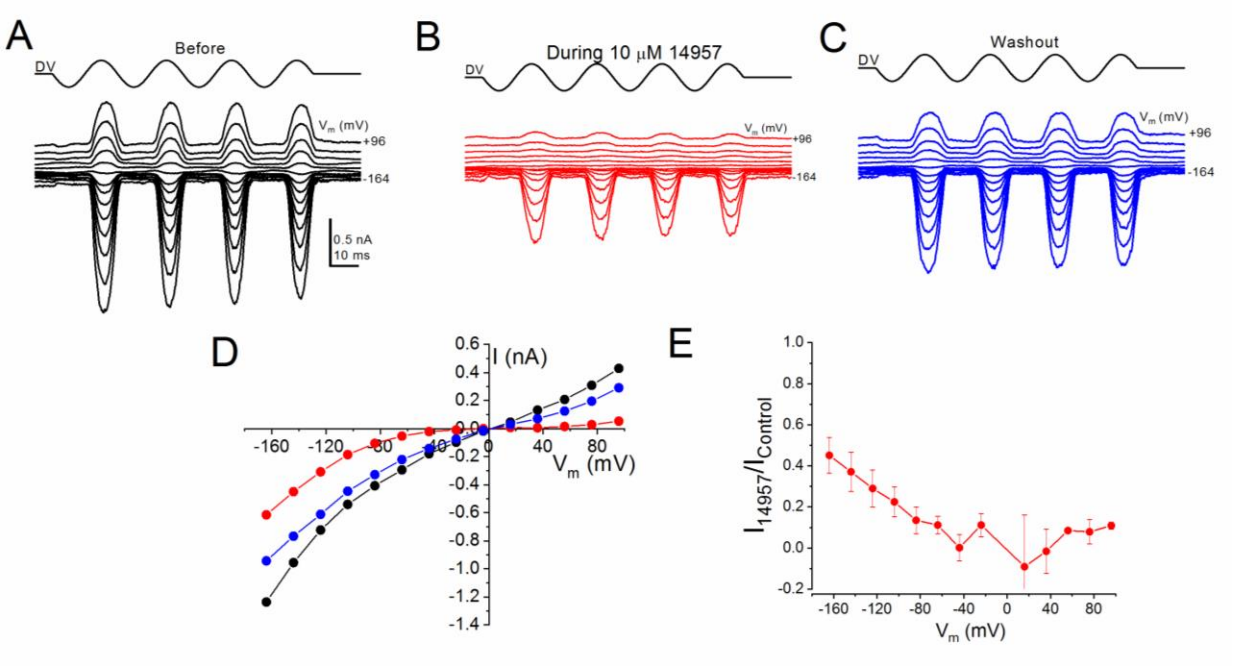

Figure 7.8: *Extracellular exposure to 10 µM compound 14957, one of the three FM 1-43 derivatives with quaternary nitrogen modifications in the hydrophilic head.*

(A-C) MET currents recorded from a P2 basal OHC between -164 and +96 mV in response to a sinewave stimulus delivered by a fluid jet (45 Hz sinusoid, ±40V driver voltage, DV) shown above each trace, before (black), during (red) and after (blue) exposure to 10 µM 14957. Compound 14957 caused a large reduction of the current size at all membrane potentials. Full recovery is seen following re-exposure to the control solution. **(D)** Current-voltage curves of the currents shown in **(A-C)** reveal the current block at all potentials during 14957 exposure and the reversibility of the block following washout. **(E)** Fractional block curve reveals the voltage-dependency of the block, with maximal block observed at slightly depolarised potentials (n=3 OHCs).

7.2.3.2.5 Derivatives with Hydrophilic Head, Alkyl Chain Modifications - 13667, 13668, 13669

Three derivatives were designed with modifications to the alkyl chain portion of their hydrophilic heads (13667, 13668 and 13669). The modifications were made to influence the space between the two positive charges. The spacer for the FM 1-43 molecule consists of three carbon atoms. Here we designed compounds bearing a spacer of 4 (13669), 5 (13667) and 6 (13668) carbons, in order to investigate how the distance between the positive charges may influence the interaction of the compound with the MET channel.

The derivatives were tested electrophysiologically for their interaction with the MET channel. When tested at 10 µM, all 3 derivatives strongly blocked the MET current, suggesting they all still interact with the channel. Shown in Figure 7.9A-C is an example of the currents obtained from a third row OHC before (black), during (red) and after (blue) the superfusion of 10 µM 13669. The current-voltage (Figure 7.9D) and fractional block curves (Figure 7.9E) generated from the raw data highlight the voltage-dependency of the observed channel block. The strongest block of the MET channel by 10 µM 13669 is observed at slightly depolarised potentials (+16 mV), and release of the block occurs at the extreme hyperpolarised and depolarised potentials, indicating that the compound is a permeant blocker of the channel. The average fractional block curves for 13667 and 13668 are presented later, in Figure 7.11D.

These results suggest that the spacing between the positive charges on the FM 1-43 molecule is not integral to its interaction with the MET channel. Interestingly, when tested in zebrafish all 3 compounds loaded into neuromast HCs however the loading patterns were different for 13668 (Figure 7.4). Compound 13668 loaded very strongly into neuromast HCs, whereas the other 2 loaded relatively weakly. As shown in Figure 7.11D, when tested electrophysiologically 13668 was also shown to be the strongest blocker of the MET channel. As 13668 had the largest spacing between its positive charges, it can be concluded that a reduced spacing may reduce the binding of the compound to the channel pore, and vice versa.

Interestingly, despite their shared block of the MET channel, none of the 3 derivatives provided any protection from the gentamicin-induced loss of OHCs when tested at 0.5 µM (Figure 7.3). When tested at 5 µM, all 3 derivatives were extremely toxic to the cochlear cultures (Figure 7.2), similarly to FM 1-43 itself.

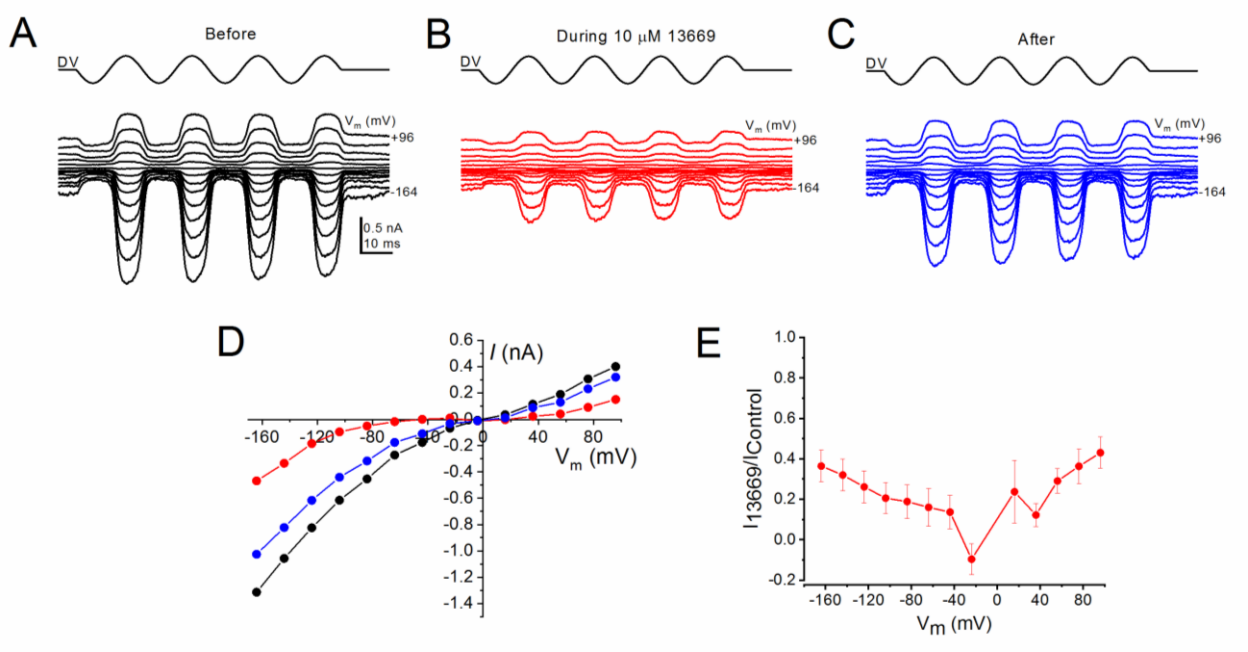

Figure 7.9: *Extracellular exposure to 10 µM compound 13669, one of the three FM 1-43 derivatives with alkyl chain modifications in the hydrophilic head*

(A-C) MET currents recorded from a P2 basal OHC between -164 and +96 mV in response to a sinewave stimulus delivered by a fluid jet (45 Hz sinusoid, ±40V driver voltage, DV) shown above each trace, before (black), during (red) and after (blue) exposure to 10 µM 13669. Compound 13669 caused a large reduction of the current size at all membrane potentials. Full recovery is seen following re-exposure to the control solution. **(D)** Current-voltage curves of the currents shown in **(A-C)** reveal the current block at all potentials during 13669 exposure and the reversibility of the block following washout. **(E)** Fractional block curve reveals the voltage-dependency of the block, with maximal block observed at slightly hyperpolarised potentials (n=4 OHCs).

7.2.3.2.6 Additional FM 1-43 Derivatives – 13666, 13698, 16327 and 28552

Four additional derivatives were synthesised based on those previously tested (7.2.3.2.2 - 7.2.3.2.5) (13666, 13698, 16327 and 28552). Compound 13666 is the zwitterionic form of 13670. Compound 13698 corresponds to bis-FM 1-43, having two lipophilic moieties, linked by a 3 carbon spacer and bearing two positive charges. The compound was designed because the Hill Coefficient, which quantifies the degree of interaction between a ligand and its binding site or the cooperativity of binding, suggests that the MET channel is able to accommodate two FM 1-43 molecules (Gale et al., 2001). Compound 16327 is a photo affinity-labelled FM 1-43 derivative. Compound 28552 was designed based on the results obtained with compounds 13696 and 13551, and is a combination of their structures.

Compounds 13666, 13698, 16327 and 28552 were tested electrophysiologically for their interaction with the MET channel. Compound 13698 was extremely hard to get into solution and prevented the possibility of current recordings due to its crystallization on the cochlear cultures following superfusion. However, when 13698 was tested in the zebrafish loading assay it did load into neuromast HCs (Figure 7.4), suggesting it does interact with, and permeate through, the MET channel.

When tested electrophysiologically, compounds 13666 and 16327 displayed a modest voltage-dependent block of the MET channel. An example of MET channel block by 10 µM 16327 is shown in Figure 7.10, with the currents recorded before (black), during (red) and after (blue) compound superfusion displayed in Figure 7.10A-C, the current-voltage curve in Figure 7.10D and the fractional block in Figure 7.10E. The average fractional block curve for 13666 is displayed later, in Figure 7.11C. When compound 28552 was superfused on top of the cochlear cultures, this ruptured the cells and current recordings could not be obtained. In the zebrafish assay all 3 compounds loaded into neuromast HCs, suggesting all still behave as permeant blockers. However, 13666 loaded very weakly – only displaying neuromast labelling when incubated at 10 µM for 10 minutes (Figure 7.4).

In mouse cochlear cultures, a wide variety of responses were observed. Compound 13666 provided no protection at either concentration tested; 13698 provided protection at both concentrations; 16327 was toxic at 5 µM and not protective at 0.5 µM; and 28552 was toxic at 5 µM and protective at 0.5 µM (Figures 7.2 and 7.3).

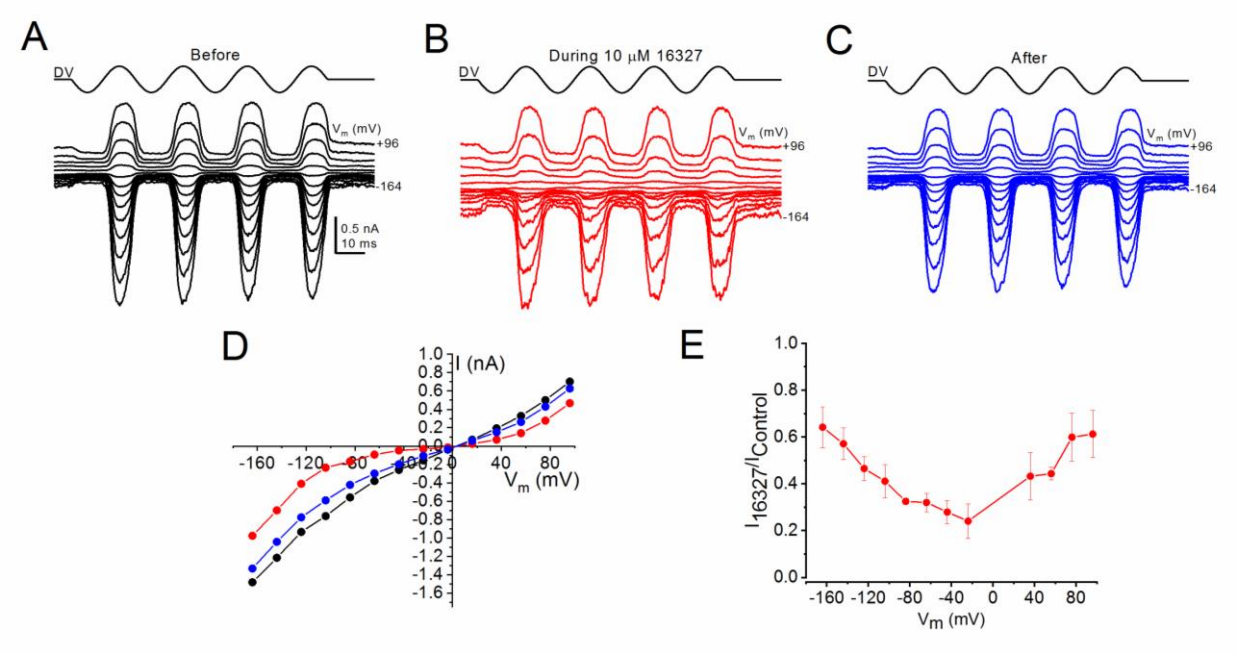

Figure 7.10: *Extracellular exposure to 10 µM compound 16327, one of the four additional FM 1-43 derivatives.*

(A-C) MET currents recorded from a P2 basal OHC between -164 and +96 mV in response to a sinewave stimulus delivered by a fluid jet (45 Hz sinusoid, ±40V driver voltage, DV) shown above each trace, before (black), during (red) and after (blue) exposure to 10 µM 16327. Compound 16327 caused a large reduction of the current size at all membrane potentials. Full recovery is seen following re-exposure to the control solution. **(D)** Current-voltage curves of the currents shown in **(A-C)** reveal the current block at all potentials during 16327 exposure and the reversibility of the block following washout. **(E)** Fractional block curve reveals the voltage-dependency of the block, with maximal block observed at slightly hyperpolarised potentials (n=4 OHCs).

7.2.3.2.7 Fractional Block Curves for all of the FM 1-43 Derivatives

The fractional block curves for all of the tested FM derivatives were compiled based on their level of MET channel block. Figure 7.11 shows the average fractional block curves for 13550 (Figure 7.11A) and also the derivatives that showed no interaction (Figure 7.11B), weak block (Figure 7.11C) or strong block (Figure 7.11D) of the MET channel. Three compounds are not shown in Figure 7.11 (13696, 13698 and 28552). Time limitations prevented 13696 from being able to be tested at 10 µM, 13698 had solubility issues and 28552 caused cell death upon application.

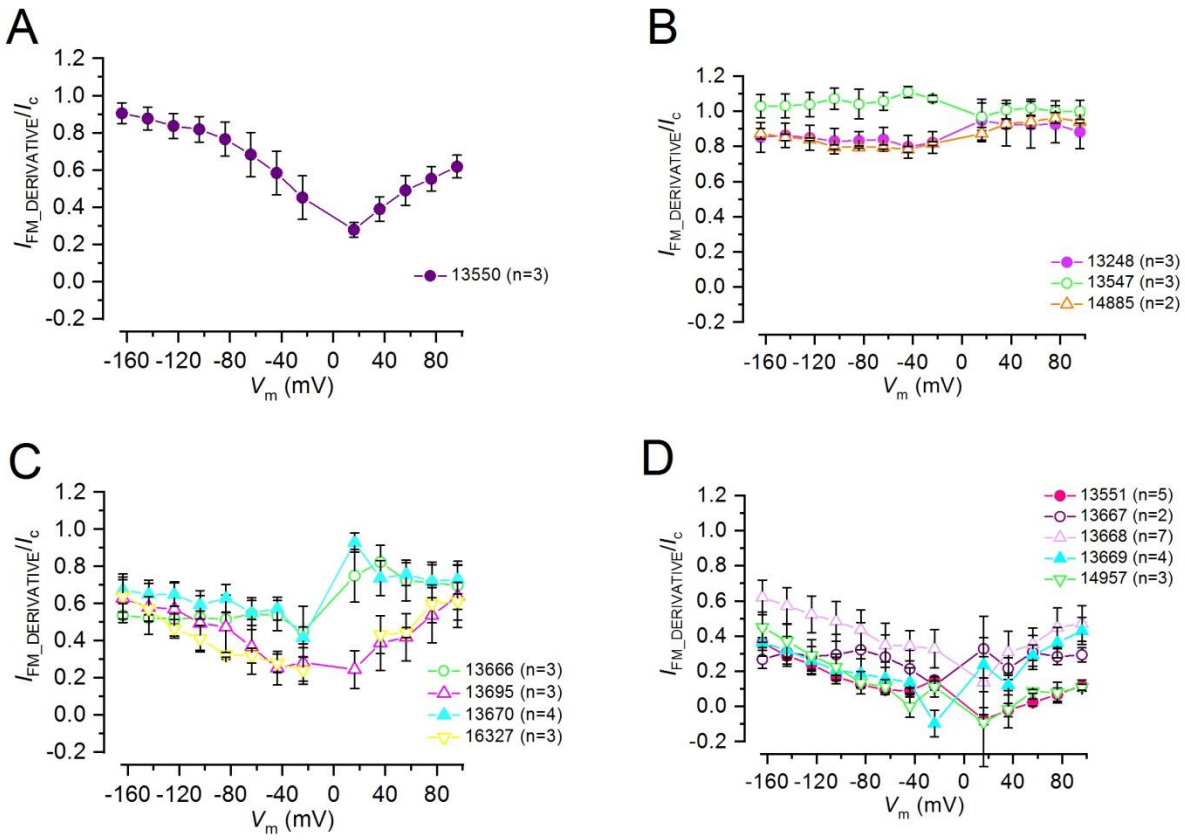

Figure 7.11: *The average fractional block curves for FM 1-43 and all but three of its derivatives at 10 µM, split in to no block, weak block and strong block of the MET channel.*

(A-D) Fractional block curves reveal that **(A)** FM 1-43 (13550) caused modest block of the MET channel. **(B)** 3 derivatives (13248, 13547 and 14885) showed no interaction. **(C)** 4 derivatives (13666, 13695, 13670 and 16327) gave a modest block and **(D)** 5 derivatives (13551, 13667, 13668, 13669 and 14957) displayed a strong block of the channel. All compounds that blocked displayed a voltage-dependent block that was greatest at intermediate and often slightly depolarised potentials. They also showed a release of block at the extreme hyperpolarised potentials, indicative of them all behaving as permeant blockers of the MET channel.

7.3 Summary

The results of this chapter have highlighted which aspects of the chemical composition of FM 1-43 are vital to its previously-documented interaction with the MET channel. FM 1-43 has three distinct structural moieties: a lipophilic tail, a central core and a hydrophilic head. Modifications were made to each moiety and we assessed the effect this had on the two aforementioned characteristics of MET channel block and reported otoprotection.

In the cochlear culture protection assay, FM 1-43 itself was toxic at 5 μM and not protective when tested at 0.5 μM. Electrophysiological recordings revealed that it behaves as a voltage-dependent blocker of the MET channel, blocking most strongly at slightly depolarised potentials and displaying a release of block when the cell membrane was stepped to extreme hyperpolarised potentials, indicating that it is a permeant blocker of the channel.

Of the 3 derivatives with modifications to their lipophilic tail (13695, 13696 and 14885), all three were toxic to cochlear cultures when tested at 5 μM and provided no protection when tested at 0.5 μM. When tested electrophysiologically, there was a variety of responses observed. Compound 13695 showed a weak, and 13696 showed a strong, voltage-dependent block of the MET channel. Compound 14885 showed no block of the channel, indicating a lack of interaction.

Both of the derivatives with modifications to their central core (13248 and 13547) did not block the MET channel and provided no protection or toxicity at either concentration tested, indicating that the central core is integral to MET channel interaction and consequent otoprotection.

Derivatives with modifications to their hydrophobic head can be divided into two classes: those missing the quaternary nitrogen and those with an extended alkyl chain spacer. Those with quaternary nitrogen modifications (13551, 13670 and 14957) all blocked the MET channel to some degree. Compound 13351 blocked strongly and protected against the gentamicin-induced loss of OHCs when tested at 0.5 μM. Compound 13670 displayed modest block of the channel and protected when tested at 5 μM. Compound 14957 strongly blocked the MET channel but was found to be highly toxic in cochlear cultures at both concentrations tested. The three derivatives with alkyl chain modifications (13667, 13668 and 13669) all strongly blocked the MET channel. When tested in cochlear cultures, however, they provided no protection at 0.5 μM and were highly toxic when tested at 5 μM.

7.4 Discussion

The results presented in this chapter serve to further indicate that the mechanism of otoprotection of FM 1-43 that had been previously reported (Gale et al., 2001), was due to its block of the MET channel and the consequent prevention of AG entry into sensory HCs. None of the FM 1-43 derivatives that showed a lack of interaction with the MET channel conferred any protection against the gentamicin-induced loss of OHCs, reinforcing that MET channel block is the mechanism of reported otoprotection of the styryl dye.

It is evident that the central core of the FM 1-43 molecule is integral to its ability to interact with the MET channel, as any modification made to this moiety prevented any observable interaction. Furthermore, the evidence presented herein surprisingly suggests that the hydrophobic head component of the molecule is less integral to MET channel interaction than the lipophilic tail. This is because all six modifications made to the hydrophobic head still allowed the derivatives to display some degree of MET channel block, whereas one of the three modifications made to the lipophilic tail prevented MET channel interaction. Moreover, when modifications were made to the central core separating the charged head from the lipophilic tail (section 7.2.3.2.3), the charged head compound did not interact with the channel without the lipophilic tail component.

Electrophysiological investigations revealed that FM 1-43 and all of its derivatives that interacted with the MET channel showed maximum block at the intermediate potentials, most often at +16 mV. Moreover, only one positive charge is needed for channel interaction, as shown by compounds 13551 and 14957 still behaving as channel blockers, and a substitution of a positive for a negative charge (13670) reduced the level of block, most likely due to electrostatic repulsion of the molecule from the negative charges within the channel's pore. The spacing between the positive charges affects the permeation of the compound, in that the compound with the longer space between the two charges (13668) loaded most strongly into zebrafish neuromast HCs compared to those with lesser spacing.

In regards to the cochlear protection assays, toxicity was observed with a large number of the FM 1-43 derivative compounds (9 of the 15 when tested at 5 μM), and only few conferred protection at either concentration tested (0.5 or 5 μM). This is perhaps not surprising, as previous studies have reported that when applied to cochlear cultures, FM 1-43 caused blebbing of the apical surface of sensory HCs after only 70 minutes (Gale et al., 2001). Due to the 48 hours duration of the cochlear culture protection assay used herein, the derivatives

would have had a much longer time to potentially permeate into HCs and exert their toxic effect, thereby explaining the result. To further assess any intrinsic toxicity of the compounds, they should have been tested alone in the absence of gentamicin to determine whether it was the gentamicin or the compound that induced the toxic effects. This would have made the interpretation of their toxicity much easier. These experiments were not completed due to time limitations. Future studies should address this concern.

8 Assessing the Effects of Aminoglycoside Antibiotics on Mitochondrial Function

8.1 Introduction

Following the entry of the AGs into sensory HCs they are believed to interact with intracellular targets such as ribosomes, the endoplasmic reticulum (ER) and mitochondria (Jiang et al., 2017; O'Sullivan et al., 2017), causing their dysfunction and the consequent induction of apoptotic cell death pathways. The assumed mitochondrial involvement in the apoptotic process has manifested as a result of several indirect lines of evidence, including: the structural similarity of bacteria (the target of AGs) and mitochondria, as well as their proposed bacterial origin (Margulis et al., 1970; Gray et al., 2001; Gray et al., 2012); the co-localisation of GTTR with mitochondrial stains such as Mitotracker (Ding et al., 1995; Steyger et al., 2003); the enhanced susceptibility to AG-induced ototoxicity resulting from mitochondrial genetic mutations (Prezant et al., 1993); and the rise in ROS levels following AG exposure – cell signalling molecules that are primarily produced by mitochondria (Clerici et al., 1996; Hirose et al., 1997; Sha and Schacht, 1999a).

Although compelling, these lines of evidence for mitochondrial involvement in the AG-induced cell death process are somewhat indirect. The aim of this chapter was to investigate the effect that the AGs may directly induce when they encounter these organelles. In order to examine this I initially used isolated rat liver mitochondria, due to the ease of isolation and the high yield that can be obtained from a single liver dissection. Following preliminary investigations, I repeated the experiments in isolated rat kidney mitochondria – an organ that is susceptible to AG damage in the form of nephrotoxicity (Mingeot-Leclerq and Tulkens, 1999; Mouedden et al., 2000). Lastly, we also investigated the effect of the AGs on intact sensory HC mitochondria, in the same mouse cochlear cultures that have been used for compound screening throughout this thesis.

As a brief introduction to the way in which mitochondrial function can be investigated; all mitochondria have five protein complexes embedded in their inner membranes, known collectively as the electron transport chain (ETC). These complexes serve to move electrons along the chain, from complex I to V (CI-V), with oxygen as the final electron acceptor. This electron flow simultaneously generates a proton gradient which manifests as a membrane potential and a pH gradient. Adenosine triphosphate (ATP) synthase utilises this proton gradient in order to produce ATP, which is then harnessed by the cell. Under usual conditions, mitochondria have a basal respiratory rate known as state 4 respiration. The maximal respiratory capacity of mitochondria is known as state 3 (or state 3U, if maximal respiration is induced by uncoupler addition as opposed to an abundance of ADP), and the ratio of the basal

to maximal respiratory rates is termed the respiratory control ratio (RCR), which gives an indication of the integrity of mitochondria by conveying how coupled the consumption of oxygen is to ATP production. The ETC is also crucially involved in the production of ROS – cell signalling molecules that are directly involved in the survival of a cell.

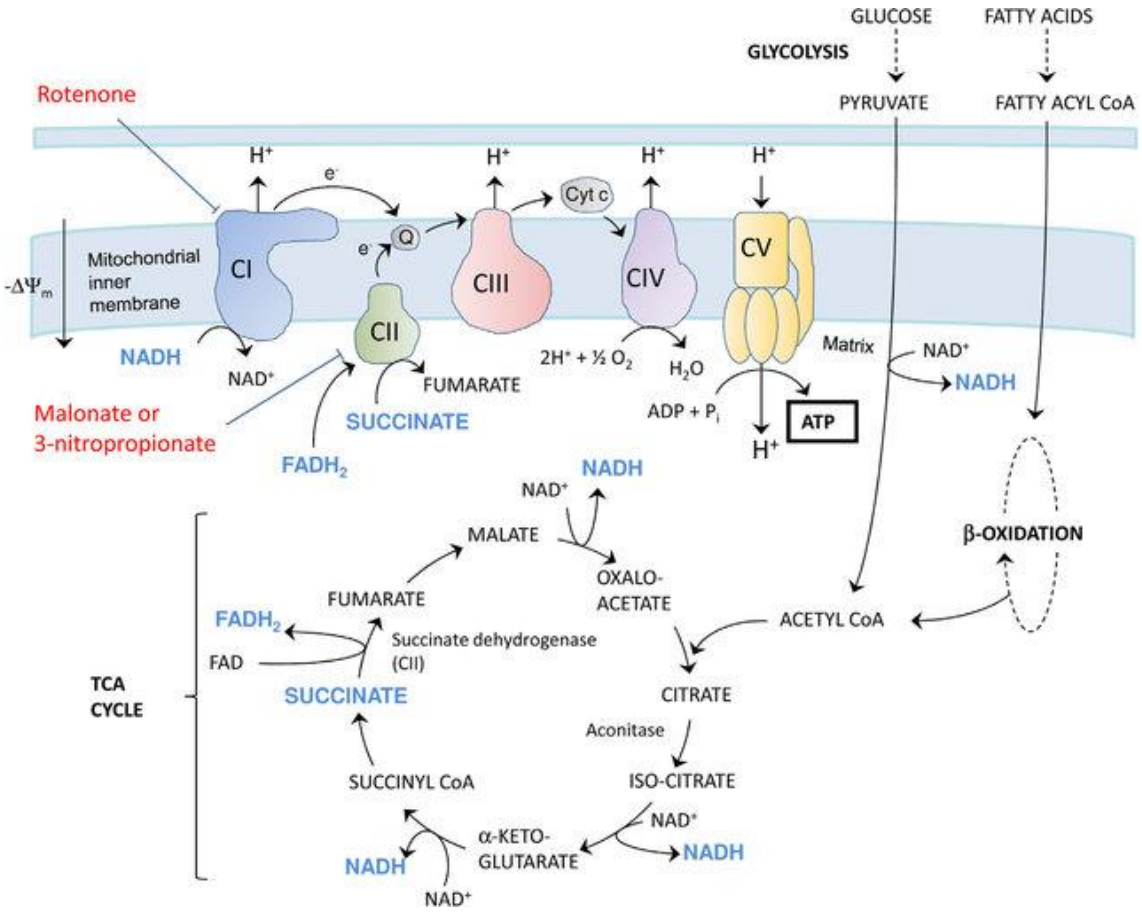

Figure 8.1: *Illustration of the mitochondrial electron transport chain, taken from Polyzos and Mcmurray, 2016.*

The ETC is the target of a large number of drugs, including several anti-cancer compounds (Rohlena et al., 2011; Olszewska and Szewczyk, 2013; Kluckova et al., 2013). Cisplatin, another nephro- and ototoxicity-inducing compound used to treat several forms of cancer (Skinner et al., 1998; Knight et al., 2005), had been reported to cause mitochondrial dysfunction as a crucial pathogenic event in its induction of nephrotoxicity (Simmons and Humes, 1979). Furthermore, previous studies investigating the effect of gentamicin on renal tissue mitochondria had reported an effect on their state 3 and state 4 respiratory activities, potentially underlying the associated nephrotoxicity (Bendirdjian et al., 1975; 1978; Simmons et al., 1980). However, documentation of the mechanism underlying this observation is lacking. Moreover, the effect of the AGs on sensory HC mitochondria is not fully understood.

Studies have reported that AGs trigger the opening of the permeability transition pore and dissipate the mitochondrial membrane potential (MtMP) (Dehne et al., 2002). AGs have also been shown to cause a rapid alteration of mitochondrial metabolism, particularly in basal OHCs when compared to IHCs and their apically-located counterparts (Jensen-Smith et al., 2012). This evidence directly correlates with the AG-induced ototoxicity pattern that I have observed throughout this thesis, suggesting a direct link between mitochondrial dysfunction and AG-induced HC death.

For this reason, I investigated whether gentamicin affected the function of the ETC in isolated mitochondria, through a series of measurements of oxygen consumption using an Oroboros Oxygraph-2K oxygen electrode. The MtMP and mitochondrial ROS (MtROS) production in isolated kidney and liver mitochondria were also investigated, as was the MtMP in intact sensory HC mitochondria using a selection of fluorescent indicators. The overarching, predominant aim of this chapter was to identify the effect that the AGs have on mitochondria and establish an assay system, so that I could then subsequently screen any identified otoprotectants against this effect, thereby investigating an additional mechanistic avenue. The mechanism of otoprotection of several compounds that I have identified herein (including the two most efficacious; see Chapter 4) remained unknown, as they do not block the HC MET channels or affect the RP, so are unlikely to prevent AG entry into the cell. By conducting this research, I was able to investigate whether these compounds may have protected sensory HCs by preventing AG-induced mitochondrial dysfunction.

8.2 Results

8.2.1 Gentamicin Stimulates State 4 and Inhibits State 3U Respiratory Activities of Isolated Rat Liver Mitochondria

Overall mitochondrial activity was assessed by measuring oxygen consumption of isolated mitochondria using an Oroboros Oxygraph-2K oxygen electrode, with the dual chamber set-up proving ideal for running control experiments simultaneously. The ETC complexes (I-V) were investigated independently, to assess any complex-dependent effect. Mitochondrial samples were equilibrated in reaction media with or without 5 mM gentamicin for 10 minutes prior to the addition of 10 mM succinate to stimulate CII, in the presence of 2.5 µM rotenone to ensure NADH generated within the tricarboxylic acid cycle did not become a confounding factor. Upon addition of the substrate, oxygen uptake increased to 240 (± 22) pmol O_2 s^{-1} ml^{-1} (n=26) within the control samples and 419 (± 48) pmol $O_2s^{-1}ml^{-1}$(n=14) in the gentamicin-treated conditions, demonstrating a significant (p = 0.0496) stimulation of CII-dependent state 4 respiration, as has previously been reported (Bendirdjian et al., 1975; 1978) (Figure 8.2). Subsequent addition of 1 µM CCCP, to uncouple oxygen consumption rates from the proton-motive force, increased the rate to 807 (± 57.43) pmol O_2 s^{-1} ml^{-1} (n=26) within the control sample. However, the gentamicin rate remained relatively stable at 406 (± 40) pmol O_2 s^{-1} ml^{-1} (n=14), demonstrating no significant change to its coupled state (Figure 8.2).

To ensure the effect was not limited to CII-dependent respiration, the same set of experiments were repeated using 5 mM pyruvate and 2 mM malate to stimulate NADH generation via pyruvate dehydrogenase and malate dehydrogenase respectively, thereby assessing CI-dependent state 4 respiration. As with the previous set of experiments, the gentamicin-treated mitochondria presented a significant (p = 0.0059) increase in state 4 respiration, increasing the rate from 149.8 (± 15.39) pmol s^{-1} ml^{-1} (n=4) in the controls to 502 (± 72) pmol O_2 s^{-1} ml^{-1} (n=4) in the gentamicin-treated conditions, but demonstrated no significant increase when treated with CCCP, 402 (± 84) pmol O_2 s^{-1} ml^{-1} (n=4) (Figure 8.2).

Furthermore, there was a significant difference in the state 3U respiratory rates between the control and gentamicin-treated conditions, both for CI (p = 0.0375) and CII-mediated (p < 0.0001) respiration (Figure 8.2). This implied that gentamicin reduces state 3U respiratory rates, as had previously been reported elsewhere in the literature (Simmons et al., 1980). All statistical comparisons in this section were made using a one-way ANOVA, followed by Tukey's multiple comparisons test.

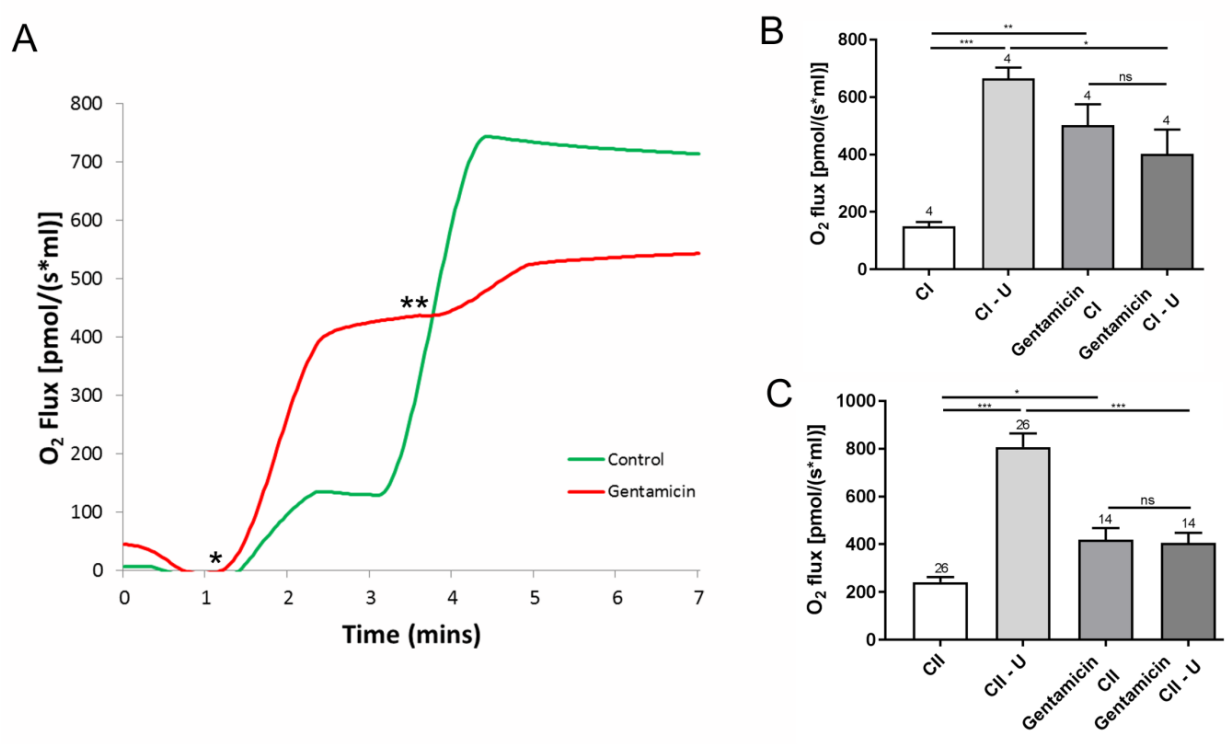

Figure 8.2: *Pre-incubation with 5 mM gentamicin for 10 minutes caused stimulation of complex I and complex II respiration (state 4) and inhibition of the maximal respiratory rates (state 3U).*

A respiratory flux trace for CII **(A)** respiration, with (red) and without (green) 5 mM gentamicin pre-incubation for 10 minutes, alongside quantification of the CI **(B)** and CII **(C)** response.

(A) Succinate addition (10 mM) (*) in the gentamicin condition caused a much larger O_2 flux response than in the control. Subsequent addition of CCCP (1µM) (**), an uncoupler of the ETC, caused O_2 flux to rise significantly in the control, whereas a greatly reduced rise was observed when pre-incubated with gentamicin. **(B)** Quantification of the CI response. Pyruvate (5 mM) and malate (2 mM) addition in the gentamicin condition caused a much larger O_2 flux response than in the control. Subsequent addition of CCCP caused O_2 flux to rise significantly in the control, whereas no such rise was seen when pre-incubated with gentamicin. **(C)** Shows quantification of the CII response, presented in **(A)**.

8.2.2 Gentamicin Reduces the Respiratory Control Ratio (RCR) of Isolated Mitochondria

Given that gentamicin stimulates state 4 and causes a concurrent reduction of state 3U respiratory rates (Figure 8.2) (Bendirdjian et al., 1975; 1978; Simmons et al., 1980), I investigated its effect upon the RCR of isolated mitochondria. The RCR is a measure of the integrity of mitochondria and the extent of the coupling between oxygen consumption and ATP production. Initial dose-response experiments were performed at a fixed 10 minutes incubation time point, with the data displaying a clear concentration-dependent increase in state 4 respiratory activities (Figure 8.3A). While the data for uncoupled (state 3U) respiration does initially appear somewhat erratic, this is likely due to the non-homogeneous nature of the mitochondrial samples, causing uniform protein addition to be extremely challenging. However, once the data is transformed into RCR values a typical dose-response effect can be observed (Figure 8.3B).

The extent to which incubation time was a factor was also investigated (Figure 8.3C), with all three concentrations tested demonstrating a linear reduction in the RCR as the length of AG-incubation time increased. Dose response curves (Figure 8.3D) were generated for state 4 respiration and an IC_{50} of 7.5 (±2.5) mM (n=2) was determined, with a Hill coefficient of 1.54 (1.24 – 1.84 95% CI).

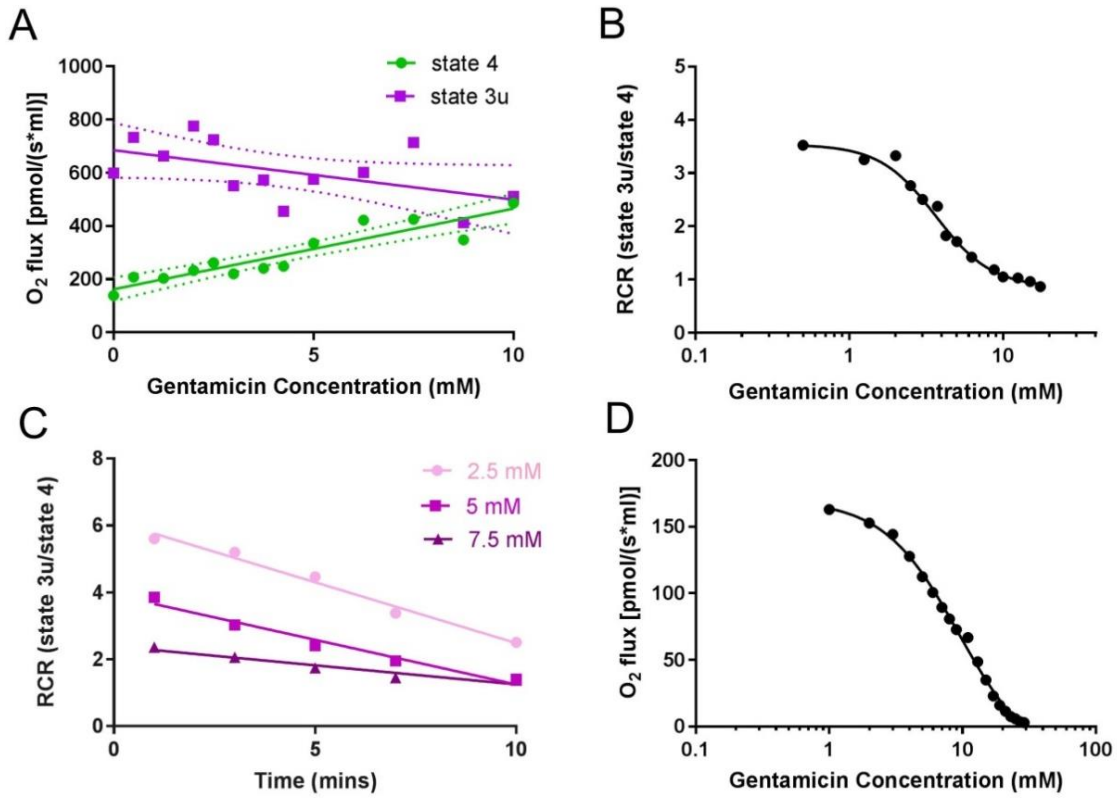

Figure 8.3: *Gentamicin reduced the respiratory control ratio (RCR) of isolated mitochondria in a dose and time-dependent manner.*

(A) Shows the increase in succinate-induced O_2 flux (state 4) with increasing gentamicin concentrations, and a simultaneous reduction in the CCCP-induced O_2 flux (state 3U). Experiments were done in the presence of 2.5 µM rotenone, to inhibit CI respiration. Lines are fit to a linear regression model, displaying 95% confidence intervals. **(B)** Shows the transformed data, with RCRs derived by dividing the CCCP state 3U rates by the succinate state 4 rates. **(C)** Shows the decrease in the RCR with increasing gentamicin incubation times, for three different concentrations (2.5, 5 and 7.5 mM). **(D)** A dose-response curve for gentamicin's effect on state 4 respiration.

8.2.3 Gentamicin Depolarises the Mitochondrial Membrane Potential (MtMP)

Given the observed effect of gentamicin on the mitochondrial RCR, I investigated its effect on the mitochondrial membrane potential (MtMP) using safranin (Krumschnabel et al., 2014). Safranin (2 µM) is a fluorescent dye that indicates the MtMP using a quenching mechanism, accumulating in mitochondria due to the negative potential inside, generated across the inner mitochondrial membrane (IMM). The MtMP is the transmembrane potential that is directly responsible for ATP production (Zorova et al., 2017); it underlies the coupling, or the RCR, of mitochondria. Previous studies have reported a loss of the MtMP in OHCs before cell death occurs (Dehne et al., 2002), further highlighting the involvement of mitochondrial dysfunction in the AG-induced cell death process.

Initial addition of safranin to the chambers generated a fluorescent signal (Figure 8.4A). Upon subsequent addition of succinate to initiate respiration a proton gradient was formed, the dye entered mitochondria and was quenched. This reduced the fluorescent signal (Figure 8.4A*), which was indicative of an MtMP being generated. Upon subsequent addition of 2.5 mM gentamicin, the signal increased, indicating a decrease in the MtMP, with successive 2.5 mM titrations further decreasing the membrane potential (Figure 8.4A↓).

Figure 8.4B shows quantification of the results. A one-way ANOVA followed by Dunnett's multiple comparisons test revealed that a significant shift in safranin signal relative to succinate only was evident at gentamicin concentrations ≥ 1 mM (p = 0.009) (n=5). As shown in Figure 8.4A, complete dissipation of the gradient was seen when using quick, successive additions of gentamicin up to a concentration of 15 mM. However, if lower concentrations of gentamicin were added (≥ 1 mM) and left incubating in the chamber then we saw a progressive depolarisation of the MtMP over time (data not shown), possibly suggesting that gentamicin must first cross the outer mitochondrial membrane (OMM) in order to exert its effect on the proteins embedded within the IMM. Alternatively, the binding of gentamicin to mitochondria has been shown to be persistent and not readily reversible when tested *in vitro* (Kornguth et al., 1980), so perhaps a certain amount of gentamicin must bind before it can exert its detrimental effect on mitochondrial function.

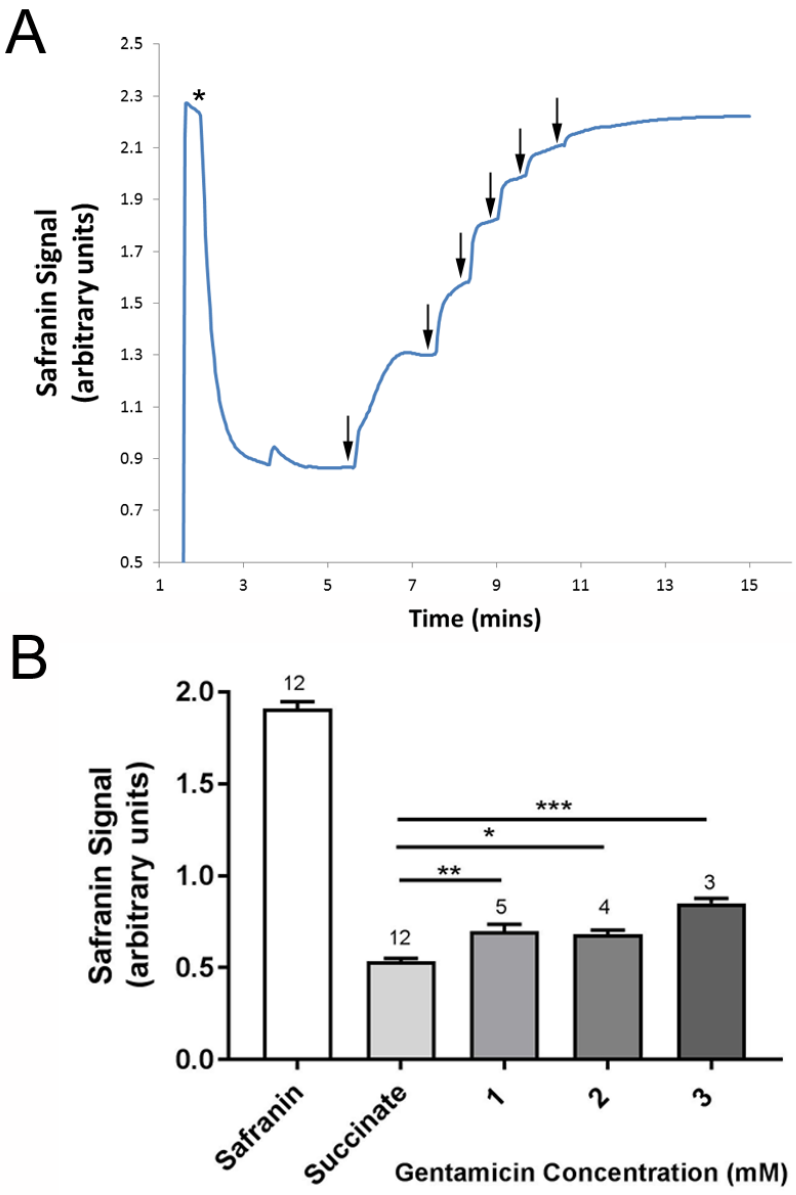

Figure 8.4: *Gentamicin depolarised the mitochondrial membrane potential (MtMP).*

(A) Succinate was added to the chamber to initiate respiration (*), generating a proton gradient and consequent polarisation of the mitochondrial membrane. This is indicated by the quenching of the safranin signal, which is indicative of the MtMP being generated. When 2.5 mM gentamicin was added to the chamber (↓) there was a sudden, direct increase in safranin signal, suggesting that gentamicin was dissipating the proton gradient and depolarising the MtMP. **(B)** Shows quantification of the results. A significant shift in safranin signal relative to succinate only was evident at gentamicin concentrations ≥ 1 mM.

8.2.4 Gentamicin Reduces Mitochondrial ROS (MtROS) Production with Succinate as the Substrate

MtROS production can be measured using Amplex Red, a dye that fluoresces dependent on hydrogen peroxide (H_2O_2) levels. Previous studies have suggested excessive ROS production to be the cause of sensory HC death, as a result of AG treatment or otherwise, with many protective approaches aimed at applying antioxidants to reduce ROS accumulation within the cell (Sha and Schacht, 2000; Wu et al., 2002; Sergi et al., 2004; Rybak and Whitworth, 2005; Xie et al., 2011; Kim et al., 2015; Negrette-Guzmán et al., 2015).

Here, endogenous ROS production was measured following the addition of succinate (*) to the Oroboros Oxygraph chambers. In Figure 8.5A, the rates of ROS production and overall concentrations in the chamber are plotted. Solid lines display overall ROS concentrations and dashed lines display ROS production rates. Green is the control and red is the gentamicin-treated condition. Evidently, 5 mM gentamicin incubation reduced the amount of ROS produced over time (Figure 8.5A). Antimycin A (2.5 µM) is an inhibitor of CIII that causes electron backflow through CI, thereby inducing ROS production. It was added as a positive control (**), and an increase in ROS was observed following its addition.

Quantification of the increase in ROS concentrations over time are plotted in Figure 8.5B. When compared to the control, a one-way ANOVA followed by Dunnett's multiple comparisons test revealed that there was a significant reduction in the amount of ROS produced over a period of 10 minutes when mitochondria were incubated with 1 (p = 0.0167) (n=3) or 5 (p = 0.0080) (n=3) mM gentamicin. Evidently, gentamicin reduces ROS production; a result which is consistent with our proposal that it acts as a mitochondrial uncoupler. This is because in order for MtROS to be produced there must be a backflow of electrons along the ETC. Uncoupling of the mitochondrial membrane prevents electron backflow, thus preventing the formation of ROS.

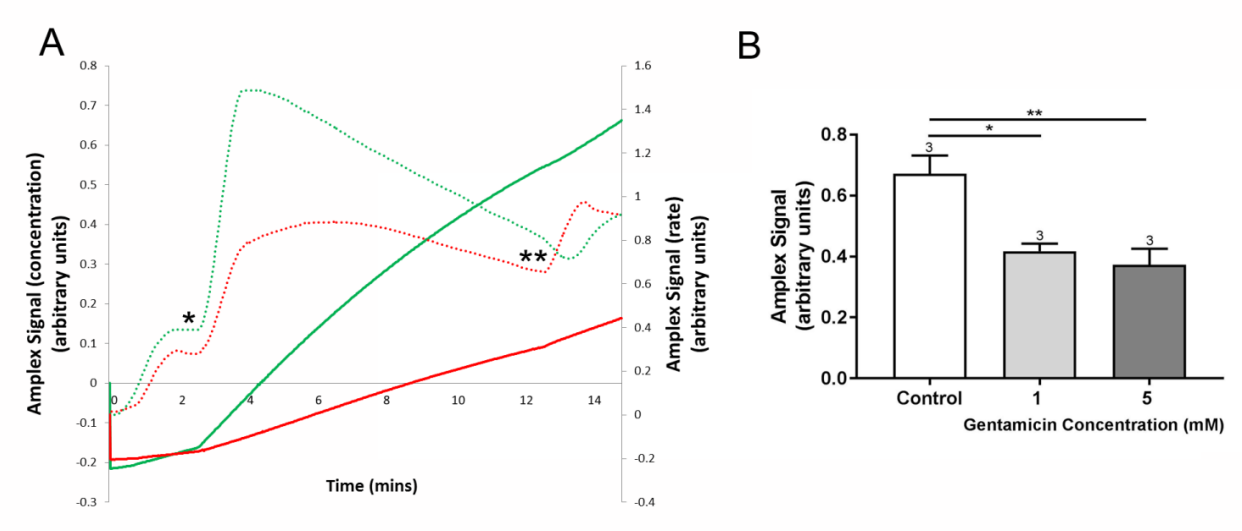

Figure 8.5: *Gentamicin reduced endogenous mitochondrial ROS (MtROS) production, consistent with our hypothesis that it behaves as a mitochondrial uncoupler.*

(A) Shows H_2O_2 levels detected over a period of 10 minutes, with the rates of production and overall concentrations plotted. Solid lines display concentrations, dashed lines display rates. Green is control, red is gentamicin. Following succinate addition (10 mM) (*), the endogenous formation of ROS was inhibited by 5 mM gentamicin. Antimycin A (2.5 µM), a known inhibitor of CIII, was added (**) as a positive control. **(B)** Shows quantification of the increase in ROS concentration over a 10 minute period. Gentamicin reduced endogenous ROS production when tested ≥ 1 mM (n=3), consistent with our proposal that it acts as a mitochondrial uncoupler.

8.2.5 Gentamicin causes State 4 Stimulation and State 3U Inhibition, RCR Reduction, MtMP Depolarisation and a Reduction in MtROS Production in Isolated Rat Kidney Mitochondria

Isolated rat liver mitochondria were used for all of the initial experiments due to the ease of isolation and the high yield of mitochondria per dissection. However, as this is not an organ that is damaged by AGs, all experiments were subsequently repeated using rat kidney mitochondria to ensure that the same effect was seen. As shown in Figure 8.6A, the same stimulation of state 4 and reduction of state 3U respiratory rates was observed, with a concurrent reduction in the RCR of kidney mitochondria (Figure 8.6B). To note, the RCR of kidney mitochondria is much lower than that of liver mitochondria, with an average RCR of 5.28 (± 0.83) (n=4) relative to that of the liver, which was 9.04 (± 0.56) (n=8). This observation has been reported elsewhere (Lash and Jones, 1993).

Depolarisation of the MtMP occurred with serial gentamicin additions (Figure 8.6C), with a complete collapse of the MtMP at gentamicin concentrations ≥ 5 mM. The lower concentration of gentamicin needed to collapse the MtMP relative to liver mitochondria is likely due to there being fewer mitochondria in the tissue sample, due to less experience in the dissection and isolation technique and the smaller size of the tissue sample meaning greater dilution by assay media throughout the isolation process. Alternatively, it could reflect the lower RCR and the smaller amount of gentamicin required to disrupt the membrane. Moreover, the time between each addition was slightly longer, perhaps giving gentamicin more time to bind or to cross the OMM and exert its effect on the IMM, if this is indeed how the antibiotic is having its effect.

Lastly, gentamicin was found to reduce ROS production in kidney mitochondria also (Figure 8.6D), with endogenous ROS levels following succinate addition (*) being greatly reduced in the gentamicin-treated condition relative to the control.

Taken together these data suggest that all mitochondria are susceptible to AG insult; however, it is the existence of suitable entry routes into specific tissue types that determines their susceptibility to AG-induced toxicity. An alternative possibility is a lack of suitable exit routes, leading to the enhanced accumulation in certain tissue types specifically.

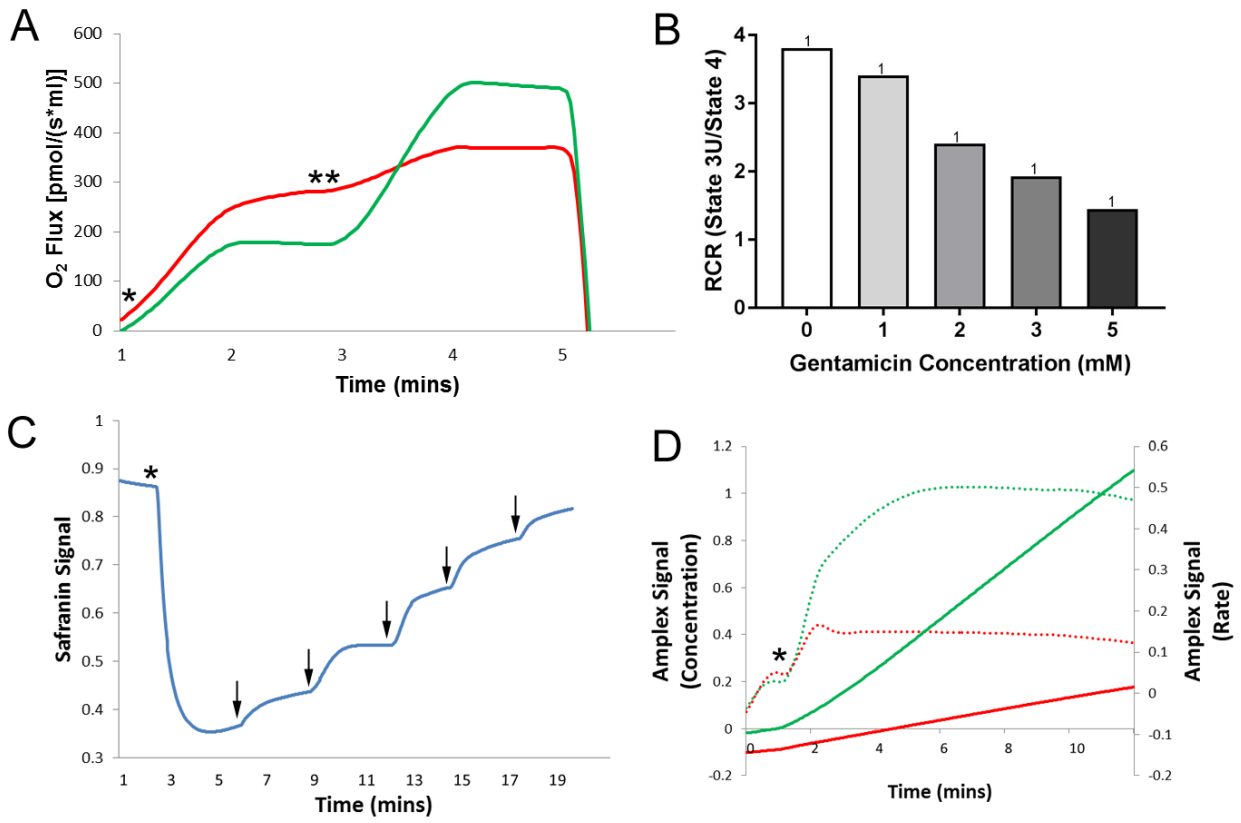

Figure 8.6: *In kidney mitochondria, gentamicin stimulated state 4 and reduced state 3U respiratory activities, reduced the RCR, depolarised the MtMP and reduced ROS production.*

All experiments detailed were replicated using kidney mitochondria, as the kidney is an organ susceptible to AG-induced (nephro-) toxicity. **(A)** Succinate addition (*) in the 5 mM gentamicin condition caused a larger O_2 flux response than in the control. Subsequent addition of CCCP (1 µM) (**) caused O_2 flux to rise significantly in the control, whereas a greatly reduced rise was seen when pre-incubated with gentamicin. **(B)** Quantification of the results shows that gentamicin caused a concentration-dependent decrease in the RCR of isolated kidney mitochondria. **(C)** Succinate was added to the chamber to initiate respiration (*), generating a proton gradient and consequent polarisation of the mitochondrial membrane. When gentamicin was added to the chamber (↓) there was a sudden, direct increase in safranin signal, suggesting that gentamicin was dissipating the proton gradient and depolarising the MtMP. **(D)** Shows H_2O_2 levels detected over a period of 10 minutes, with the rates of production and overall concentrations plotted. Solid lines display concentrations, dashed lines display rates. Green is control, red is gentamicin. Following succinate addition (10 mM) (*), the endogenous formation of ROS was inhibited by gentamicin.

8.2.6 Gentamicin causes MtMP Depolarisation in Sensory HC Mitochondria

*This research was conducted by Nerissa Kirkwood, University of Sussex.

To further confirm that the effect I had observed in isolated mitochondria would also occur in intact cell systems, we investigated the effect of gentamicin on the MtMP in the mitochondria of HCs in mouse cochlear cultures. Previous studies had shown a location-dependent effect of gentamicin on cochlear culture HCs; with basal OHCs losing their mitochondrial metabolic activity more rapidly than those located in the apical coil (Jensen-Smith et al., 2012).

Cells were pre-loaded with Rhodamine-123, a fluorescent dye that stains mitochondria based on an active MtMP. If the MtMP is dissipated, the fluorescence signal diminishes (Rahn et al., 1991). Cells were bathed in extracellular solution and gentamicin was added to a final concentration of 5 mM. Figure 8.7 shows the HC fluorescence over a period of 26 minutes. Between 0 and 14 minutes, there was no change in the fluorescence detected (Figure 8.7A-D). By 16 minutes incubation time, however, the MtMP in some HCs had dissipated, as indicated by the asterisk in Figure 8.7E. By 26 minutes, almost all of the HCs in the cochlear region under investigation showed a loss of their MtMPs (Figure 8.7J). This directly correlates with what we had observed previously in the isolated mitochondrial assay systems, adding further confirmation that this may be the process underlying AG-induced ototoxicity.

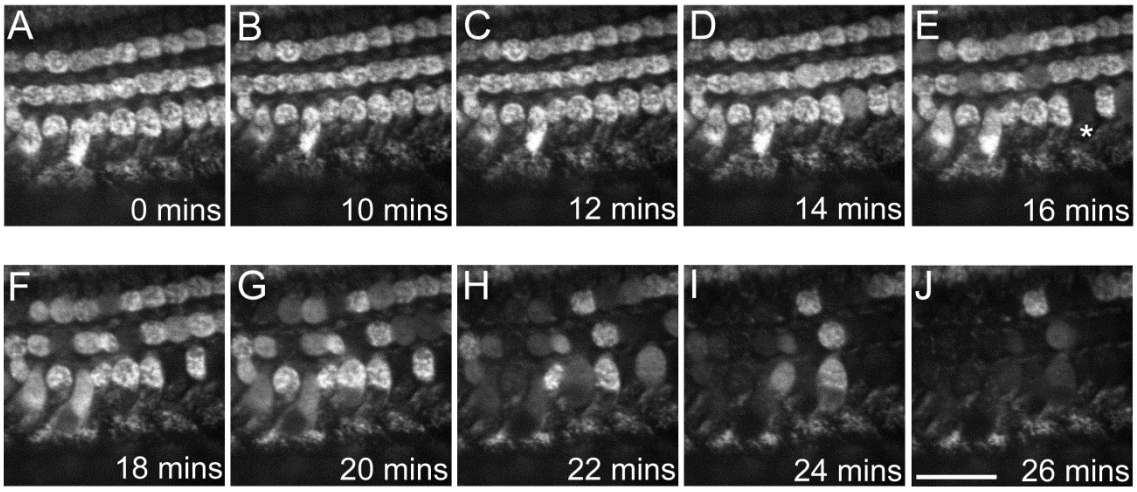

Figure 8.7: *Extracellular exposure to 5 mM gentamicin caused a loss of MtMPs in mouse cochlear culture HCs after ≥ 16 minutes incubation time.*

(A-J) Rhodamine-123 fluorescence in cochlear culture OHCs at differing time points following extracellular exposure to 5 mM gentamicin. Loss of fluorescence begins at 16 minutes post-exposure, with complete loss visible in one OHC (*). The decrease in fluorescence indicates a

collapse of the MtMP. By 26 minutes post-exposure the majority of OHCs in the ROI had reduced Rhodamine-123 fluorescence indicating a widespread loss of MtMP. Experiment was performed at room temperature (20 -22 °C). Scale bar is 25 µm.

8.2.7 Tocris Library Otoprotectant 13143 Prevents the Gentamicin-Induced Stimulation of State 4 Respiration

One of the most effective otoprotectants that I identified in this thesis, 13143 (see Chapter 4), was shown to have no interaction with the HC MET channel or affect the RP of the cell. Although shown to reduce GTTR entry into HCs, this was assumed to be independent of its mechanism of protection due to the lack of effect on the MET channel current or the RP of the cell; the two processes that could influence the AG-uptake process. This meant that the mechanism of protection of this compound remained unknown. For this reason, I investigated whether 13143 was able to prevent the gentamicin-induced effect on the respiratory activities of isolated mitochondria. Using an Oroboros Oxygraph I compared the state 4 respiratory rates of isolated mitochondria when incubated with 5 mM gentamicin alone or 5 mM gentamicin alongside 25 µM 13143.

In Figure 8.8A-D the otoprotective effect of 13143 is shown. Partial protection against the 48 hours, 5 µM gentamicin-induced loss of OHCs is observed with co-incubation of 0.5 µM 13143, and complete protection is seen with 1 µM. Shown in Figure 8.8E is the stimulation of CII-driven state 4 respiration caused by 5 mM gentamicin (red), and also the reduction of this stimulatory effect as a result of co-incubation with 25 µM 13143 (purple). Quantification of the response is shown in Figure 8.8F. A one-way ANOVA followed by Tukey's post hoc test revealed a significant difference in the gentamicin-induced stimulation of CII-driven state 4 oxygen consumption rates when mitochondria were co-incubated with 25 µM 13143 (p = 0.0039) (n=3). The average state 4 respiratory rate of the mitochondria treated with 5 mM gentamicin was 712 (± 68.4) pmol O_2 s^{-1} ml^{-1} (n=3) and in those co-treated with 13143 it was 396 (± 13.9) pmol O_2 s^{-1} ml^{-1} (n=3). However, the maximal respiratory rate (state 3U) was greatly reduced, measuring 907.3 (± 33.9) pmol O_2 s^{-1} ml^{-1} (n=3) in the gentamicin-treated conditions and 600.7 (± 39.0) pmol O_2 s^{-1} ml^{-1} (n=3) in those co-incubated with 13143. Consequently, RCR conversions revealed the resulting RCR of gentamicin-treated mitochondria to be 1.31 (± 0.19) and 1.51 (± 0.05) when co-incubated with 13143. The difference was not

significant. However, dissimilarly to what was observed with gentamicin alone, 13143 co-incubation did restore a significant difference between the state 4 and state 3U respiratory activities (p = 0.0042) (n=3).

Taken together, these data implied that this may be the mechanism of protection of 13143 – protecting by preventing the gentamicin-induced dysfunction of mitochondrial activity that subsequently leads to HC apoptosis induction. However, the mitochondrial RCR is still reduced to approximately the same value and the overall activity is considerably lower, suggesting that 13143 may simply be exacerbating the ETC disruption caused by gentamicin.

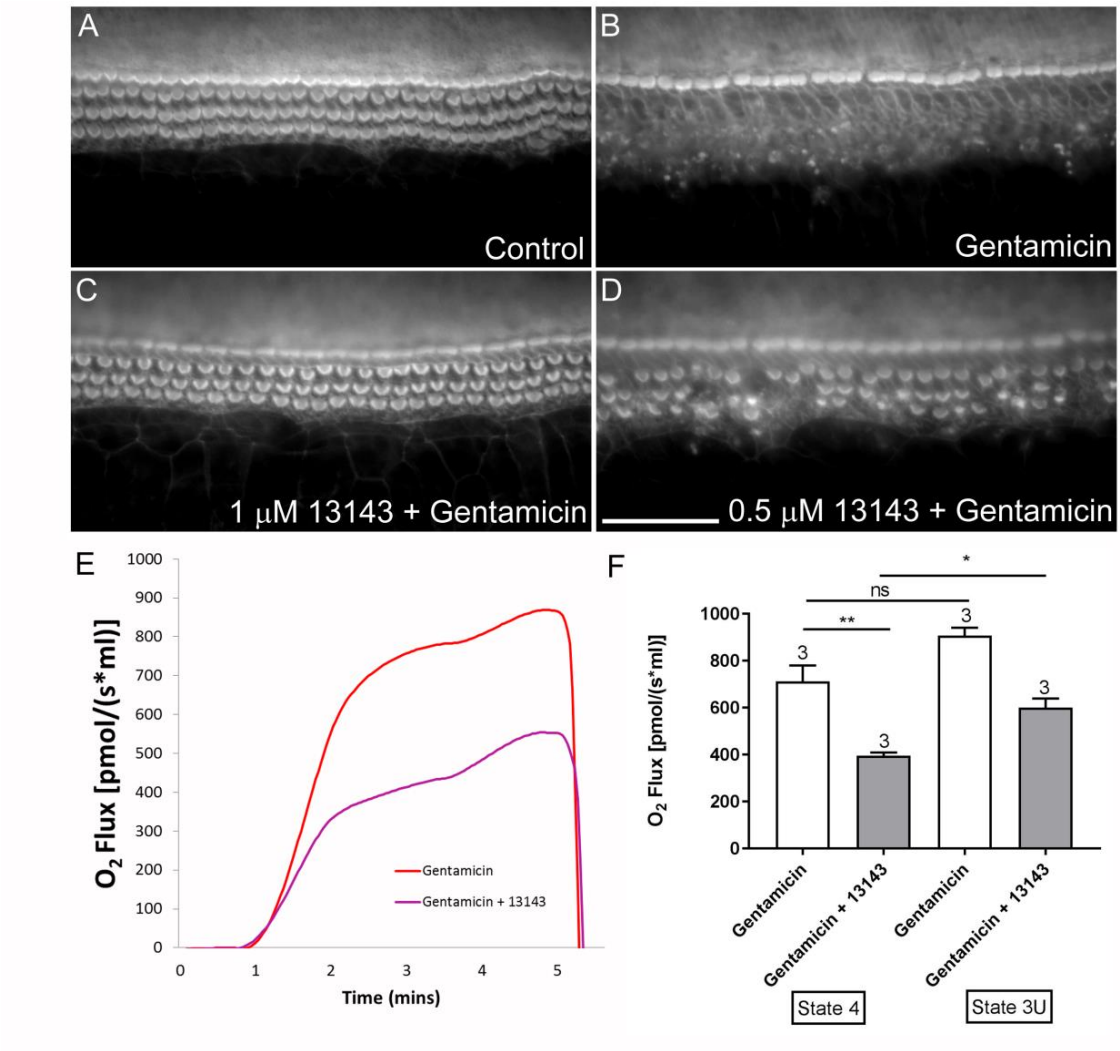

Figure 8.8: *Compound 13143 protected sensory HCs against gentamicin damage in mouse cochlear cultures and also prevented the gentamicin-induced stimulation of mitochondrial state 4 respiration in isolated rat liver mitochondria.*

Cochlear cultures were treated for 48 hours with either **(A)** 0.5% DMSO, **(B)** 5 μM gentamicin and 0.5% DMSO, 5 μM gentamicin and **(C)** 1 μM or **(D)** 0.5 μM 13143. Scale bar is 50 μm. **(E)**

Oroboros Oxygraph recordings of oxygen consumption showed that co-incubation of 25 µM 13143 (purple) reduced the 5 mM gentamicin-induced stimulation of CII-driven state 4 respiration. **(F)** Quantification revealed that 25 µM 13143 co-incubation significantly reduced gentamicin's stimulation of state 4 respiration (p = 0.0081) and also caused an increase in state 3U activity, relative to state 4 (n=3).

8.2.8 Tocris Library Otoprotectant 13097 does not Prevent AG-Induced Mitochondrial Dysfunction

The most effective otoprotectant that I identified in this thesis, 13097 (see Chapter 4), was shown to protect with a remarkable efficacy. However, mechanistic investigations revealed that it had no effect on the MET channel current or the RP of the cell, and was also shown to have no effect on the loading of GTTR into cochlear HCs. Consequently, the mechanism of protection was assumed to be intracellular. For this reason, I investigated whether 13097 was able to prevent the gentamicin-induced effect on the respiratory activities of isolated mitochondria.

Figure 8.9A-D shows the protective effect of 13097, completely protecting against the 5 µM gentamicin-induced OHC damage when co-incubated at a concentration of 10 nM. In Figure 8.9E the gentamicin-induced stimulation of state 4 and inhibition of state 3U respiratory activities is shown (red). Also shown is evidence that 13097 does not prevent this effect (purple), at any concentration tested (≤ 200 µM). Figure 8.9F shows quantification of the state 4 response and Figure 8.9G shows quantification of the state 3U response. A one-way ANOVA followed by Dunnett's multiple comparison's test revealed that no significant difference between the gentamicin alone and gentamicin alongside 13097 conditions were detected with either gentamicin-induced effect.

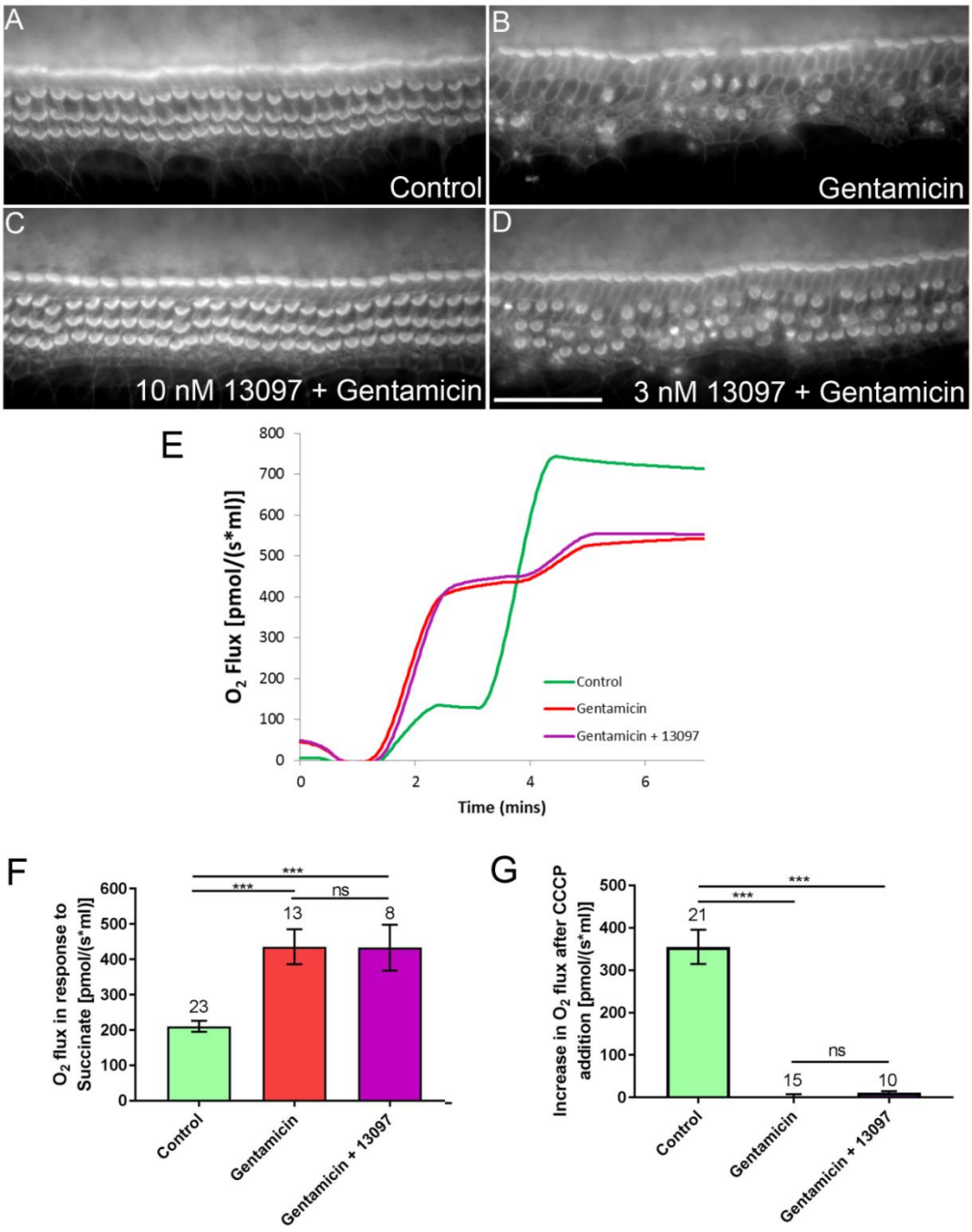

Figure 8.9: *Compound 13097 protected sensory HCs against gentamicin damage in mouse cochlear cultures but did not prevent gentamicin's effects on isolated rat liver mitochondria.*

Cochlear cultures were treated for 48 hours with either **(A)** 0.5% DMSO, **(B)** 5 µM gentamicin and 0.5% DMSO, 5 µM gentamicin and **(C)** 10 nM or **(D)** 3 nM 13097. Scale bar is 50 µm. **(E)** Oroboros Oxygraph recordings of oxygen consumption rates revealed that co-incubation of 200 µM 13097 (purple) did not prevent the 5 mM gentamicin-induced stimulation of CII-driven state 4 respiration (red). **(F-G)** Quantification of the respiratory rates revealed no significant difference in the oxygen fluxes of mitochondria treated with 5 mM gentamicin alone or gentamicin alongside 200 µM 13097.

8.3 Summary

Here I have presented evidence of the direct effect of gentamicin on the respiratory activities of isolated rat liver and kidney mitochondria, showing that it stimulated state 4 and inhibited state 3U respiratory rates, thereby reducing the mitochondrial RCR. I have also demonstrated that gentamicin caused a collapse of the MtMP, which would lead to a reduction in ATP production. I propose that the AGs behave as uncouplers of the mitochondrial ETC; increasing the permeability of the membrane and thus preventing the tight coupling of oxygen consumption to ATP production. This working hypothesis is supported by evidence that it reduces the production of MtROS (Figure 8.5 and 8.5D), which is only produced by electron backflow - a process requiring coupled mitochondria. I also showed the gentamicin-induced reduction of the MtMP in sensory HCs of mouse cochlear cultures, confirming that the effects observed in isolated mitochondria are also applicable to those in intact cell systems. Lastly, I tested the two most effective otoprotectants that I identified within this thesis to see if they prevented the observed effect of gentamicin on mitochondria, as their mechanism of protection remained unknown. One compound (13143) prevented the gentamicin-induced stimulation of state 4 respiration and one (13097) did not.

To summarise on the effect of AGs on mitochondria, it is my working hypothesis that once the AGs have accumulated inside a cell at a high enough concentration, they begin to cause the dysfunction of mitochondria. They potentially form holes in mitochondrial membranes similarly to how they attack bacteria (Kadurugamuwa et al., 1993), or perhaps in a similar way to classic mitochondrial uncouplers such as CCCP, which work as protonophores by translocating protons across the lipid membrane (Lim et al., 2001); leading to the opening of the permeability transition pore that underlies the characteristic mitochondrial swelling associated with apoptosis (Ganote and Armstrong, 2003). The increased permeability causes the dissipation of the proton gradient and MtMP (Dehne et al., 2002; Miyazono et al., 2018) that is tightly regulated in order to allow the correct production of ATP required by the cell. Consequently, mitochondria will be unable to produce as much ATP on demand – for instance, in the event of AG damage and the need for additional ATP to aid its clearance. Studies have shown reduced ATP levels in whole kidneys following *in vivo* gentamicin treatment (Simmons et al., 1980), supporting this postulation.

This hypothesis is further supported by evidence that valinomycin, another antibiotic, induces the same effect as classic mitochondrial uncouplers – increasing mitochondrial membrane permeability to K^+ ions, thereby reducing the MtMP (Safiulina et al., 2006).

8.4 Discussion

The evidence that I have presented in this chapter is important in that I show a potentially direct effect of the AGs on the functional activities of mitochondria and propose a mechanism of action underlying the effect. Although often assumed to interact with mitochondria and affect their respiratory activities, most lines of evidence for this postulation are indirect and a unified process has not yet been established. If this research is validated by future studies, this could represent a direct line of evidence to reveal how the AGs induce mitochondrial dysfunction once inside a cell, thereby enabling screening for otoprotection mechanisms in terms of intracellular, mitochondrial dysfunction.

Doubt in the validity of the experimental results presented in this chapter arises from the concentration of gentamicin used in the experiments. In order to see an effect on mitochondria, gentamicin had to be incubated in the millimolar range for at least 2 to 3 minutes. When compared to the cochlear culture gentamicin-kill assay used throughout this thesis, which used 5 µM gentamicin for 48 hours, concerns for the discrepancy in concentration arise. Ideally, mitochondria would have been incubated with a much lower concentration for a much longer time, to mimic the cochlear culture assay conditions. However, when using the Oroboros Oxygraph machinery, mitochondria left spinning in the chambers lose their integrity and begin to uncouple as soon as 15 minutes post-incubation. This is because a magnetic stirrer bar is used to keep the mitochondria in suspension in the solution; however, the mechanical damage induced by this setup caused the mitochondria to uncouple over time, resulting in a reduction in the RCR which then skewed meaningful interpretation of the results. Consequently, it was not possible to extend the incubation time and reduce the AG concentration to make the two assay types more comparable.

Although the concentration discrepancy poses a valid concern, a previous study investigating the effect of gentamicin on renal cells *in vivo* revealed a very similar response (Simmons et al., 1980). The researchers gave daily administrations of gentamicin to rats for 7 days, after which they harvested their kidneys and performed similar experiments on mitochondria isolated from the organ. They also observed a gentamicin-induced stimulation of state 4 and inhibition of state 3U respiration, which adds validity to the results obtained herein. Moreover, the researchers found a very high concentration of gentamicin had accumulated in the kidney cortex (damage to which underlies nephrotoxicity) relative to the hepatic concentrations (Simmons et al., 1980); thus further supporting the argument that it is the tissue-selective enhanced accumulation that underlies the specificity of AG toxicity.

Further validation of the effects I observed in isolated mitochondria comes from the investigation of MtMP changes in the HCs of cochlear cultures. All of the effects seen in isolated mitochondria (respiratory state stimulations and inhibitions, RCR and MtMP reductions and the prevention of ROS production) are tightly linked to the collapse of the MtMP. In cochlear cultures, the evident MtMP collapse therefore implies that each of the documented effects would be applicable to mitochondria in whole-cells also. We observed the collapse of HC MtMPs after 16 minutes extracellular exposure to 5 mM gentamicin. What remains to be determined is what concentration of gentamicin would accumulate intracellularly when this MtMP collapse is observed. Because the cochlear cultures are stripped of their SV during the dissection process, the EP would not be present to act as a driving force for AG entry, as is usually the case *in vivo*. Moreover, the EP only starts to develop in mice *in vivo* around P7, so it would not be present in the cochlear cultures irrespective of SV removal. Electrophysiological experiments would need to be conducted to assess the HC's resting potential, so as to establish what driving force would exist across the MET channel, in order to determine the entry rates of the antibiotics and their consequent accumulation within the cell. Volumetric calculations of the HC size would also be required for this calculation. Furthermore, the speed at which HCs lose their MtMP may be quicker *in vivo* due to the differing temperatures. The experiments were performed at room temperature (20-22°C); however, if performed at body temperature (37°C), due to the kinetics involved in the entry rates, AGs might have entered more rapidly and caused a loss of the MtMPs more rapidly also.

Another intriguing factor emerging from this research concerns the lack of MtROS production. After exposure to AGs, large spikes of ROS are observed in cochlear HCs before they undergo apoptosis (Clerici et al., 1996; Hirose et al., 1997; Sha and Schacht, 1999a). This was one line of evidence that suggested mitochondrial involvement in the AG-induced cell death process, as mitochondria are the main source of ROS within the cell. However, there are other sources of ROS production (Brand, 2010; Phaniendra et al., 2015), so this issue remains to be further investigated. Given the results presented within this chapter, it would suggest that AG-induced ROS production is not mitochondrial in nature. Perhaps if one could block MtROS production, by way of uncoupler addition, for example, and then investigate whether ROS spikes still occur in cells before apoptosis, this would add confirmation to our hypothesis of AG-induced mitochondrial uncoupling preventing MtROS formation.

Interestingly, past researchers investigating the effect of gentamicin on mitochondrial activity found that after harvesting mitochondria from the kidney and liver of rats exposed to daily administration of gentamicin (Simmons et al., 1980), liver mitochondria showed no difference

when compared to controls, dissimilarly to what was found in those isolated from the kidney. This implied that only the mitochondria of organs susceptible to AG damage are affected by the antibiotics. However, here I have demonstrated the same effect of gentamicin on both kidney and liver mitochondria. What this suggests is that all mitochondria are susceptible to AG damage; however, it is the entry and exit rates into specific organs, and the consequent accumulation, that determines whether an organ's mitochondria are affected by the antibiotics.

The results presented herein confirm mitochondrial involvement in AG-induced ototoxicity whilst also potentially contesting the opposing postulation that it is the ER (or more specifically, its calcium signalling to mitochondria) that underlies the phenomenon, as other researchers have more recently suggested (Esterberg et al., 2013; 2014; 2016; Hailey et al., 2017; O'Sullivan et al., 2017). Here we demonstrated that the same effects that have been observed in whole-cell systems, both kidney and cochlea, before the onset of AG-induced cell death occur in the isolated mitochondrial systems used in this chapter. Mitochondria in isolation receive no signalling input from the ER, which implies that mitochondria are susceptible to the reported AG effects independent of any input from the ER or its calcium signalling pathways. This is consistent with previous reports of mitochondrial alterations as the earliest and most predominant event observed in neomycin-induced cell death in zebrafish lateral line systems (Owens et al., 2007).

The evident preventative effect of Tocris compound 13143 on gentamicin's stimulation of state 4 respiration could be independent of its mechanism of protection, similarly to its effect on GTTR loading as presented in Chapter 4. This presumption arose due to the lack of any effect observed with 13097. Both compounds are K_v7 channel blockers, with 13097 (XE 991) identified as an improved version of 13143 (linopirdine) for use as a cognitive enhancer (Zaczek et al., 1998; Greene et al., 2017). Consequently, it was assumed that both compounds would protect HCs in a similar way. It therefore remains to be determined whether the preservation of mitochondrial function is indeed the mechanism of otoprotection of 13143. In order to investigate this further, assessment of MtMPs in cochlear culture sensory hair cells exposed to gentamicin alone (Figure 8.7) or gentamicin alongside 13143 would reveal whether this effect potentially underlay the identified HC protection.

To conclude, the research presented in this chapter provides an exciting new prospect for the investigation of the mechanism of action of identified otoprotectants. If confirmed to be the true effect of the AGs, the potential for screening prospects is enormous. Although the

Oroboros Oxygraph only has two chambers, and so only allows the comparison of two mitochondrial samples at any one time, there are larger-scale versions of the machinery. Seahorse Biosciences have utilised the same principle of oxygen consumption assays for the assessment of mitochondria activity; however, their machines can hold up to 96 well plates and can be used both with isolated mitochondria and whole cells (Plitzko and Loesgen, 2018). If the effects I observed in the Oroboros Oxygraph could be replicated in Seahorse machinery, then we could use this for high-throughput screening of potential otoprotectants, especially when compared to the much lower throughput of our cochlear culture screening procedures.

9 Final Summary and Conclusions

Within this thesis I present a number of potential novel otoprotectants, to the identification and validation of which I have contributed. These compounds are capable of protecting against the AG-induced loss of sensory hair cells that underlies the ototoxicity associated with the clinical use of the antibiotics. In terms of the identification of compounds that provide any otoprotective effect in mammalian models I discuss 25 novel compounds: 13 compounds from the Tocris Ion Channel library of ion channel interactors and 1 Tocris compound derivative (Chapter 4); the d-Tubocurarine-related alkaloid berbamine and a similar neuromuscular blocker that was commercially bought (Chapter 5); the FDA-approved drug carvedilol and 4 of its synthesised derivatives (Chapter 6); and 4 FM 1-43 derivatives synthesised in house (Chapter 7). Additionally, I have confirmed the protective nature of d-Tubocurarine and questioned that of FM 1-43, whilst extending the knowledge base of their otoprotective profiles.

After thoroughly screening for any potentially adverse effects of all of the newly-identified otoprotectants investigated in this thesis, 5 compounds remained that have the potential to be used in a clinical setting. These 5 compounds emerged from the Tocris Ion Channel library screen (13097, 13142, 13143, 13154 and 13222), all of which displayed otoprotective properties and also no adverse effects throughout the comprehensive screening process. These compounds are now awaiting *in vivo* validation of their otoprotective abilities, for confirmation that they protect, and do not induce any off-target side-effects, when used in a whole mouse model.

Of the 5 compounds with the potential for clinical application, 3 of them block sensory hair cell MET channels (13142, 13154 and 13222), suggesting block of AG entry to be their mechanism of protection. The remaining two (13097 and 13143) do not interact with the MET channel. They do interact with $I_{K,neo}$, the other membrane channel that could influence the AG uptake process, however their modest block of this channel did not depolarise the OHCs, suggesting that they do not prevent AG entry but rather protect intracellularly. Although both avenues of otoprotection should thus continue to be investigated, I would argue that an intracellular, non-MET blocking approach may be the most successful. Compounds 13097 (XE 991) and 13143 (linopirdine) both protect mammalian hair cells at extremely low concentrations. Both protecting in the low nanomolar range, these compounds protect with a much greater efficacy than any other identified in this thesis and also reported elsewhere in the literature. It is

evident that they do not block the MET channel or prevent AG loading into hair cells. Extrapolating, this implies that they are likely to be working intracellularly, for example by way of preventing apoptosis induction in sensory hair cells. Compound 13143 may be protecting by preventing AG-induced mitochondrial dysfunction (Chapter 8), however this remains to be confirmed with additional experimentation.

The research presented in this thesis has highlighted the importance of a thorough screening procedure when searching for otoprotectants with the potential for use in a clinical setting. A large number of the potential novel protectants identified herein (approximately 80%) were ineligible for testing *in vivo* due to the adverse side-effects they were shown to cause in mouse cochlear cultures, and therefore may induce in a whole mouse model. Consequently, it is vital that thorough screening procedures are always adhered to throughout this investigatory process.

I have confirmed that the use of zebrafish pre-screening and a two-model system using the zebrafish lateral line and mouse cochlear cultures for otoprotectant discovery is a viable and successful procedure, with the majority of compounds shown to protect in mouse cochlear cultures also identified as protectors in the preliminary zebrafish screens. However, although useful for initial trials, follow-up experiments with extensive additional screening in mammalian systems should always be conducted.

Lastly, I have shown that chemical compound modification based on the way in which a compound provides protection is a viable method for the production of alternative and additional otoprotectants. In each otoprotectant screening chapter presented herein, selected compounds were structurally modified and this led to the production of novel compounds capable of protecting against AG-induced sensory hair cell loss. Some of these modifications led to improved protective efficacy and also a reduction of unwanted, adverse side-effects. This confirms that the modification of compounds based on a compound's mechanism of protection is a viable method for the generation of novel otoprotectants.

Bibliography

Akbar, S., Alorainy, M.S., 2014. The current status of beta blockers' use in the management of hypertension. Saudi Med. J. 35, 1307–1317.

Al-Ghamdi, H., 2011. Carvedilol in the treatment of portal hypertension. Saudi J. Gastroenterol. 17, 155. https://doi.org/10.4103/1319-3767.77251

Alharazneh, A., Luk, L., Huth, M., Monfared, A., Steyger, P.S., Cheng, A.G., Ricci, A.J., 2011. Functional Hair Cell Mechanotransducer Channels Are Required for Aminoglycoside Ototoxicity. PLoS ONE 6, e22347. https://doi.org/10.1371/journal.pone.0022347

Al-Malky, G., Dawson, S.J., Sirimanna, T., Bagkeris, E., Suri, R., 2015. High-frequency audiometry reveals high prevalence of aminoglycoside ototoxicity in children with cystic fibrosis. J. Cyst. Fibros. 14, 248–254. https://doi.org/10.1016/j.jcf.2014.07.009

Amaral, E., Guatimosim, S., Guatimosim, C., 2011. Using the Fluorescent Styryl Dye FM1-43 to Visualize Synaptic Vesicles Exocytosis and Endocytosis in Motor Nerve Terminals, in: Chiarini-Garcia, H., Melo, R.C.N. (Eds.), Light Microscopy. Humana Press, Totowa, NJ, pp. 137–148. https://doi.org/10.1007/978-1-60761-950-5_8

Ariano, R.E., Zelenitsky, S.A., Kassum, D.A., 2008. Aminoglycoside-Induced Vestibular Injury: Maintaining a Sense of Balance. Ann. Pharmacother. 42, 1282–1289. https://doi.org/10.1345/aph.1L001

Assad, J.A., Shepherd, G.M., Corey, D.P., 1991. Tip-link integrity and mechanical transduction in vertebrate hair cells. Neuron 7, 985–994.

Betz, W.J., Mao, F., Smith, C.B., 1996. Imaging exocytosis and endocytosis. Curr. Opin. Neurobiol. 6, 365–371. https://doi.org/10.1016/S0959-4388(96)80121-8

Beurg, M., Evans, M.G., Hackney, C.M., Fettiplace, R., 2006. A Large-Conductance Calcium-Selective Mechanotransducer Channel in Mammalian Cochlear Hair Cells. J. Neurosci. 26, 10992–11000. https://doi.org/10.1523/JNEUROSCI.2188-06.2006

Beurg, M., Fettiplace, R., 2017. PIEZO2 as the anomalous mechanotransducer channel in auditory hair cells: Mechanosensitive channels in cochlear hair cells. J. Physiol. 595, 7039–7048. https://doi.org/10.1113/JP274996

Beurg, M., Fettiplace, R., Nam, J.-H., Ricci, A.J., 2009. Localization of inner hair cell mechanotransducer channels using high-speed calcium imaging. Nat. Neurosci. 12, 553–558. https://doi.org/10.1038/nn.2295

Beurg, M., Kim, K.X., Fettiplace, R., 2014. Conductance and block of hair-cell mechanotransducer channels in transmembrane channel–like protein mutants. J. Gen. Physiol. 144, 55–69. https://doi.org/10.1085/jgp.201411173

Brownell, W. E., 1984. Microscopic observation of cochlear hair cell motility, Scan. Elect. Microscopy, 1984/III, 1401–1406.

Cannizzaro, E., Cannizzaro, C., Plescia, F., Martines, F., Soleo, L., Pira, E., Lo Coco, D., 2014. Exposure to ototoxic agents and hearing loss: A review of current knowledge. Hear. Balance Commun. 12, 166–175. https://doi.org/10.3109/21695717.2014.964939

Chen, Y., Huang, W.G., Zha, D.J., Qiu, J.H., Wang, J.L., Sha, S.H., Schacht, J., 2007. Aspirin attenuates gentamicin ototoxicity: From the laboratory to the clinic. Hear. Res. 226, 178–182. https://doi.org/10.1016/j.heares.2006.05.008

Chiu, L.L., Cunningham, L.L., Raible, D.W., Rubel, E.W., Ou, H.C., 2008. Using the Zebrafish Lateral Line to Screen for Ototoxicity. J. Assoc. Res. Otolaryngol. 9, 178–190. https://doi.org/10.1007/s10162-008-0118-y

Chung, Y.W., Kim, Y.S., Ahn, J.-C., Chung, P.-S., Rhee, C.-K., 2007. Effect of low level laser on ototoxicity prevention of FM1-43 in postnatal organotypic culture of rat utricles, in: Kollias, N., Choi, B., Zeng, H., Malek, R.S., Wong, B.J., Ilgner, J.F.R., Gregory, K.W., Tearney, G.J., Hirschberg, H., Madsen, S.J. (Eds.), . p. 64241I. https://doi.org/10.1117/12.700622

Clerici, W.J., Hensley, K., DiMartino, D.L., Butterfield, D.A., 1996. Direct detection of ototoxicant-induced reactive oxygen species generation in cochlear explants. Hear. Res. 98, 116–124. https://doi.org/10.1016/0378-5955(96)00075-5

Coffin, A.B., Rubel, E.W., Raible, D.W., 2013a. Bax, Bcl2, and p53 Differentially Regulate Neomycin- and Gentamicin-Induced Hair Cell Death in the Zebrafish Lateral Line. J. Assoc. Res. Otolaryngol. 14, 645–659. https://doi.org/10.1007/s10162-013-0404-1

Coffin, A.B., Williamson, K.L., Mamiya, A., Raible, D.W., Rubel, E.W., 2013b. Profiling drug-induced cell death pathways in the zebrafish lateral line. Apoptosis 18, 393–408. https://doi.org/10.1007/s10495-013-0816-8

Conly, J., Gold, W., Shafran, S., 1994. Once-daily aminoglycoside dosing: A new look at an old drug. Can. J. Infect. Dis. J. Can. Mal. Infect. 5, 205–206.

Corey, D.P., 2003. New TRP channels in hearing and mechanosensation. Neuron 39, 585–588.

Corns, L.F., Johnson, S.L., Kros, C.J., Marcotti, W., 2014. Calcium entry into stereocilia drives adaptation of the mechanoelectrical transducer current of mammalian cochlear hair cells. Proc. Natl. Acad. Sci. 111, 14918–14923. https://doi.org/10.1073/pnas.1409920111

Cox, E.C., White, J.R., Flaks, J.G., 1964. STREPTOMYCIN ACTION AND THE RIBOSOME. Proc. Natl. Acad. Sci. 51, 703–709. https://doi.org/10.1073/pnas.51.4.703

Crawford, A.C., Evans, M.G., Fettiplace, R., 1989. Activation and adaptation of transducer currents in turtle hair cells. J. Physiol. 419, 405–434.

Dai, C.F., Mangiardi, D., Cotanche, D.A., Steyger, P.S., 2006. Uptake of fluorescent gentamicin by vertebrate sensory cells in vivo. Hear. Res. 213, 64–78. https://doi.org/10.1016/j.heares.2005.11.011

Dallos, P., 1996. Overview: cochlear neurophysiology. A.N. Popper, R.R. Fay (Eds.), The Cochlea, Springer, New York (1996), pp. 1-43

Dallos, P., 2008. Cochlear amplification, outer hair cells and prestin. Curr. Opin. Neurobiol. 18, 370–376. https://doi.org/10.1016/j.conb.2008.08.016

Dallos, P., Harris, D., 1978. Properties of auditory nerve responses in absence of outer hair cells. J. Neurophysiol. 41, 365–383. https://doi.org/10.1152/jn.1978.41.2.365

Dallos, P., Santos-Sacchi, J., Flock, A., 1982. Intracellular recordings from cochlear outer hair cells. Science 218, 582–584.

Davies, J., Davis, B.D., 1968. Misreading of ribonucleic acid code words induced by aminoglycoside antibiotics. The effect of drug concentration. J. Biol. Chem. 243, 3312–3316.

de Groot, J.C., Meeuwsen, F., Ruizendaal, W.E., Veldman, J.E., 1990. Ultrastructural localization of gentamicin in the cochlea. Hear. Res. 50, 35–42.

Dehne, N., Rauen, U., de Groot, H., Lautermann, J., 2002. Involvement of the mitochondrial permeability transition in gentamicin ototoxicity. Hear. Res. 169, 47–55. https://doi.org/10.1016/S0378-5955(02)00338-6

Ding, D., Jin, X., Zhao, J., 1995. Accumulation sites of kanamycin in cochlear basal membrane cells. Zhonghua Er Bi Yan Hou Ke Za Zhi 30, 323–325.

Drew, L.J., Wood, J.N., 2007. FM1-43 is a Permeant Blocker of Mechanosensitive Ion Channels in Sensory Neurons and Inhibits Behavioural Responses to Mechanical Stimuli. Mol. Pain 3, 1744-8069-3–1. https://doi.org/10.1186/1744-8069-3-1

Eatock, R.A., Corey, D.P., Hudspeth, A.J., 1987. Adaptation of mechanoelectrical transduction in hair cells of the bullfrog's sacculus. J. Neurosci. Off. J. Soc. Neurosci. 7, 2821–2836.

eHealthMe, 2017. Carvedilol and Multaq drug interactions – from FDA reports. CA.Available at. http://www.ehealthme.com/drug-interaction/carvedilol/multaq/Accessed date: 23 June 2018.

El Mouedden, M., 2000. Gentamicin-Induced Apoptosis in Renal Cell Lines and Embryonic Rat Fibroblasts. Toxicol. Sci. 56, 229–239. https://doi.org/10.1093/toxsci/56.1.229

Eltahawy, A.T., Bahnassy, A.A., 1996. Aminoglycoside prescription, therapeutic monitoring and nephrotoxicity at a university hospital in Saudi Arabia. J. Chemother. Florence Italy 8, 278–283. https://doi.org/10.1179/joc.1996.8.4.278

Erostegui, C., Norris, C.H., Bobbin, R.P., 1994. In vitro pharmacologic characterization of a cholinergic receptor on outer hair cells. Hear. Res. 74, 135–147. https://doi.org/10.1016/0378-5955(94)90182-1

Esterberg, R., Coffin, A.B., Ou, H., Simon, J.A., Raible, D.W., Rubel, E.W., 2013. Fish in a dish: drug discovery for hearing habilitation. Drug Discov. Today Dis. Models 10, e23–e29. https://doi.org/10.1016/j.ddmod.2012.02.001

Esterberg, R., Hailey, D.W., Rubel, E.W., Raible, D.W., 2014. ER-Mitochondrial Calcium Flow Underlies Vulnerability of Mechanosensory Hair Cells to Damage. J. Neurosci. 34, 9703–9719. https://doi.org/10.1523/JNEUROSCI.0281-14.2014

Farris, H.E., LeBlanc, C.L., Goswami, J., Ricci, A.J., 2004. Probing the pore of the auditory hair cell mechanotransducer channel in turtle: Pharmacology of mechanotransduction. J. Physiol. 558, 769–792. https://doi.org/10.1113/jphysiol.2004.061267

Fausti, S.A., Henry, J.A., Helt, W.J., Phillips, D.S., Frey, R.H., Noffsinger, D., Larson, V.D., Fowler, C.G., 1999. An individualized, sensitive frequency range for early detection of ototoxicity. Ear Hear. 20, 497–505.

Fausti, S.A., Henry, J.A., Schaffer, H.I., Olson, D.J., Frey, R.H., McDonald, W.J., 1992. High-frequency audiometric monitoring for early detection of aminoglycoside ototoxicity. J. Infect. Dis. 165, 1026–1032.

Fee, W.E., 1980. AMINOGLYCOSIDE OTOTOXICITY IN THE HUMAN. The Laryngoscope 90, 1–19. https://doi.org/10.1288/00005537-198010001-00001

Fettiplace, R., 2016. Is TMC1 the Hair Cell Mechanotransducer Channel? Biophys. J. 111, 3–9. https://doi.org/10.1016/j.bpj.2016.05.032

Fettiplace, R., 2009. Defining features of the hair cell mechanoelectrical transducer channel. Pflüg. Arch. - Eur. J. Physiol. 458, 1115–1123. https://doi.org/10.1007/s00424-009-0683-x

Forge, A., Richardson, G., 1993. Freeze fracture analysis of apical membranes in cochlear cultures: differences between basal and apical-coil outer hair cells and effects of neomycin. J. Neurocytol. 22, 854–867.

Forge, A., Schacht, J., 2000. Aminoglycoside antibiotics. Audiol. Neurootol. 5, 3–22. https://doi.org/10.1159/000013861

Fu, A.L., Dong, Z.H., Sun, M.J., 2006. Protective effect of N-acetyl-l-cysteine on amyloid β-peptide-induced learning and memory deficits in mice. Brain Res. 1109, 201–206. https://doi.org/10.1016/j.brainres.2006.06.042

Gale, J.E., Marcotti, W., Kennedy, H.J., Kros, C.J., Richardson, G.P., 2001. FM1-43 Dye Behaves as a Permeant Blocker of the Hair-Cell Mechanotransducer Channel. J. Neurosci. 21, 7013.

Gale, J.E., Meyers, J.R., Periasamy, A., Corwin, T., 2002. Survival of bundleless hair cells and subsequent bundle replacement in the bullfrog's saccule. J. Neurobiol. 50, 81–92. https://doi.org/10.1002/neu.10002

Ganote, C.E., Armstrong, S.C., 2003. Effects of CCCP-induced mitochondrial uncoupling and cyclosporin A on cell volume, cell injury and preconditioning protection of isolated rabbit cardiomyocytes. J. Mol. Cell. Cardiol. 35, 749–759.

Garinis, A.C., Cross, C.P., Srikanth, P., Carroll, K., Feeney, M.P., Keefe, D.H., Hunter, L.L., Putterman, D.B., Cohen, D.M., Gold, J.A., Steyger, P.S., 2017. The cumulative effects of intravenous antibiotic treatments on hearing in patients with cystic fibrosis. J. Cyst. Fibros. 16, 401–409. https://doi.org/10.1016/j.jcf.2017.01.006

Glowatzki, E., Ruppersberg, J.P., Zenner, H.-P., Rüsch, A., 1997. Mechanically and ATP-induced currents of mouse outer hair cells are independent and differentially blocked by d-tubocurarine. Neuropharmacology 36, 1269–1275. https://doi.org/10.1016/S0028-3908(97)00108-1

Goh, J.W., Pennefather, P.S., 1987. Pharmacological and physiological properties of the after-hyperpolarization current of bullfrog ganglion neurones. J. Physiol. 394, 315–330. https://doi.org/10.1113/jphysiol.1987.sp016872

Gonzalez L. S., Spencer J. P., 1998. Aminoglycosides: a practical review. Am. Fam. Phys. 58, 1811–1820.

Goodyear, R.J., Richardson, G.P., 2003. A Novel Antigen Sensitive to Calcium Chelation That is Associated with the Tip Links and Kinocilial Links of Sensory Hair Bundles. J. Neurosci. 23, 4878–4887. https://doi.org/10.1523/JNEUROSCI.23-12-04878.2003

Grati, M., Kachar, B., 2011. Myosin VIIa and sans localization at stereocilia upper tip-link density implicates these Usher syndrome proteins in mechanotransduction. Proc. Natl. Acad. Sci. 108, 11476–11481. https://doi.org/10.1073/pnas.1104161108

Gray, M.W., 2012. Mitochondrial evolution. Cold Spring Harb. Perspect. Biol. 4, a011403. https://doi.org/10.1101/cshperspect.a011403

Gray, M.W., Burger, G., Lang, B.F., 2001. The origin and early evolution of mitochondria. Genome Biol. 2, REVIEWS1018.

Greene, D.L., Kang, S., Hoshi, N., 2017. XE991 and Linopirdine Are State-Dependent Inhibitors for Kv7/KCNQ Channels that Favor Activated Single Subunits. J. Pharmacol. Exp. Ther. 362, 177–185. https://doi.org/10.1124/jpet.117.241679

Hackney, C.M., Furness, D.N., 2013. The composition and role of cross links in mechanoelectrical transduction in vertebrate sensory hair cells. J. Cell Sci. 126, 1721–1731. https://doi.org/10.1242/jcs.106120

Hailey, D.W., Esterberg, R., Linbo, T.H., Rubel, E.W., Raible, D.W., 2017. Fluorescent aminoglycosides reveal intracellular trafficking routes in mechanosensory hair cells. J. Clin. Invest. 127, 472–486. https://doi.org/10.1172/JCI85052

Harris, J.A., Cheng, A.G., Cunningham, L.L., MacDonald, G., Raible, D.W., Rubel, E.W., 2003. Neomycin-Induced Hair Cell Death and Rapid Regeneration in the Lateral Line of Zebrafish (Danio rerio). JARO - J. Assoc. Res. Otolaryngol. 4, 219–234. https://doi.org/10.1007/s10162-002-3022-x

Heller, J., 1984. Effect of some simple manoeuvres on the course of acute renal failure after gentamycin treatment in rats. Int. Urol. Nephrol. 16, 243–251.

Hibino, H., Kurachi, Y., 2006. Molecular and Physiological Bases of the K^+ Circulation in the Mammalian Inner Ear. Physiology 21, 336–345. https://doi.org/10.1152/physiol.00023.2006

Hirose, K., Hockenbery, D.M., Rubel, E.W., 1997. Reactive oxygen species in chick hair cells after gentamicin exposure in vitro. Hear. Res. 104, 1–14.

Hirose, Y., Sugahara, K., Kanagawa, E., Takemoto, Y., Hashimoto, M., Yamashita, H., 2016. Quercetin protects against hair cell loss in the zebrafish lateral line and guinea pig cochlea. Hear. Res. 342, 80–85. https://doi.org/10.1016/j.heares.2016.10.001

Housley, G.D., Ashmore, J.F., 1991. Direct Measurement of the Action of Acetylcholine on Isolated Outer Hair Cells of the Guinea Pig Cochlea. Proc. R. Soc. B Biol. Sci. 244, 161–167. https://doi.org/10.1098/rspb.1991.0065

Huth, M.E., Ricci, A.J., Cheng, A.G., 2011. Mechanisms of Aminoglycoside Ototoxicity and Targets of Hair Cell Protection. Int. J. Otolaryngol. 2011, 1–19. https://doi.org/10.1155/2011/937861

Imamura, S., Adams, J.C., 2003. Distribution of Gentamicin in the Guinea Pig Inner Ear after Local or Systemic Application. JARO - J. Assoc. Res. Otolaryngol. 4, 176–195. https://doi.org/10.1007/s10162-002-2036-8

Indzhykulian, A.A., Stepanyan, R., Nelina, A., Spinelli, K.J., Ahmed, Z.M., Belyantseva, I.A., Friedman, T.B., Barr-Gillespie, P.G., Frolenkov, G.I., 2013. Molecular Remodeling of Tip Links

Underlies Mechanosensory Regeneration in Auditory Hair Cells. PLoS Biol. 11, e1001583. https://doi.org/10.1371/journal.pbio.1001583

Ishii, T.M., Maylie, J., Adelman, J.P., 1997. Determinants of Apamin and *d* -Tubocurarine Block in SK Potassium Channels. J. Biol. Chem. 272, 23195–23200. https://doi.org/10.1074/jbc.272.37.23195

Jensen-Smith, H.C., Hallworth, R., Nichols, M.G., 2012. Gentamicin Rapidly Inhibits Mitochondrial Metabolism in High-Frequency Cochlear Outer Hair Cells. PLoS ONE 7, e38471. https://doi.org/10.1371/journal.pone.0038471

Jia, F., Ruan, S., Liu, N., Fu, L., 2017. Synergistic Antitumor Effects of Berbamine and Paclitaxel through ROS/Akt Pathway in Glioma Cells. Evid. Based Complement. Alternat. Med. 2017, 1–8. https://doi.org/10.1155/2017/8152526

Jiang, M., Karasawa, T., Steyger, P.S., 2017. Aminoglycoside-Induced Cochleotoxicity: A Review. Front. Cell. Neurosci. 11. https://doi.org/10.3389/fncel.2017.00308

Johnson, S.L., Beurg, M., Marcotti, W., Fettiplace, R., 2011. Prestin-Driven Cochlear Amplification Is Not Limited by the Outer Hair Cell Membrane Time Constant. Neuron 70, 1143–1154. https://doi.org/10.1016/j.neuron.2011.04.024

Kadurugamuwa, J.L., Clarke, A.J., Beveridge, T.J., 1993. Surface action of gentamicin on Pseudomonas aeruginosa. J. Bacteriol. 175, 5798–5805.

Kandel, E., Schwartz, J., Jessell, T., Siegelbaum, S., J Hudspeth, A., 2013. Principles of Neural Science, Fifth Edition.

Karasawa T., Steyger P.S. 2011. Intracellular mechanisms of aminoglycoside-induced cytotoxicity. Integr. Biol.;3:879–886. doi: 10.1039/c1ib00034a.

Kaus, S., 1987. The Effect of Aminoglycoside Antibiotics on the Lateral Line Organ of Aplocheilus lineatus (Cyprinodontidae). Acta Otolaryngol. (Stockh.) 103, 291–298. https://doi.org/10.3109/00016488709107285

Kazmierczak, P., Sakaguchi, H., Tokita, J., Wilson-Kubalek, E.M., Milligan, R.A., Müller, U., Kachar, B., 2007. Cadherin 23 and protocadherin 15 interact to form tip-link filaments in sensory hair cells. Nature 449, 87–91. https://doi.org/10.1038/nature06091

Kenyon, E.J., Kirkwood, N.K., Kitcher, S.R., O'Reilly, M., Derudas, M., Cantillon, D.M., Goodyear, R.J., Secker, A., Baxendale, S., Bull, J.C., Waddell, S.J., Whitfield, T.T., Ward, S.E., Kros, C.J., Richardson, G.P., 2017. Identification of ion-channel modulators that protect against aminoglycoside-induced hair cell death. JCI Insight 2. https://doi.org/10.1172/jci.insight.96773

Kikuchi, K., Hilding, D., 1965. The Development of the Organ of Corti in the Mouse. Acta Otolaryngol. (Stockh.) 60, 207–221. https://doi.org/10.3109/00016486509127003

Kim, S.J., Ho Hur, J., Park, C., Kim, H.J., Oh, G.S., Lee, J.N., Yoo, S.J., Choe, S.K., So, H.S., Lim, D.J., Moon, S.K., Park, R., 2015. Bucillamine prevents cisplatin-induced ototoxicity through induction of glutathione and antioxidant genes. Exp. Mol. Med. 47, e142–e142. https://doi.org/10.1038/emm.2014.112

Kimura, R.S., 1966. Hairs of the cochlear sensory cells and their attachment to the tectorial membrane. Acta Otolaryngol. (Stockh.) 61, 55–72.

Kindt, K.S., Finch, G., Nicolson, T., 2012. Kinocilia Mediate Mechanosensitivity in Developing Zebrafish Hair Cells. Dev. Cell 23, 329–341. https://doi.org/10.1016/j.devcel.2012.05.022

Kirkwood, N.K., O'Reilly, M., Derudas, M., Kenyon, E.J., Huckvale, R., van Netten, S.M., Ward, S.E., Richardson, G.P., Kros, C.J., 2017. d-Tubocurarine and Berbamine: Alkaloids That Are Permeant Blockers of the Hair Cell's Mechano-Electrical Transducer Channel and Protect from Aminoglycoside Toxicity. Front. Cell. Neurosci. 11. https://doi.org/10.3389/fncel.2017.00262

Kluckova, K., Bezawork-Geleta, A., Rohlena, J., Dong, L., Neuzil, J., 2013. Mitochondrial complex II, a novel target for anti-cancer agents. Biochim. Biophys. Acta BBA - Bioenerg. 1827, 552–564. https://doi.org/10.1016/j.bbabio.2012.10.015

Knight, K.R.G., Kraemer, D.F., Neuwelt, E.A., 2005. Ototoxicity in Children Receiving Platinum Chemotherapy: Underestimating a Commonly Occurring Toxicity That May Influence Academic and Social Development. J. Clin. Oncol. 23, 8588–8596. https://doi.org/10.1200/JCO.2004.00.5355

Koo, J.-W., Quintanilla-Dieck, L., Jiang, M., Liu, J., Urdang, Z.D., Allensworth, J.J., Cross, C.P., Li, H., Steyger, P.S., 2015. Endotoxemia-mediated inflammation potentiates aminoglycoside-induced ototoxicity. Sci. Transl. Med. 7, 298ra118-298ra118. https://doi.org/10.1126/scitranslmed.aac5546

Kornguth, M.L., Bayer, W.H., Kunin, C.M., 1980. Binding of gentamicin to subcellular fractions of rabbit kidney: inhibition by spermine and other polyamines. J. Antimicrob. Chemother. 6, 121–131. https://doi.org/10.1093/jac/6.1.121

Kros, C.J., Rusch, A., and Richardson, G.P. (1992). Mechano-Electrical Transducer Currents in Hair Cells of the Cultured Neonatal Mouse Cochlea. Proc. R. Soc. Lond. B *249*, 185–193.

Kros, C.J., 1996. Physiology of mammalian cochlear hair cells. In Springer Handbook of Auditory Research, Vol. 8: The Cochlea, ed. Dallos, P., Popper, A.N. & Fay, R.R., p318-385. Springer-Verlag, New York.

Kros, C.J., and Desmonds, T. 2015. Drug-induced hearing loss: Infection raises the odds. Science Translational Medicine *7*, 298fs31–fs298fs31.

Kros, C.J., Marcotti, W., van Netten, S.M., Self, T.J., Libby, R.T., Brown, S.D.M., Richardson, G.P., and Steel, K.P., 2002. Reduced climbing and increased slipping adaptation in cochlear hair cells of mice with Myo7a mutations. Nat Neurosci *5*, 41–47.

Kruger, M., Boney, R., Ordoobadi, A.J., Sommers, T.F., Trapani, J.G., Coffin, A.B., 2016. Natural Bizbenzoquinoline Derivatives Protect Zebrafish Lateral Line Sensory Hair Cells from Aminoglycoside Toxicity. Front. Cell. Neurosci. 10. https://doi.org/10.3389/fncel.2016.00083

Krumschnabel, G., Eigentler, A., Fasching, M., Gnaiger, E., 2014. Use of Safranin for the Assessment of Mitochondrial Membrane Potential by High-Resolution Respirometry and Fluorometry, in: Methods in Enzymology. Elsevier, pp. 163–181. https://doi.org/10.1016/B978-0-12-416618-9.00009-1

Kurima, K., Ebrahim, S., Pan, B., Sedlacek, M., Sengupta, P., Millis, B.A., Cui, R., Nakanishi, H., Fujikawa, T., Kawashima, Y., Choi, B.Y., Monahan, K., Holt, J.R., Griffith, A.J., Kachar, B., 2015. TMC1 and TMC2 Localize at the Site of Mechanotransduction in Mammalian Inner Ear Hair Cell Stereocilia. Cell Rep. 12, 1606–1617. https://doi.org/10.1016/j.celrep.2015.07.058

Kushner, B., Allen, P.D., Crane, B.T., 2016. Frequency and Demographics of Gentamicin Use: Otol. Neurotol. 37, 190–195. https://doi.org/10.1097/MAO.0000000000000937

Lash, L.H., Jones, D.P. (Eds.), 1993. Front Matter, in: Mitochondrial Dysfunction. Academic Press, p. iii. https://doi.org/10.1016/B978-0-12-461205-1.50002-3

Lee, J.H., Park, C., Kim, S.J., Kim, H.J., Oh, G.S., Shen, A., So, H.S., Park, R., 2013. Different uptake of gentamicin through TRPV1 and TRPV4 channels determines cochlear hair cell vulnerability. Exp. Mol. Med. 45, e12–e12. https://doi.org/10.1038/emm.2013.25

Lerner, S.A., Schmitt, B.A., Seligsohn, R., Matz, G.J., 1986. Comparative study of ototoxicity and nephrotoxicity in patients randomly assigned to treatment with amikacin or gentamicin. Am. J. Med. 80, 98–104.

Lezi, E., Swerdlow, R.H., 2012. Mitochondria in Neurodegeneration, in: Scatena, R., Bottoni, P., Giardina, B. (Eds.), Advances in Mitochondrial Medicine. Springer Netherlands, Dordrecht, pp. 269–286. https://doi.org/10.1007/978-94-007-2869-1_12

Li, H., Steyger, P.S., 2009. Synergistic ototoxicity due to noise exposure and aminoglycoside antibiotics. Noise Health 11, 26–32.

Lim, M.L.., Minamikawa, T., Nagley, P., 2001. The protonophore CCCP induces mitochondrial permeability transition without cytochrome *c* release in human osteosarcoma cells. FEBS Lett. 503, 69–74. https://doi.org/10.1016/S0014-5793(01)02693-X

Majumder, P., Moore, P.A., Richardson, G.P., Gale, J.E., 2017. Protecting Mammalian Hair Cells from Aminoglycoside-Toxicity: Assessing Phenoxybenzamine's Potential. Front. Cell. Neurosci. 11. https://doi.org/10.3389/fncel.2017.00094

Marcotti, W., Corns, L.F., Desmonds, T., Kirkwood, N.K., Richardson, G.P., Kros, C.J., 2014. Transduction without Tip Links in Cochlear Hair Cells Is Mediated by Ion Channels with Permeation Properties Distinct from Those of the Mechano-Electrical Transducer Channel. J. Neurosci. 34, 5505–5514. https://doi.org/10.1523/JNEUROSCI.4086-13.2014

Marcotti, W., Kros, C.J., 1999. Developmental expression of the potassium current $I_{K,n}$ contributes to maturation of mouse outer hair cells. J. Physiol. 520, 653–660. https://doi.org/10.1111/j.1469-7793.1999.00653.x

Marcotti, W., Van Netten, S.M., Kros, C.J., 2005. The aminoglycoside antibiotic dihydrostreptomycin rapidly enters mouse outer hair cells through the mechano -electrical transducer channels: Aminoglycoside entry into hair cells. J. Physiol. 567, 505–521. https://doi.org/10.1113/jphysiol.2005.085951

Margulis, L., 1970. Origin of eukaryotic cells. Yale University Press, New Haven, CT

McRorie, T.I., Bosso, J., Randolph, L., 1989. Aminoglycoside ototoxicity in cystic fibrosis. Evaluation by high-frequency audiometry. Am. J. Dis. Child. 1960 143, 1328–1332.

Meng, Z., Li, T., Ma, X., Wang, X., Van Ness, C., Gan, Y., Zhou, H., Tang, J., Lou, G., Wang, Y., Wu, J., Yen, Y., Xu, R., Huang, W., 2013. Berbamine Inhibits the Growth of Liver Cancer Cells and Cancer-Initiating Cells by Targeting Ca2+/Calmodulin-Dependent Protein Kinase II. Mol. Cancer Ther. 12, 2067–2077. https://doi.org/10.1158/1535-7163.MCT-13-0314

Mingeot-Leclercq, M.P., Tulkens, P.M., 1999. Aminoglycosides: nephrotoxicity. Antimicrob. Agents Chemother. 43, 1003–1012.

Miyazono, Y., Hirashima, S., Ishihara, N., Kusukawa, J., Nakamura, K., Ohta, K., 2018. Uncoupled mitochondria quickly shorten along their long axis to form indented spheroids, instead of rings, in a fission-independent manner. Sci. Rep. 8, 350. https://doi.org/10.1038/s41598-017-18582-6

Nagai, J., Takano, M., 2014. Entry of aminoglycosides into renal tubular epithelial cells via endocytosis-dependent and endocytosis-independent pathways. Biochem. Pharmacol. 90, 331–337. https://doi.org/10.1016/j.bcp.2014.05.018

Negrette-Guzmán, M., García-Niño, W.R., Tapia, E., Zazueta, C., Huerta-Yepez, S., León-Contreras, J.C., Hernández-Pando, R., Aparicio-Trejo, O.E., Madero, M., Pedraza-Chaverri, J., 2015. Curcumin Attenuates Gentamicin-Induced Kidney Mitochondrial Alterations: Possible Role of a Mitochondrial Biogenesis Mechanism. Evid. Based Complement. Alternat. Med. 2015, 1–16. https://doi.org/10.1155/2015/917435

Neveux, S., Smith, N.K., Roche, A., Blough, B.E., Pathmasiri, W., Coffin, A.B., 2017. Natural Compounds as Occult Ototoxins? Ginkgo biloba Flavonoids Moderately Damage Lateral Line Hair Cells. J. Assoc. Res. Otolaryngol. JARO 18, 275–289. https://doi.org/10.1007/s10162-016-0604-6

Nin, F., Hibino, H., Doi, K., Suzuki, T., Hisa, Y., Kurachi, Y., 2008. The endocochlear potential depends on two K+ diffusion potentials and an electrical barrier in the stria vascularis of the inner ear. Proc. Natl. Acad. Sci. 105, 1751–1756. https://doi.org/10.1073/pnas.0711463105

Oliver, D., Knipper, M., Derst, C., Fakler, B., 2003. Resting potential and submembrane calcium concentration of inner hair cells in the isolated mouse cochlea are set by KCNQ-type potassium channels. J. Neurosci. Off. J. Soc. Neurosci. 23, 2141–2149.

Olszewska, A., Szewczyk, A., 2013. Mitochondria as a pharmacological target: Magnum overview. IUBMB Life 65, 273–281. https://doi.org/10.1002/iub.1147

O'Sullivan, M.E., Perez, A., Lin, R., Sajjadi, A., Ricci, A.J., Cheng, A.G., 2017. Towards the Prevention of Aminoglycoside-Related Hearing Loss. Front. Cell. Neurosci. 11. https://doi.org/10.3389/fncel.2017.00325

Ou, H.C., Cunningham, L.L., Francis, S.P., Brandon, C.S., Simon, J.A., Raible, D.W., Rubel, E.W., 2009. Identification of FDA-Approved Drugs and Bioactives that Protect Hair Cells in the Zebrafish (Danio rerio) Lateral Line and Mouse (Mus musculus) Utricle. J. Assoc. Res. Otolaryngol. 10, 191–203. https://doi.org/10.1007/s10162-009-0158-y

Owens, K.N., Coffin, A.B., Hong, L.S., Bennett, K.O., Rubel, E.W., Raible, D.W., 2009. Response of mechanosensory hair cells of the zebrafish lateral line to aminoglycosides reveals distinct cell death pathways. Hear. Res. 253, 32–41. https://doi.org/10.1016/j.heares.2009.03.001

Owens, K.N., Santos, F., Roberts, B., Linbo, T., Coffin, A.B., Knisely, A.J., Simon, J.A., Rubel, E.W., Raible, D.W., 2008. Identification of Genetic and Chemical Modulators of Zebrafish Mechanosensory Hair Cell Death. PLoS Genet. 4, e1000020. https://doi.org/10.1371/journal.pgen.1000020

Pan, B., Akyuz, N., Liu, X.-P., Asai, Y., Nist-Lund, C., Kurima, K., Derfler, B.H., György, B., Limapichat, W., Walujkar, S., Wimalasena, L.N., Sotomayor, M., Corey, D.P., Holt, J.R., 2018. TMC1 Forms the Pore of Mechanosensory Transduction Channels in Vertebrate Inner Ear Hair Cells. Neuron 99, 736-753.e6. https://doi.org/10.1016/j.neuron.2018.07.033

Petersen, L., Rogers, C., 2015. Aminoglycoside-induced hearing deficits – a review of cochlear ototoxicity. South Afr. Fam. Pract. 57, 77–82. https://doi.org/10.1080/20786190.2014.1002220

Pickles, J.O., Brix, J., Comis, S.D., Gleich, O., Köppl, C., Manley, G.A., Osborne, M.P., 1989. The organization of tip links and stereocilia on hair cells of bird and lizard basilar papillae. Hear. Res. 41, 31–41. https://doi.org/10.1016/0378-5955(89)90176-7

Pickles, J.O., 2008. An Introduction to the Physiology of Hearing (Academic Press).

Polyzos, A. A., McMurray, C.T. 2017. The chicken or the egg: mitochondrial dysfunction as a cause or consequence of toxicity in Huntington's disease. Mech Ageing Dev;161:181–97.

Prezant, T.R., Agapian, J.V., Bohlman, M.C., Bu, X., Öztas, S., Qiu, W.-Q., Arnos, K.S., Cortopassi, G.A., Jaber, L., Rotter, J.I., Shohat, M., Fischel-Ghodsian, N., 1993. Mitochondrial ribosomal RNA mutation associated with both antibiotic–induced and non–syndromic deafness. Nat. Genet. 4, 289–294. https://doi.org/10.1038/ng0793-289

Purves, D., Augustine, G.J., Fitzpatrick, D., et al., editors. 2001. Neuroscience. 2nd edition. Sunderland (MA): Sinauer Associates. Two Kinds of Hair Cells in the Cochlea. Available from: https://www.ncbi.nlm.nih.gov/books/NBK11122/

Purves, D., Augustine, G.J., Fitzpatrick, D., Hall, W.C., LaMantia, A., White, L.E., 2012. Neuroscience. Fifth Edition.

Quraishi, I.H., Raphael, R.M., 2008. Generation of the Endocochlear Potential: A Biophysical Model. Biophys. J. 94, L64–L66. https://doi.org/10.1529/biophysj.107.128082

Rahn, C.A., Bombick, D.W., Doolittle, D.J., 1991. Assessment of mitochondrial membrane potential as an indicator of cytotoxicity. Fundam. Appl. Toxicol. Off. J. Soc. Toxicol. 16, 435–448.

Reddy, P.H., 2009. Role of mitochondria in neurodegenerative diseases: mitochondria as a therapeutic target in Alzheimer's disease. CNS Spectr. 14, 8–13; discussion 16-18.

Richardson, G.P., Forge, A., Kros, C.J., Fleming, J., Brown, S.D., Steel, K.P., 1997. Myosin VIIA is required for aminoglycoside accumulation in cochlear hair cells. J. Neurosci. Off. J. Soc. Neurosci. 17, 9506–9519.

Richardson, G.P., Russell, I.J., 1991. Cochlear cultures as a model system for studying aminoglycoside induced ototoxicity. Hear. Res. 53, 293–311.

Rizzi, M.D., Hirose, K., 2007. Aminoglycoside ototoxicity: Curr. Opin. Otolaryngol. Head Neck Surg. 15, 352–357. https://doi.org/10.1097/MOO.0b013e3282ef772d

Rohlena, J., Dong, L.-F., Ralph, S.J., Neuzil, J., 2011. Anticancer Drugs Targeting the Mitochondrial Electron Transport Chain. Antioxid. Redox Signal. 15, 2951–2974. https://doi.org/10.1089/ars.2011.3990

Roth, B., Bruns, V., 1992. Postnatal development of the rat organ of Corti: II. Hair cell receptors and their supporting elements. Anat. Embryol. (Berl.) 185, 571–581. https://doi.org/10.1007/BF00185616

Russell., I.J, Sellick, P.M. 1983. Low-frequency characteristics of intracellularly recorded receptor potentials in guinea-pig cochlear hair cells. The Journal of Physiology. 338:179–206. doi: 10.1113/jphysiol.1983.sp014668.

Rybak, L.P., Whitworth, C.A., 2005. Ototoxicity: therapeutic opportunities. Drug Discov. Today 10, 1313–1321. https://doi.org/10.1016/S1359-6446(05)03552-X

Safiulina, D., Veksler, V., Zharkovsky, A., Kaasik, A., 2006. Loss of mitochondrial membrane potential is associated with increase in mitochondrial volume: Physiological role in neurones. J. Cell. Physiol. 206, 347–353. https://doi.org/10.1002/jcp.20476

Santos, F., MacDonald, G., Rubel, E.W., Raible, D.W., 2006. Lateral line hair cell maturation is a determinant of aminoglycoside susceptibility in zebrafish (Danio rerio). Hear. Res. 213, 25–33. https://doi.org/10.1016/j.heares.2005.12.009

Schacht, J., Talaska, A.E., Rybak, L.P., 2012. Cisplatin and Aminoglycoside Antibiotics: Hearing Loss and Its Prevention. Anat. Rec. Adv. Integr. Anat. Evol. Biol. 295, 1837–1850. https://doi.org/10.1002/ar.22578

Seiler, C., Nicolson, T., 1999. Defective calmodulin-dependent rapid apical endocytosis in zebrafish sensory hair cell mutants. J. Neurobiol. 41, 424–434.

Selimoglu, E., 2007. Aminoglycoside-induced ototoxicity. Curr. Pharm. Des. 13, 119–126.

Sergi, B., Fetoni, A.R., Ferraresi, A., Troiani, D., Azzena, G.B., Paludetti, G., Maurizi, M., 2004. The role of antioxidants in protection from ototoxic drugs. Acta Oto-Laryngol. Suppl. 42–45.

Sha, S.H. and Schacht, J., 1999a. Formation of reactive oxygen species following bioactivation of gentamicin. Free Rad Biol Med 26:341–347.

Sha, S.-H., Schacht, J., 2000. Antioxidants attenuate gentamicin-induced free radical formation in vitro and ototoxicity in vivo: D-methionine is a potential protectant. Hear. Res. 142, 34–40. https://doi.org/10.1016/S0378-5955(00)00003-4

Simmons, C.F., Bogusky, R.T., Humes, H.D., 1980. Inhibitory effects of gentamicin on renal mitochondrial oxidative phosphorylation. J. Pharmacol. Exp. Ther. 214, 709.

Skinner, R., Pearson, A.D., English, M.W., Price, L., Wyllie, R.A., Coulthard, M.G., Craft, A.W., 1998. Cisplatin dose rate as a risk factor for nephrotoxicity in children. Br. J. Cancer 77, 1677–1682.

Smith, C.B., Betz, W.J., 1996. Simultaneous independent measurement of endocytosis and exocytosis. Nature 380, 531–534. https://doi.org/10.1038/380531a0

Song, J., Yan, H.Y., Popper, A.N., 1995. Damage and recovery of hair cells in fish canal (but not superficial) neuromasts after gentamicin exposure. Hear. Res. 91, 63–71.

Stafylas, P.C., Sarafidis, P.A., 2008. Carvedilol in hypertension treatment. Vasc. Health Risk Manag. 4, 23–30.

Stavroulaki, P., Vossinakis, I.C., Dinopoulou, D., Doudounakis, S., Adamopoulos, G., Apostolopoulos, N., 2002. Otoacoustic emissions for monitoring aminoglycoside-induced ototoxicity in children with cystic fibrosis. Arch. Otolaryngol. Head Neck Surg. 128, 150–155.

Steyger, P.S., Peters, S.L., Rehling, J., Hordichok, A., Dai, C.F., 2003. Uptake of Gentamicin by Bullfrog Saccular Hair Cells in vitro. JARO - J. Assoc. Res. Otolaryngol. 4, 565–578. https://doi.org/10.1007/s10162-003-4002-5

Stone, J.S., Cotanche, D.A., 2007. Hair cell regeneration in the avian auditory epithelium. Int. J. Dev. Biol. 51, 633–647. https://doi.org/10.1387/ijdb.072408js

Takeuchi, S., Ando, M., Kakigi, A., 2000. Mechanism Generating Endocochlear Potential: Role Played by Intermediate Cells in Stria Vascularis. Biophys. J. 79, 2572–2582. https://doi.org/10.1016/S0006-3495(00)76497-6

Tao, C., Riyuan, L., Shuolong, Y., Liangwei, X., Shiming, Y., 2014. Combinational Administration of Aminoglycosides and Loop Diuretics as An Efficient Strategy to Establish Deafness Models in Rats. J. Otol. 9, 91–96. https://doi.org/10.1016/S1672-2930(14)50021-9

Tasaki, I., Spyropoulos, C.S., 1959. STRIA VASCULARIS AS SOURCE OF ENDOCOCHLEAR POTENTIAL. J. Neurophysiol. 22, 149–155. https://doi.org/10.1152/jn.1959.22.2.149

Thomas, A.J., Wu, P., Raible, D.W., Rubel, E.W., Simon, J.A., Ou, H.C., 2015. Identification of Small Molecule Inhibitors of Cisplatin-Induced Hair Cell Death: Results of a 10,000 Compound Screen in the Zebrafish Lateral Line. Otol. Neurotol. 36, 519–525. https://doi.org/10.1097/MAO.0000000000000487

Ton, C., Parng, C., 2005. The use of zebrafish for assessing ototoxic and otoprotective agents. Hear. Res. 208, 79–88. https://doi.org/10.1016/j.heares.2005.05.005

Tran Ba Huy, P., Bernard, P., Schacht, J., 1986. Kinetics of gentamicin uptake and release in the rat. Comparison of inner ear tissues and fluids with other organs. J. Clin. Invest. 77, 1492–1500. https://doi.org/10.1172/JCI112463

Vacher, P., Vacher, A.-M., Mollard, P., 1998. Tubocurarine blocks a calcium-dependent potassium current in rat tumoral pituitary cells. Mol. Cell. Endocrinol. 139, 131–142. https://doi.org/10.1016/S0303-7207(98)00066-5

Vilfan, A., Duke, T., 2003. Two Adaptation Processes in Auditory Hair Cells Together Can Provide an Active Amplifier. Biophys. J. 85, 191–203. https://doi.org/10.1016/S0006-3495(03)74465-8

Vlasits, A.L., Simon, J.A., Raible, D.W., Rubel, E.W., Owens, K.N., 2012. Screen of FDA-approved drug library reveals compounds that protect hair cells from aminoglycosides and cisplatin. Hear. Res. 294, 153–165. https://doi.org/10.1016/j.heares.2012.08.002

Wang, Q., Steyger, P.S., 2009. Trafficking of Systemic Fluorescent Gentamicin into the Cochlea and Hair Cells. J. Assoc. Res. Otolaryngol. 10, 205–219. https://doi.org/10.1007/s10162-009-0160-4

Wang, S., Zhang, Q., Zhang, Yuxin, Zhang, Yanling, Wu, Q., Li, S., Qiao, Y., 2016. Identification of berbamine dihydrochloride from barberry as an anti-adipogenic agent by high-content imaging assay. J. Tradit. Chin. Med. Sci. 3, 91–99. https://doi.org/10.1016/j.jtcms.2016.07.007

Wangemann, P., 2006. Supporting sensory transduction: cochlear fluid homeostasis and the endocochlear potential: Cochlear homeostasis. J. Physiol. 576, 11–21. https://doi.org/10.1113/jphysiol.2006.112888

Wangemann, P., 2002. K+ cycling and the endocochlear potential. Hear. Res. 165, 1–9.

Wargo, K.A., Edwards, J.D., 2014. Aminoglycoside-induced nephrotoxicity. J. Pharm. Pract. 27, 573–577. https://doi.org/10.1177/0897190014546836

Woiwode, U., Sievers-Engler, A., Lämmerhofer, M., 2016. Preparation of fluorescent labeled gentamicin as biological tracer and its characterization by liquid chromatography and high resolution mass spectrometry. J Pharm Biomed Anal 121, 307–315. https://doi.org/10.1016/j.jpba.2015.12.053Wu, W.-J., Sha, S.-H., Schacht, J., 2002. Recent Advances in Understanding Aminoglycoside Ototoxicity and Its Prevention. Audiol. Neurotol. 7, 171–174. https://doi.org/10.1159/000058305

Xie, J., Talaska, A.E., Schacht, J., 2011. New developments in aminoglycoside therapy and ototoxicity. Hear. Res. 281, 28–37. https://doi.org/10.1016/j.heares.2011.05.008

Zaczek, R., Chorvat, R.J., Saye, J.A., Pierdomenico, M.E., Maciag, C.M., Logue, A.R., Fisher, B.N., Rominger, D.H., Earl, R.A., 1998. Two new potent neurotransmitter release enhancers, 10,10-bis(4-pyridinylmethyl)-9(10H)-anthracenone and 10,10-bis(2-fluoro-4-pyridinylmethyl)-9(10H)-anthracenone: comparison to linopirdine. J. Pharmacol. Exp. Ther. 285, 724–730.

Zhang, C.M., Gao, L., Zheng, Y.J., Yang, H.T., 2012. Berbamine protects the heart from ischemia/reperfusion injury by maintaining cytosolic Ca(2+) homeostasis and preventing calpain activation. Circ. J. Off. J. Jpn. Circ. Soc. 76, 1993–2002.

Zhao, Y., Lv, J.J., Chen, J., Jin, X.B., Wang, M.W., Su, Z.H., Wang, L.Y., Zhang, H.Y., 2016. Berbamine inhibited the growth of prostate cancer cells in vivo and in vitro via triggering intrinsic pathway of apoptosis. Prostate Cancer Prostatic Dis. 19, 358–366. https://doi.org/10.1038/pcan.2016.29

Zhao, Y., Yamoah, E.N., Gillespie, P.G., 1996. Regeneration of broken tip links and restoration of mechanical transduction in hair cells. Proc. Natl. Acad. Sci. U. S. A. 93, 15469–15474.

Zheng, J., Madison, L.D., Oliver, D., Fakler, B., Dallos, P., 2002. Prestin, the Motor Protein of Outer Hair Cells. Audiol. Neurotol. 7, 9–12. https://doi.org/10.1159/000046855

Zheng, J., Shen, W., He, D.Z.Z., Long, K.B., Madison, L.D., Dallos, P., 2000. Prestin is the motor protein of cochlear outer hair cells. Nature 405, 149–155. https://doi.org/10.1038/35012009

Zorova, L.D., Popkov, V.A., Plotnikov, E.Y., Silachev, D.N., Pevzner, I.B., Jankauskas, S.S., Babenko, V.A., Zorov, S.D., Balakireva, A.V., Juhaszova, M., Sollott, S.J., Zorov, D.B., 2017. Mitochondrial membrane potential. Anal. Biochem. https://doi.org/10.1016/j.ab.2017.07.009